EuroIntervention
2024;20:e1465-e1475
published online e-edition December 2024
DOI: 10.4244/EIJ-D-24-00096

ORIGINAL RESEARCH

Computed tomography versus near-infrared spectroscopy for the assessment of coronary atherosclerosis

Anantharaman Ramasamy[1,2], MBChB, PhD; Ramya Parasa[1,2], MBBS; Hessam Sokooti[3], PhD; Xiaotong Zhang[4], MSc; Ibrahim Halil Tanboga[5], MD, PhD; Pieter Kitslaar[3,4], MSc; Alexander Broersen[4], PhD; Krishnaraj S. Rathod[1,2], PhD; Rajiv Amersey[1], FRCP; Ajay Jain[1], MD; Mick Ozkor[1], MD; Johan H.C. Reiber[3,4], PhD; Jouke Dijkstra[4], PhD; Patrick W. Serruys[6,7], MD, PhD; James C. Moon[1,8], MD; Anthony Mathur[1,2], MD, PhD; Ryo Torii[9], MSc, PhD; Francesca Pugliese[1,2], MD, PhD; Andreas Baumbach[1,2], MD, PhD; Christos V. Bourantas[1,2,8]*, MD, PhD

**Corresponding author: Barts Heart Centre, St Bartholomew's Hospital, West Smithfield, London, EC1A 7BE, United Kingdom. E-mail: c.bourantas@nhs.net*

This paper also includes supplementary data published online at: https://eurointervention.pcronline.com/doi/10.4244/EIJ-D-24-00096

ABSTRACT

BACKGROUND: Coronary computed tomography angiography (CCTA) has been proposed as an alternative to intravascular imaging for assessing plaque pathology.

AIMS: We aimed to assess the efficacy of CCTA against near-infrared spectroscopy-intravascular ultrasound (NIRS-IVUS) in evaluating atheroma burden and composition and for guiding coronary interventions.

METHODS: Seventy patients with a chronic coronary syndrome were recruited and underwent CCTA and NIRS-IVUS. The imaging data were matched, and the estimations of lumen, vessel wall and plaque dimensions and composition of the two modalities were compared. The primary endpoint of the study was the efficacy of CCTA in detecting lipid-rich plaques identified by NIRS-IVUS. Secondary endpoints included the performance of CCTA in evaluating coronary artery pathology in the studied segments and its value in stent sizing, using NIRS-IVUS as the reference standard.

RESULTS: In total, 186 vessels were analysed. The attenuated plaque volume on CCTA had weak accuracy in detecting lipid-rich plaques (58%; p=0.029). Compared to NIRS-IVUS, CCTA underestimated the lumen volume (309.2 mm^3 vs 420.4 mm^3; p=0.001) and plaque dimensions (total atheroma volume 116.1 mm^3 vs 292.8 mm^3; p<0.001 and percentage atheroma volume 27.67% vs 41.06%; p<0.001) and overestimated the lipid component (lipid core burden index 48.6 vs 33.8; p=0.007). In the 86 lesions considered for revascularisation, CCTA underestimated the reference vessel area (8.16 mm^2 vs 12.30 mm^2; p<0.001) and overestimated the lesion length (23.5 mm vs 19.0 mm; p=0.029) compared to NIRS-IVUS.

CONCLUSIONS: CCTA has limited efficacy in assessing plaque composition and quantifying lumen and plaque dimensions and tissue types, which may potentially impact revascularisation planning.

KEYWORDS: intravascular ultrasound; MSCT; non-invasive imaging; stable angina

SUBMITTED ON 27/01/2024 - REVISION RECEIVED ON 1st 30/06/2024 / 2nd 07/08/2024 - ACCEPTED ON 20/08/2024

Intravascular imaging enables the accurate assessment of coronary artery pathology, evaluates the implications of novel pharmacotherapies on atheroma burden and morphology and assesses post-percutaneous coronary intervention (PCI) results especially in high-risk patients and complex lesions[1]. However, intravascular imaging is invasive, is usually used in patients with advanced coronary artery disease, does not allow assessment of the entire coronary tree, and is associated with both an increased cost and a small, albeit non-negligible, risk of complications[2].

Non-invasive imaging, specifically coronary computed tomography angiography (CCTA), has emerged as an alternative imaging modality for assessing plaque pathology[3]. Histological studies have shown that CCTA has value in characterising plaque composition and burden and has been increasingly used to examine the potency of emerging pharmacotherapies and their effects on plaque morphology[4]. In parallel, there is an increased interest in the value of CCTA in guiding PCI[5]. Nevertheless, so far there has been no prospective study specifically designed to assess the efficacy of CCTA in assessing plaque composition, quantifying lumen and vessel wall dimensions and guiding revascularisation against state-of-the-art intravascular imaging.

Methods

STUDY POPULATION

The Evaluation of the Efficacy of Computed Tomographic Coronary Angiography in Assessing Coronary Artery Morphology and Physiology study (ClinicalTrials.gov: NCT03556644) is a prospective, multivessel coronary imaging study that was designed to compare CCTA and NIRS-IVUS estimations. The study protocol has been published previously[6]. In brief, 70 patients with a chronic coronary syndrome and obstructive coronary artery disease on invasive coronary angiography undergoing further assessment (pressure wire or intravascular imaging) or treatment with PCI were recruited. All patients underwent a CCTA, followed by multivessel NIRS-IVUS imaging assessment. The patients were then treated according to their clinical indication. The recruited patients provided written consent prior to enrolment. The study was approved by the local ethics committee (Research Ethics Committee [REC] reference: 17/SC/0566) and was performed in accordance with the Declaration of Helsinki. The NIRS-IVUS and CCTA data acquisition, analysis and coregistration are described in **Supplementary Appendix 1**.

Impact on daily practice

This is the first prospective study assessing the efficacy of optimal coronary computed tomography angiography (CCTA) in estimating the extent of coronary artery disease, quantifying plaque burden and composition and guiding percutaneous coronary interventions compared to state-of-the-art near-infrared spectroscopy-intravascular ultrasound (NIRS-IVUS) imaging. In our study, the necrotic core volume in CCTA had moderate efficacy in detecting lipid-rich plaques. CCTA also underestimated lumen and plaque dimensions in the segments that had been assessed by both modalities and had limited efficacy in assessing plaque composition. In lesions that were revascularised, CCTA underestimated the reference vessel area and was unable to accurately estimate lesion length and, thus, indicated implantation of smaller stents compared to NIRS-IVUS.

DATA ANALYSIS AND STUDY ENDPOINTS

PRIMARY ENDPOINT

The primary endpoint of this study is the efficacy of plaque composition on CCTA in detecting lipid-rich plaque, using NIRS-IVUS as the reference standard. A plaque on NIRS-IVUS was defined as a segment with plaque burden (PB) ≥40% over three consecutive frames[7]. Plaques were considered separate if there was a segment with a length of >5 mm between them. In CCTA, there is no established PB cutoff to define plaques. Therefore, in this study, receiver operating characteristic (ROC) curve analysis was performed to identify the optimal PB cutoff that predicted a PB ≥40% on NIRS-IVUS. This was used to define plaques on CCTA similarly to NIRS-IVUS (i.e., a segment with at least three consecutive frames with increased PB). In total, 50 vessels from 15 patients were randomly selected to identify the optimal PB cutoff for predicting plaques. This test set was also used to identify plaque components on CCTA that corresponded to the presence of lipid tissue on the 2 mm block chemogram on NIRS-IVUS[8], and these plaque components were used to build a model that enabled prediction of the presence of lipid tissue on CCTA. The performance of the model to detect lipid-rich plaques – defined as a plaque with at least one yellow block chemogram – was tested in the remaining dataset (136 vessels). A further analysis was performed to examine the efficacy of CCTA to identify lipid-rich plaques with and without increased calcific component (defined as the presence of calcific tissue with an arc >90 on NIRS-IVUS)[9].

Abbreviations

BA	Bland-Altman	**LoA**	limits of agreement
CaBI	calcific burden index	**MLA**	minimum lumen area
CCTA	coronary computed tomography angiography	**NIRS-IVUS**	near-infrared spectroscopy-intravascular ultrasound
DS	diameter stenosis	**NPV**	negative predictive value
EEM	external elastic membrane	**PAV**	percentage atheroma volume
HU	Hounsfield units	**PB**	plaque burden
ICC	intraclass correlation coefficient	**PPV**	positive predictive value
LCBI	lipid core burden index	**TAV**	total atheroma volume

SECONDARY ENDPOINTS

The secondary endpoints of the study included the following:

1. The agreement between NIRS-IVUS and CCTA for quantifying the lumen, vessel wall and plaque dimensions, as well as plaque burden and composition at the segment level. For each segment of interest assessed by NIRS-IVUS and CCTA, the lumen, vessel, total atheroma (TAV) and percentage atheroma volumes (PAV) were estimated on NIRS-IVUS and CCTA and compared. Plaque composition comparison was performed using the lipid core burden index (LCBI), calcific burden index (CaBI) and maximum LCBI in a 4 mm segment ($maxLCBI_{4mm}$).

2. The accuracy of CCTA in identifying high-risk lesions. Previous prospective NIRS-IVUS studies have shown that lesions with a large lipid content ($maxLCBI_{4mm}$ >325 and $maxLCBI_{4mm}$ >400)[10,11] on NIRS-IVUS are at risk of causing events. Therefore, we performed a further analysis to examine whether plaque components derived by CCTA can accurately predict these lesions.

3. The value of CCTA in guiding revascularisation. Intravascular imaging has an established role in identifying the optimal landing zone (based on the current consensus, segments with a PB <50%) and stent diameter defined by the external elastic membrane (EEM) diameter in the distal reference segment (rounded down by <0.5 mm)[12]. These criteria were used by the analyst who did the NIRS-IVUS analysis to determine the optimal stent size based on the NIRS-IVUS estimations for all lesions treated with PCI or that were considered for PCI and underwent functional assessment. In CCTA, there is no specific PB cutoff for identifying disease-free landing zones. Therefore, as before, ROC curve analysis was performed in the test set of 50 vessels to identify the optimal PB cutoff on CCTA that predicted a PB >50% on NIRS-IVUS. This cutoff was used by the analyst who performed the CCTA segmentation to define the optimal stent size and diameter based on the CCTA annotations in lesions that were treated with or considered for revascularisation. Tandem lesions on CCTA, with interpolated disease-free segments with a length <10 mm, that corresponded to the same lesion on NIRS-IVUS were treated as a single lesion, and the stent length on CCTA was estimated from the proximal reference segment of the most proximal lesion and the distal reference segment of the most distal lesion. Moreover, we examined the efficacy of CCTA to assess plaque composition and identify compositional predictors associated with periprocedural complications and worse prognosis and, in particular, the presence of $maxLCBI_{4mm}$ >600, which has been found to be a predictor of microvascular obstruction post-PCI; we also evaluated its efficacy in identifying the presence of a vessel diameter <3.5 mm in calcific lesions, of circumferential calcification, and of an arc of calcium >270° for a length >5 mm, all of which are established predictors of stent underexpansion[13,14].

Statistical analysis

Continuous variables are presented as median (interquartile range [IQR]) or mean±standard deviation (SD) – depending on their distribution – while categorical variables are presented as absolute values and percentages. The estimations of NIRS-IVUS and CCTA on the same subject were compared using Wilcoxon signed-rank tests for continuous variables or the McNemar test for categorical variables. The agreement of the two modalities for continuous variables was tested using intraclass correlation coefficients (ICC) under a two-way random-effects model, considering absolute agreement and average measurements. The kappa statistic was used for agreement between categorical variables. The Pearson correlation coefficient was implemented to examine the linear relationship between the two modalities, and Bland-Altman (BA) analysis was used to assess bias and determine the limits of agreement (LoA) between CCTA and NIRS-IVUS measurements. In parametric BA analysis, the bias was calculated as the mean or median difference between the two approaches depending on distribution, while the LoA were defined as a range centred around the mean bias±1.96 x SD. For non-parametric BA analysis, the median bias and the 2.5th-97.5th percentiles were computed using quantile regression. We chose non-parametric BA analysis for the lesion- and segment-level analyses due to the small sample size and the non-normal distribution of the differences[15,16]. The association between two categorical variables was assessed by Cramer's V value.

For the study's primary endpoint, the volumes of three tissue types (necrotic core, fibrofatty, necrotic core + fibrofatty) from 50 vessels were estimated and compared with the presence of lipid tissue on the 2 mm block chemogram from NIRS-IVUS. ROC curve analysis was performed, and the area under the curve (AUC) was used to assess the performance of these three tissue categories in identifying lipid on the block chemogram. The necrotic core volume was found to perform best, and the optimal cutoff (1 mm^3; 95% confidence interval [CI]: 0.84-1.36 mm^3) was applied to the remaining dataset. The primary endpoint of the study – the efficacy of CCTA in detecting fibroatheroma classified on NIRS-IVUS – was assessed by diagnostic performance measures (AUC, sensitivity, specificity, positive [PPV] and negative [NPV] predictive values).

All statistical tests were two-tailed, and statistical significance was set at $p<0.05$; analyses were performed using R software, v. 4.2.2 (R Foundation for Statistical Computing) using "lme4", "psych", "dplyr", "rms" and "ggplot2" packages.

Results

PATIENT BASELINE CHARACTERISTICS

The baseline characteristics of the 70 patients recruited in our study are summarised in **Supplementary Table 1**. CCTA images were reviewed by two independent experts who graded image quality. One patient was excluded because of poor image quality due to increased calcific burden. In addition, 9 vessels were excluded because of poor matching between CCTA and NIRS-IVUS. Therefore, in total 64 patients (186 vessels; 23,605 matched NIRS-IVUS and CCTA cross-sections) were included in the final analysis **(Supplementary Figure 1)**.

PRIMARY ENDPOINT: EFFICACY OF CCTA IN DETECTING LIPID-RICH PLAQUES

The necrotic core volume cutoff (≥1 mm^3), found to best predict the presence of lipid-rich block chemogram in 50 vessels, was

applied in the remaining dataset (49 patients, 136 vessels) to assess plaque phenotype. Of the 75 lipid-rich plaques detected by NIRS-IVUS, CCTA correctly detected 53 lipid-rich plaques but misclassified 44 others as lipid-rich. The sensitivity of CCTA was 70.7% (IQR 59-81%), specificity was 46.3% (IQR 35-58%), PPV was 55% (IQR 44-65%), NPV was 63% (IQR 50-75%) and accuracy was 58% (IQR 50-66%; p=0.010; AUC=0.585, 95% CI: 0.510-0.660; p=0.029).

CCTA showed a similar ability in detecting non-calcified lipid-rich plaques compared to calcified lipid-rich plaques with a sensitivity of 70.9% versus 66.7%, specificity 47.0% versus 40.6%, PPV 46.2% versus 9.0%, NPV 71.6% versus 93.0%, accuracy 56.4% versus 42.7% and AUC 0.590 versus 0.536; p=0.434, respectively.

COMPARISON OF NIRS-IVUS AND CCTA AT THE SEGMENT LEVEL

In total, 186 vessels were included in the final analysis. The mean length of the studied segments was 76.9±27.4 mm. An example of matched CCTA and NIRS-IVUS spread-out plots are shown in **Figure 1**. The ICC and the Pearson correlation coefficient were high for the lumen volume, vessel volume and TAV, moderate for the PAV and CaBI, and weak for the LCBI and $maxLCBI_{4mm}$ **(Table 1)**. CCTA underestimated the lumen and vessel volumes, TAV and PAV, and overestimated the LCBI, but there was no difference between the two modalities for the CaBI or $maxLCBI_{4mm}$ **(Figure 2)**. However, the LoA were wide for these latter two metrics **(Figure 3)**.

CCTA FOR DETECTING HIGH-RISK LESIONS

In the 186 vessels that were assessed by NIRS-IVUS, 32 plaques had a $maxLCBI_{4mm}$ >400, and 40 plaques had a $maxLCBI_{4mm}$ >325. The accuracy of CCTA to detect high-risk plaques was moderate **(Central illustration)** and was not different for plaques with $maxLCBI_{4mm}$ >325 and $maxLCBI_{4mm}$ >400 (sensitivity: 63.5% and 68.1%; specificity: 67.4% and 65.6%; PPV: 47.1% and 37.6%; NPV: 80.2% and 87.1%; and AUC: 0.683 and 0.675; p=0.796, respectively).

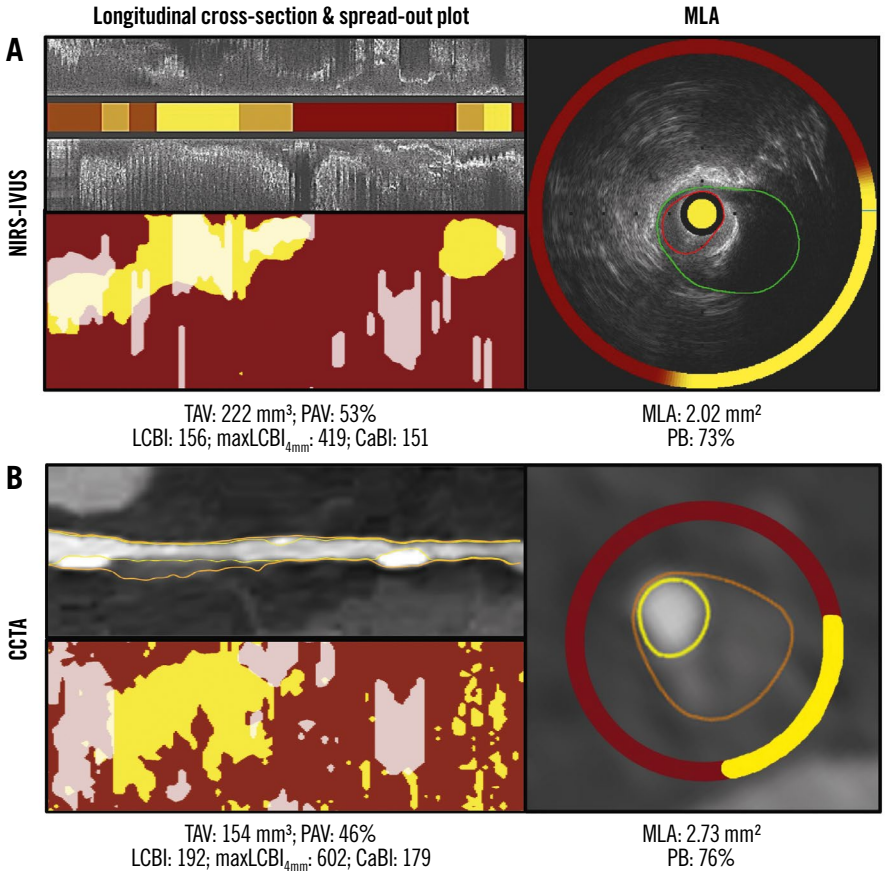

Figure 1. *Lumen, vessel wall and spread-out plaque composition analysis of the NIRS-IVUS and CCTA images. A) portrays a longitudinal segment of interest in a left anterior descending artery on NIRS-IVUS, while (B) portrays the corresponding segment of interest on CCTA. The spread-out plots displaying lipid and calcific tissue distribution are also displayed. The TAV, PAV, LCBI, CaBI and $maxLCBI_{4mm}$ estimations of both modalities are shown at the bottom. The cross-sections showing the MLA with the annotated lumen and vessel wall borders and the circumferential distribution of tissue types on NIRS-IVUS and CCTA are portrayed in the images on the right in (A) and (B). CaBI: calcific burden index; CCTA: coronary computed tomography angiography; LCBI: lipid core burden index; $maxLCBI_{4mm}$: maximum LCBI in a 4 mm segment; MLA: minimum lumen area; NIRS-IVUS: near-infrared spectroscopy-intravascular ultrasound; PAV: percentage atheroma volume; PB: plaque burden; TAV: total atheroma volume*

Table 1. Segment-level comparison of the estimations of NIRS-IVUS and CCTA imaging.

Estimations	NIRS-IVUS	CCTA	*p*-value	Median bias (95% LoA)	r	*p*-value	ICC	*p*-value
Lumen volume, mm³	420.4 (223.8-612.8)	309.2 (176.7-463.8)	0.001	89.4 (–52.9, 411.8)	0.98 (0.97-0.98)	<0.001	0.97 (0.96-0.98)	<0.001
Vessel volume, mm³	735.0 (385.2-1,059.4)	454.6 (247.5-672.1)	<0.001	251.3 (–7.2, 847.9)	0.95 (0.93-0.96)	<0.001	0.95 (0.94-0.96)	<0.001
TAV, mm³	292.8 (149.4-465.2)	116.1 (64.9-229.7)	<0.001	139.9 (–61.1, 535.3)	0.80 (0.74-0.84)	<0.001	0.86 (0.81-0.90)	<0.001
PAV, %	41.06 (33.75-47.86)	27.67 (20.61-37.17)	<0.001	10.60 (–10.94, 31.60)	0.48 (0.36-0.58)	<0.001	0.64 (0.52-0.73)	<0.001
LCBI	34 (5-91)	49 (11-126)	0.007	–10 (–524, 175)	0.18 (0.04-0.32)	0.012	0.26 (0.14-0.45)	0.020
$MaxLCBI_{4mm}$	228 (60-407)	240 (53-549)	0.182	–30 (–716, 510)	0.33 (0.19-0.45)	<0.001	0.48 (0.30-0.61)	<0.001
CaBI	59 (17-131)	61 (16-130)	0.865	3.8 (–181.9, 150.3)	0.66 (0.57-0.73)	<0.001	0.79 (0.73-0.85)	<0.001

Values are median (interquartile range) unless otherwise stated. CaBI: calcific burden index; CCTA: coronary computed tomography angiography; ICC: intraclass correlation coefficient; LCBI: lipid core burden index; LoA: limits of agreement; $maxLCBI_{4mm}$: maximum LCBI in a 4 mm segment; NIRS-IVUS: near-infrared spectroscopy-intravascular ultrasound; PAV: percentage atheroma volume; r: Pearson's correlation coefficient; TAV: total atheroma volume

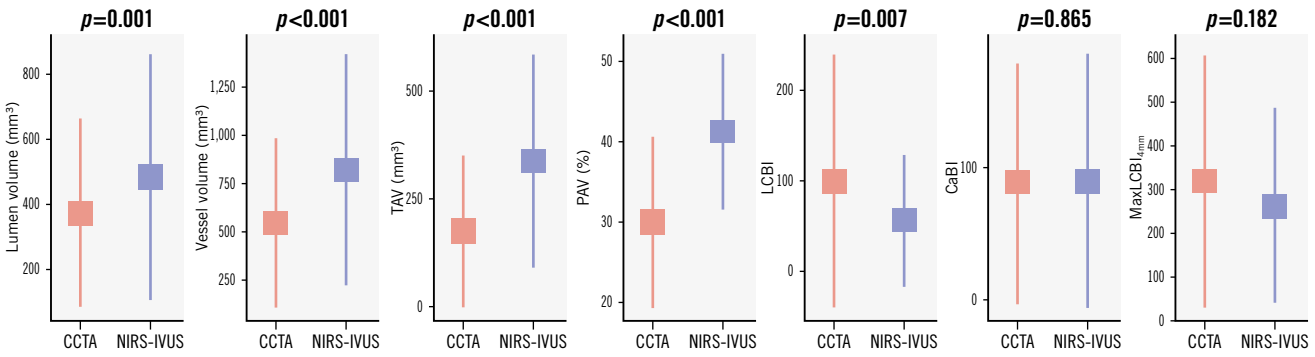

Figure 2. *Segment-level analysis comparison of NIRS-IVUS and CCTA estimations for lumen volume, vessel volume, TAV, PAV, LCBI, CaBI and maxLCBI$_{4mm}$. CaBI: calcific burden index; CCTA: coronary computed tomography angiography; LCBI: lipid core burden index; maxLCBI$_{4mm}$: maximum LCBI in a 4 mm segment; NIRS-IVUS: near-infrared spectroscopy-intravascular ultrasound; PAV: percentage atheroma volume; TAV: total atheroma volume*

CCTA FOR GUIDING REVASCULARISATION

Revascularisation with PCI or coronary artery bypass grafting (CABG) was performed in lesions with severe stenosis (angiographic diameter stenosis [DS] >90%) or in lesions with moderate stenosis (30-90%) and objective evidence of ischaemia on invasive or non-invasive imaging. In total, 86 lesions that were considered for revascularisation **(Central illustration)** were assessed by both NIRS-IVUS and CCTA (58 lesions treated with PCI, 7 lesions with CABG, and 21 lesions were found to be non-flow-limiting on functional assessment and were treated conservatively). In these lesions, the reference vessel area was larger on NIRS-IVUS (12.30 [IQR 9.17-16.0] mm² vs 8.16 [IQR 6.55-11.0] mm²; p<0.001), while lesion length was longer on CCTA (23.5 [IQR 14.0-39.3] mm vs 19.0 [IQR 11.6-32.7] mm; p=0.029) **(Table 2)**. There was no agreement between the two modalities for the LBCI, while for the CaBI, the median values were similar, but the bias and the LoA were large between NIRS-IVUS and CCTA. CCTA showed moderate accuracy in identifying lesions with $maxLCBI_{4mm}$ >600 (accuracy 0.583), for detecting vessel diameter <3.5 mm (accuracy 0.613) in calcified lesions and circumferential calcification (accuracy 0.750) and good accuracy for detecting >270° arc of calcium for a length of >5 mm (accuracy 0.885) **(Supplementary Table 2)**.

The results were different when analysis focused on lesions that were treated with PCI; their mean length by NIRS-IVUS was 19.7 (IQR 14.8-32.9) mm and by CCTA was 21.0 (IQR 14.3-36.3) mm; p=0.415. Although there was no significant difference in the estimated stent length between the two modalities, the LoA were large between NIRS-IVUS and CCTA estimations **(Table 3)**. In addition, the distal reference vessel area on NIRS-IVUS was 11.70 (IQR 9.01-15.60) mm² and on CCTA was 7.83 (IQR 6.58-10.40) mm²; p<0.001. Based on these measurements, PCI guided by NIRS-IVUS would have resulted in the deployment of a stent with a mean diameter of 3.5 mm and post-dilatation with a 3.75 mm balloon, while using CCTA, the mean stent diameter would have been 3 mm, and post-dilatation would have been performed with a 3 mm balloon.

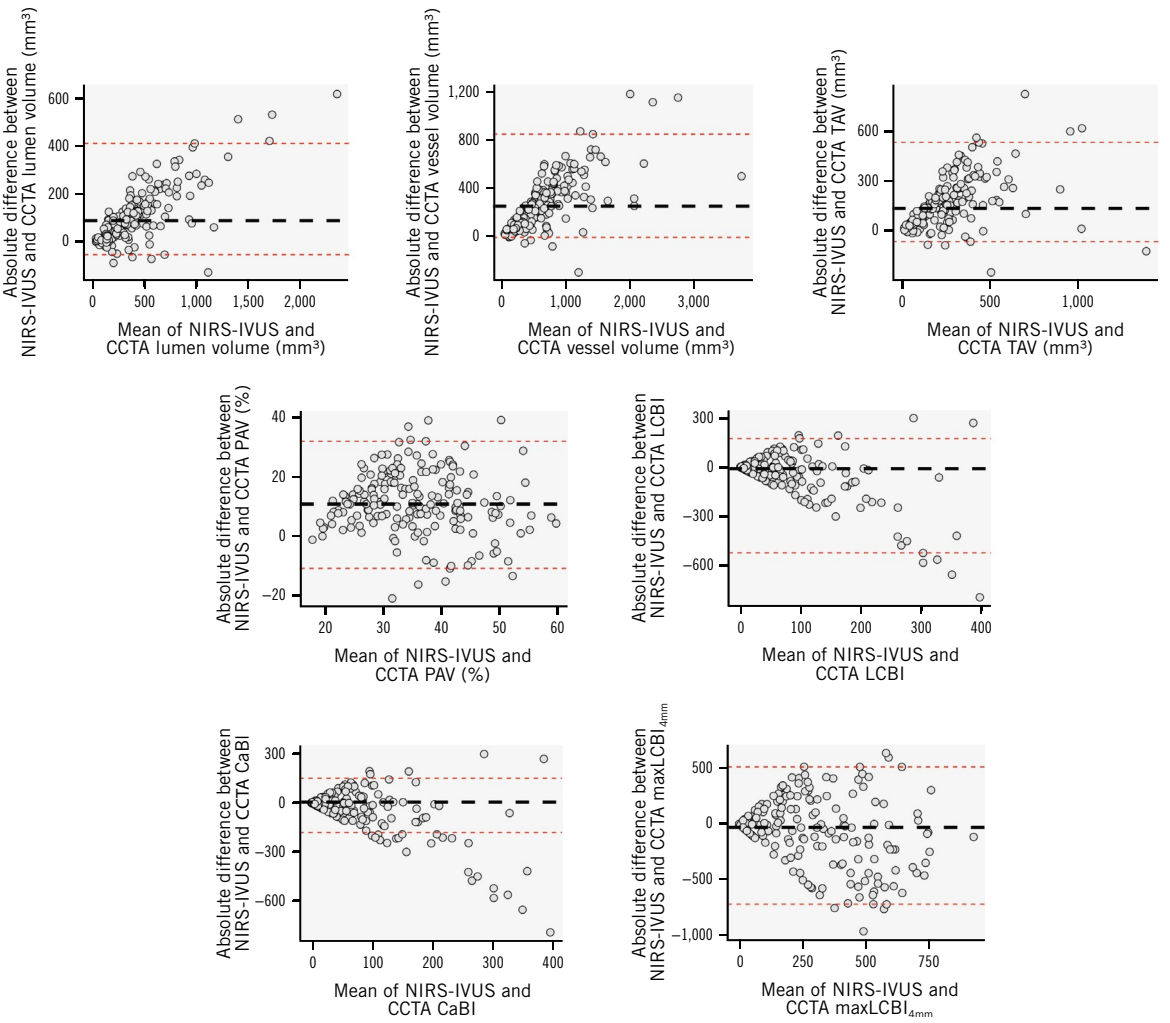

Figure 3. *BA analyses of the mean differences between NIRS-IVUS and CCTA estimations at a segment level for lumen and vessel volumes, TAV, PAV, LCBI, CaBI and maxLCBI$_{4mm}$. BA: Bland-Altman; CaBI: calcific burden index; CCTA: coronary computed tomography angiography; LCBI: lipid core burden index; maxLCBI$_{4mm}$: maximum LCBI in a 4 mm segment; NIRS-IVUS: near-infrared spectroscopy-intravascular ultrasound; PAV: percentage atheroma volume; TAV: total atheroma volume*

The location of the minimum lumen area (MLA) and the proximal and distal landing zones on NIRS-IVUS and CCTA in the 58 vessels treated with PCI are shown in **Supplementary Figure 2**. In 17 lesions, the difference in the distance of the proximal or distal landing zone between NIRS-IVUS and CCTA estimations was >5 mm; in 11 cases, CCTA indicated implantation of significantly longer stents, and in 8 cases, it indicated significantly shorter stents compared to NIRS-IVUS. The overestimation of the stent length with CCTA was mainly attributed to the presence of calcific plaques near the reference segment, resulting in an overestimation of the PB in these locations due to the blooming artefacts. Conversely, CCTA failed to detect fibrotic plaques seen on NIRS-IVUS, resulting in an underestimation of the stent length in fibrotic lesions with diffuse disease **(Figure 4)**.

LCBI values derived from NIRS-IVUS were significantly lower than that of CCTA, but there was no significant difference in the CaBI values between the two modalities. The performance of CCTA in identifying a maxLCBI$_{4mm}$ >600 or calcific extent associated with stent underexpansion is shown in **Supplementary Table 2**.

Discussion

This is the first prospective study to examine the efficacy of CCTA in assessing coronary artery pathology using state-of-the-art intravascular imaging as the reference standard. We found that (1) necrotic core volume measured by CCTA had a limited efficacy in detecting fibroatheromas, (2) CCTA had limitations in evaluating lumen and plaque dimensions and plaque composition, and (3) this resulted in suboptimal stent sizing in lesions considered for PCI.

Previous studies comparing NIRS-IVUS and CCTA have shown that CCTA has a value in assessing the lumen and vessel wall dimensions and quantifying plaque components[17]. The first studies showed that CCTA overestimated lumen dimensions[18], but more recent reports have contradicted these

EuroIntervention — Central Illustration

Efficacy of CCTA compared to NIRS-IVUS for assessing plaque pathology and guiding revascularisation.

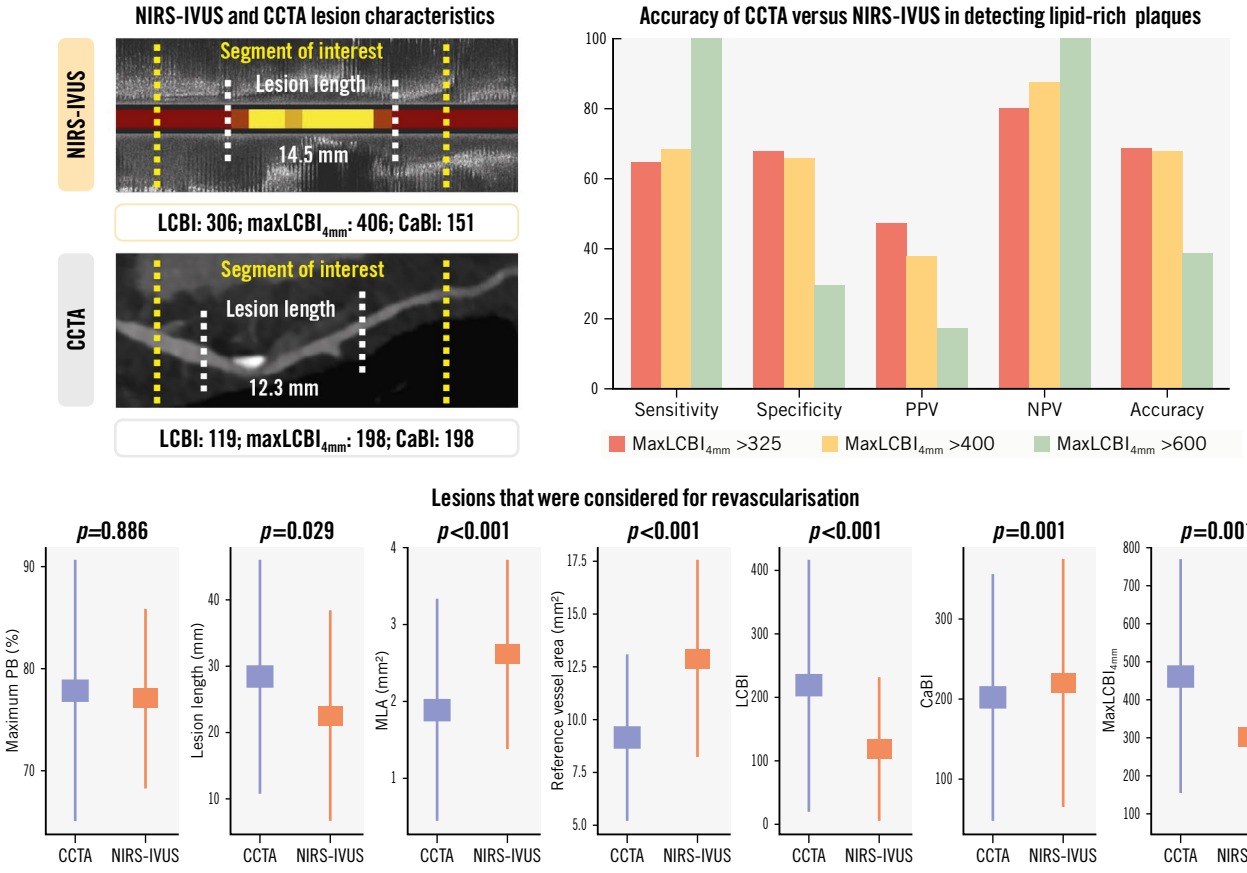

Anantharaman Ramasamy *et al.* • *EuroIntervention* 2024;20:e1465-e1475 • DOI: 10.4244/EIJ-D-24-00096

CaBI: calcific burden index; CCTA: coronary computed tomography angiography; LCBI: lipid core burden index; maxLCBI$_{4mm}$: maximum LCBI in a 4 mm segment; MLA: minimum lumen area; NIRS-IVUS: near-infrared spectroscopy-intravascular ultrasound; NPV: negative predictive value; PB: plaque burden; PPV: positive predictive value

findings, indicating that CCTA underestimates lumen area and PB[19]. Differences in CCTA scanners and reconstruction methods as well as limitations in image coregistration are likely to be responsible for the inconsistent results[19-21]. The present analysis overcomes the above limitations as it has been prospectively designed to examine the performance of CCTA in assessing lumen and vessel wall dimensions at the segment level and characterise plaque composition. In contrast to previous reports, this analysis was appropriately powered for the primary endpoint, and it was conducted using a 3rd-generation CT scanner. Furthermore, it implemented a thorough protocol for comparing CCTA and NIRS-IVUS estimations that involved (1) assessment of the entire coronary artery tree by NIRS-IVUS rather than specific vessels or lesions so as to avoid bias; (2) administration of the same amount of nitrates during NIRS-IVUS and CCTA imaging to have the same vasodilatory effect[22]; (3) use of an optimal CCTA reconstruction algorithm for data reconstruction that appears to perform better than the algorithms used in clinical practice[19]; and (4) the implementation of a retrospective gating method to identify the end-diastolic NIRS-IVUS frames in order to analyse only frames acquired at the same phase of the cardiac cycle[23] and avoid the effect of the change in coronary pressure during the cardiac cycle on the lumen and plaque dimensions and the backward-forward motion of the NIRS-IVUS probe during the cardiac cycle that can affect the quantification of the TAV and PAV and accurate CCTA coregistration[24]. In addition, all analyses were performed blindly, and we developed a dedicated software to match frame-by-frame the NIRS-IVUS and CCTA data **(Supplementary Figure 3)**; we modified the output of the CCTA analysis and generated spread-out plots of plaque composition to compare this with the output of NIRS-IVUS.

We found a high agreement between CCTA and NIRS-IVUS for the lumen, vessel and plaque dimensions but also large biases, with the CCTA underestimating these metrics.

Table 2. Comparison of the estimations of NIRS-IVUS and CCTA in lesions that were considered for revascularisation.

Estimations	NIRS-IVUS	CCTA	*p*-value	Median bias (95% LoA)	r	*p*-value	ICC	*p*-value
Lesion length, mm	19.0 (11.6, 32.7)	23.5 (14.0, 39.3)	0.029	–2.6 (–19.1, 4.3)	0.81 (0.72, 0.88)	<0.001	0.89 (0.84, 0.93)	<0.001
MLA*, mm^2	2.22 (1.71, 3.21)	1.49 (0.76, 2.38)	<0.001	0.77 (–0.70, 2.20)	0.63 (0.47, 0.75)	<0.001	0.76 (0.64, 0.85)	<0.001
Reference lumen area, mm^2	6.81 (4.87, 9.10)	6.30 (4.68, 9.02)	0.279	0.70 (–2.24, 3.28)	0.70 (0.56, 0.80)	<0.001	0.82 (0.71, 0.89)	<0.001
Reference vessel area, mm^2	12.30 (9.17, 16.0)	8.16 (6.55, 11.0)	<0.001	4.01 (0.39, 8.60)	0.63 (0.46, 0.75)	<0.001	0.77 (0.63, 0.86)	<0.001
Maximum PB*, %	77.9 (72.2, 82.6)	78.0 (69.0, 87.3)	0.886	–0.3 (–15.4, 16.0)	0.48 (0.28, 0.64)	<0.001	0.63 (0.42, 0.76)	<0.001
LCBI	79 (34, 179)	149 (86, 283)	<0.001	–39 (–445, 130)	0.02 (–0.22, 0.25)	0.897	0.03 (–0.56, 0.39)	0.455
$MaxLCBI_{4mm}$	286 (128, 437)	449 (175, 721)	<0.001	–124 (–616, 326)	0.12 (–0.12, 0.34)	0.335	0.20 (–0.28, 0.50)	0.179
CaBI	195 (106, 310)	192 (81.3, 289)	0.001	26.0 (–83.0, 158)	0.66 (0.50, 0.77)	<0.001	0.79 (0.67, 0.87)	<0.001

Values are median (interquartile range) unless otherwise stated. *Lesions that were predilated before NIRS-IVUS (n=6) were excluded from the MLA and the maximum PB analyses. CaBI: calcific burden index; CCTA: coronary computed tomography angiography; ICC: intraclass correlation coefficient; LCBI: lipid core burden index; LoA: limits of agreement; $maxLCBI_{4mm}$: maximum LCBI in a 4 mm segment; MLA: minimum lumen area; NIRS-IVUS: near-infrared spectroscopy-intravascular ultrasound; PB: plaque burden; r: Pearson's correlation coefficient

Table 3. Comparison of the estimations of NIRS-IVUS and CCTA in lesions that were treated with PCI.

Estimations	NIRS-IVUS	CCTA	*p*-value	Median bias (95% LoA)	r	*p*-value	ICC	*p*-value
Lesion length, mm	19.7 (14.8, 32.9)	21.0 (14.3, 36.3)	0.415	–2.6 (–10.9, 4.3)	0.90 (0.84, 0.94)	<0.001	0.95 (0.91, 0.97)	<0.001
MLA*, mm^2	1.84 (1.63, 2.38)	1.20 (0.62, 2.20)	0.001	0.66 (–0.92, 1.72)	0.69 (0.50, 0.81)	<0.001	0.77 (0.61, 0.86)	<0.001
Reference lumen area, mm^2	6.26 (4.75, 8.63)	5.87 (4.69, 8.41)	0.344	0.70 (–2.24, 2.05)	0.67 (0.48, 0.80)	<0.001	0.80 (0.65, 0.89)	<0.001
Reference vessel area, mm^2	11.7 (9.01, 15.6)	7.83 (6.58, 10.4)	<0.001	3.86 (–0.53, 8.72)	0.55 (0.32, 0.72)	<0.001	0.70 (0.47, 0.83)	<0.001
Maximum PB*, %	80.3 (76.6, 83.8)	81.2 (70.5, 89.7)	0.825	–0.3 (–15.8, 16.2)	0.61 (0.40, 0.76)	<0.001	0.64 (0.39, 0.79)	0.002
LCBI	70 (29, 155)	178 (53, 290)	0.003	–33 (–464, 130)	–0.06 (–0.34, 0.23)	0.694	0.00 (–0.78, 0.44)	0.500
$MaxLCBI_{4mm}$	290 (105, 427)	454 (148, 734)	0.006	–188 (–669, 335)	0.07 (–0.22, 0.35)	0.643	0.12 (–0.57, 0.51)	0.335
CaBI	190 (112, 296)	178 (58, 296)	0.004	34 (–93, 162)	0.66 (0.46, 0.79)	<0.001	0.79 (0.62, 0.88)	<0.001

Values are median (interquartile range) unless otherwise stated. *Lesions that were predilated before NIRS-IVUS (n=6) were excluded from the MLA and the maximum PB analyses. CaBI: calcific burden index; CCTA: coronary computed tomography angiography; ICC: intraclass correlation coefficient; LCBI: lipid core burden index; LoA: limits of agreement; $maxLCBI_{4mm}$: maximum LCBI in a 4 mm segment; MLA: minimum lumen area; NIRS-IVUS: near-infrared spectroscopy-intravascular ultrasound; PB: plaque burden; r: Pearson's correlation coefficient

Conversely, the correlation between the two modalities was weak for plaque components, with the CCTA overestimating both lipid and calcific components. BA analysis showed a large bias and wide LoA even for the calcific tissue, for which CCTA is regarded a reliable imaging modality. A careful examination of the spread-out plots showed that, in specific cases, the Hounsfield unit (HU) values in the lumen were high, resulting in a false classification of the defined plaque as calcific tissue. Replacing the tissue types in disease-free segments by the media – an option that is provided by the analysis software – resulted in an improvement in the correlation between the two modalities for the calcific tissue; however, the LoA were still large as this adjustment did not enable correction of tissue misclassification in diseased segments **(Supplementary Figure 4)**. These results underscore the limitations of software that use HU cutoffs to assess tissue composition and highlight the need to develop advanced machine-learning methods that will be trained either by histology or high-resolution intravascular imaging and will enable more accurate plaque characterisation[25].

The limited agreement between CCTA and NIRS-IVUS for assessing plaque composition influenced its performance in detecting fibroatheromas. The necrotic core volume had moderate accuracy in detecting lipid-rich plaques. These

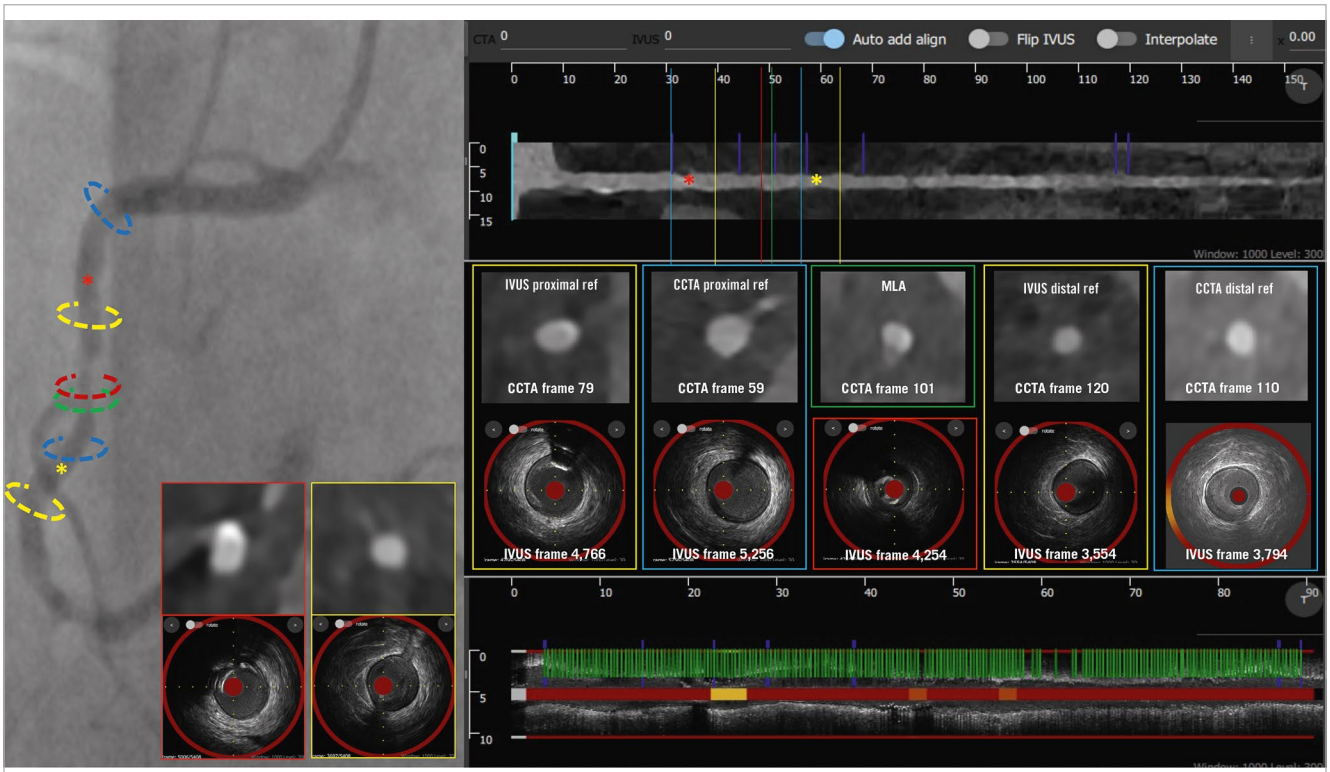

Figure 4. *Case example of NIRS-IVUS- and CCTA-guided right coronary artery PCI. The treated lesion is shown on the coronary angiogram, along with CCTA and NIRS-IVUS longitudinal images. The location of the MLA on NIRS-IVUS (red) and CCTA (green) are different. The NIRS-IVUS proximal and distal reference areas are marked in yellow, while the CCTA proximal and distal reference areas are marked in blue. There was a significant difference in the landing zone estimations between NIRS-IVUS and CCTA; CCTA overestimated the PB in the calcific segment proximal to the lesion, while distally it missed a fibrotic plaque compared to NIRS-IVUS. CaBI: calcific burden index; CCTA: coronary computed tomography angiography; IVUS: intravascular ultrasound; MLA: minimum lumen area; NIRS-IVUS: near-infrared spectroscopy-intravascular ultrasound; PB: plaque burden; PCI: percutaneous coronary intervention*

findings are in line with a recent study by Tanisawa et al which showed that 40% of the low-attenuation plaques on CCTA were classified as non-lipid-rich plaques on NIRS-IVUS[26]. In addition, several retrospective analyses have shown that the attenuated plaque volume and the morphological features on CCTA can detect vulnerable plaques but with limited accuracy[27,28]. Radiomics analysis seems to provide an effective alternative to detect high-risk plaques[29].

Finally, the limited efficacy of CCTA in assessing vessel dimensions affected its performance in guiding stent sizing. We found that CCTA would result in implantation of smaller stents and has limited efficacy in accurately determining stent length compared to NIRS-IVUS as the reference standard. Our results are in line with the findings of the P3 study[30] that reported a moderate correlation and wide LoA between the estimations of optical coherence tomography and CCTA for lesion length and reference vessel diameter. In addition, CCTA was weak in identifying lipid-rich plaques that were likely to cause no-reflow during revascularisation and moderate in characterising calcium extent that has been associated with stent underexpansion. The above findings are clinically relevant as they underscore the advantages and limitations of CCTA in guiding revascularisation and should be taken into account by ongoing but also future studies assessing the potential of CCTA in guiding PCI (ClinicalTrials.gov: NCT05253677).

Limitations

Although this study is the first prospective clinical study to enable a thorough evaluation of CCTA in assessing coronary artery pathology against high-resolution NIRS-IVUS imaging – which is U.S. Food and Drug Administration-approved for detecting high-risk lesions and patients – it has several limitations. First, it is a single-centre study; however, this facilitated the implementation of a robust protocol for image comparison and enabled NIRS-IVUS imaging of long segments. Additionally, CCTA imaging was performed with a 3rd-generation scanner using a specific reconstruction protocol; therefore, it is unclear whether these findings apply to previous-generation, or photon-counting, CT scanners and different reconstruction protocols. Moreover, patients with stable angina were included in this analysis, so it is unclear whether our findings apply to patients with acute coronary syndrome that have more advanced atherosclerotic plaques. Furthermore, this study enabled evaluation of the performance of CCTA in detecting lesion characteristics related to stent underexpansion but did not allow comparison of the score, as CCTA cannot detect the presence of calcific nodules, which

are included in the IVUS score[14]. Moreover, stent sizing in lesions considered for revascularisation was performed based on specific PB cutoffs – derived after performing ROC curve analysis to find the best value that predicted a PB of 50% on IVUS; it is unclear whether these results would have been different if a different PB cutoff had been used for defining the landing zones on CCTA. However, considering that CCTA tends to overestimate lesion length in calcific lesions and underestimate its length in fibrotic lesions, we believe that a different cutoff is unlikely to have resulted in a high agreement between the estimations of the two modalities. Finally, although it is the largest study in the field, including >23,000 matched cross-sections, the number of the studied segments and lesions considered for revascularisation remains relatively small.

Conclusions

Our head-to-head comparison of CCTA and NIRS-IVUS showed that CCTA has limitations in detecting the lipid component, measuring the lumen and plaque dimensions and characterising plaque components. This may have an impact on its value in guiding revascularisation.

Authors' affiliations

1. Department of Cardiology, Barts Heart Centre, St. Bartholomew's Hospital, London, United Kingdom; 2. Centre for Cardiovascular Medicine and Devices, William Harvey Research Institute, Queen Mary University London, London, United Kingdom; 3. Medis Medical Imaging Systems, Leiden, the Netherlands; 4. Division of Image Processing, Department of Radiology, Leiden University Medical Center, Leiden, the Netherlands; 5. Department of Biostatistics and Cardiology, Nisantasi University Medical School, Istanbul, Turkey; 6. Faculty of Medicine, National Heart & Lung Institute, Imperial College London, London, United Kingdom; 7. Department of Cardiology, University of Galway, Galway, Ireland; 8. Institute of Cardiovascular Sciences, University College London, London, United Kingdom; 9. Department of Mechanical Engineering, University College London, London, United Kingdom

Funding

This study is jointly funded by the British Heart Foundation (PG/17/18/32883), University College London Biomedical Resource Centre (BRC492B) and Rosetrees Trust (A1773). There was additional funding from the project LSHM19028 PRAGMATICS, which is cofunded by the PPP Allowance made available by Health~Holland, Top Sector Life Sciences & Health, to stimulate public-private partnerships. A. Ramasamy, R. Parasa, A. Mathur, A. Baumbach and C.V. Bourantas are funded by Barts NIHR Biomedical Research Centre, London, United Kingdom.

Conflict of interest statement

The authors have no conflicts of interest to declare.

References

1. Lee JM, Choi KH, Song YB, Lee JY, Lee SJ, Lee SY, Kim SM, Yun KH, Cho JY, Kim CJ, Ahn HS, Nam CW, Yoon HJ, Park YH, Lee WS, Jeong JO, Song PS, Doh JH, Jo SH, Yoon CH, Kang MG, Koh JS, Lee KY, Lim YH, Cho YH, Cho JM, Jang WJ, Chun KJ, Hong D, Park TK, Yang JH, Choi SH, Gwon HC, Hahn JY; RENOVATE-COMPLEX-PCI Investigators. Intravascular Imaging-Guided or Angiography-Guided Complex PCI. *N Engl J Med*. 2023;388:1668-79.

2. Bourantas CV, Garcia-Garcia HM, Torii R, Zhang YJ, Westwood M, Crake T, Serruys PW. Vulnerable plaque detection: an unrealistic quest or a feasible objective with a clinical value? *Heart*. 2016;102:581-9.

3. Ferencik M, Mayrhofer T, Bittner DO, Emami H, Puchner SB, Lu MT, Meyersohn NM, Ivanov AV, Adami EC, Patel MR, Mark DB, Udelson JE, Lee KL, Douglas PS, Hoffmann U. Use of High-Risk Coronary Atherosclerotic Plaque Detection for Risk Stratification of Patients With Stable Chest Pain: A Secondary Analysis of the PROMISE Randomized Clinical Trial. *JAMA Cardiol*. 2018;3:144-52.

4. Lee SE, Chang HJ, Sung JM, Park HB, Heo R, Rizvi A, Lin FY, Kumar A, Hadamitzky M, Kim YJ, Conte E, Andreini D, Pontone G, Budoff MJ, Gottlieb I, Lee BK, Chun EJ, Cademartiri F, Maffei E, Marques H, Leipsic JA, Shin S, Choi JH, Chinnaiyan K, Raff G, Virmani R, Samady H, Stone PH, Berman DS, Narula J, Shaw LJ, Bax JJ, Min JK. Effects of Statins on Coronary Atherosclerotic Plaques: The PARADIGM Study. *JACC Cardiovasc Imaging*. 2018;11:1475-84.

5. Collet C, Sonck J, Leipsic J, Monizzi G, Buytaert D, Kitslaar P, Andreini D, De Bruyne B. Implementing Coronary Computed Tomography Angiography in the Catheterization Laboratory. *JACC Cardiovasc Imaging*. 2021;14:1846-55.

6. Ramasamy A, Safi H, Moon JC, Andiapen M, Rathod KS, Maurovich-Horvat P, Bajaj R, Serruys PW, Mathur A, Baumbach A, Pugliese F, Torii R, Bourantas CV. Evaluation of the Efficacy of Computed Tomographic Coronary Angiography in Assessing Coronary Artery Morphology and Physiology: Rationale and Study Design. *Cardiology*. 2020;145:285-93.

7. García-García HM, Gomez-Lara J, Gonzalo N, Garg S, Shin ES, Goedhart D, Serruys PW. A comparison of the distribution of necrotic core in bifurcation and non-bifurcation coronary lesions: an in vivo assessment using intravascular ultrasound radiofrequency data analysis. *EuroIntervention*. 2010;6:321-7.

8. Gardner CM, Tan H, Hull EL, Lisauskas JB, Sum ST, Meese TM, Jiang C, Madden SP, Caplan JD, Burke AP, Virmani R, Goldstein J, Muller JE. Detection of lipid core coronary plaques in autopsy specimens with a novel catheter-based near-infrared spectroscopy system. *JACC Cardiovasc Imaging*. 2008;1:638-48.

9. Räber L, Koskinas KC, Yamaji K, Taniwaki M, Roffi M, Holmvang L, Garcia Garcia HM, Zanchin T, Maldonado R, Moschovitis A, Pedrazzini G, Zaugg S, Dijkstra J, Matter CM, Serruys PW, Lüscher TF, Kelbaek H, Karagiannis A, Radu MD, Windecker S. Changes in Coronary Plaque Composition in Patients With Acute Myocardial Infarction Treated With High-Intensity Statin Therapy (IBIS-4): A Serial Optical Coherence Tomography Study. *JACC Cardiovasc Imaging*. 2019;12:1518-28.

10. Erlinge D, Maehara A, Ben-Yehuda O, Bøtker HE, Maeng M, Kjøller-Hansen L, Engstrøm T, Matsumura M, Crowley A, Dressler O, Mintz GS, Fröbert O, Persson J, Wiseth R, Larsen AI, Okkels Jensen L, Nordrehaug JE, Bleie Ø, Omerovic E, Held C, James SK, Ali ZA, Muller JE, Stone GW; PROSPECT II Investigators. Identification of vulnerable plaques and patients by intracoronary near-infrared spectroscopy and ultrasound (PROSPECT II): a prospective natural history study. *Lancet*. 2021;397:985-95.

11. Waksman R, Di Mario C, Torguson R, Ali ZA, Singh V, Skinner WH, Artis AK, Cate TT, Powers E, Kim C, Regar E, Wong SC, Lewis S, Wykrzykowska J, Dube S, Kazziha S, van der Ent M, Shah P, Craig PE, Zou Q, Kolm P, Brewer HB, Garcia-Garcia HM; LRP Investigators. Identification of patients and plaques vulnerable to future coronary events with near-infrared spectroscopy intravascular ultrasound imaging: a prospective, cohort study. *Lancet*. 2019;394:1629-37.

12. Ali ZA, Maehara A, Généreux P, Shlofmitz RA, Fabbiocchi F, Nazif TM, Guagliumi G, Meraj PM, Alfonso F, Samady H, Akasaka T, Carlson EB, Leesar MA, Matsumura M, Ozan MO, Mintz GS, Ben-Yehuda O, Stone GW; ILUMIEN III: OPTIMIZE PCI Investigators. Optical coherence tomography compared with intravascular ultrasound and with angiography to guide coronary stent implantation (ILUMIEN III: OPTIMIZE PCI): a randomised controlled trial. *Lancet*. 2016;388:2618-28.

13. Terada K, Kubo T, Madder RD, Ino Y, Takahata M, Shimamura K, Shiono Y, Nishi T, Emori H, Higashioka D, Khalifa AKM, Wada T, Akasaka T. Near-infrared spectroscopy to predict microvascular obstruction after primary percutaneous coronary intervention. *EuroIntervention*. 2021;17:e999-1006.

14. Zhang M, Matsumura M, Usui E, Noguchi M, Fujimura T, Fall KN, Zhang Z, Nazif TM, Parikh SA, Rabbani LE, Kirtane AJ, Collins MB, Leon MB, Moses JW, Karmpaliotis D, Ali ZA, Mintz GS, Maehara A. Intravascular Ultrasound-Derived Calcium Score to Predict Stent Expansion in Severely Calcified Lesions. *Circ Cardiovasc Interv*. 2021;14:e010296.

15. Chen LA, Kao CL. Parametric and nonparametric improvements in Bland and Altman's assessment of agreement method. *Stat Med*. 2021;40:2155-76.

16. Ma C, Wang X, Xia L, Cheng X, Qiu L. Effect of sample size and the traditional parametric, nonparametric, and robust methods on the establishment of reference intervals: Evidence from real world data. *Clin Biochem*. 2021;92:67-70.

17. Collet C, Chevalier B, Cequier A, Fajadet J, Dominici M, Helqvist S, Van Boven AJ, Dudek D, McClean D, Almeida M, Piek JJ, Tenekecioglu E, Bartorelli A, Windecker S, Serruys PW, Onuma Y. Diagnostic Accuracy of Coronary CT Angiography for the Evaluation of Bioresorbable Vascular Scaffolds. *JACC Cardiovasc Imaging*. 2018;11:722-32.

18. Voros S, Rinehart S, Qian Z, Joshi P, Vazquez G, Fischer C, Belur P, Hulten E, Villines TC. Coronary atherosclerosis imaging by coronary CT angiography: current status, correlation with intravascular interrogation and meta-analysis. *JACC Cardiovasc Imaging*. 2011;4:537-48.

19. Ramasamy A, Hamid A Khan A, Cooper J, Simon J, Maurovich-Horvat P, Bajaj R, Kitslaar P, Amersey R, Jain A, Deaner A, Reiber JH, Moon JC, Dijkstra J, Serruys PW, Mathur A, Baumbach A, Torii R, Pugliese F, Bourantas CV. Implications of computed tomography reconstruction algorithms on coronary atheroma quantification: Comparison with intravascular ultrasound. *J Cardiovasc Comput Tomogr*. 2023;17:43-51.

20. Puchner SB, Ferencik M, Maehara A, Stolzmann P, Ma S, Do S, Kauczor HU, Mintz GS, Hoffmann U, Schlett CL. Iterative Image Reconstruction Improves the Accuracy of Automated Plaque Burden Assessment in Coronary CT Angiography: A Comparison With Intravascular Ultrasound. *AJR Am J Roentgenol*. 2017;208:777-84.

21. Motoyama S, Ito H, Sarai M, Nagahara Y, Miyajima K, Matsumoto R, Doi Y, Kataoka Y, Takahashi H, Ozaki Y, Toyama H, Katada K. Ultra-High-Resolution Computed Tomography Angiography for Assessment of Coronary Artery Stenosis. *Circ J*. 2018;82:1844-51.

22. Shaw LJ, Blankstein R, Bax JJ, Ferencik M, Bittencourt MS, Min JK, Berman DS, Leipsic J, Villines TC, Dey D, Al'Aref S, Williams MC, Lin F, Baskaran L, Litt H, Litmanovich D, Cury R, Gianni U, van den Hoogen I, R van Rosendael A, Budoff M, Chang HJ, E Hecht H, Feuchtner G, Ahmadi A, Ghoshajra BB, Newby D, Chandrashekhar YS, Narula J. Society of Cardiovascular Computed Tomography / North American Society of Cardiovascular Imaging - Expert Consensus Document on Coronary CT Imaging of Atherosclerotic Plaque. *J Cardiovasc Comput Tomogr*. 2021;15:93-109.

23. Bajaj R, Huang X, Kilic Y, Jain A, Ramasamy A, Torii R, Moon J, Koh T, Crake T, Parker MK, Tufaro V, Serruys PW, Pugliese F, Mathur A, Baumbach A, Dijkstra J, Zhang Q, Bourantas CV. A deep learning methodology for the automated detection of end-diastolic frames in intravascular ultrasound images. *Int J Cardiovasc Imaging*. 2021;37:1825-37.

24. Erdogan E, Huang X, Cooper J, Jain A, Ramasamy A, Bajaj R, Torii R, Moon J, Deaner A, Costa C, Garcia-Garcia HM, Tufaro V, Serruys PW, Pugliese F, Mathur A, Dijkstra J, Baumbach A, Zhang Q, Bourantas CV. End-diastolic segmentation of intravascular ultrasound images enables more reproducible volumetric analysis of atheroma burden. *Catheter Cardiovasc Interv*. 2022;99:706-13.

25. Ramasamy A, Sokooti H, Zhang X, Tzorovili E, Bajaj R, Kitslaar P, Broersen A, Amersey R, Jain A, Ozkor M, Reiber JHC, Dijkstra J, Serruys PW, Moon JC, Mathur A, Baumbach A, Torii R, Pugliese F, Bourantas CV. Novel near-infrared spectroscopy-intravascular ultrasound-based deep-learning methodology for accurate coronary computed tomography plaque quantification and characterization. *Eur Heart J Open*. 2023;3:oead090.

26. Tanisawa H, Matsumoto H, Cadet S, Higuchi S, Ohya H, Isodono K, Irie D, Kaneko K, Sumida A, Hirano T, Otaki Y, Kitamura R, Slomka PJ, Dey D, Shinke T. Quantification of Low-Attenuation Plaque Burden from Coronary CT Angiography: A Head-to-Head Comparison with Near-Infrared Spectroscopy Intravascular US. *Radiol Cardiothorac Imaging*. 2023;5:e230090.

27. Williams MC, Kwiecinski J, Doris M, McElhinney P, D'Souza MS, Cadet S, Adamson PD, Moss AJ, Alam S, Hunter A, Shah ASV, Mills NL, Pawade T, Wang C, Weir McCall J, Bonnici-Mallia M, Murrills C, Roditi G, van Beek EJR, Shaw LJ, Nicol ED, Berman DS, Slomka PJ, Newby DE, Dweck MR, Dey D. Low-Attenuation Noncalcified Plaque on Coronary Computed Tomography Angiography Predicts Myocardial Infarction: Results From the Multicenter SCOT-HEART Trial (Scottish Computed Tomography of the HEART). *Circulation*. 2020;141:1452-62.

28. Deseive S, Straub R, Kupke M, Broersen A, Kitslaar PH, Massberg S, Hadamitzky M, Hausleiter J. Quantification of coronary low-attenuation plaque volume for long-term prediction of cardiac events and reclassification of patients. *J Cardiovasc Comput Tomogr*. 2018;12:118-24.

29. Chen Q, Pan T, Wang YN, Schoepf UJ, Bidwell SL, Qiao H, Feng Y, Xu C, Xu H, Xie G, Gao X, Tao XW, Lu M, Xu PP, Zhong J, Wei Y, Yin X, Zhang J, Zhang LJ. A Coronary CT Angiography Radiomics Model to Identify Vulnerable Plaque and Predict Cardiovascular Events. *Radiology*. 2023;307:e221693.

30. Sonck J, Nagumo S, Norgaard BL, Otake H, Ko B, Zhang J, Mizukami T, Maeng M, Andreini D, Takahashi Y, Jensen JM, Ihdayhid A, Heggermont W, Barbato E, Mileva N, Munhoz D, Bartunek J, Updegrove A, Collinsworth A, Penicka M, Van Hoe L, Leipsic J, Koo BK, De Bruyne B, Collet C. Clinical Validation of a Virtual Planner for Coronary Interventions Based on Coronary CT Angiography. *JACC Cardiovasc Imaging*. 2022;15:1242-55.

Supplementary data

Supplementary Appendix 1. Data acquisition and analysis.

Supplementary Table 1. Baseline demographics of the studied patients.

Supplementary Table 2. Accuracy of CCTA in assessing plaque features associated with microvascular obstruction or stent underexpansion on NIRS-IVUS imaging.

Supplementary Figure 1. Study flowchart.

Supplementary Figure 2. Estimations of NIRS-IVUS and CCTA for the MLA and the proximal and distal reference segments for the 58 cases that were revascularised with PCI.

Supplementary Figure 3. NIRS-IVUS and CCTA coregistration software.

Supplementary Figure 4. A case example highlighting the limitations of Hounsfield unit-based plaque composition assessment.

The supplementary data are published online at: https://eurointervention.pcronline.com/doi/10.4244/EIJ-D-24-00096

Supplementary data

Supplementary Appendix 1. Data acquisition and analysis.

NIRS-IVUS data acquisition

Coronary angiography and intravascular imaging were performed within 4 weeks following CCTA imaging according to local Barts Health NHS Trust protocol.[6] All patients received 400 micrograms of intracoronary nitrate prior to image acquisition. Following diagnostic coronary angiography, intravascular imaging (2.4F Makoto™ 35-65MHz, NIRS-IVUS imaging System, Infraredx, Burlington, USA) was performed in all 3 major epicardial vessels and their side branches with diameter ≥2mm. The NIRS-IVUS catheter was advanced approximately 5mm distal to the most distal side branch seen on coronary angiography and it was then pulled-back to the ostium of the vessel at a constant speed of 0.5mm/s using an automated pullback device. Lesion pre-dilatation was performed with a 2mm semi-compliant balloon, only in cases where there was a critical stenosis prohibiting advancement of the NIRS-IVUS imaging catheter. The NIRS-IVUS images were acquired at 30fps and transferred to workstation for offline analysis.

CCTA data acquisition

CCTA was performed using a 3rd-generation dual-source CT scanner prior to NIRS-IVUS imaging (Somatom Force, Siemens Healthineers, Forchheim, Germany).[6] All patients received sublingual nitroglycerin tablets (400 micrograms) and intravenous metoprolol (maximum 40mg) if their heart rate was >70 beats per minute. The CCTA scanning parameters included prospective ECG-triggered sequential scan mode, gantry rotation time of 250ms, 128 x 2 x 0.5mm collimation with z-flying focal spot for both detectors, minimum tube voltage of 100kV – as recommended by a recent consensus document on plaque assessment – defined by the CarekV algorithm and tube current determined by the scanner. The raw CCTA data were reconstructed using a medium smooth kernel (b40f), slice thickness 0.50mm with 0.30mm increments, and highest strength model-based iterative reconstruction (ADMIRE 5). This reconstruction approach was selected as it has been previously shown that it enables more accurate quantification of the vessel wall and plaque dimensions.[19]

Data analysis

NIRS-IVUS and CCTA analysis

Data analysis was performed by 3 expert operators to avoid bias. The coronary angiography, CCTA and NIRS-IVUS imaging data were reviewed by an expert cardiologist (1st analyst) who used anatomical landmarks and in particular, the origin of side branches to identify the segment of interest defined as the segment that had a lumen diameter≥2mm on CCTA and was assessed by NIRS-IVUS. Stented segments and segments with artefacts or poor image quality were excluded from the analysis.

NIRS-IVUS analysis was performed for the segments of interest by an independent expert (2nd analyst) with established reproducibility, blinded to the CCTA datasets.[19] Segmentation was performed using the QCU-CMS software (Version 4.69, Leiden, University Medical Center, The Netherlands). First, the NIRS-IVUS end-diastolic frames were automatically detected using an in-house deep-learning methodology,[23] and in these frames, the lumen and external elastic membrane (EEM) borders were manually annotated. The presence and circumferential extent of lipid core tissue in the analysed NIRS-IVUS frames were extracted from the chemogram, which is a two-dimensional colour-coded display of the presence of lipid core with X-axis showing the position along the length of the vessel and Y-axis showing the position along the circumference of the vessel. The presence of calcific tissue and its circumferential extent was also annotated, whenever this was present in NIRS-IVUS frames. This information was used to create a spread-out plot for each studied vessel that enabled evaluation of tissue distribution with the lipid tissue shown in yellow and the calcific in semi-transparent white colour while the fibrotic tissue was displayed in red colour (Figure 1).[19] These data were used to compute the lipid core burden index (LCBI) defined as the proportion of the spread-out plot portraying lipid tissue multiplied by 1000 and the calcific burden index (CaBI) that enables quantification of the calcific component. Moreover, the $maxLCBI_{4mm}$ was estimated, that reflects the maximum amount of lipid component in a 4mm segment.

The CCTA imaging data consisting of the segment of interest were analysed offline by an expert analyst (3rd analyst) with known reproducibility, blinded to the intravascular imaging analysis.[19] CCTA analysis was performed using a commercially available software (QAngioCT Research Edition 3.1, Medis Medical Imaging Systems, The Netherlands). The coronary tree was extracted and for the segments of

interest the expert manually annotated the lumen and vessel borders at every 0.5mm. Pre-specified software Hounsfield units (HU) cut-offs were used to characterise plaque composition and define the presence of necrotic core (-30 to 75HU) and calcific tissue (>350HU). Tissues distribution in the annotated CCTA images were plotted in a two-dimensional image similar to NIRS-IVUS with the x-axis portraying the longitudinal location and the y-axis, the circumferential distribution of the lipid and calcific tissue (Figure 1). For each segment, similar to NIRS-IVUS, the necrotic core and calcific tissue distribution were used to estimate the LCBI, CaBI and the $maxLCBI_{4mm}$.

CCTA and NIRS-IVUS co-registration

The frame-by-frame matching of the CCTA and NIRS-IVUS imaging data was performed by the analyst that defined the segment of interest (1st analyst) using an in-house dedicated non-commercial software (QAngioCT IVUS Matcher, Medis Medical Imaging Systems Leiden, The Netherlands). This allowed simultaneous visualization of the CCTA and NIRS-IVUS cross-sectional images and identification of anatomical landmarks such as coronary ostia and side branches that were seen in both modalities. These were used to match corresponding cross-sections while linear interpolation was used for matching of frames in between cross-sections, enabling every end-diastolic NIRS-IVUS frame to be matched with a CCTA cross-section. This process that has been described previously in detail, enables exact matching of the NIRS-IVUS and CCTA data and identification of corresponding lesions.[19]

Supplementary Table 1. Baseline demographics of the studied patients.

	Studied vessels (n=70)
Age (years)	62±9
Gender (male)	56 (80.0%)
Current smoker	5 (7.1%)
Family history of CAD	41 (58.6%)
Co-morbidities	
Diabetes mellitus	24 (34.3%)
Hypertension	39 (55.7%)
Hypercholesterolemia	48 (68.6%)
Renal failure*	4 (5.7%)
Previous PCI	15 (21.4%)
LV function	
Good LV function	66 (94.3%)
Impaired LV function**	4 (5.7%)
Studied vessels by NIRS-IVUS	
Total number of vessels	197
LAD/diagonal branches	67 (34.0%)
LCx/intermediate/obtuse marginal branches	81 (41.1%)
RCA	49 (24.9%)

Table footnote: CAD, coronary artery disease; LAD, left anterior descending artery; LCx, left circumflex artery; LV, left ventricle; NIRS-IVUS, near-infrared spectroscopy–intravascular ultrasound; PCI, percutaneous coronary intervention.

*Renal failure is defined as an estimated glomerular filtration rate of <60ml/min/1.73m^2

**Impaired LV function is defined as LV ejection fraction of <50%.

Supplementary Table 2. Accuracy of CCTA in assessing plaque features associated with microvascular obstruction or stent underexpansion on NIRS-IVUS imaging.

NIRS-IVUS metrics	Specificity	Sensitivity	Positive predictive value	Negative predictive value	Accuracy
Lesions considered for revascularisation					
$maxLCBI_{4mm}$>600	0.615 (0.486, 0.733)	0.286 (0.037, 0.710)	0.074 (0.009, 0.243)	0.889 (0.759, 0.963)	0.583 (0.461, 0.698)
Vessel diameter <3.5mm	1.000 (0.900, 1.000)	0.275 (0.146, 0.439)	1.000 (0.715, 1.000)	0.547 (0.417, 0.672)	0.613 (0.494, 0.724)
Circumferential calcification (360^o)	0.857 (0.728, 0.941)	0.522 (0.306, 0.732)	0.632 (0.384, 0.837)	0.792 (0.659, 0.892)	0.750 (0.634, 0.845)
Length of >270 ^{o} arc of calcium for >5mm	0.957 (0.781, 0.999)	0.333 (0.008, 0.906)	0.500 (0.013, 0.987)	0.917 (0.730, 0.990)	0.885 (0.698, 0.976)
Lesions treated with PCI					
$maxLCBI_{4mm}$>600	0.545 (0.388, 0.696)	0.250 (0.006, 0.806)	0.048 (0.001, 0.238)	0.889 (0.708, 0.976)	0.521 (0.372, 0.667)
Vessel diameter <3.5mm	1.000 (0.877, 1.000)	0.304 (0.132, 0.529)	1.000 (0.590, 1.000)	0.636 (0.478, 0.776)	0.686 (0.541, 0.809)
Circumferential calcification (360^o)	0.900 (0.735, 0.979)	0.611 (0.357, 0.827)	0.786 (0.492, 0.953)	0.794 (0.621, 0.913)	0.792 (0.650, 0.895)
Length of >270 ^{o} arc of calcium for >5mm	0.938 (0.698, 0.998)	0.333 (0.008, 0.906)	0.500 (0.013, 0.987)	0.882 (0.636, 0.985)	0.842 (0.604, 0.966)

Table footnote: CCTA, computed tomography coronary angiography; LCBI, lipid core burden index; NIRS-IVUS, near infrared spectroscopy-intravascular ultrasound.

Supplementary Figure 1. Study flowchart.

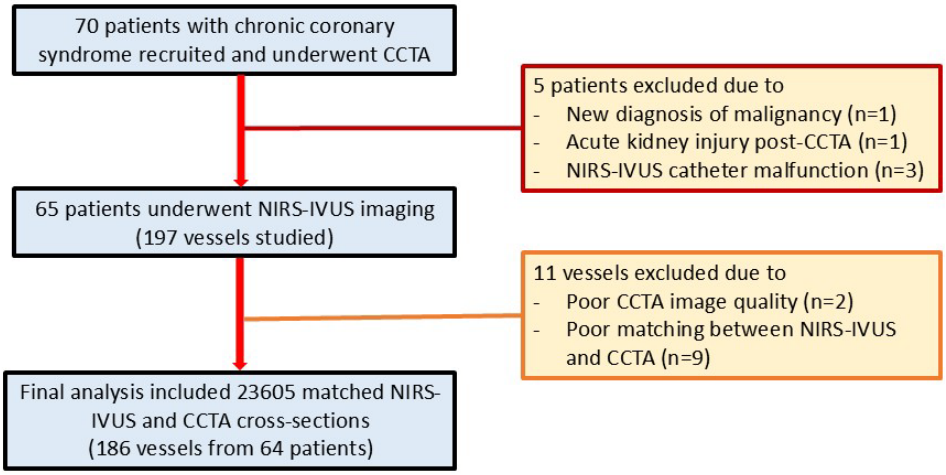

Supplementary Figure 2. Estimations of NIRS-IVUS and CCTA for the MLA and the proximal and distal reference segments for the 58 cases that were revascularised with PCI. Coronary angiogram showing the location of the treated lesion on the left, the longitudinal CCTA image on the top panel and the longitudinal IVUS image on the bottom panel. The blue lines in the longitudinal images indicate corresponding frames. The middle panel shows the MLA in NIRS-IVUS and CCTA, as well as the corresponding proximal and distal reference segments in both modalities. The locations of these frames are indicated with a straight line in the CCTA longitudinal image. In cases where there is a large discrepancy (>5mm) between NIRS-IVUS and CCTA for the reference segments, additional cross-sectional images of both modalities are provided to highlight the reasons for the difference between NIRS-IVUS and CCTA.

Case 1

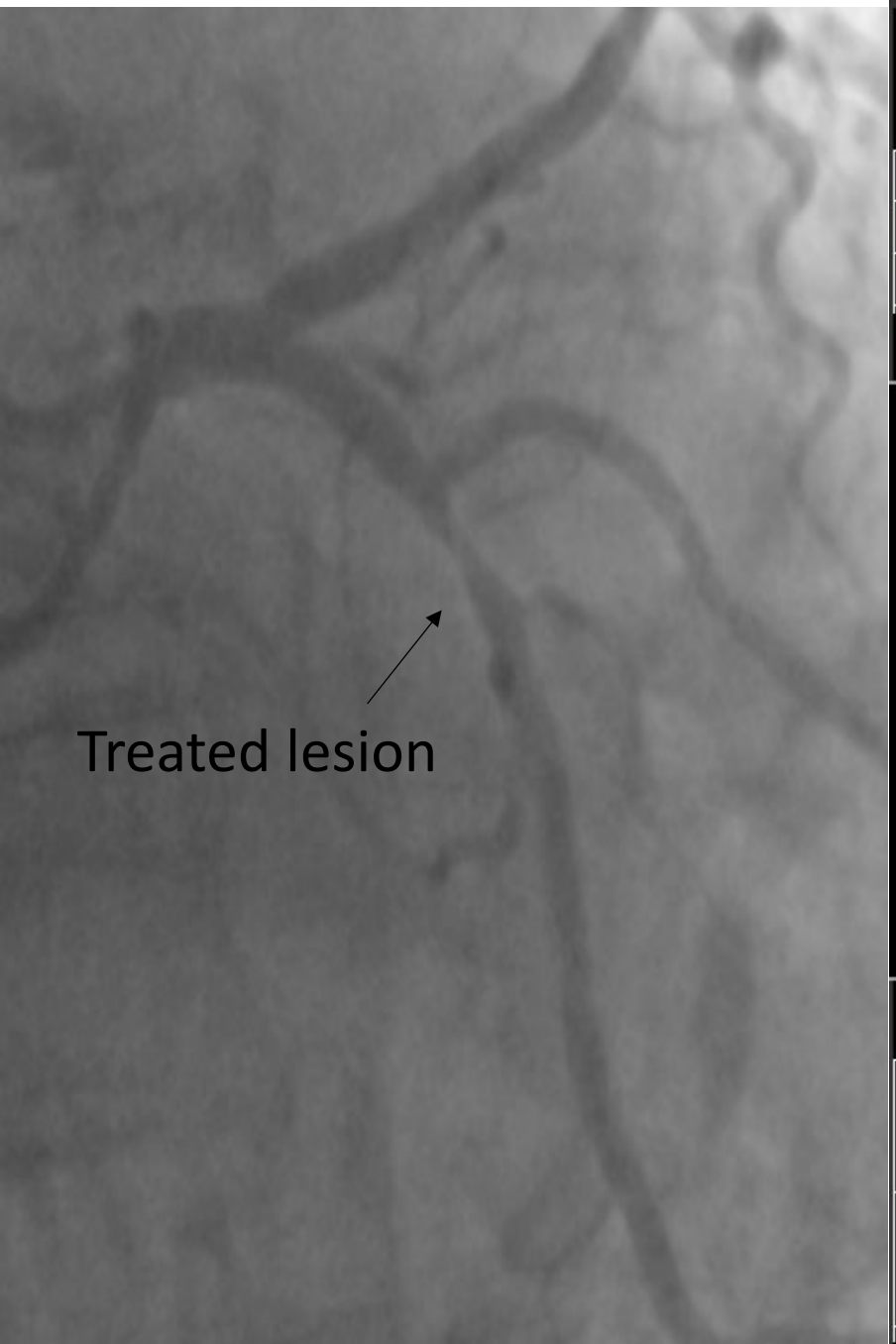
Treated lesion

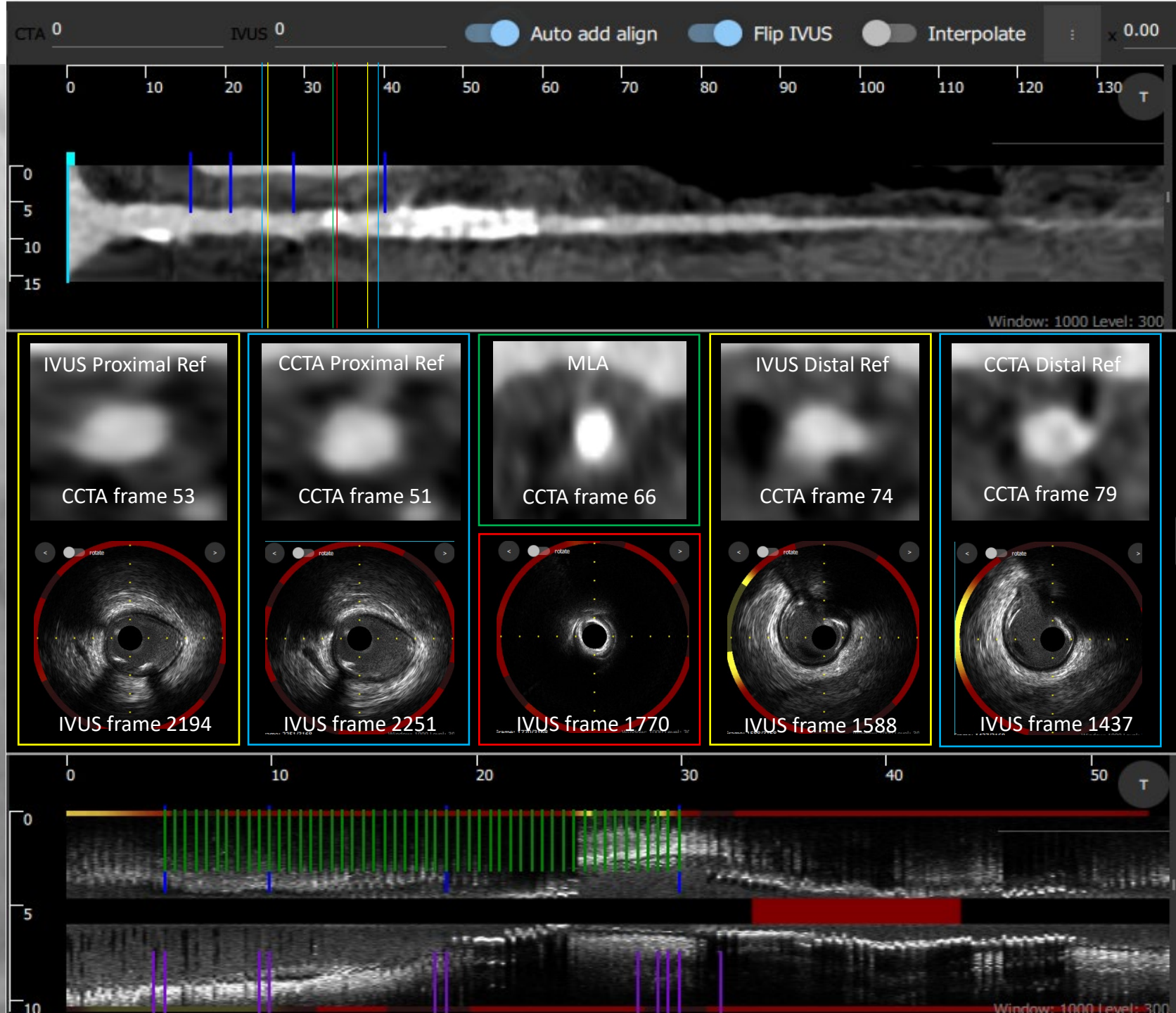
CTA 0
IVUS 0
Auto add align
Flip IVUS
Interpolate
0.00
0 10 20 30 40 50 60 70 80 90 100 110 120 130
0 5 10 15
Window: 1000 Level: 300
IVUS Proximal Ref
CCTA frame 53
IVUS frame 2194
CCTA Proximal Ref
CCTA frame 51
IVUS frame 2251
MLA
CCTA frame 66
IVUS frame 1770
IVUS Distal Ref
CCTA frame 74
IVUS frame 1588
CCTA Distal Ref
CCTA frame 79
IVUS frame 1437
0 10 20 30 40 50
0 5 10
Window: 1000 Level: 300

Case 2

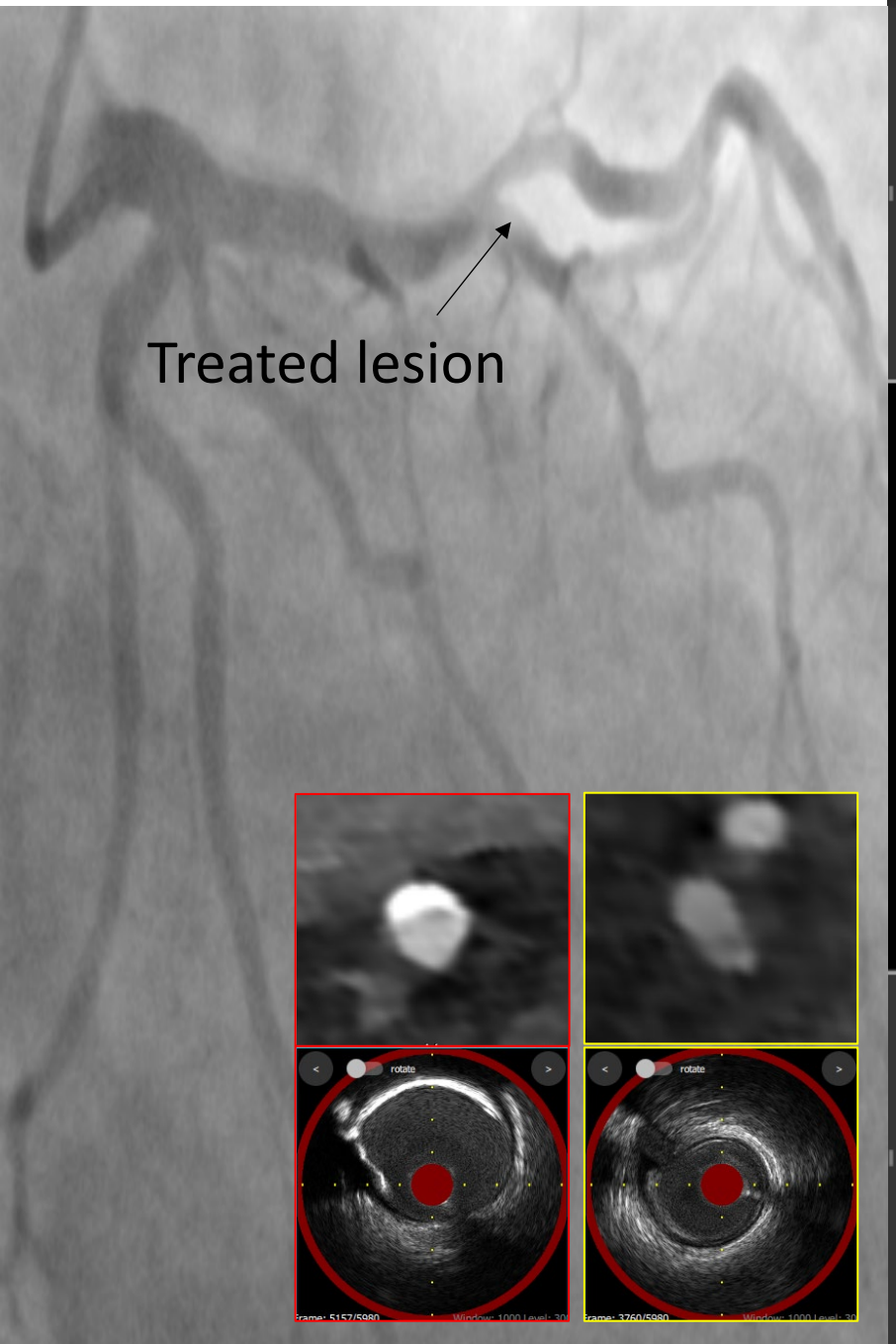
Treated lesion

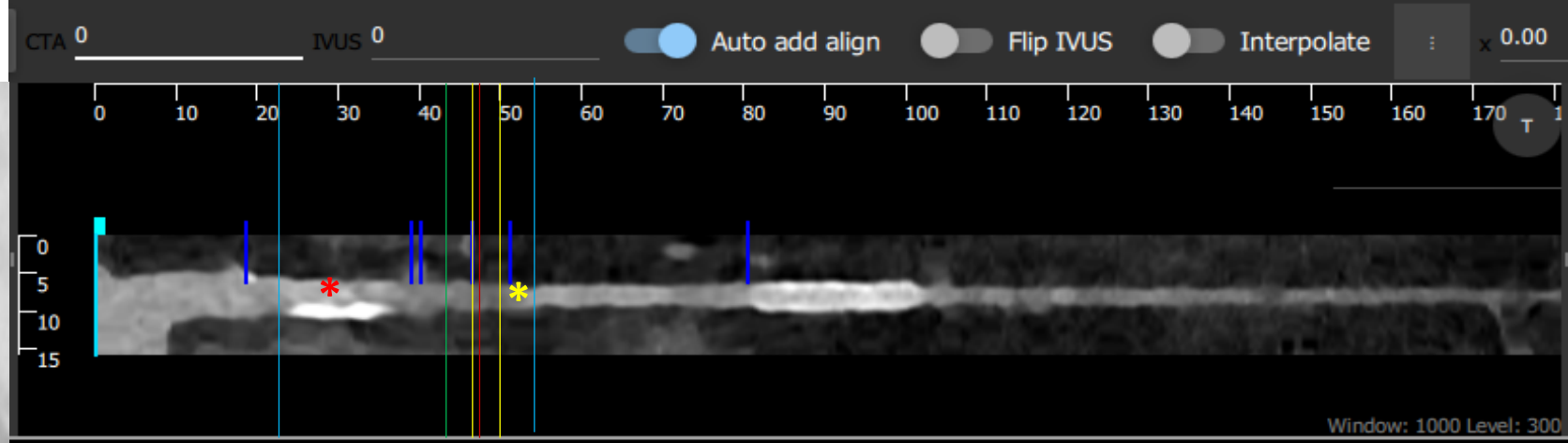
CTA 0
IVUS 0
Auto add align
Flip IVUS
Interpolate
x 0.00
0 10 20 30 40 50 60 70 80 90 100 110 120 130 140 150 160 170
0 5 10 15
Window: 1000 Level: 300

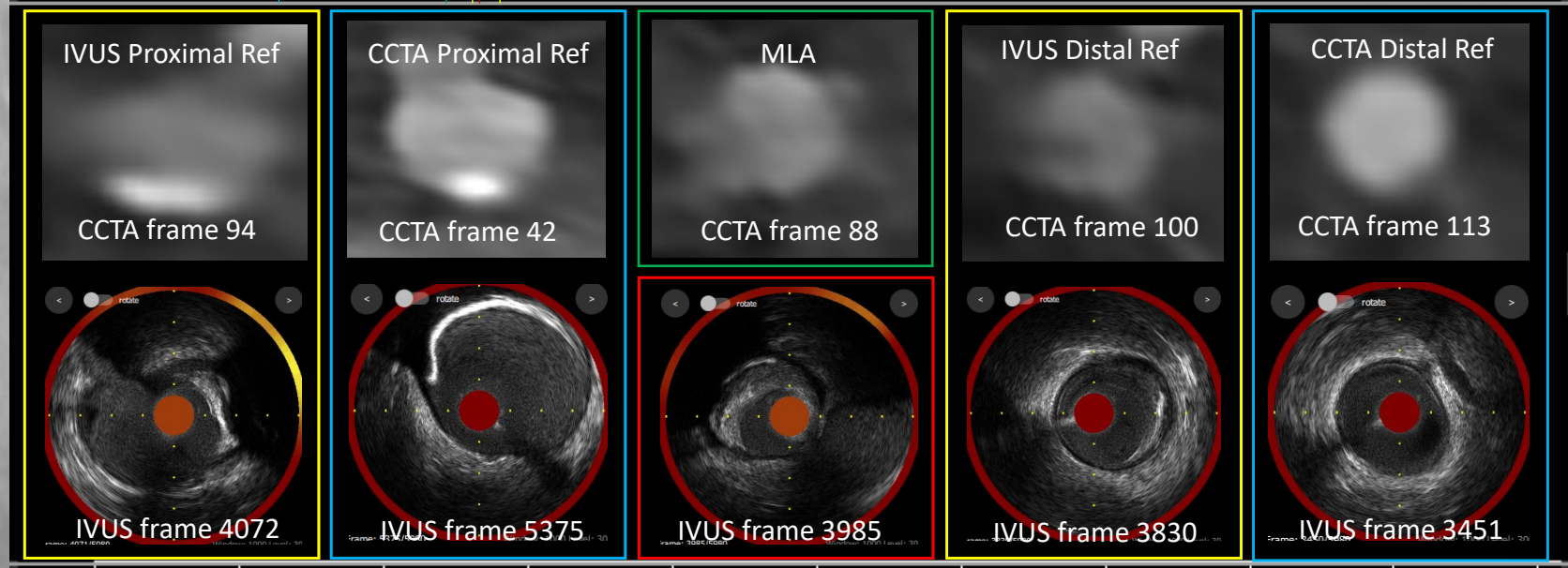
IVUS Proximal Ref
CCTA frame 94
IVUS frame 4072
CCTA Proximal Ref
CCTA frame 42
IVUS frame 5375
MLA
CCTA frame 88
IVUS frame 3985
IVUS Distal Ref
CCTA frame 100
IVUS frame 3830
CCTA Distal Ref
CCTA frame 113
IVUS frame 3451

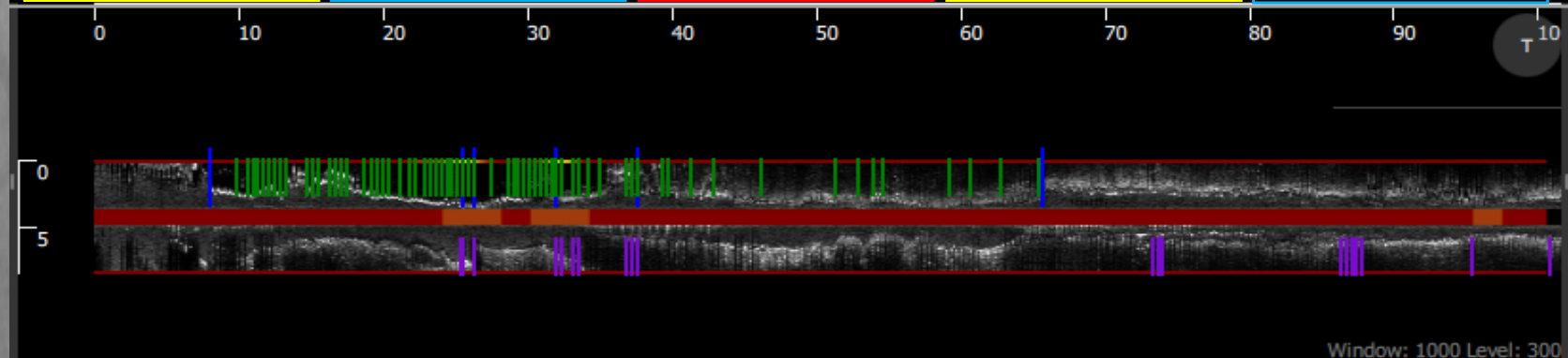
0 10 20 30 40 50 60 70 80 90 100
0 5
Window: 1000 Level: 300

Case 3


Treated lesion

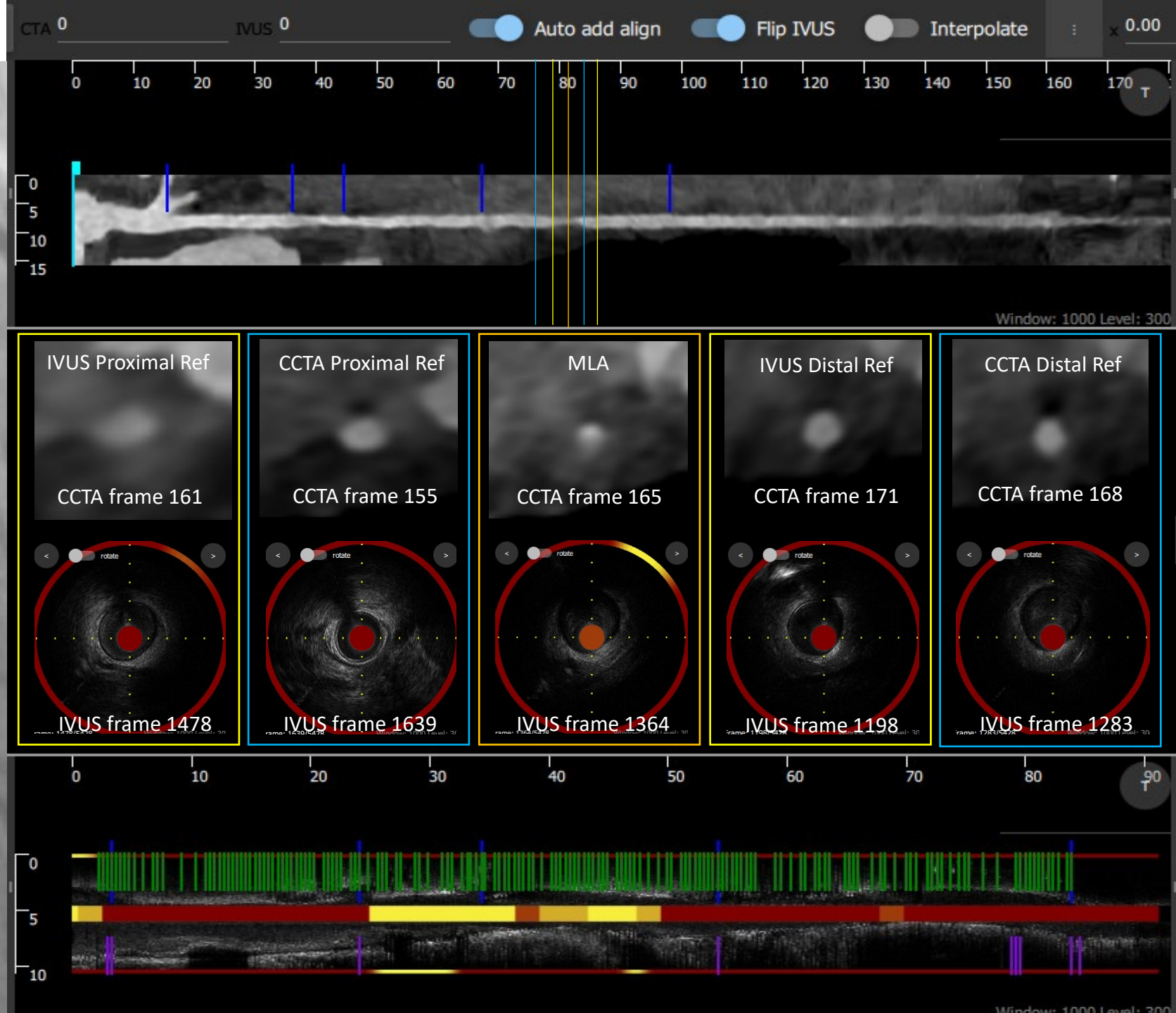
CTA 0
IVUS 0
Auto add align
Flip IVUS
Interpolate
0.00
0 10 20 30 40 50 60 70 80 90 100 110 120 130 140 150 160 170
0 5 10 15
Window: 1000 Level: 300
IVUS Proximal Ref
CCTA frame 161
IVUS frame 1478
CCTA Proximal Ref
CCTA frame 155
IVUS frame 1639
MLA
CCTA frame 165
IVUS frame 1364
IVUS Distal Ref
CCTA frame 171
IVUS frame 1198
CCTA Distal Ref
CCTA frame 168
IVUS frame 1283
0 10 20 30 40 50 60 70 80 90
0 5 10

Case 4

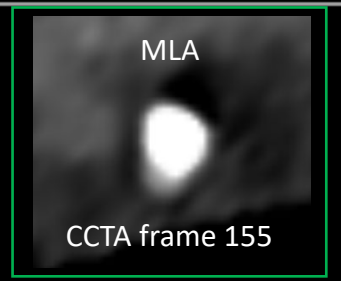

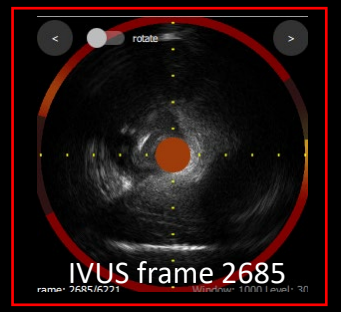

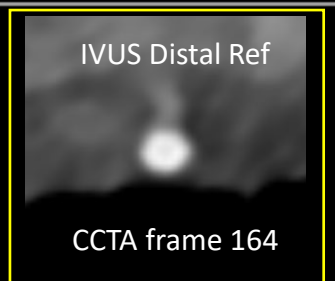

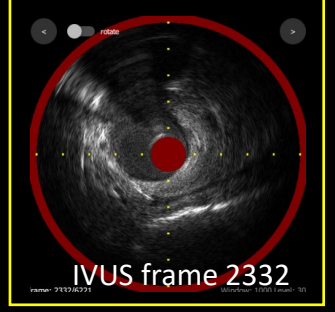

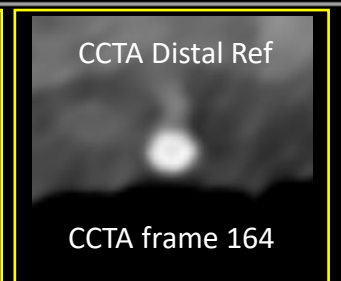

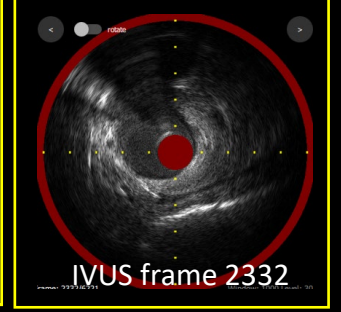

Poor image quality of CCTA did not allow clear visualisation of the lumen and vessel wall. Lesion length and proximal reference areas could not be estimated.

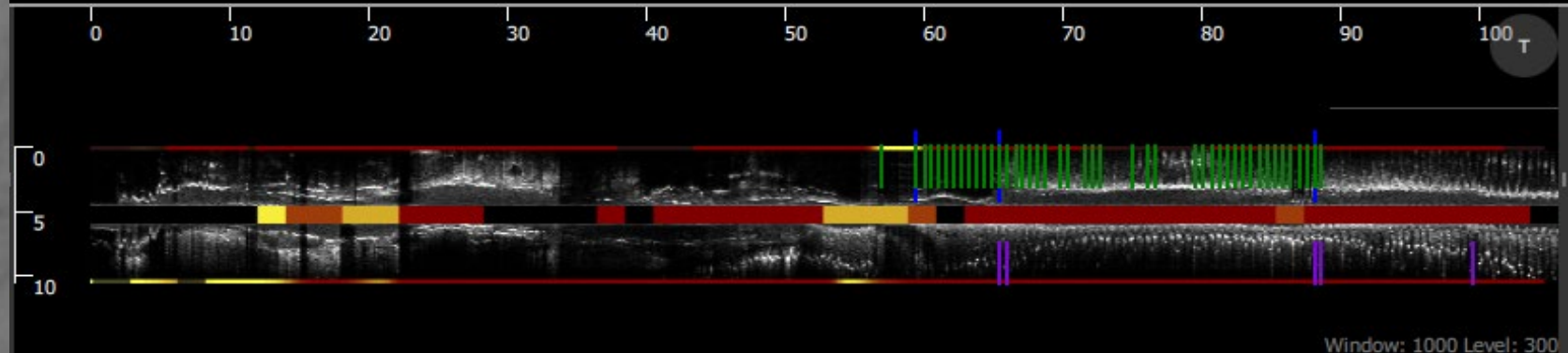

Case 5


Treated lesion

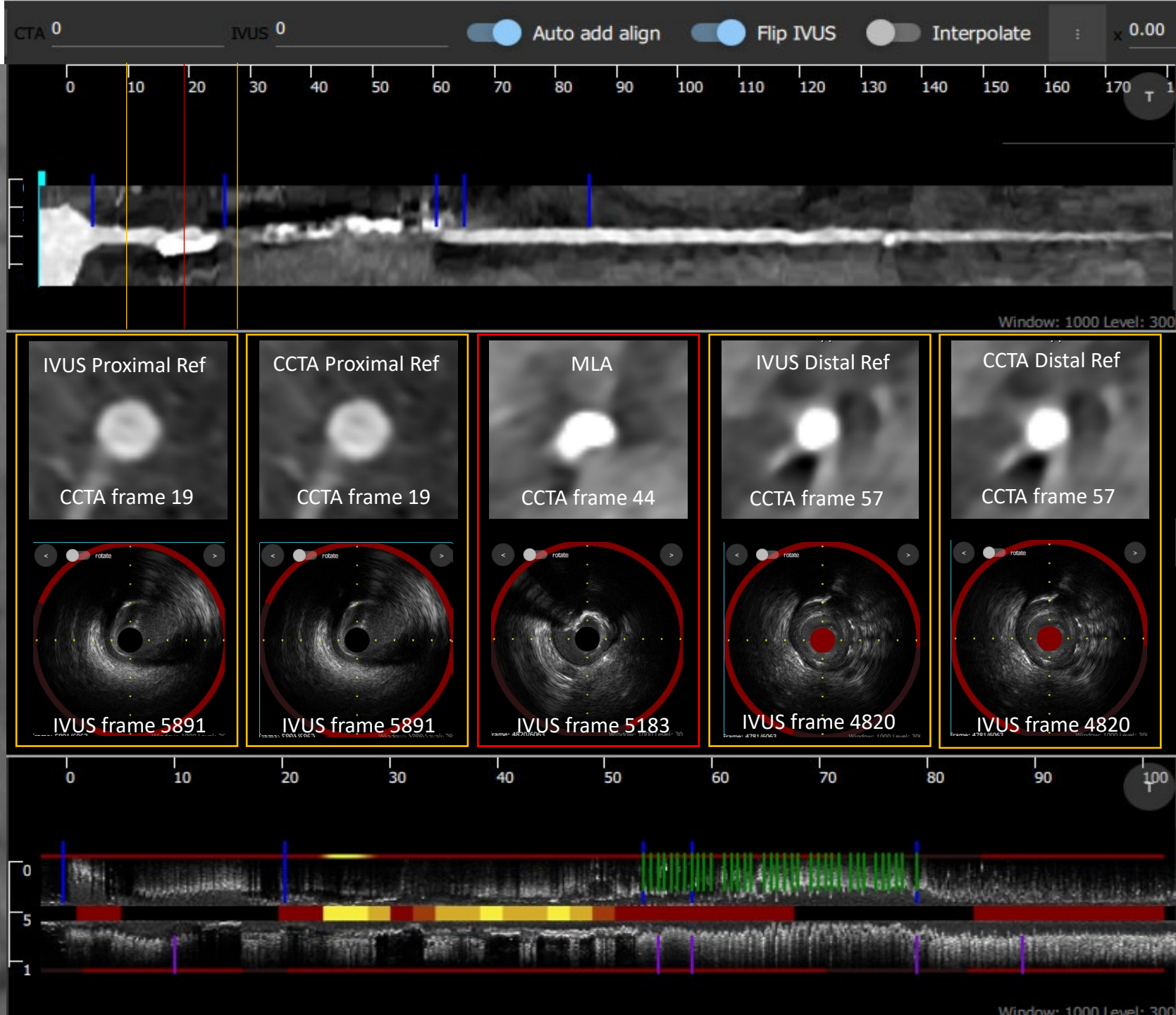
CTA 0
IVUS 0
Auto add align
Flip IVUS
Interpolate
0.00
0 10 20 30 40 50 60 70 80 90 100 110 120 130 140 150 160 170
Window: 1000 Level: 300
IVUS Proximal Ref
CCTA frame 19
IVUS frame 5891
CCTA Proximal Ref
CCTA frame 19
IVUS frame 5891
MLA
CCTA frame 44
IVUS frame 5183
IVUS Distal Ref
CCTA frame 57
IVUS frame 4820
CCTA Distal Ref
CCTA frame 57
IVUS frame 4820
0 10 20 30 40 50 60 70 80 90 100
0
5
1
Window: 1000 Level: 300

Case 6

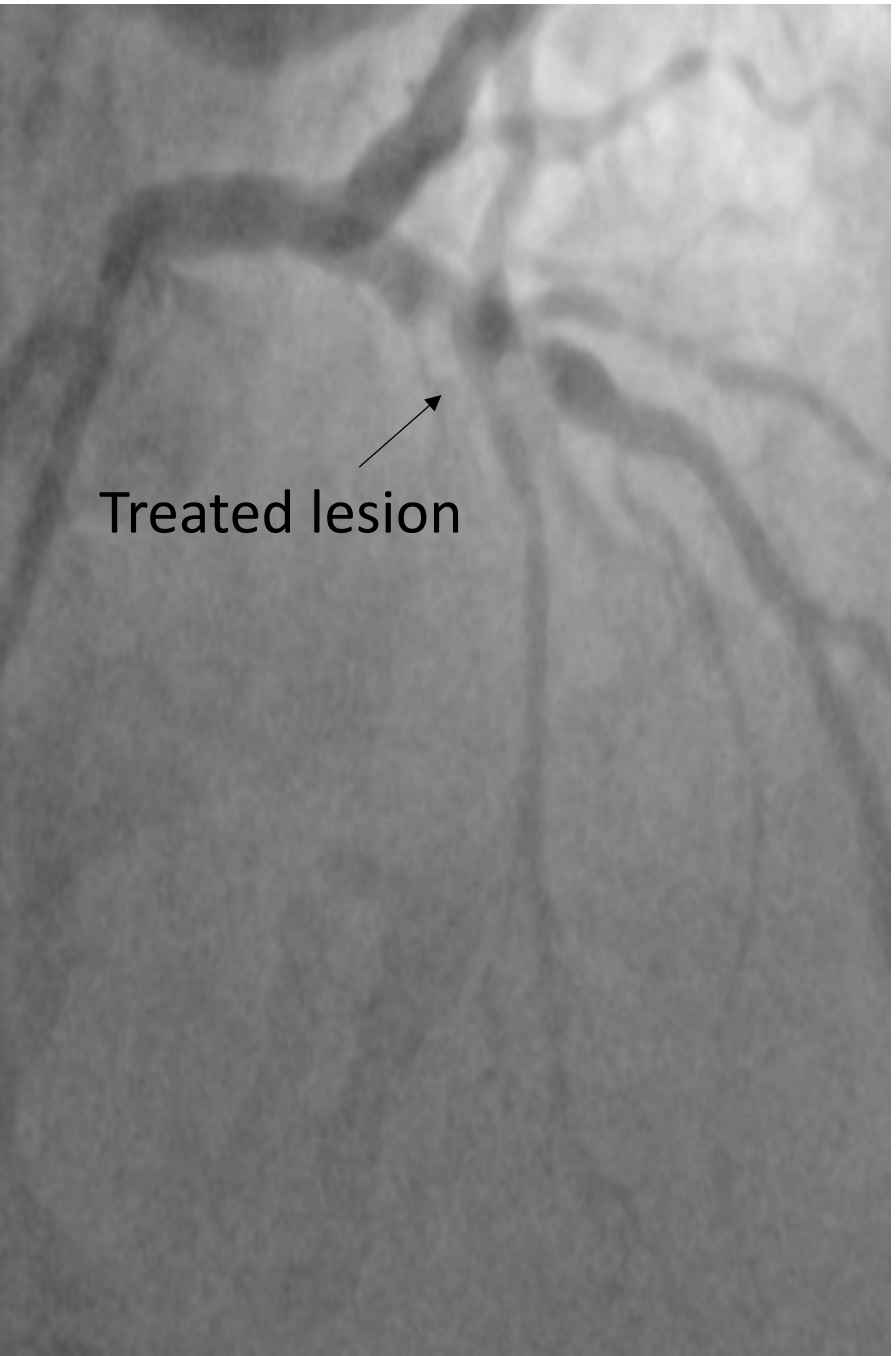
Treated lesion

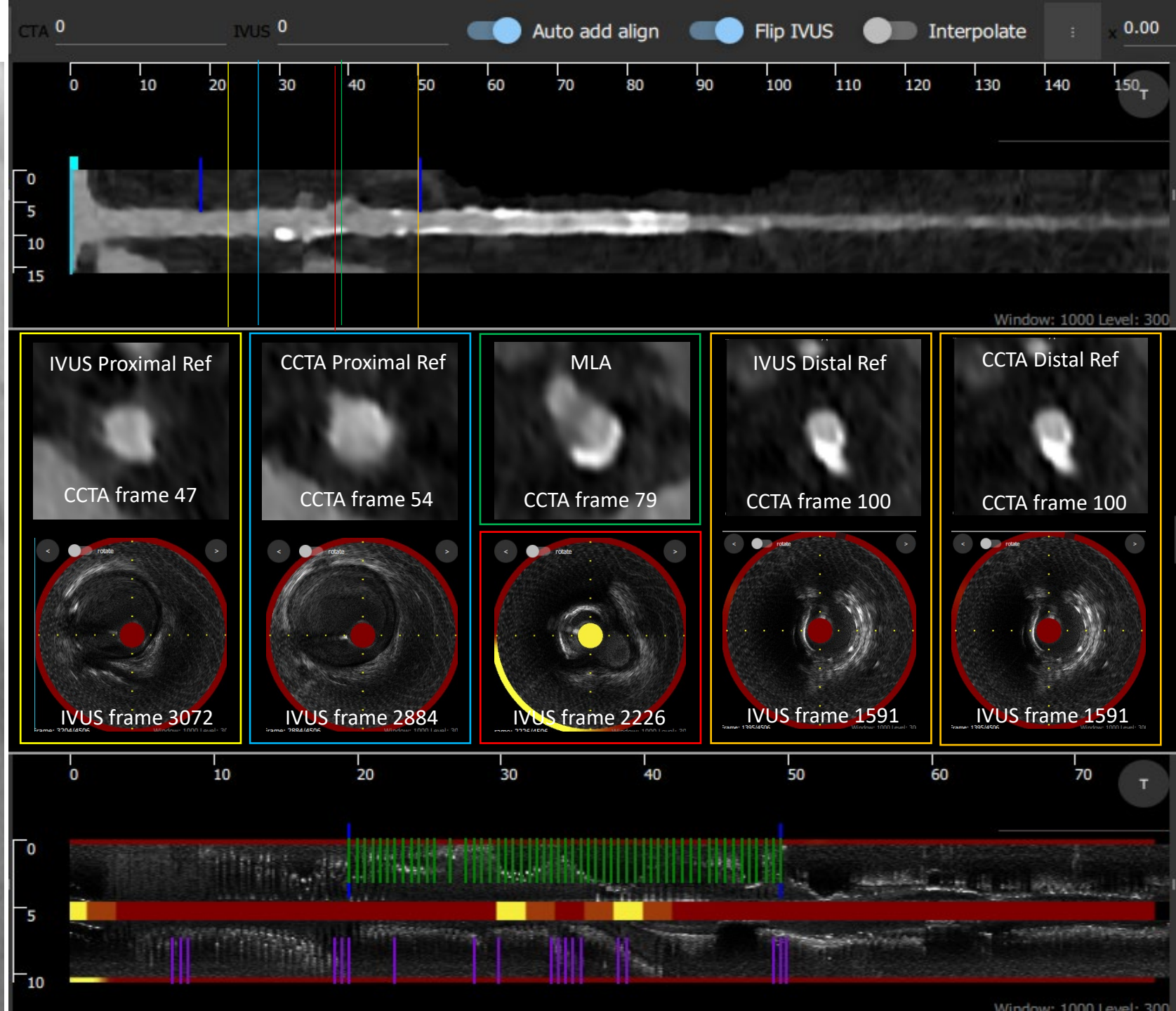
CTA 0
IVUS 0
Auto add align
Flip IVUS
Interpolate
0.00
Window: 1000 Level: 300
IVUS Proximal Ref
CCTA frame 47
IVUS frame 3072
CCTA Proximal Ref
CCTA frame 54
IVUS frame 2884
MLA
CCTA frame 79
IVUS frame 2226
IVUS Distal Ref
CCTA frame 100
IVUS frame 1591
CCTA Distal Ref
CCTA frame 100
IVUS frame 1591
Window: 1000 Level: 300

Case 7


Treated lesion

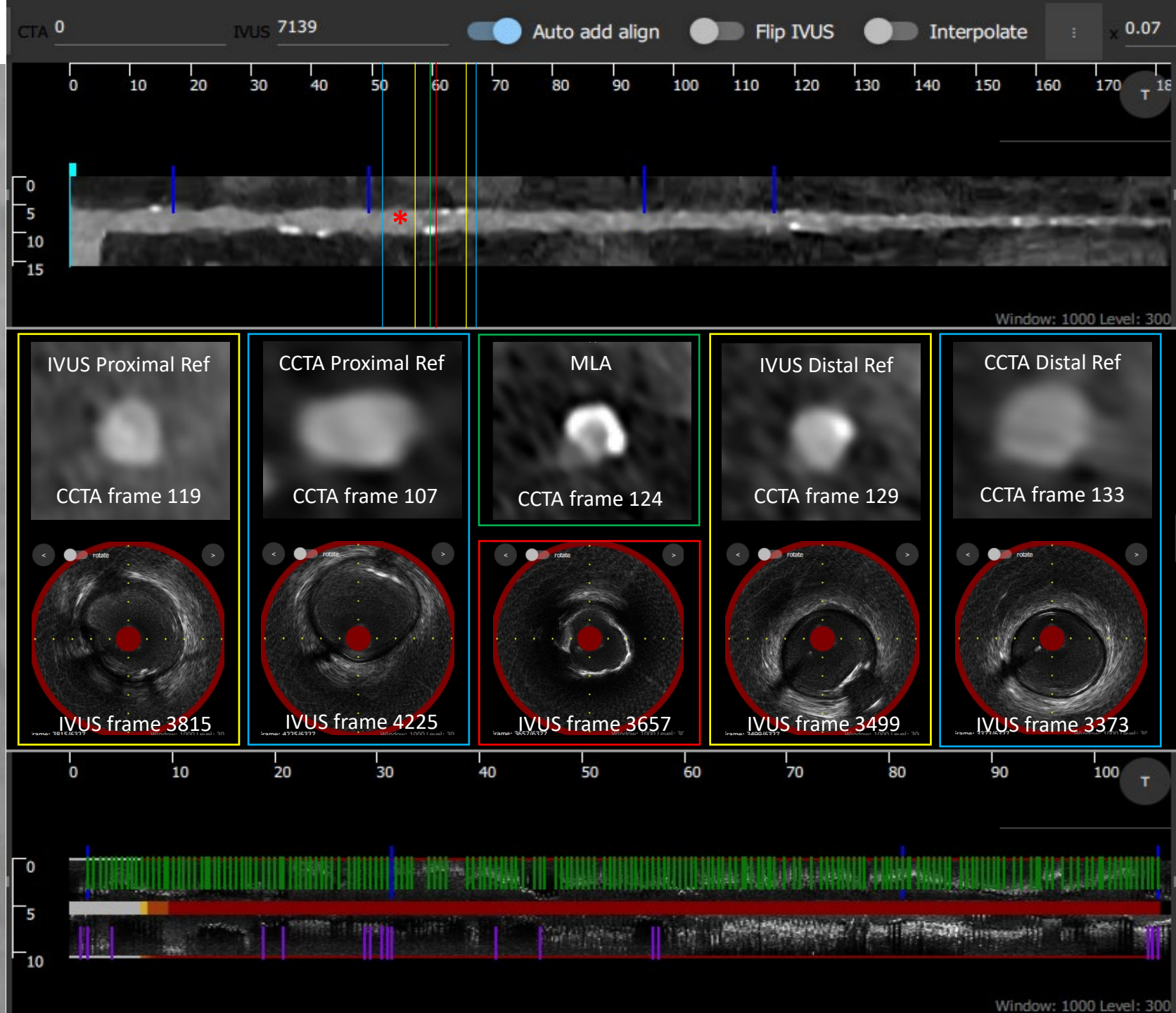
CTA 0
IVUS 7139
Auto add align
Flip IVUS
Interpolate
0.07
Window: 1000 Level: 300
IVUS Proximal Ref
CCTA frame 119
IVUS frame 3815
CCTA Proximal Ref
CCTA frame 107
IVUS frame 4225
MLA
CCTA frame 124
IVUS frame 3657
IVUS Distal Ref
CCTA frame 129
IVUS frame 3499
CCTA Distal Ref
CCTA frame 133
IVUS frame 3373
Window: 1000 Level: 300

Case 8

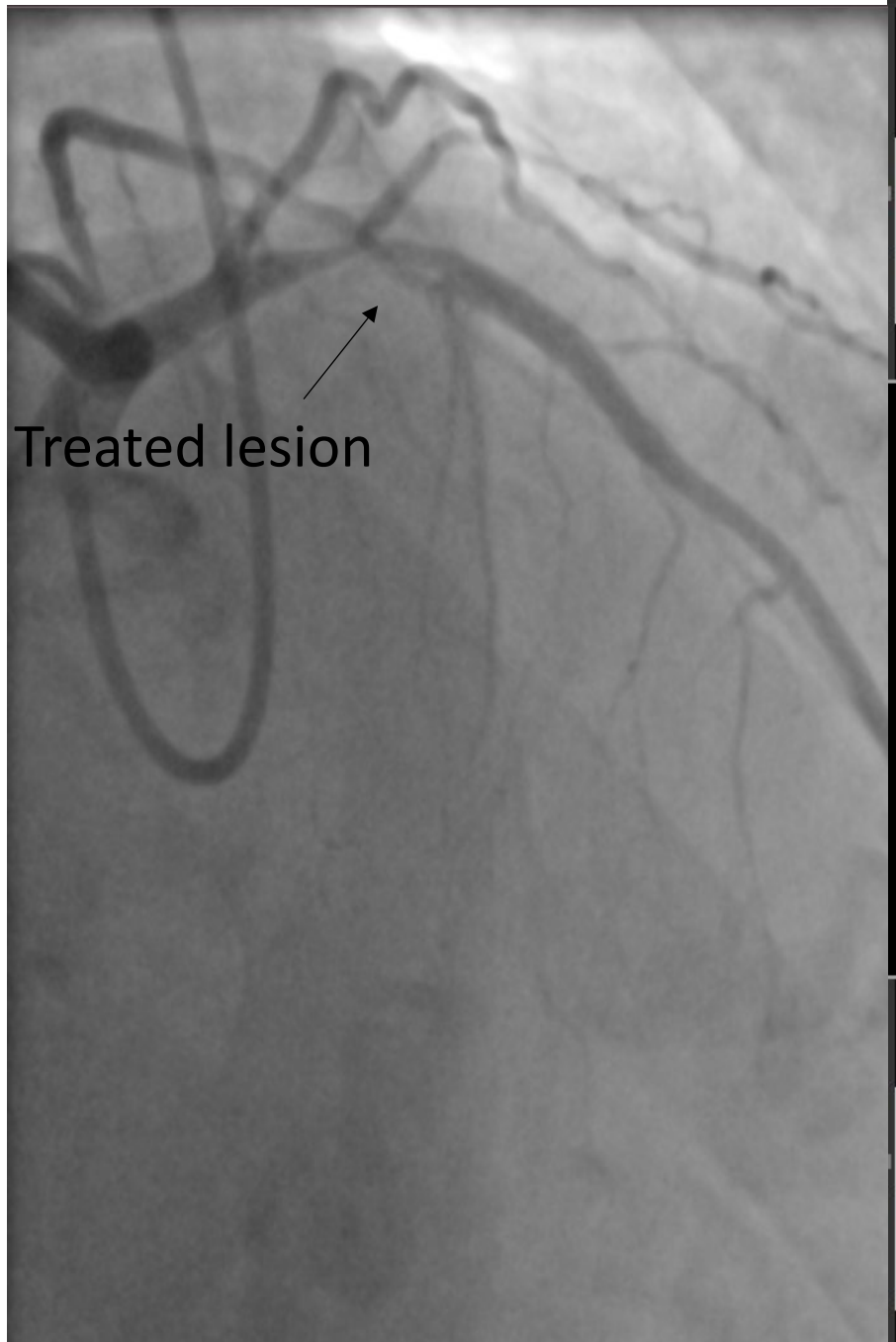
Treated lesion

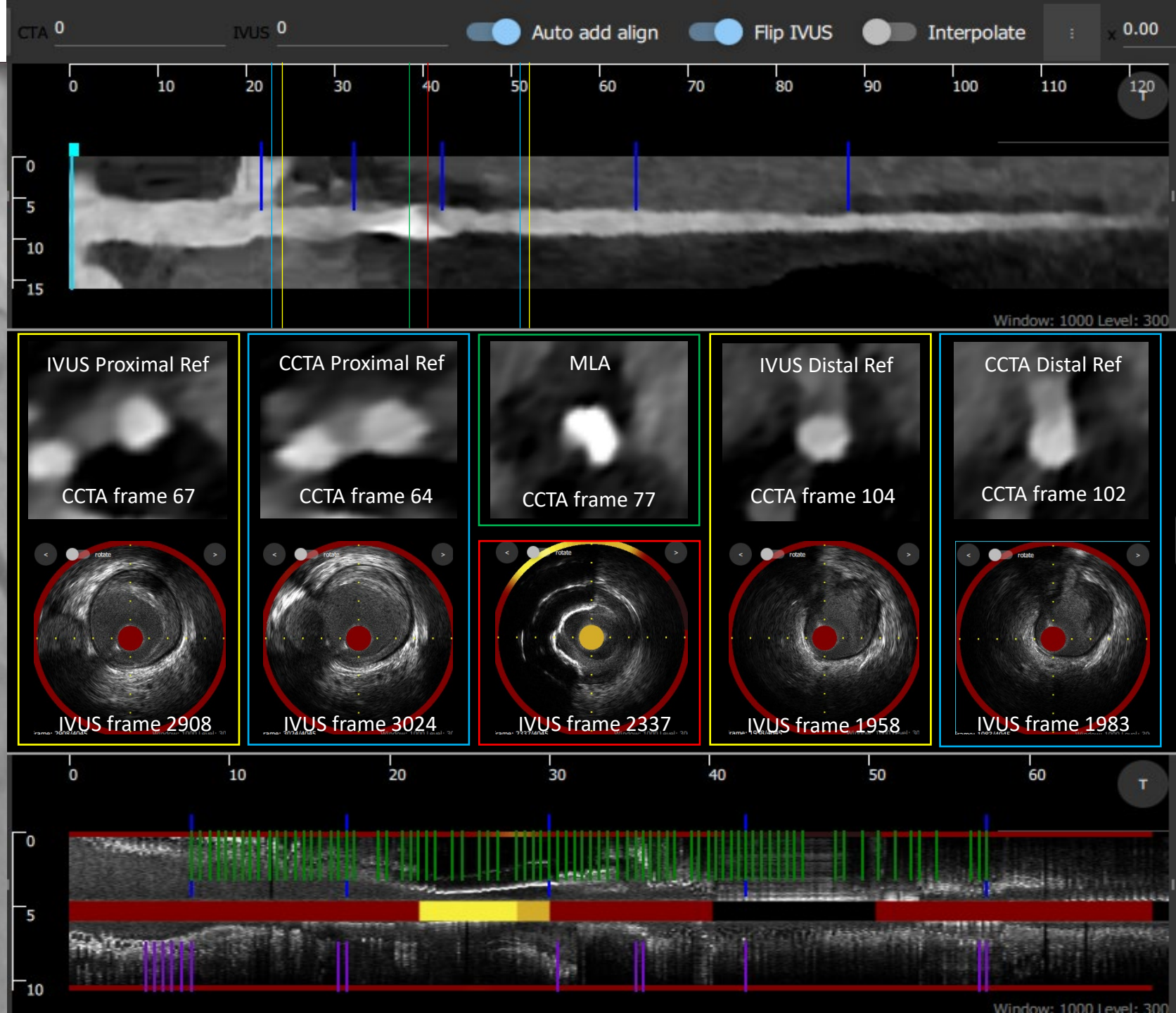
CTA 0
IVUS 0
Auto add align
Flip IVUS
Interpolate
0.00
0 10 20 30 40 50 60 70 80 90 100 110 120
0 5 10 15
Window: 1000 Level: 300
IVUS Proximal Ref
CCTA frame 67
IVUS frame 2908
CCTA Proximal Ref
CCTA frame 64
IVUS frame 3024
MLA
CCTA frame 77
IVUS frame 2337
IVUS Distal Ref
CCTA frame 104
IVUS frame 1958
CCTA Distal Ref
CCTA frame 102
IVUS frame 1983
0 10 20 30 40 50 60
0 5 10
Window: 1000 Level: 300

Case 9

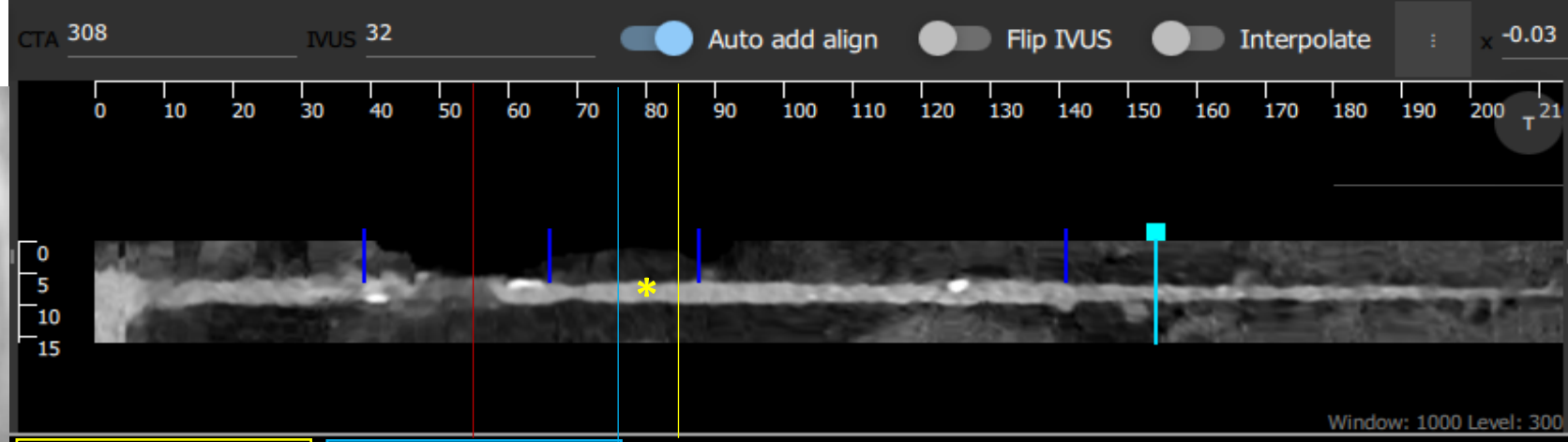

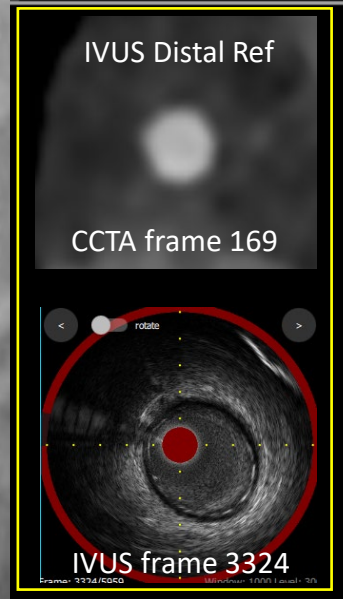

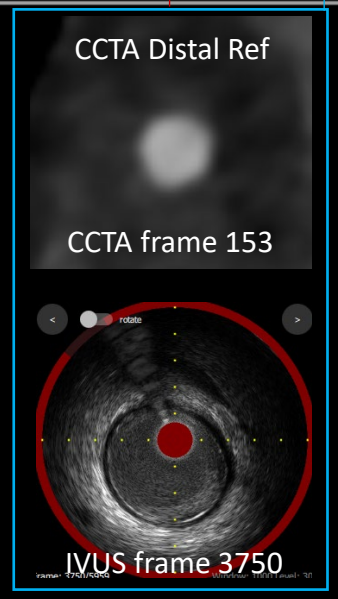

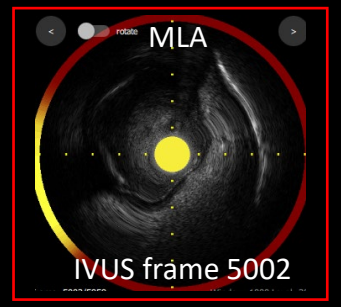

Poor CCTA image quality did not allow clear visualisation of the lumen and vessel wall in the proximal vessel so proximal reference and MLA could not be estimated accurately. Diffuse plaque with PB>50% in the proximal vessel back to the ostium on NIRS-IVUS imaging.

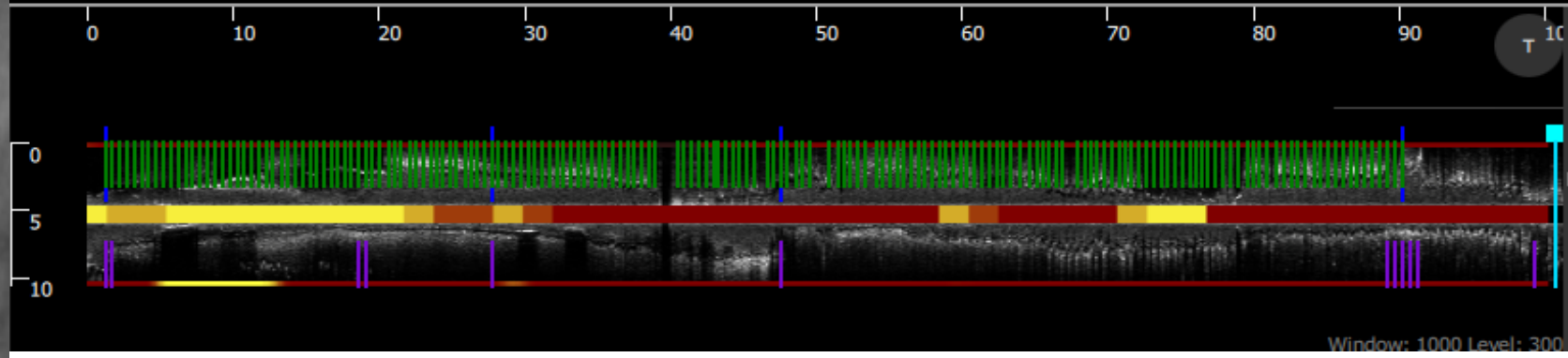

Case 10

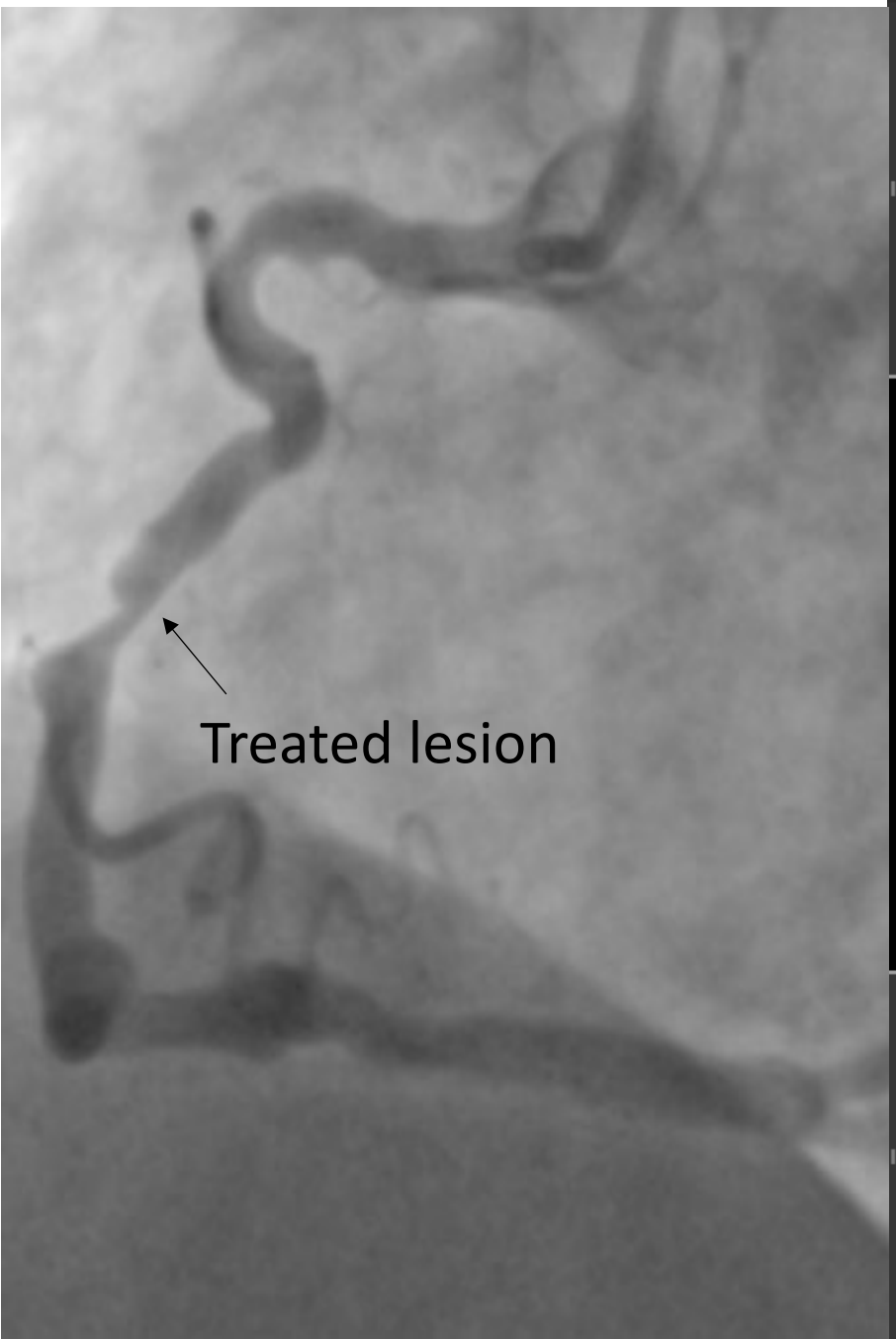
Treated lesion

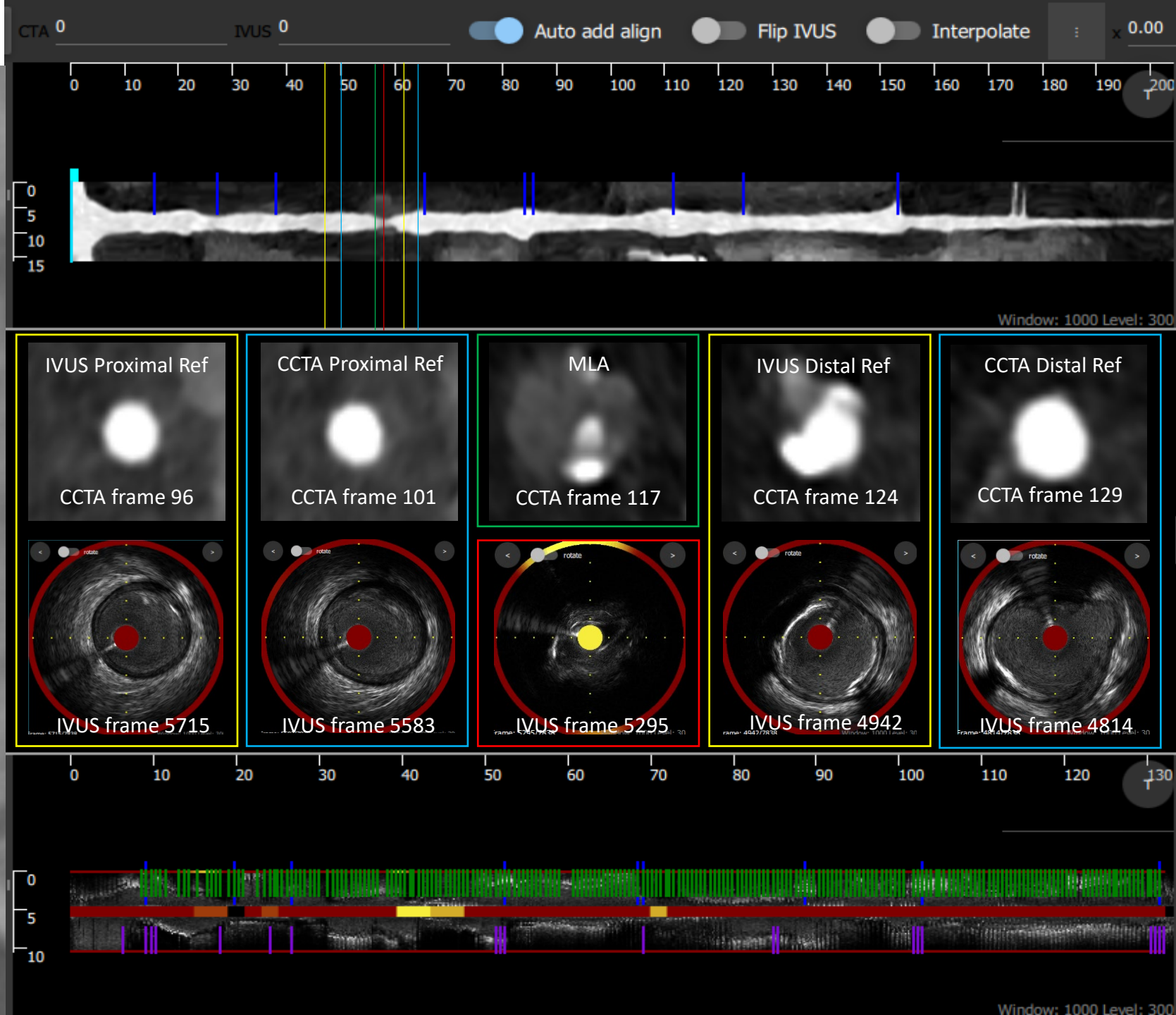
CTA 0
IVUS 0
Auto add align
Flip IVUS
Interpolate
0.00
Window: 1000 Level: 300
IVUS Proximal Ref
CCTA frame 96
IVUS frame 5715
CCTA Proximal Ref
CCTA frame 101
IVUS frame 5583
MLA
CCTA frame 117
IVUS frame 5295
IVUS Distal Ref
CCTA frame 124
IVUS frame 4942
CCTA Distal Ref
CCTA frame 129
IVUS frame 4814
Window: 1000 Level: 300

Case 11

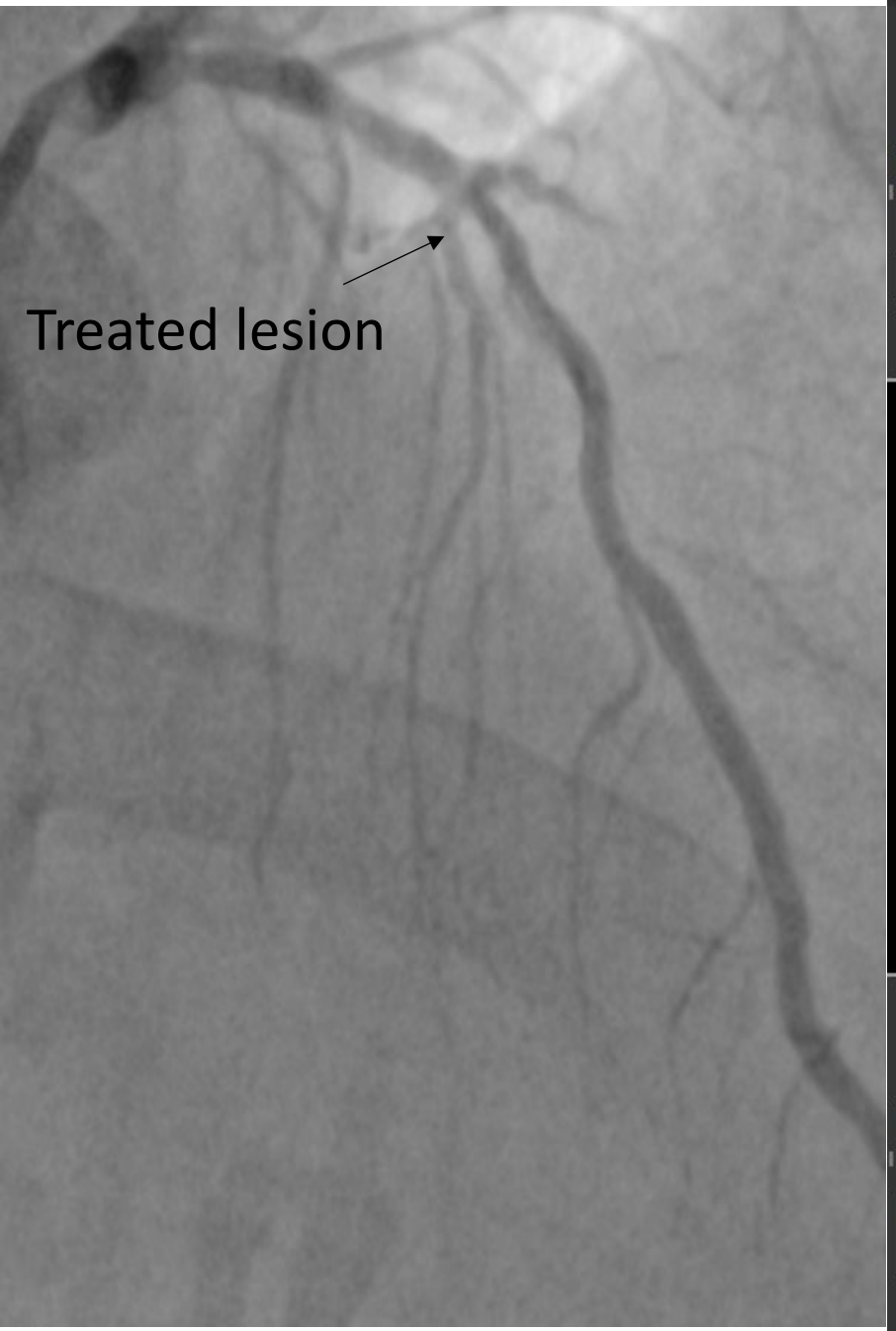
Treated lesion

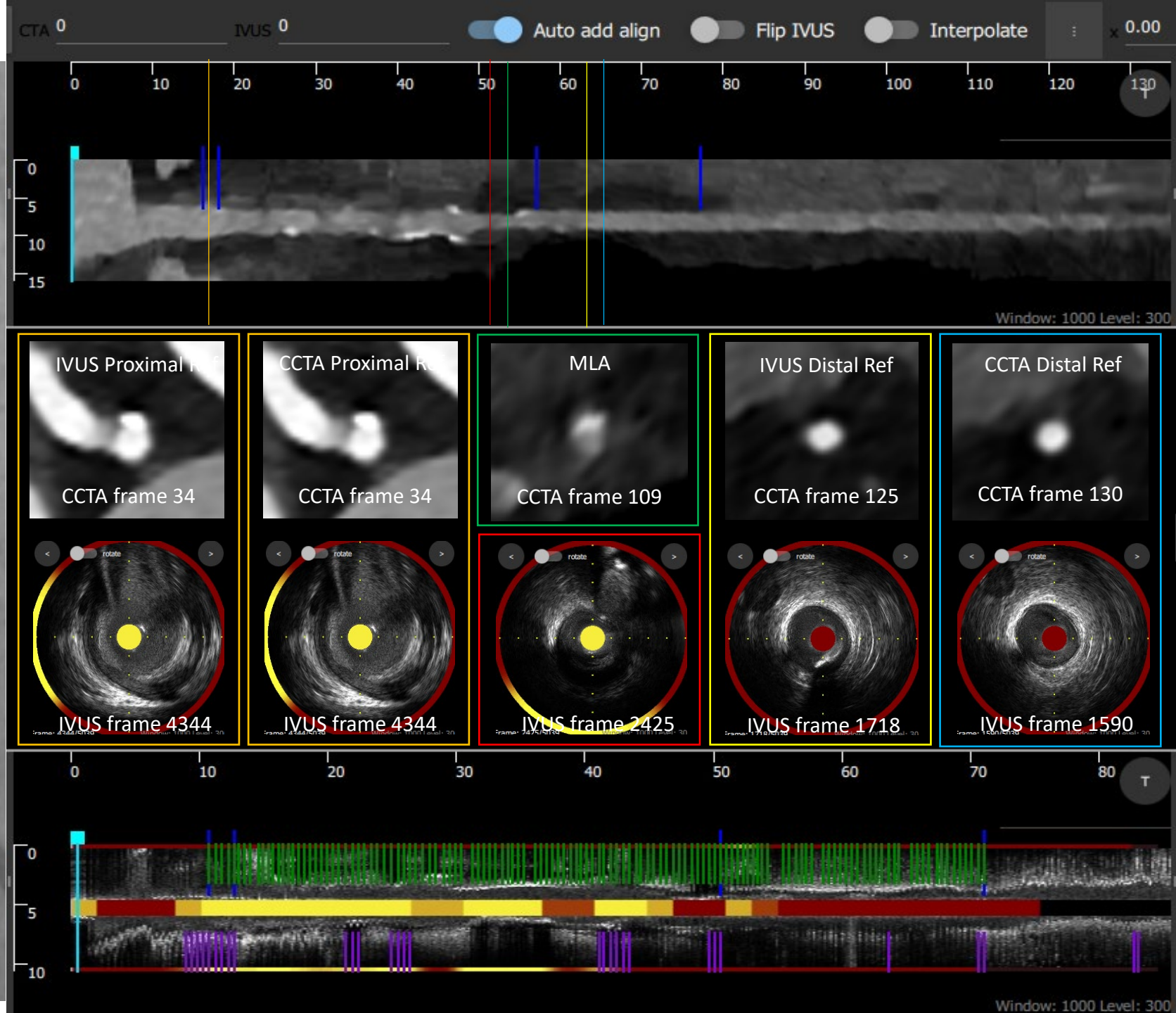
CTA 0
IVUS 0
Auto add align
Flip IVUS
Interpolate
0.00
Window: 1000 Level: 300
IVUS Proximal Ref
CCTA frame 34
IVUS frame 4344
CCTA Proximal Ref
CCTA frame 34
IVUS frame 4344
MLA
CCTA frame 109
IVUS frame 2425
IVUS Distal Ref
CCTA frame 125
IVUS frame 1718
CCTA Distal Ref
CCTA frame 130
IVUS frame 1590
Window: 1000 Level: 300

Case 12

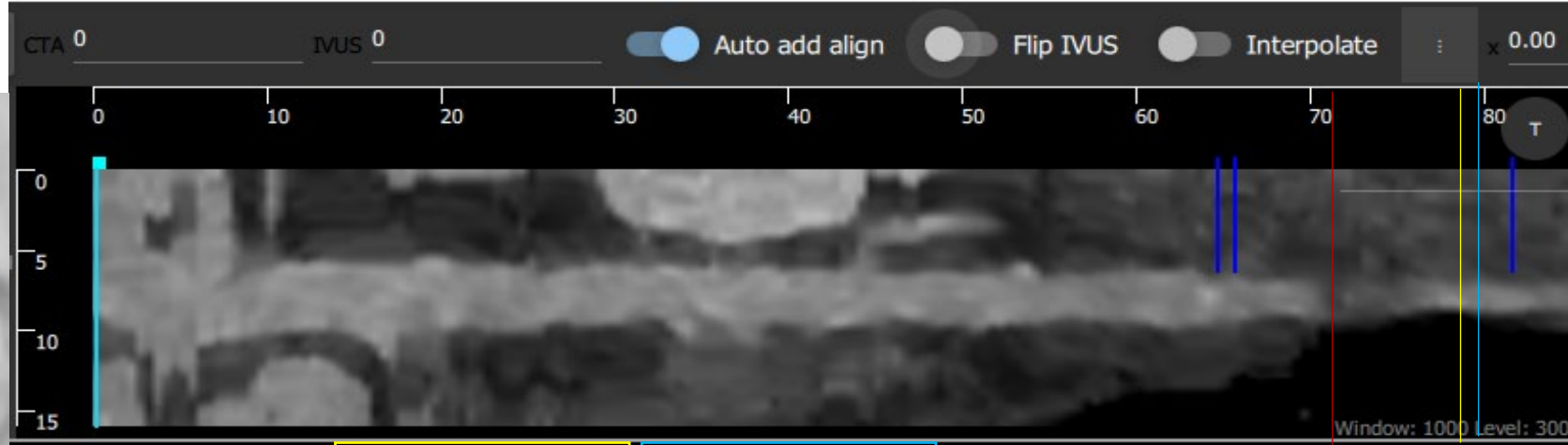

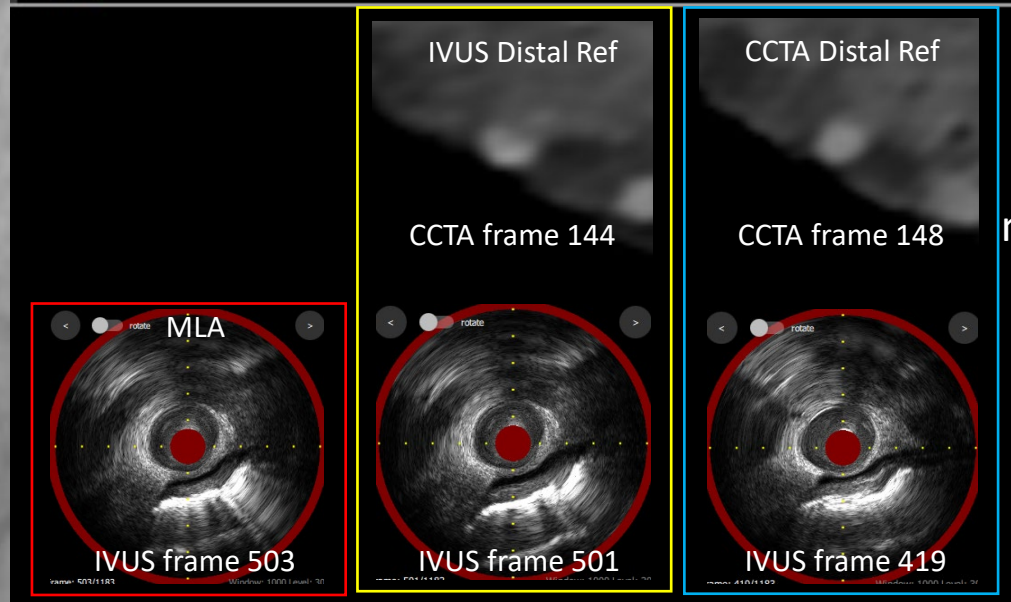

Poor image quality of CCTA did not allow accurate visualisation of the lumen and vessel wall at the MLA and proximal segment. The MLA of NIRS-IVUS and distal references are shown.

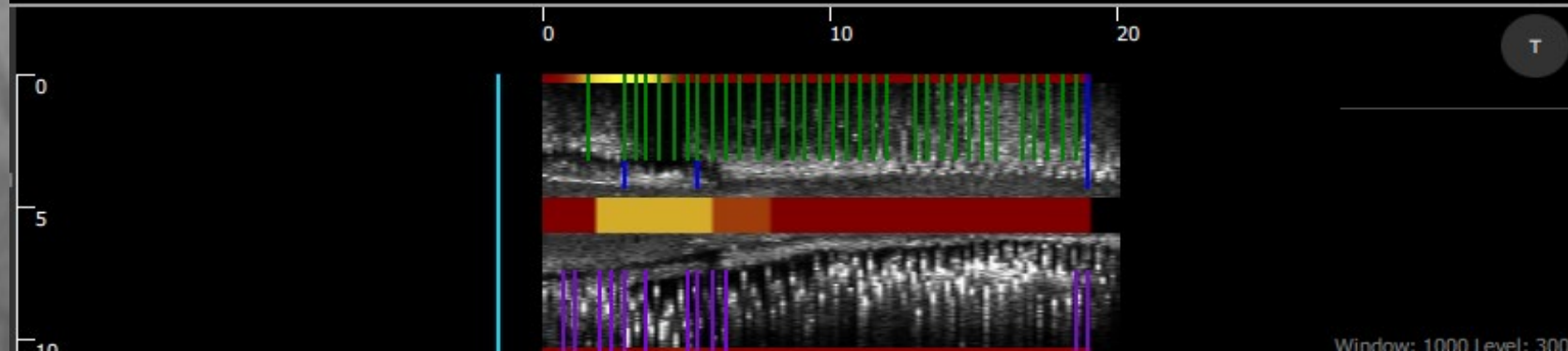

Case 13


Treated lesion

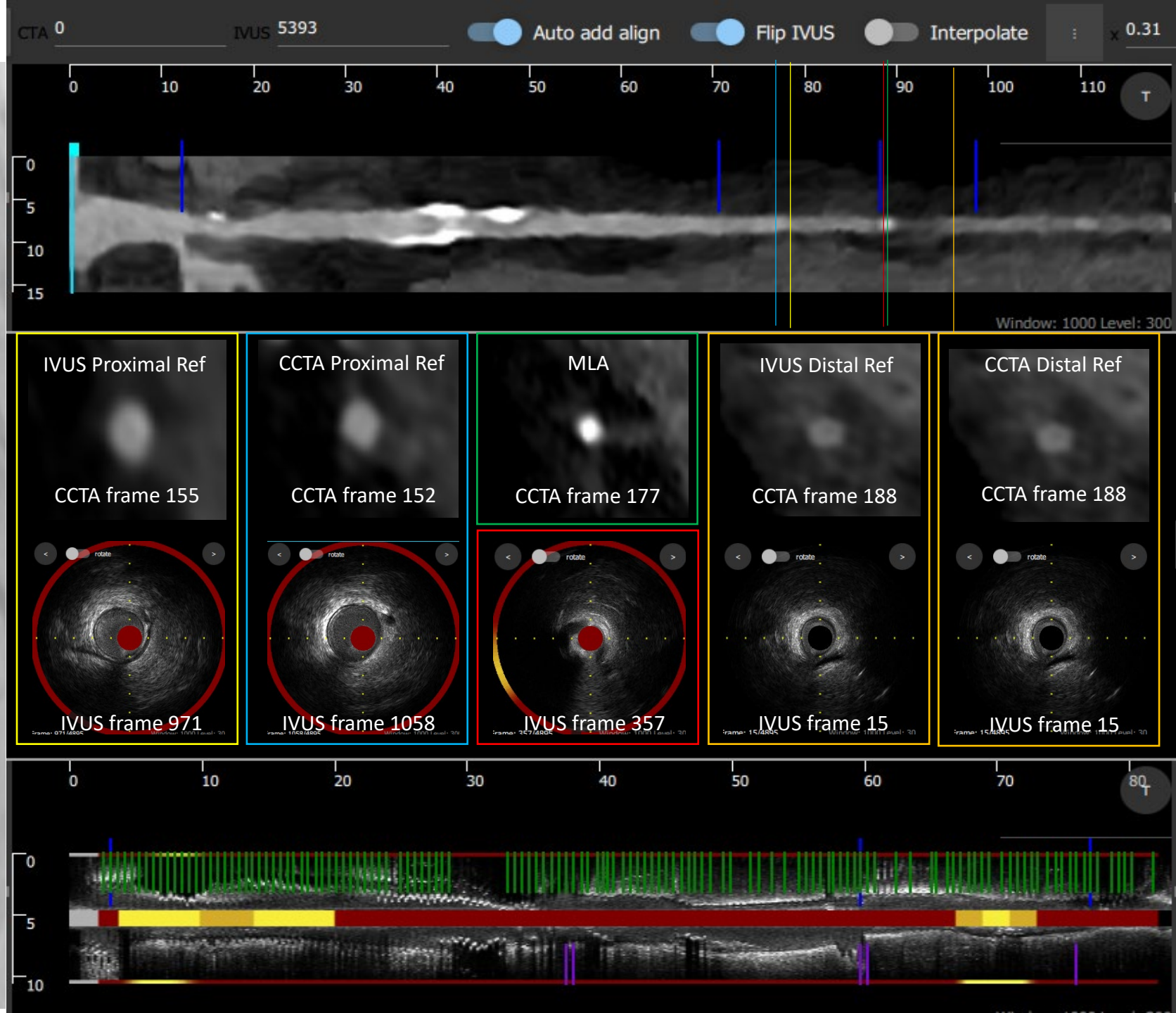
CTA 0
IVUS 5393
Auto add align
Flip IVUS
Interpolate
0.31
Window: 1000 Level: 300
IVUS Proximal Ref
CCTA frame 155
IVUS frame 971
CCTA Proximal Ref
CCTA frame 152
IVUS frame 1058
MLA
CCTA frame 177
IVUS frame 357
IVUS Distal Ref
CCTA frame 188
IVUS frame 15
CCTA Distal Ref
CCTA frame 188
IVUS frame 15

Case 14

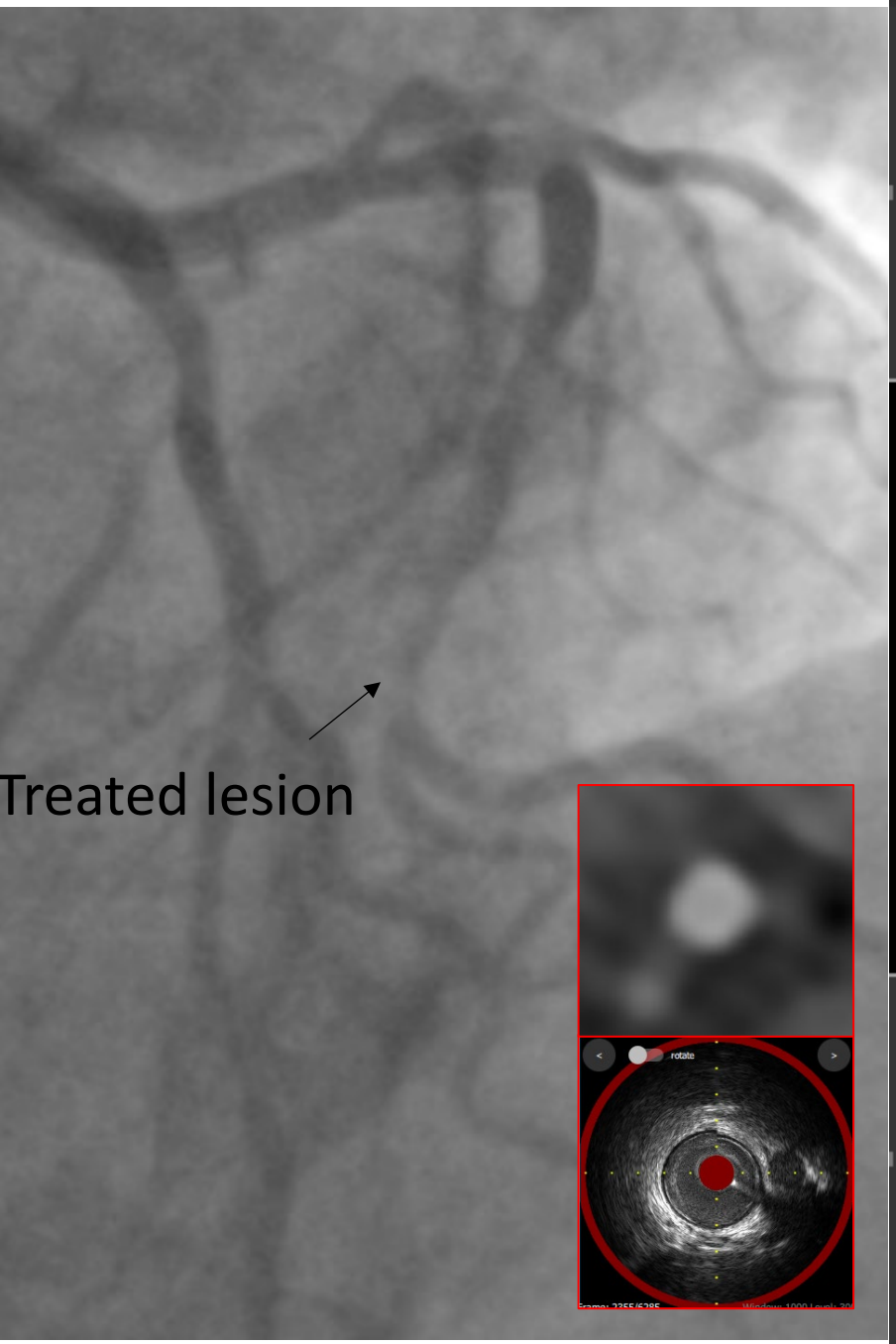
Treated lesion

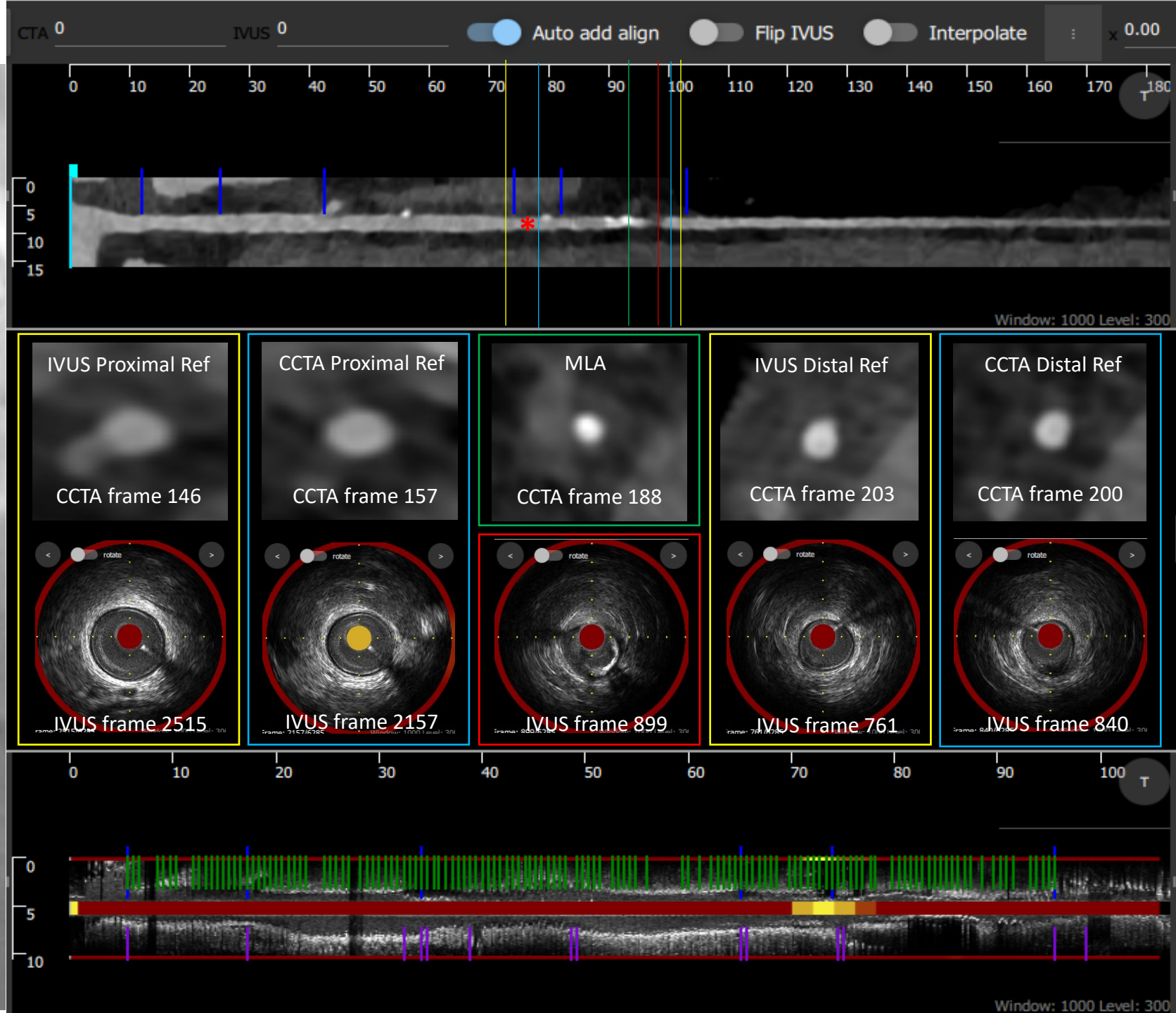
CTA 0
IVUS 0
Auto add align
Flip IVUS
Interpolate
0.00
0 10 20 30 40 50 60 70 80 90 100 110 120 130 140 150 160 170 180
0 5 10 15
Window: 1000 Level: 300
IVUS Proximal Ref
CCTA frame 146
IVUS frame 2515
CCTA Proximal Ref
CCTA frame 157
IVUS frame 2157
MLA
CCTA frame 188
IVUS frame 899
IVUS Distal Ref
CCTA frame 203
IVUS frame 761
CCTA Distal Ref
CCTA frame 200
IVUS frame 840
0 10 20 30 40 50 60 70 80 90 100
0 5 10
Window: 1000 Level: 300

Case 15

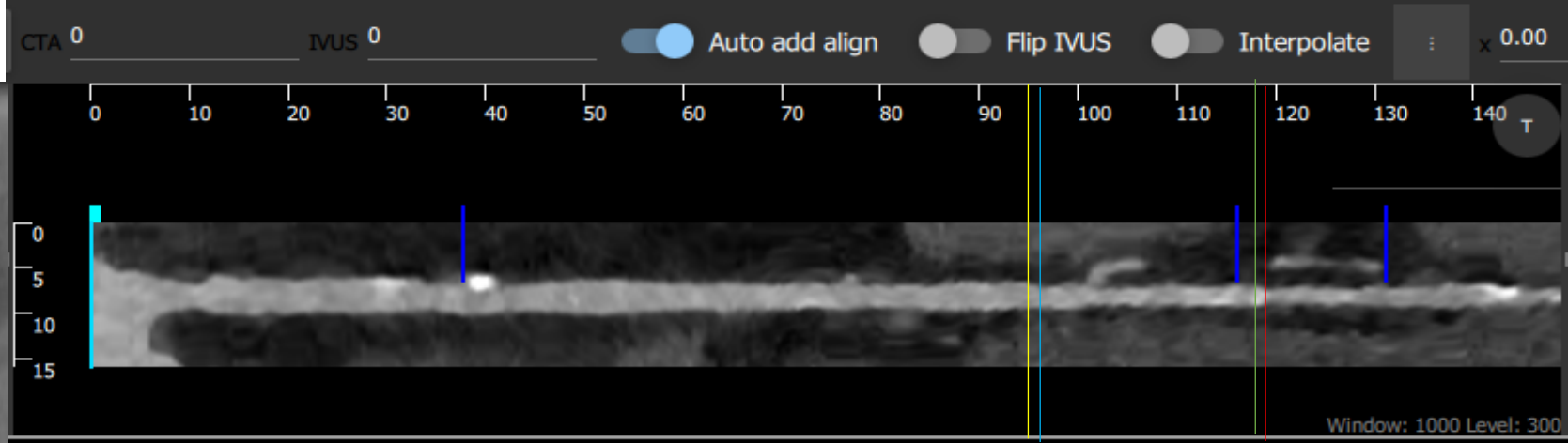

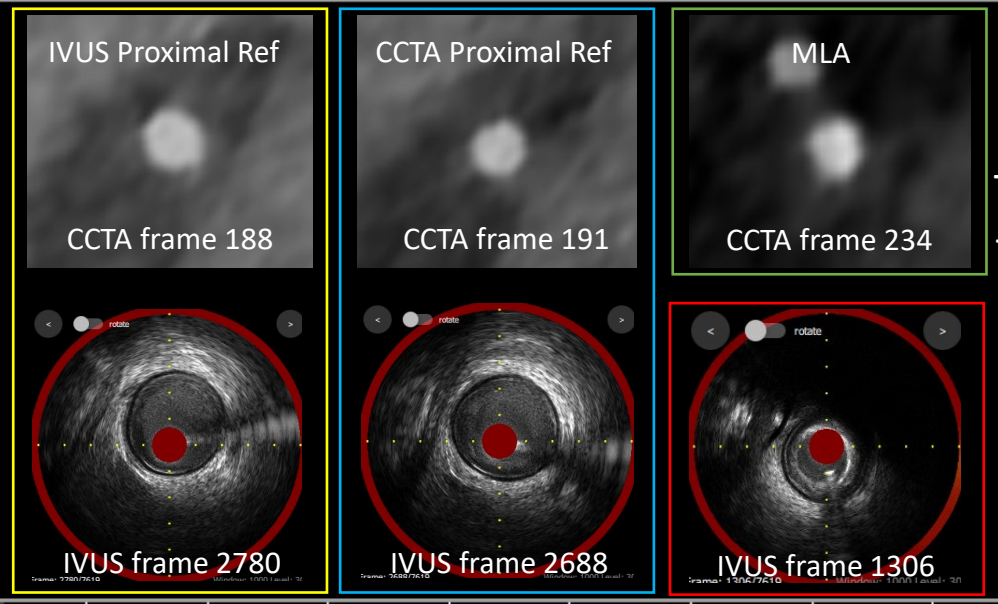

The NIRS-IVUS pullback started in the lesion, so the distal reference areas and lesion length were not estimated

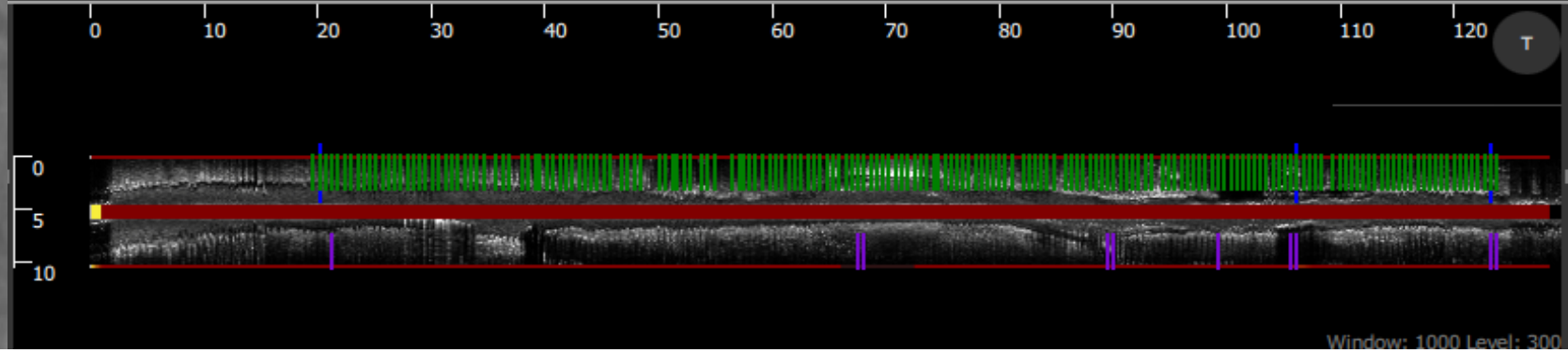

Case 16

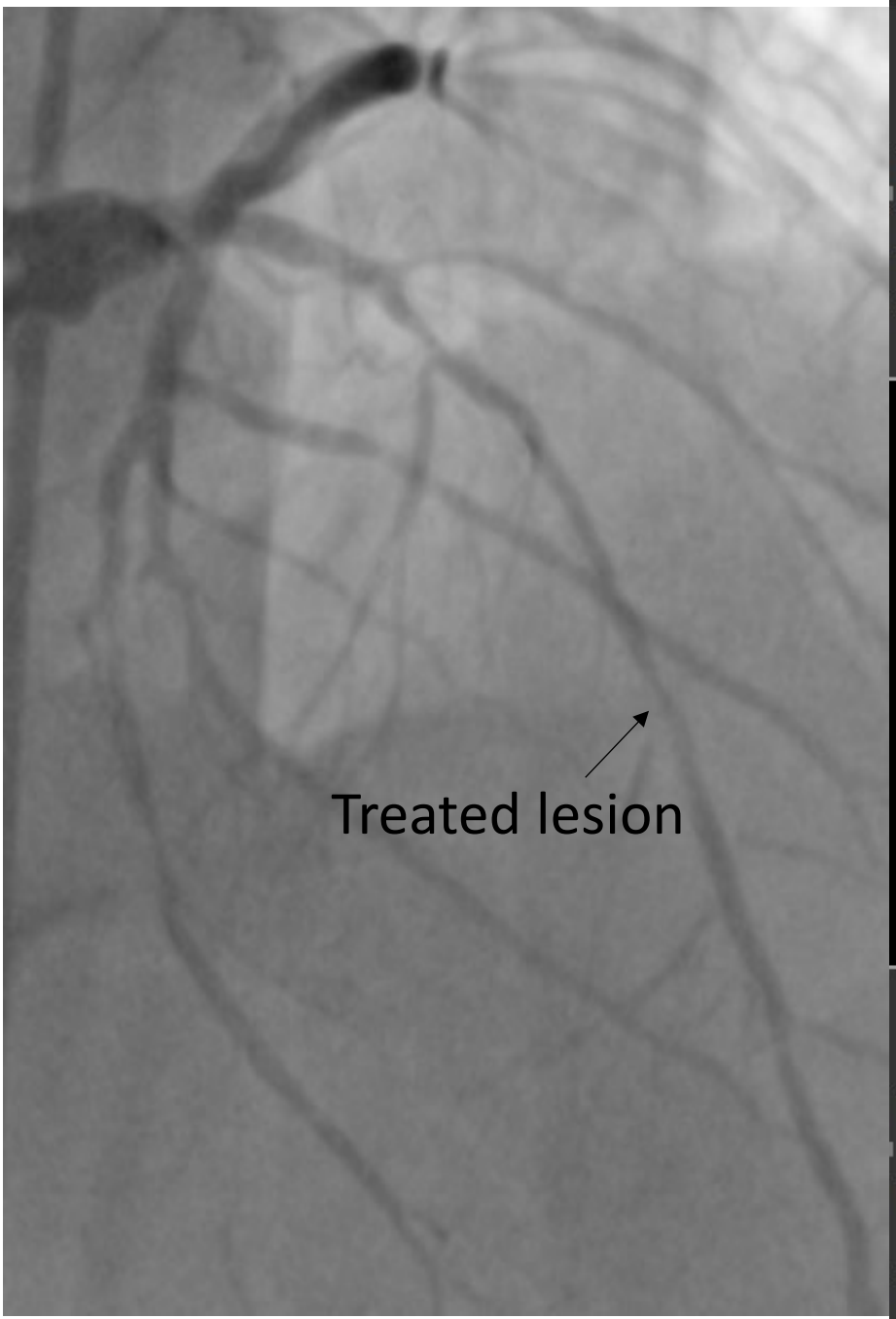

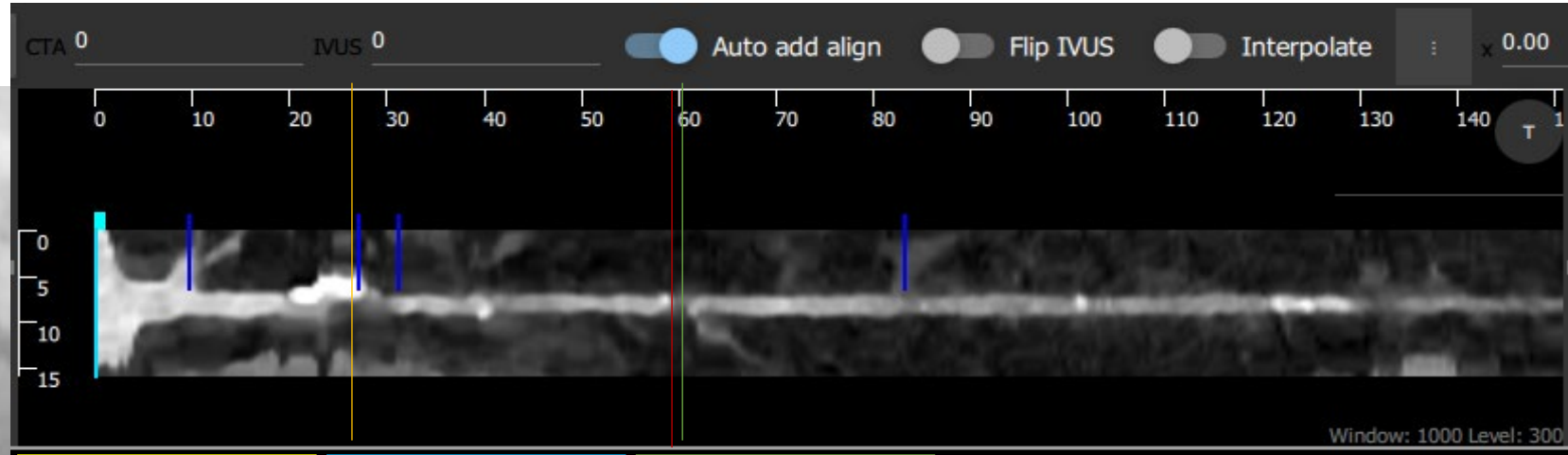

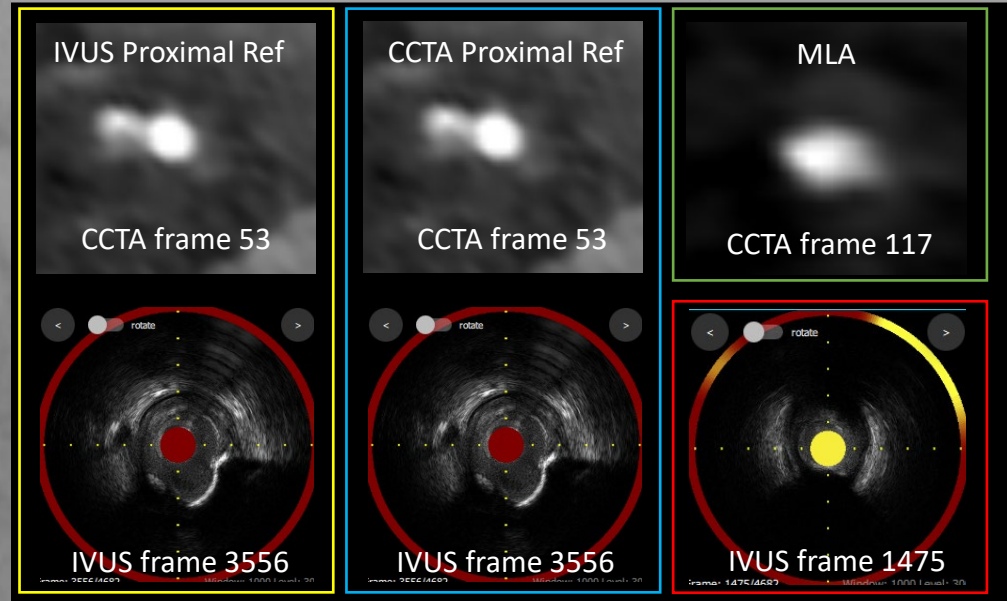

The NIRS-IVUS pullback started in the lesion, so the distal reference areas and lesion length were not estimated. There was diffuse plaque with PB>50% in the entire pullback back to left main stem so the proximal reference area was placed just proximal to the D1 branch where the stent was placed.

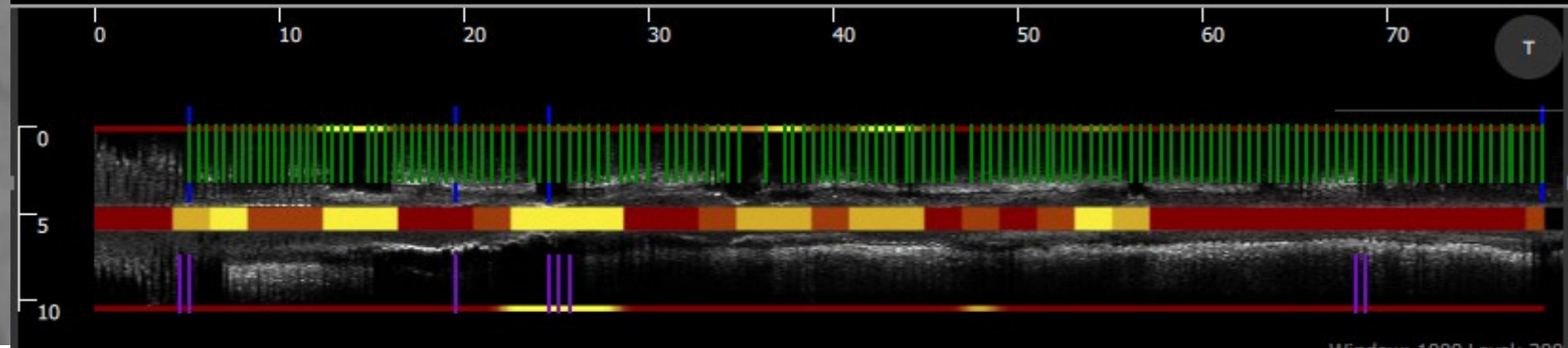

Case 17

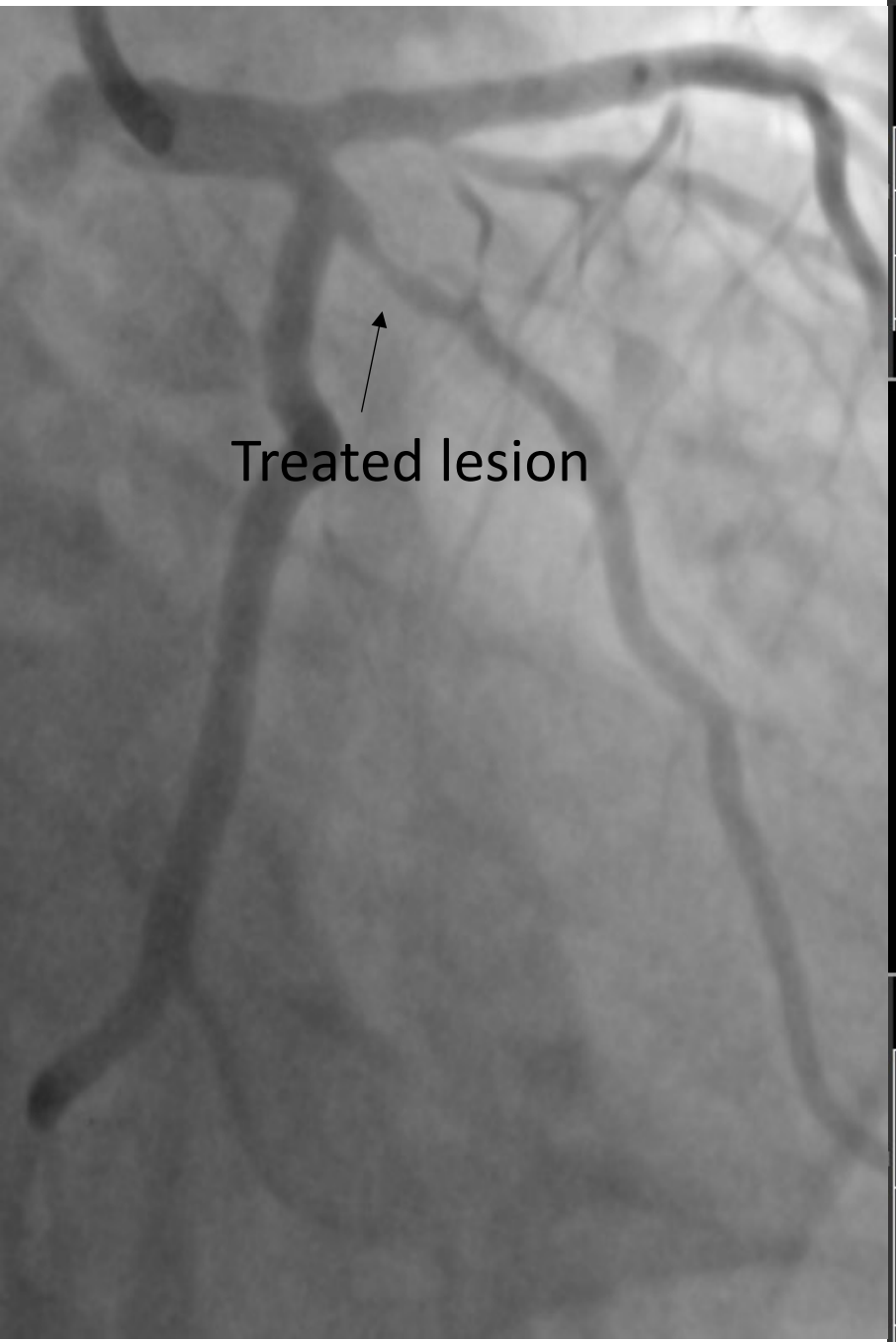
Treated lesion

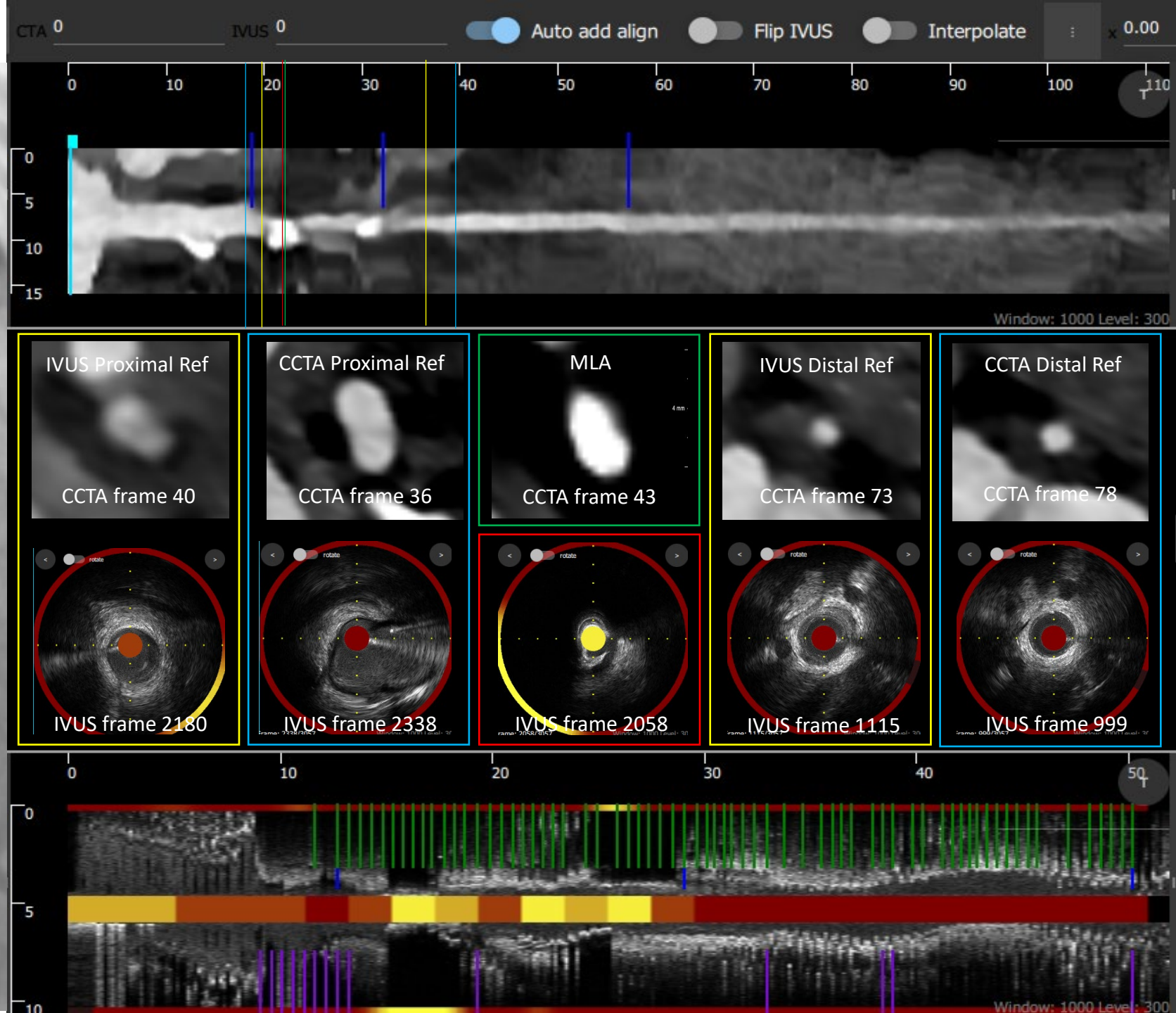
CTA 0
IVUS 0
Auto add align
Flip IVUS
Interpolate
0.00
Window: 1000 Level: 300
IVUS Proximal Ref
CCTA frame 40
IVUS frame 2180
CCTA Proximal Ref
CCTA frame 36
IVUS frame 2338
MLA
CCTA frame 43
IVUS frame 2058
IVUS Distal Ref
CCTA frame 73
IVUS frame 1115
CCTA Distal Ref
CCTA frame 78
IVUS frame 999
Window: 1000 Level: 300

Case 18

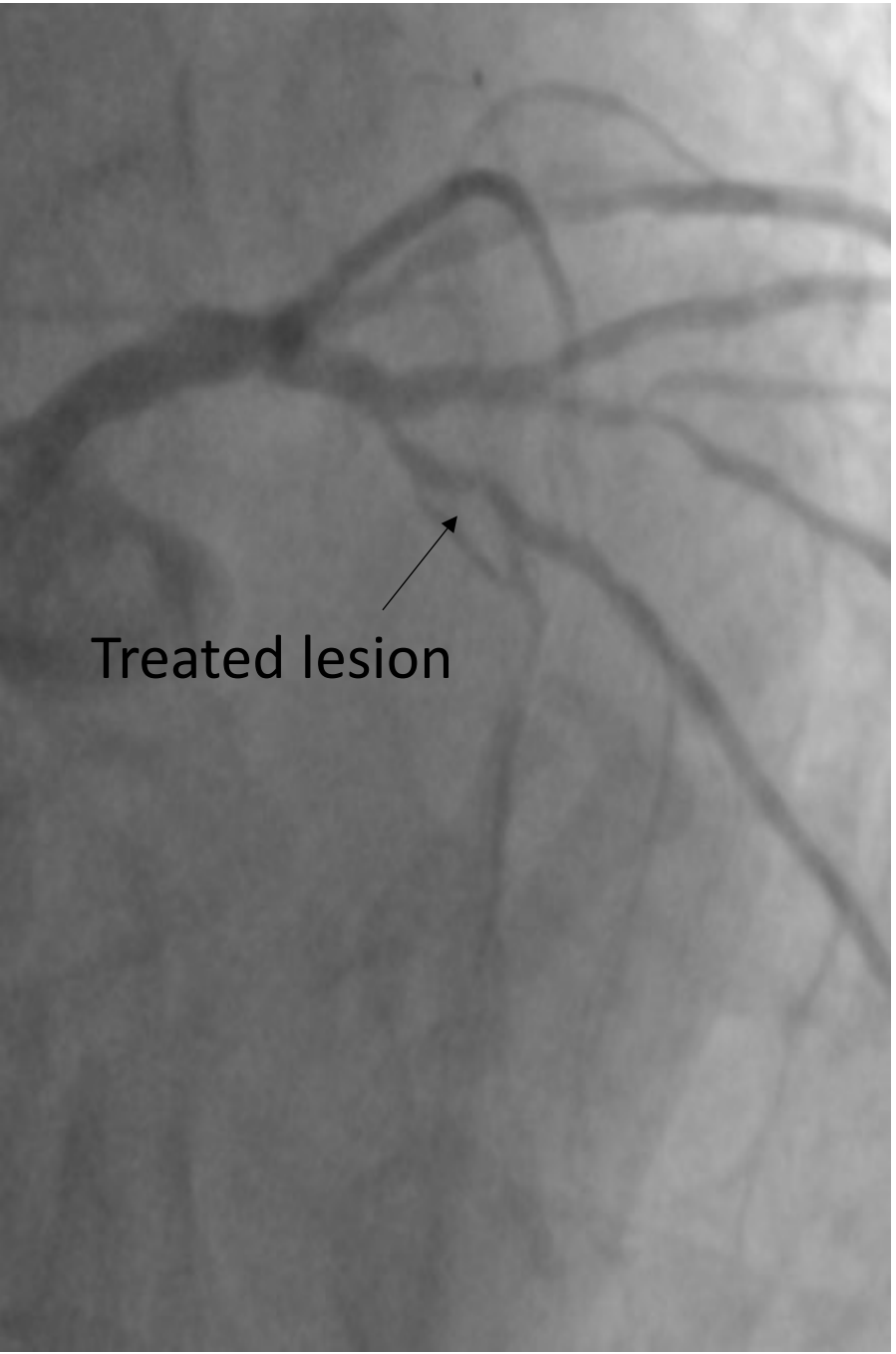
Treated lesion

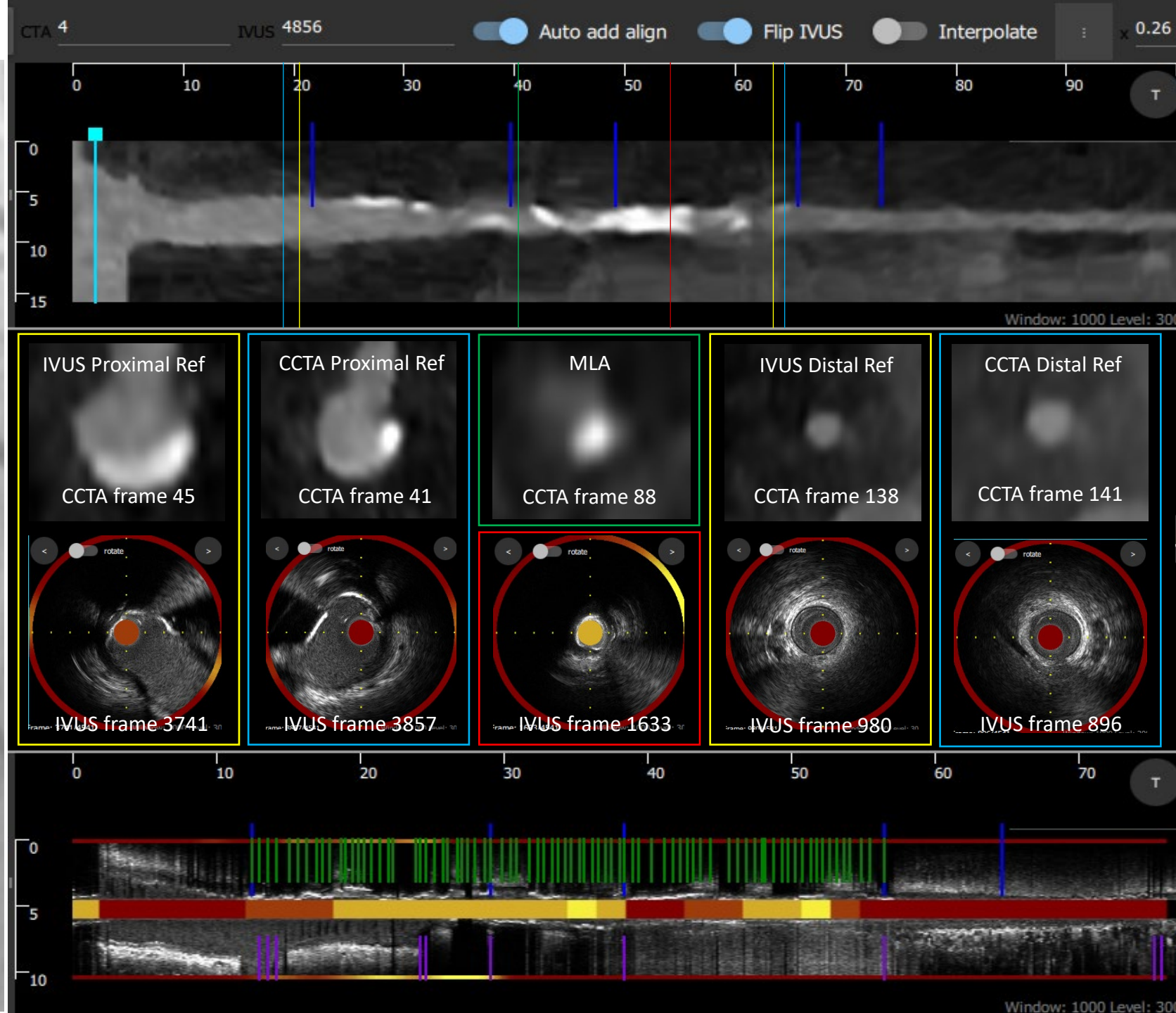
CTA 4
IVUS 4856
Auto add align
Flip IVUS
Interpolate
0.26
Window: 1000 Level: 30
IVUS Proximal Ref
CCTA frame 45
IVUS frame 3741
CCTA Proximal Ref
CCTA frame 41
IVUS frame 3857
MLA
CCTA frame 88
IVUS frame 1633
IVUS Distal Ref
CCTA frame 138
IVUS frame 980
CCTA Distal Ref
CCTA frame 141
IVUS frame 896
Window: 1000 Level: 30

Case 19

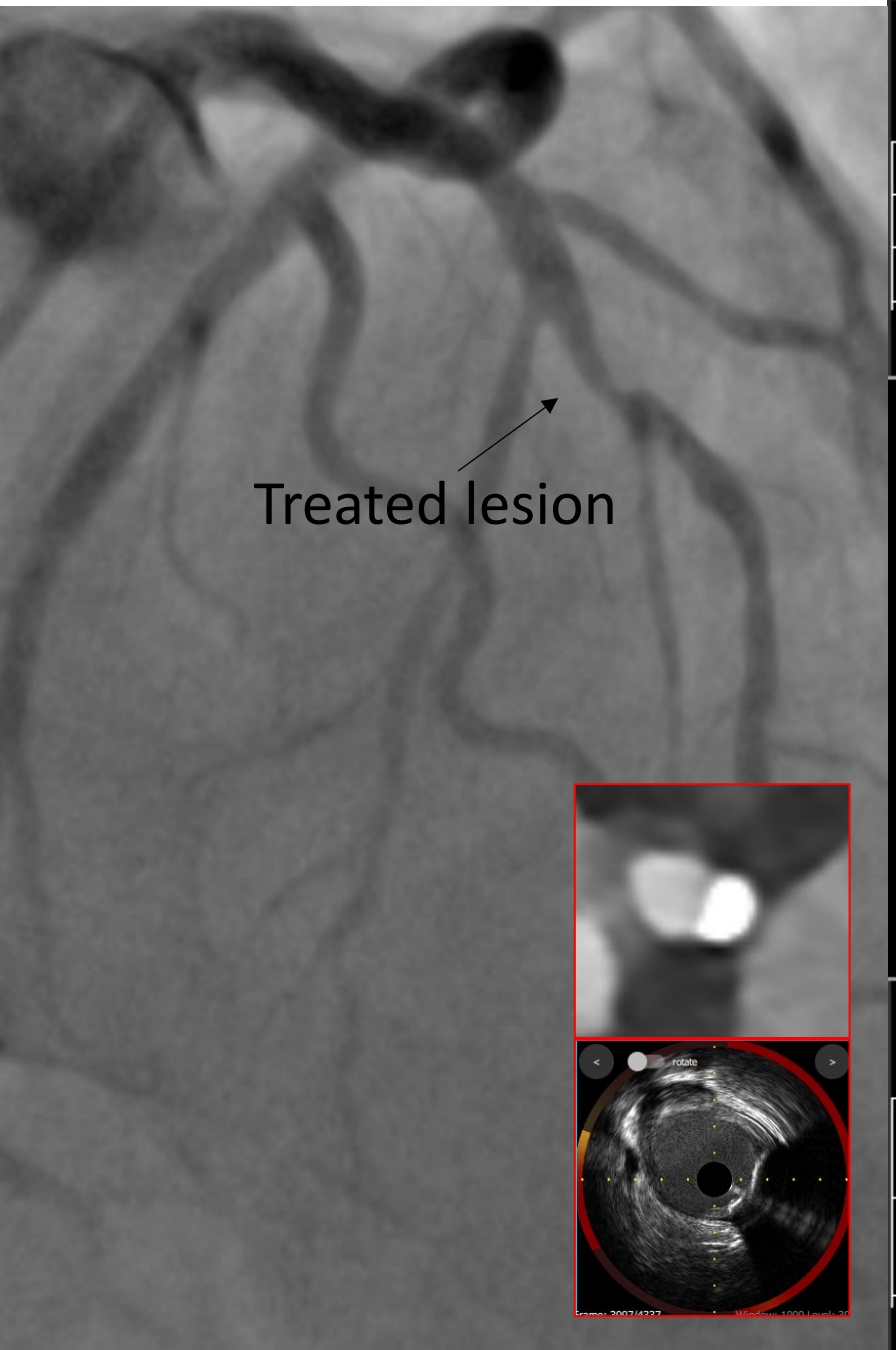
Treated lesion


CTA 0
IVUS 5723
Auto add align
Flip IVUS
Interpolate
-0.56
Window: 1000 Level: 300
IVUS Proximal Ref
CCTA frame 77
IVUS frame 3528
CCTA Proximal Ref
CCTA frame 49
IVUS frame 4332
MLA
CCTA frame 87
IVUS frame 3241
IVUS Distal Ref
CCTA frame 117
IVUS frame 2361
CCTA Distal Ref
CCTA frame 121
IVUS frame 2252
Window: 1000 Level: 300

Case 20

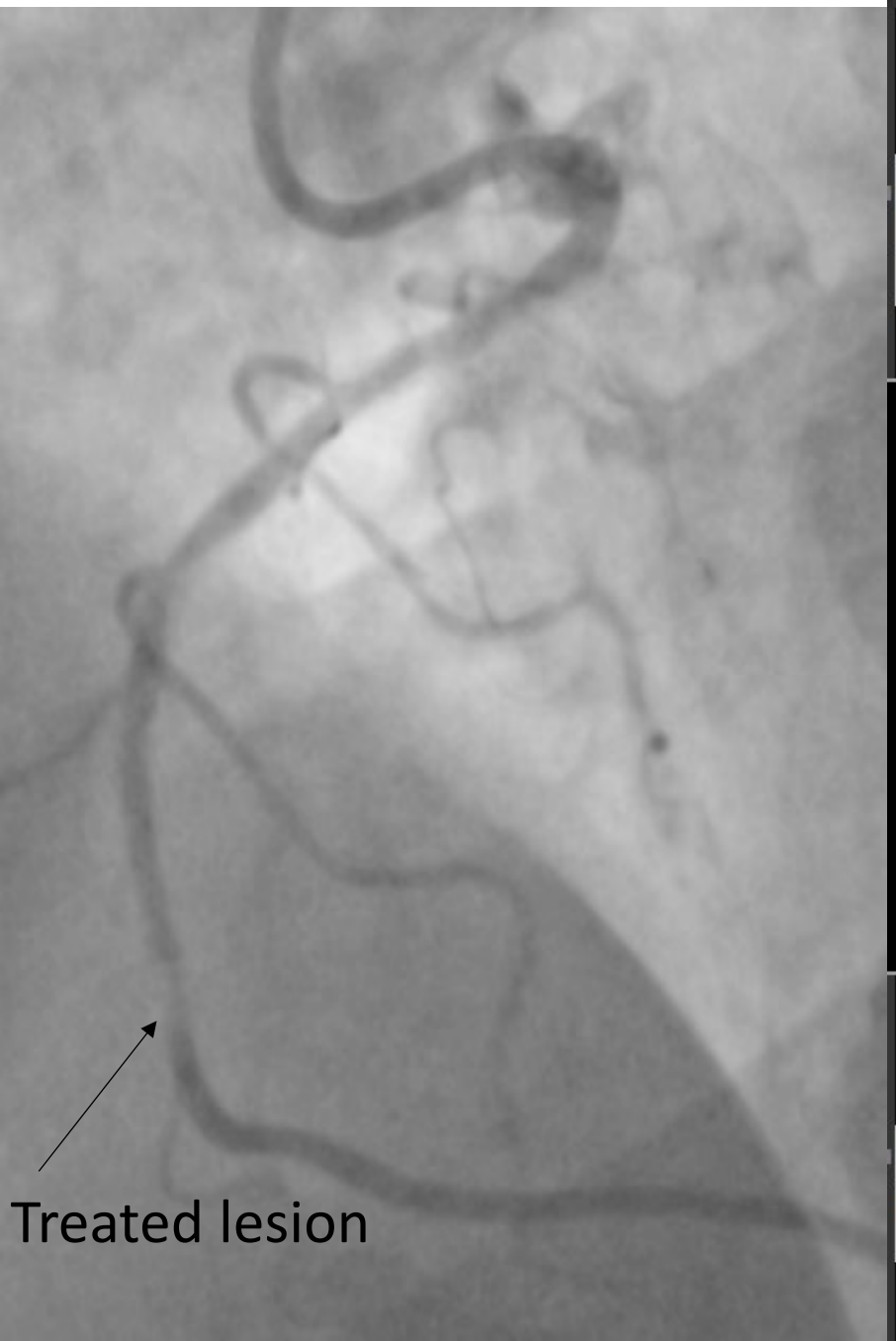
Treated lesion

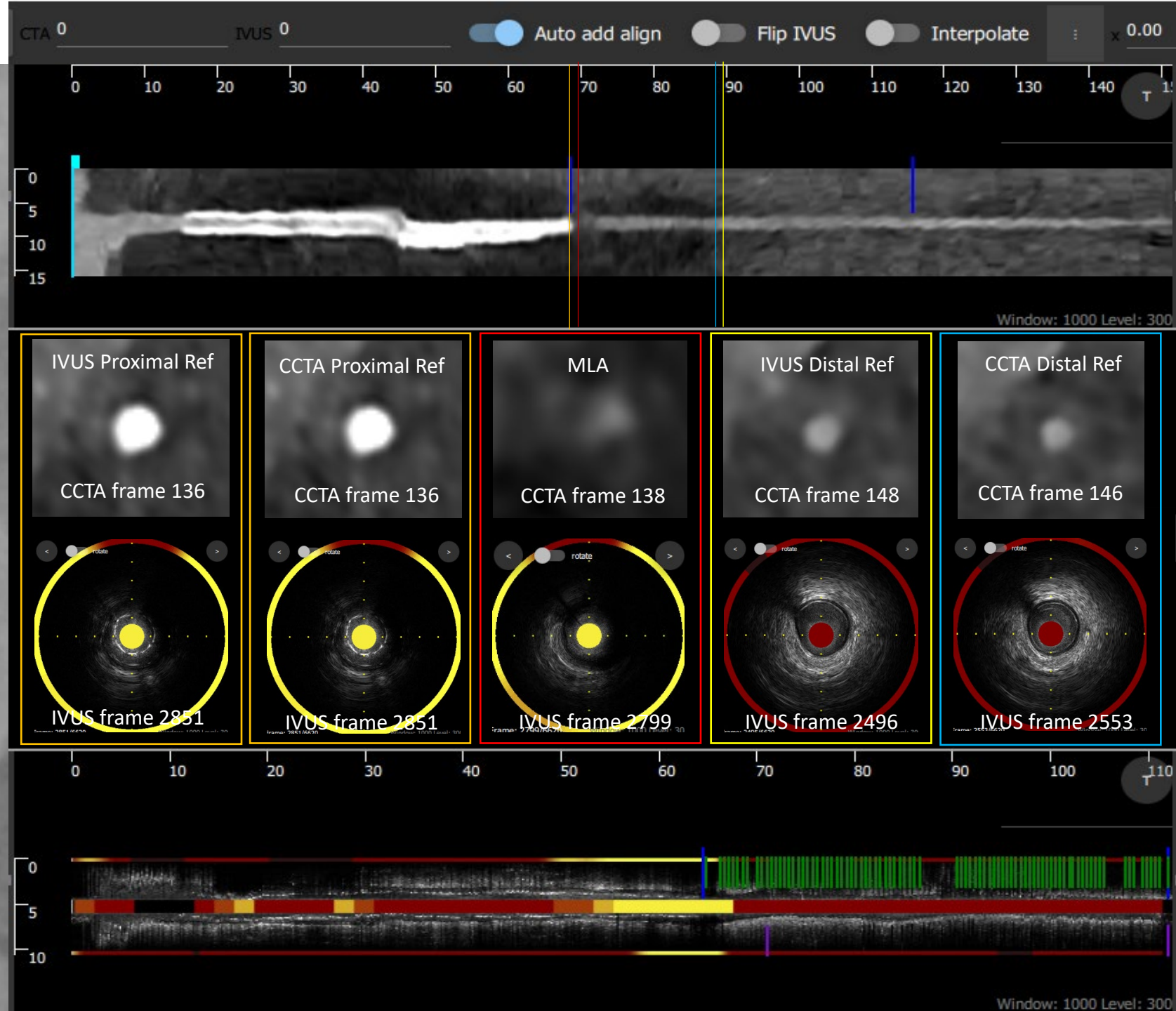
CTA 0
IVUS 0
Auto add align
Flip IVUS
Interpolate
0.00
0 10 20 30 40 50 60 70 80 90 100 110 120 130 140
0 5 10 15
Window: 1000 Level: 300
IVUS Proximal Ref
CCTA frame 136
IVUS frame 2851
CCTA Proximal Ref
CCTA frame 136
IVUS frame 2851
MLA
CCTA frame 138
IVUS frame 2799
IVUS Distal Ref
CCTA frame 148
IVUS frame 2496
CCTA Distal Ref
CCTA frame 146
IVUS frame 2553
0 10 20 30 40 50 60 70 80 90 100 110
0 5 10
Window: 1000 Level: 300

Case 21


Treated lesion

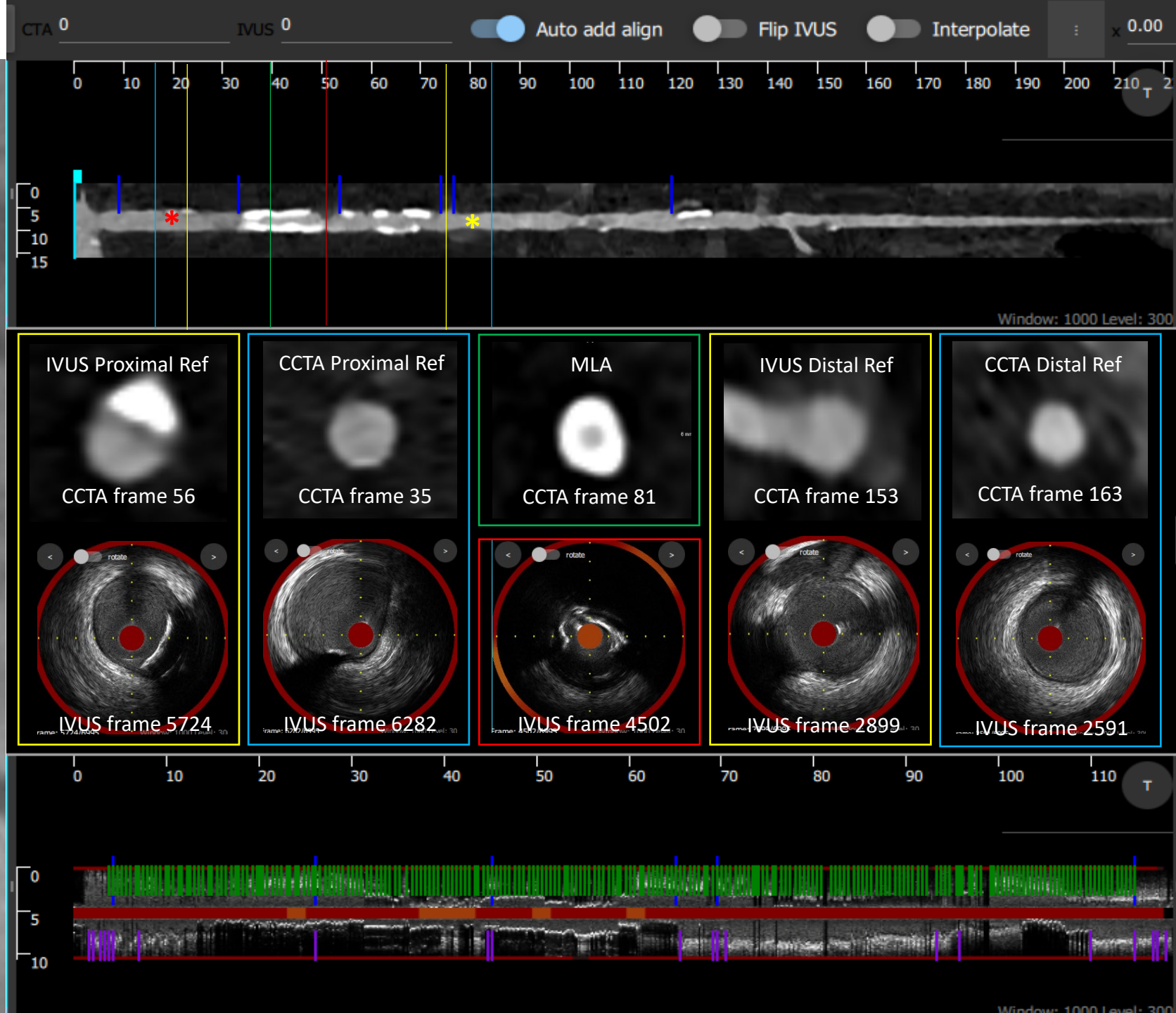
CTA 0
IVUS 0
Auto add align
Flip IVUS
Interpolate
0.00
0 10 20 30 40 50 60 70 80 90 100 110 120 130 140 150 160 170 180 190 200 210
0 5 10 15
Window: 1000 Level: 300
IVUS Proximal Ref
CCTA frame 56
IVUS frame 5724
CCTA Proximal Ref
CCTA frame 35
IVUS frame 6282
MLA
CCTA frame 81
IVUS frame 4502
IVUS Distal Ref
CCTA frame 153
IVUS frame 2899
CCTA Distal Ref
CCTA frame 163
IVUS frame 2591
0 10 20 30 40 50 60 70 80 90 100 110
0 5 10
Window: 1000 Level: 300

Case 22

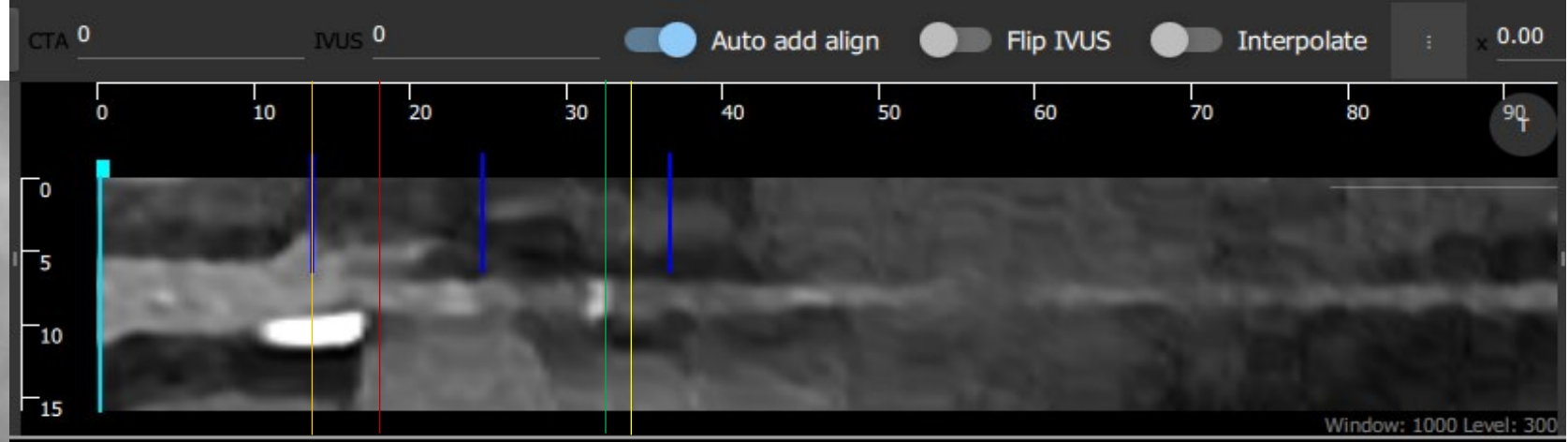

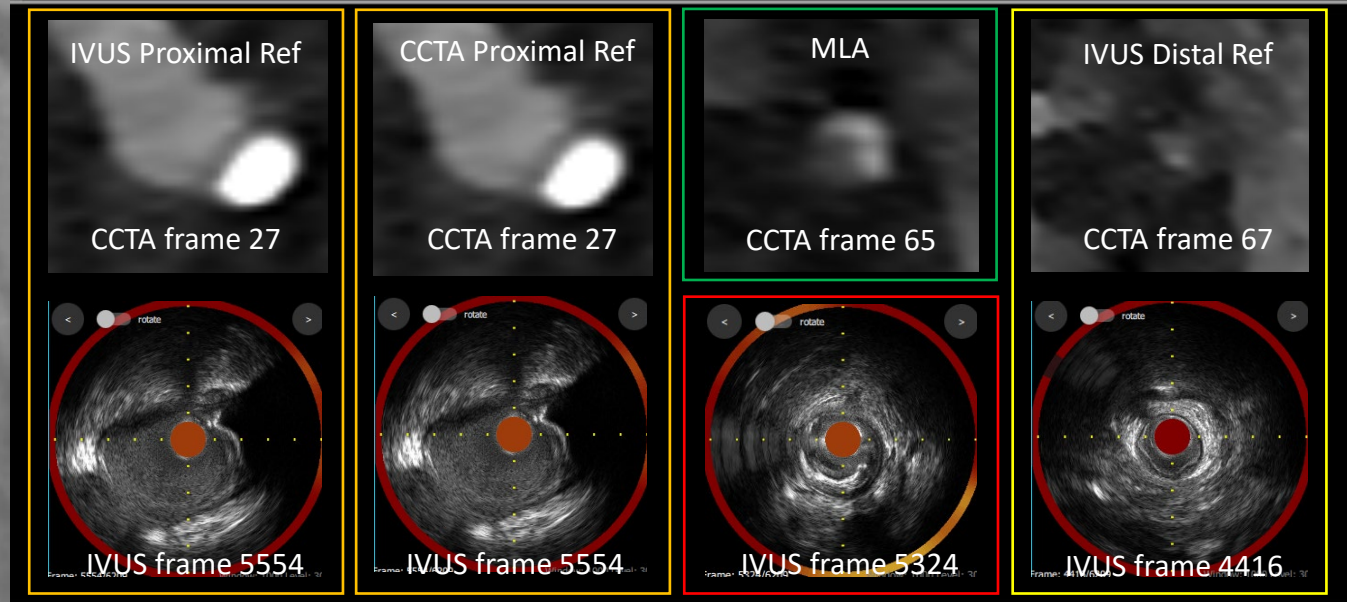

Very poor CT image quality (sub-totally occluded LAD at the time of CTCA image acquisition) did not allow accurate assessment of distal reference areas

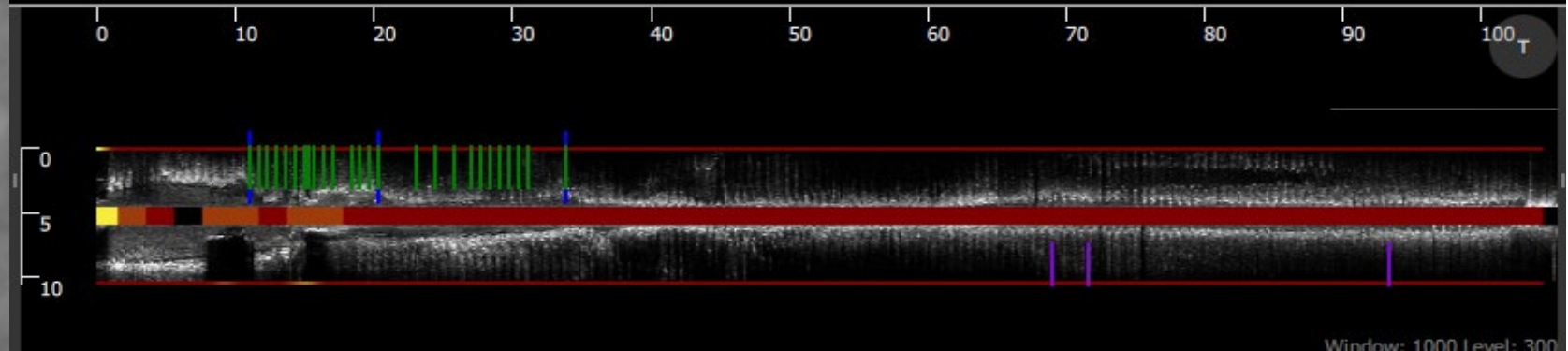

Case 23

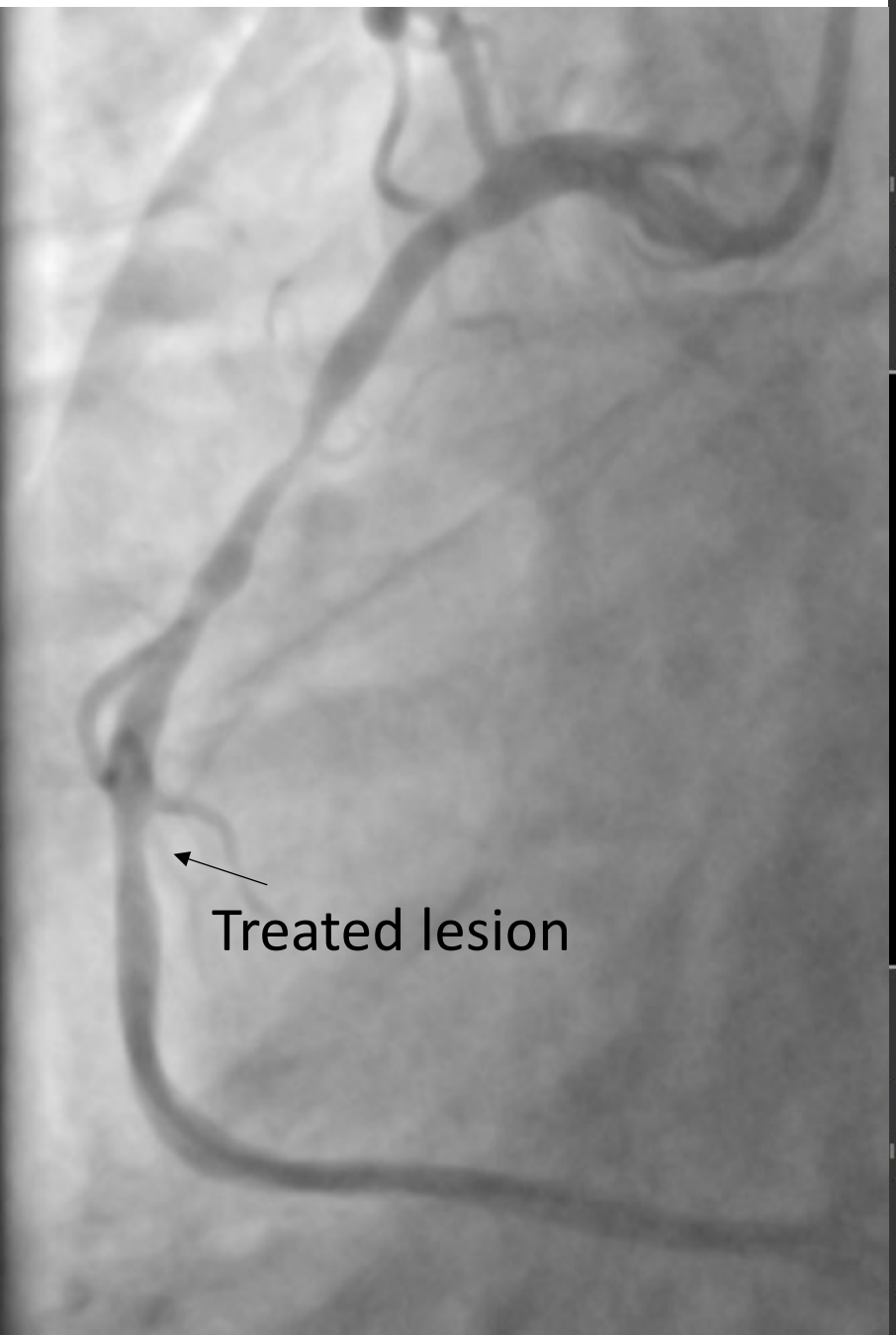
Treated lesion

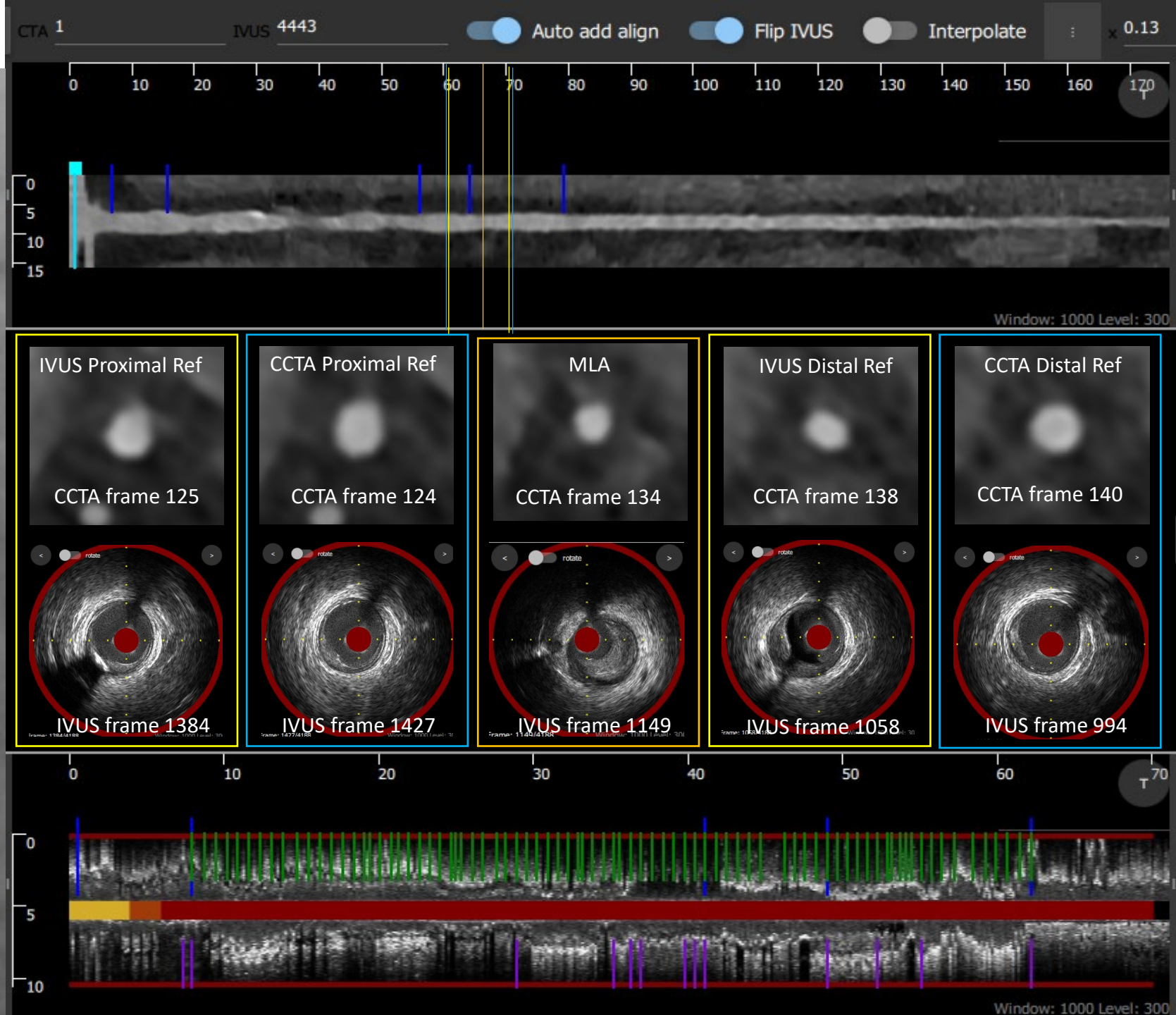
CTA 1
IVUS 4443
Auto add align
Flip IVUS
Interpolate
0.13
Window: 1000 Level: 300
IVUS Proximal Ref
CCTA frame 125
IVUS frame 1384
CCTA Proximal Ref
CCTA frame 124
IVUS frame 1427
MLA
CCTA frame 134
IVUS frame 1149
IVUS Distal Ref
CCTA frame 138
IVUS frame 1058
CCTA Distal Ref
CCTA frame 140
IVUS frame 994
Window: 1000 Level: 300

Case 24


Treated lesion

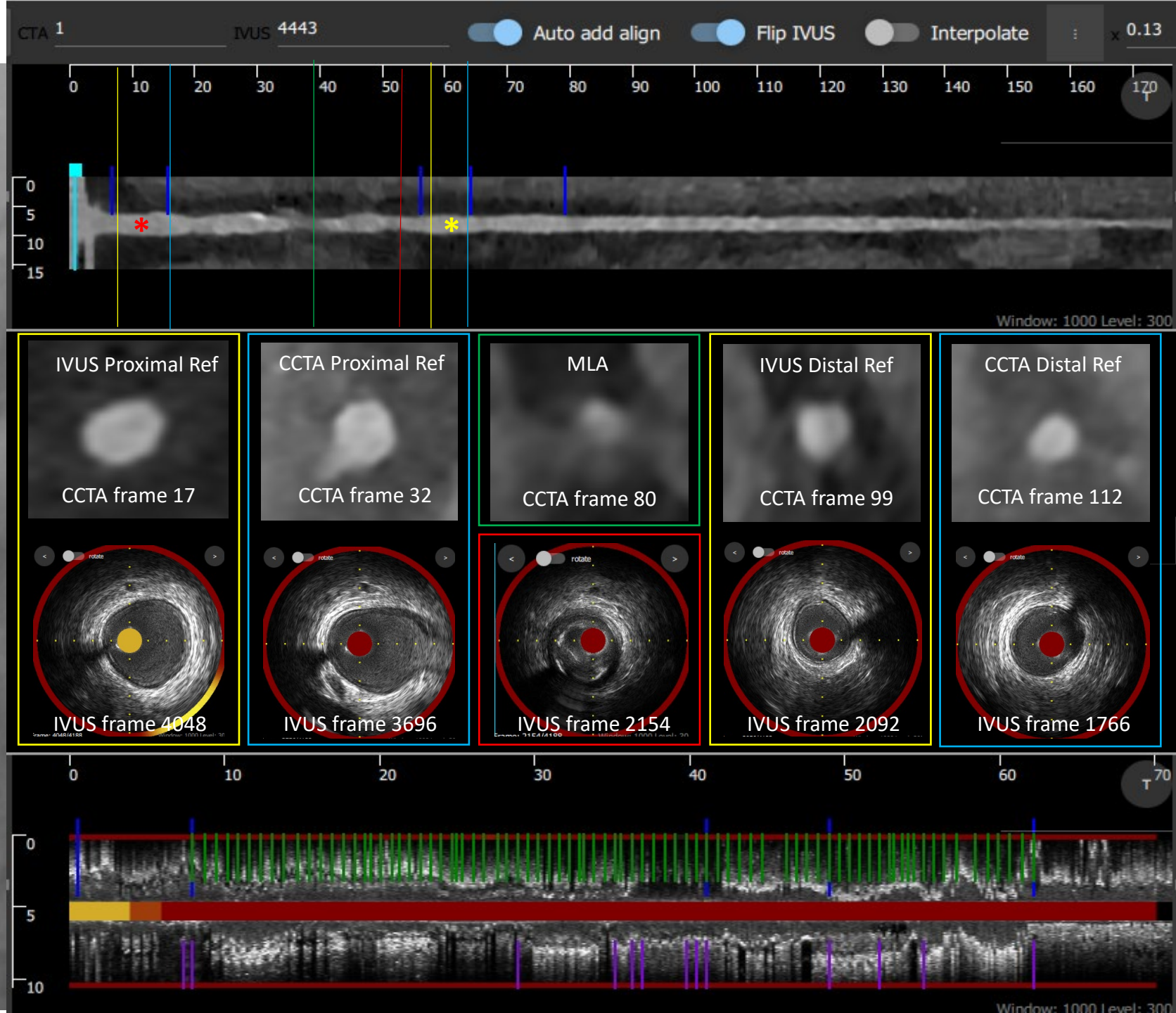
CTA 1
IVUS 4443
Auto add align
Flip IVUS
Interpolate
0.13
Window: 1000 Level: 300
IVUS Proximal Ref
CCTA frame 17
IVUS frame 4048
CCTA Proximal Ref
CCTA frame 32
IVUS frame 3696
MLA
CCTA frame 80
IVUS frame 2154
IVUS Distal Ref
CCTA frame 99
IVUS frame 2092
CCTA Distal Ref
CCTA frame 112
IVUS frame 1766
Window: 1000 Level: 300

Case 25


Treated lesion


CTA 0
IVUS 0
Auto add align
Flip IVUS
Interpolate
0.00
Window: 1000 Level: 300
IVUS Proximal Ref
CCTA frame 23
IVUS frame 3533
CCTA Proximal Ref
CCTA frame 26
IVUS frame 3433
MLA
CCTA frame 85
IVUS frame 1496
IVUS Distal Ref
CCTA frame 99
IVUS frame 1320
CCTA Distal Ref
CCTA frame 99
IVUS frame 1320
Window: 1000 Level: 300

Case 26

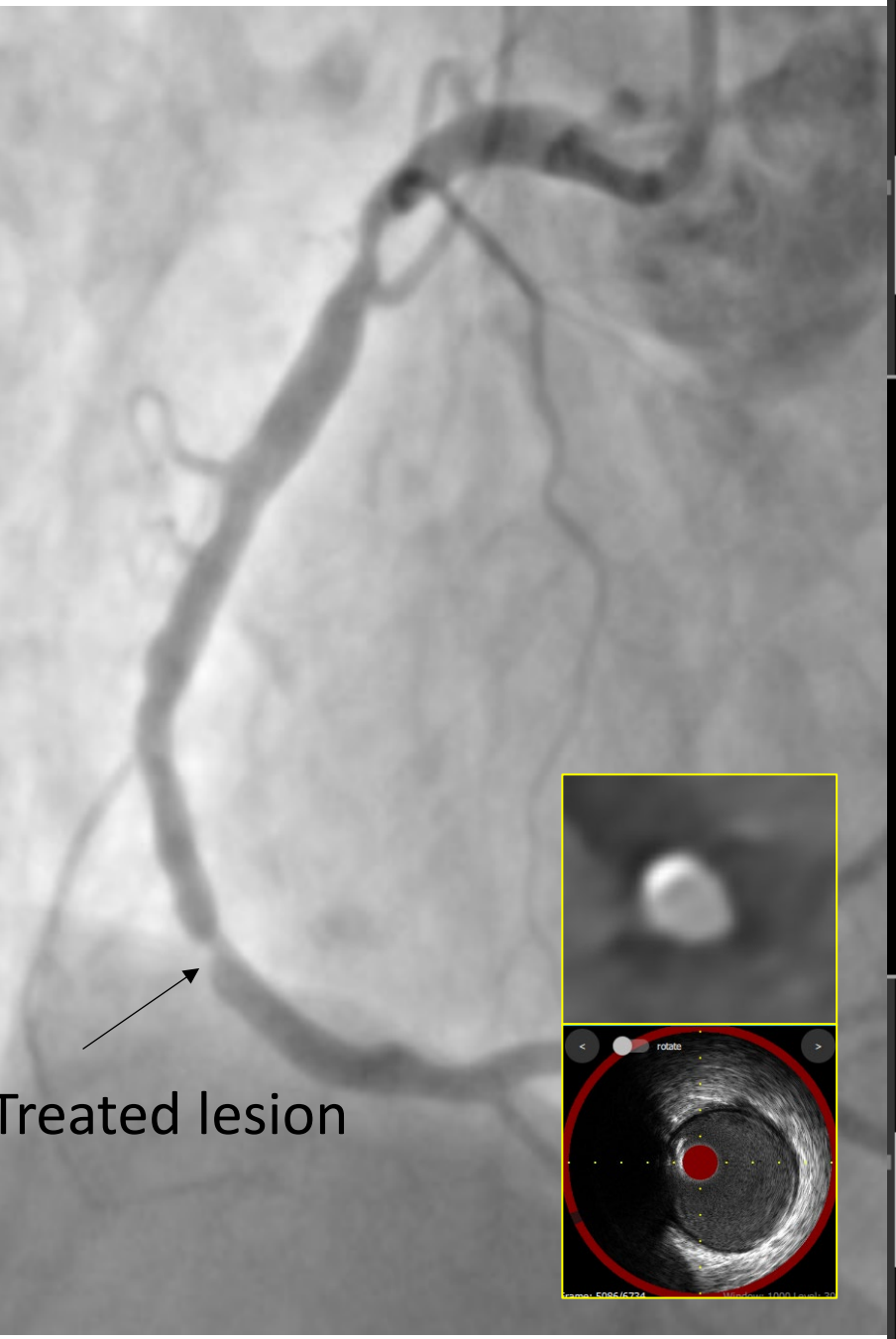
Treated lesion

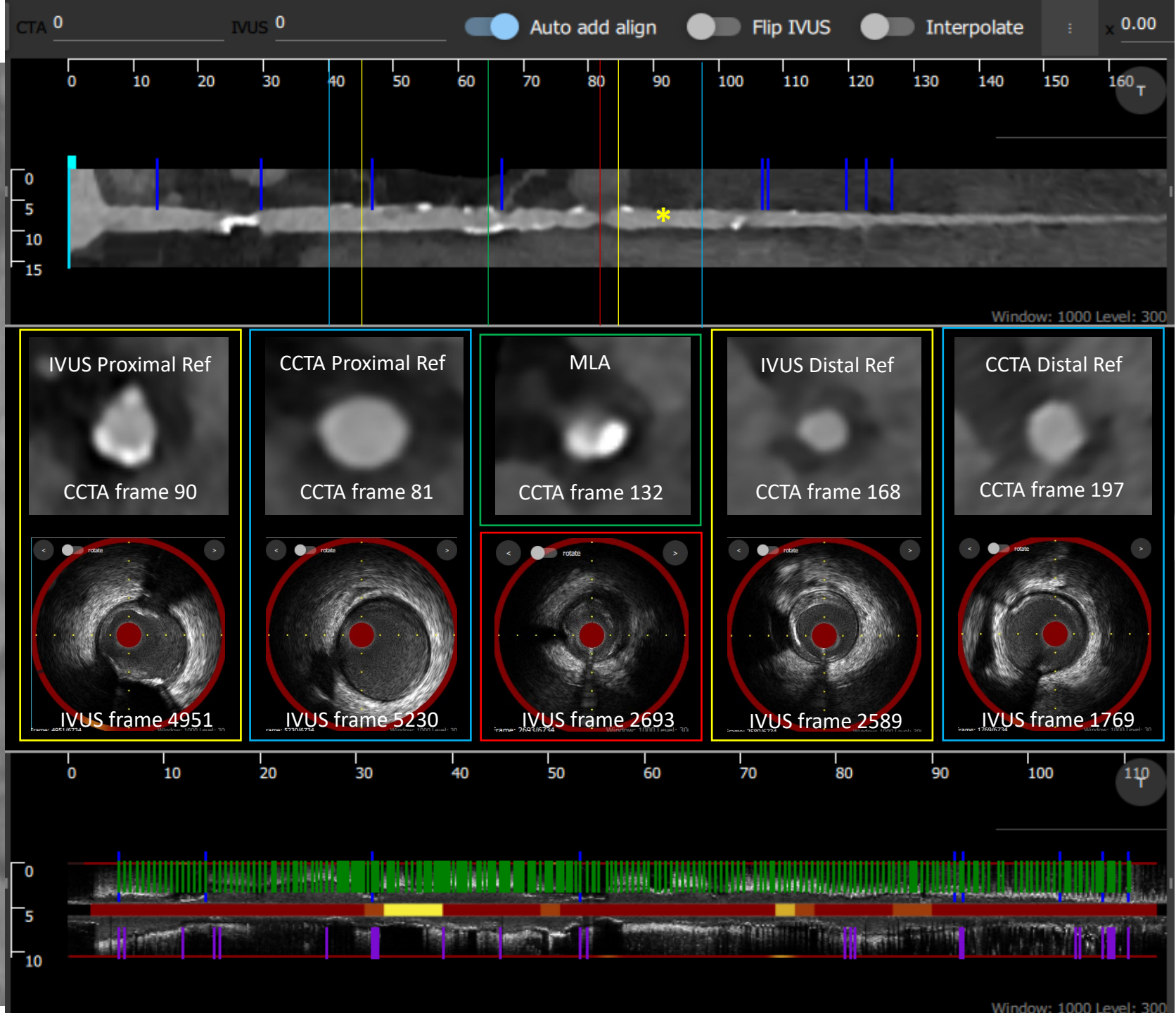
CTA 0
IVUS 0
Auto add align
Flip IVUS
Interpolate
0.00
0 10 20 30 40 50 60 70 80 90 100 110 120 130 140 150 160
0 5 10 15
Window: 1000 Level: 300
IVUS Proximal Ref
CCTA frame 90
IVUS frame 4951
CCTA Proximal Ref
CCTA frame 81
IVUS frame 5230
MLA
CCTA frame 132
IVUS frame 2693
IVUS Distal Ref
CCTA frame 168
IVUS frame 2589
CCTA Distal Ref
CCTA frame 197
IVUS frame 1769
0 10 20 30 40 50 60 70 80 90 100 110
0 5 10
Window: 1000 Level: 300

Case 27

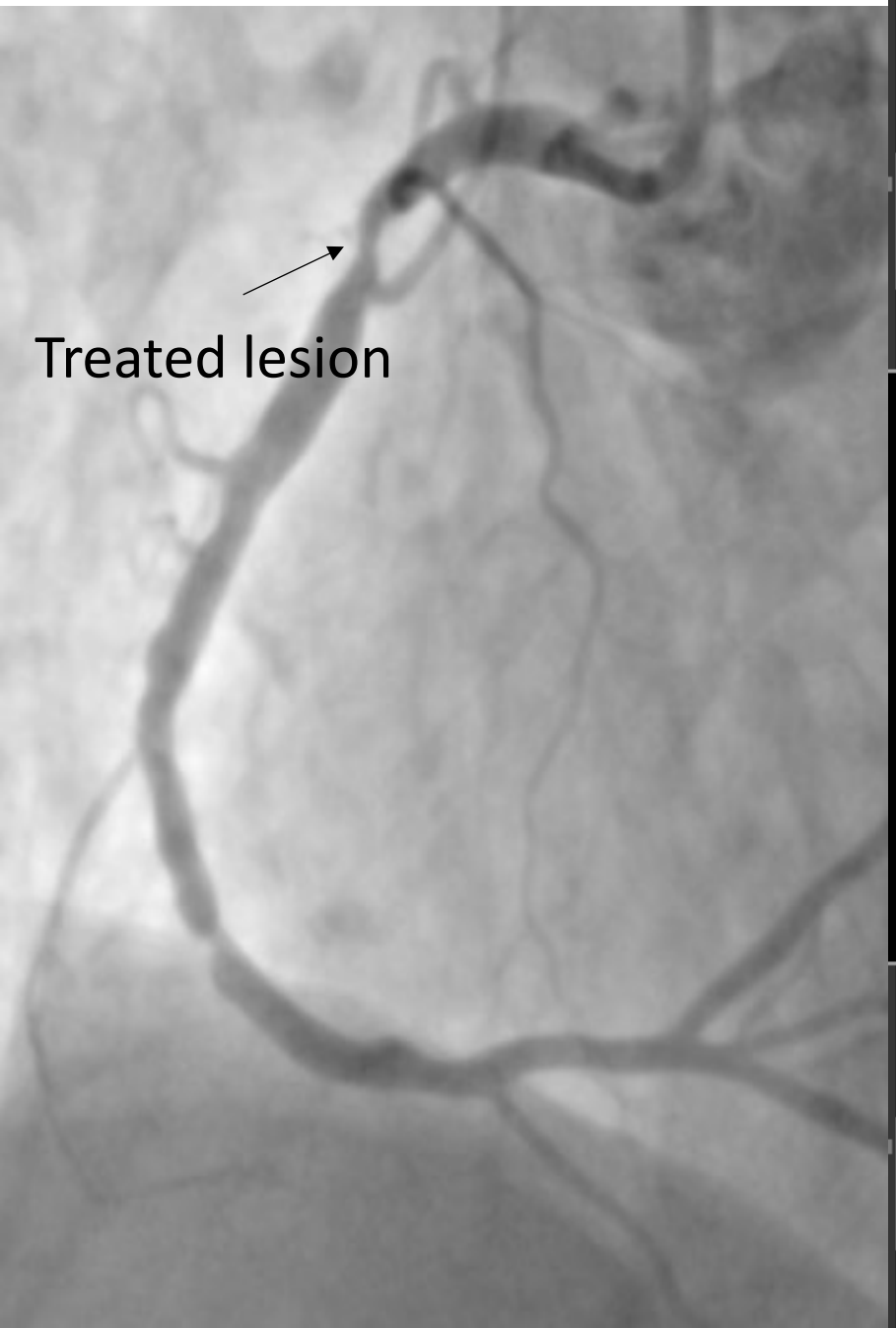
Treated lesion

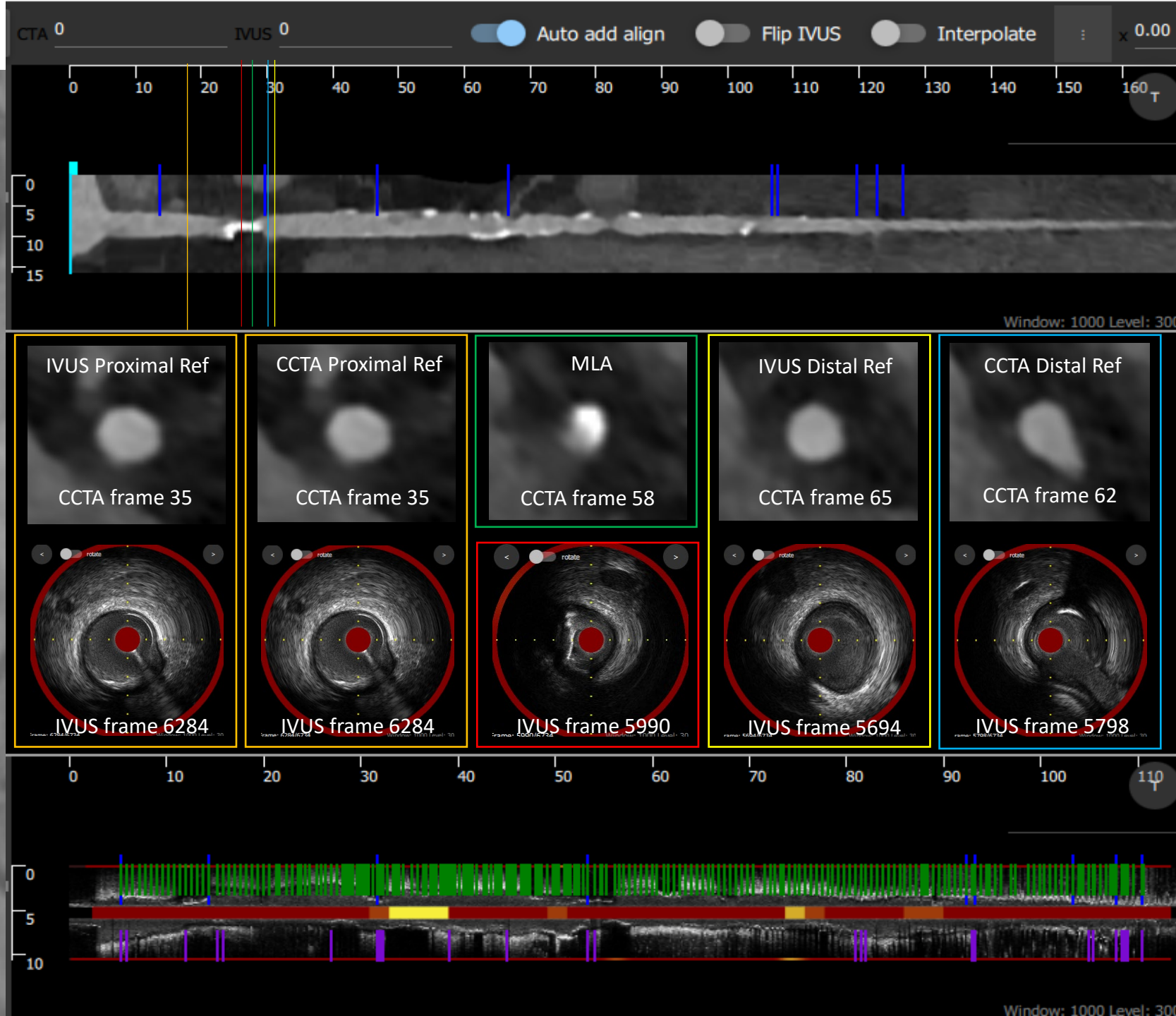
CTA 0
IVUS 0
Auto add align
Flip IVUS
Interpolate
0.00
0 10 20 30 40 50 60 70 80 90 100 110 120 130 140 150 160
0 5 10 15
Window: 1000 Level: 300
IVUS Proximal Ref
CCTA frame 35
IVUS frame 6284
CCTA Proximal Ref
CCTA frame 35
IVUS frame 6284
MLA
CCTA frame 58
IVUS frame 5990
IVUS Distal Ref
CCTA frame 65
IVUS frame 5694
CCTA Distal Ref
CCTA frame 62
IVUS frame 5798
0 10 20 30 40 50 60 70 80 90 100 110
0 5 10
Window: 1000 Level: 300

Case 28

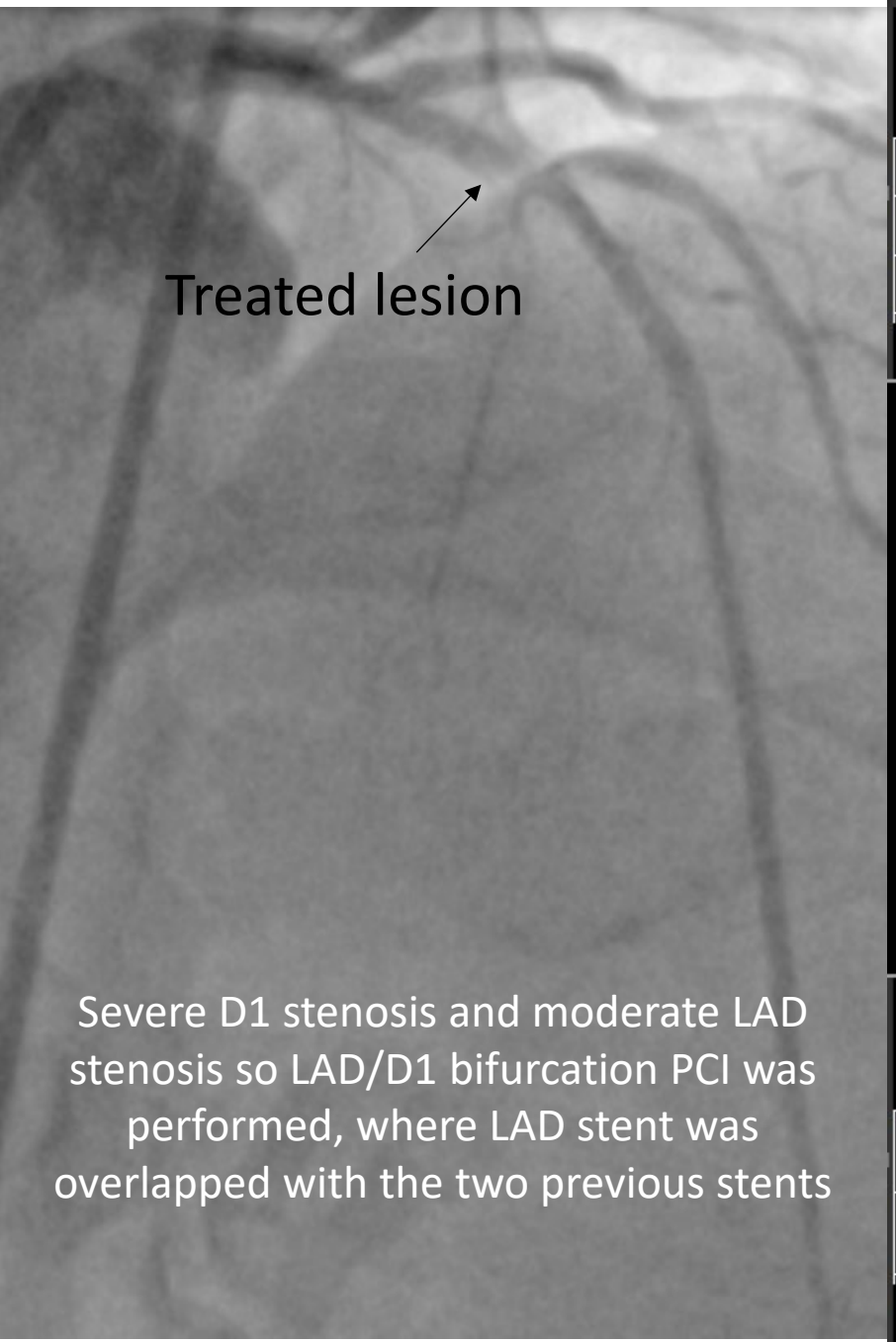

Severe D1 stenosis and moderate LAD stenosis so LAD/D1 bifurcation PCI was performed, where LAD stent was overlapped with the two previous stents

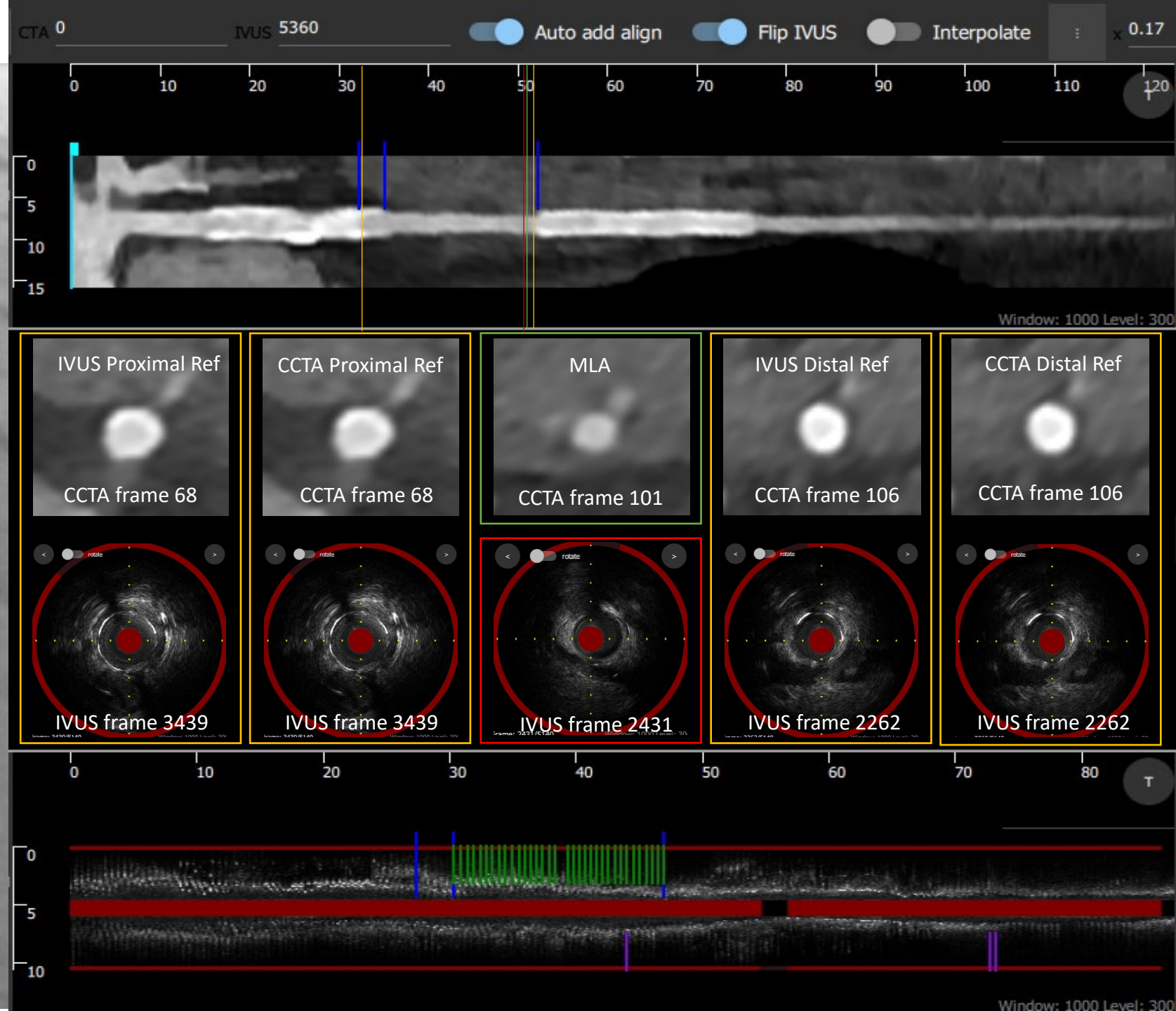

Case 29

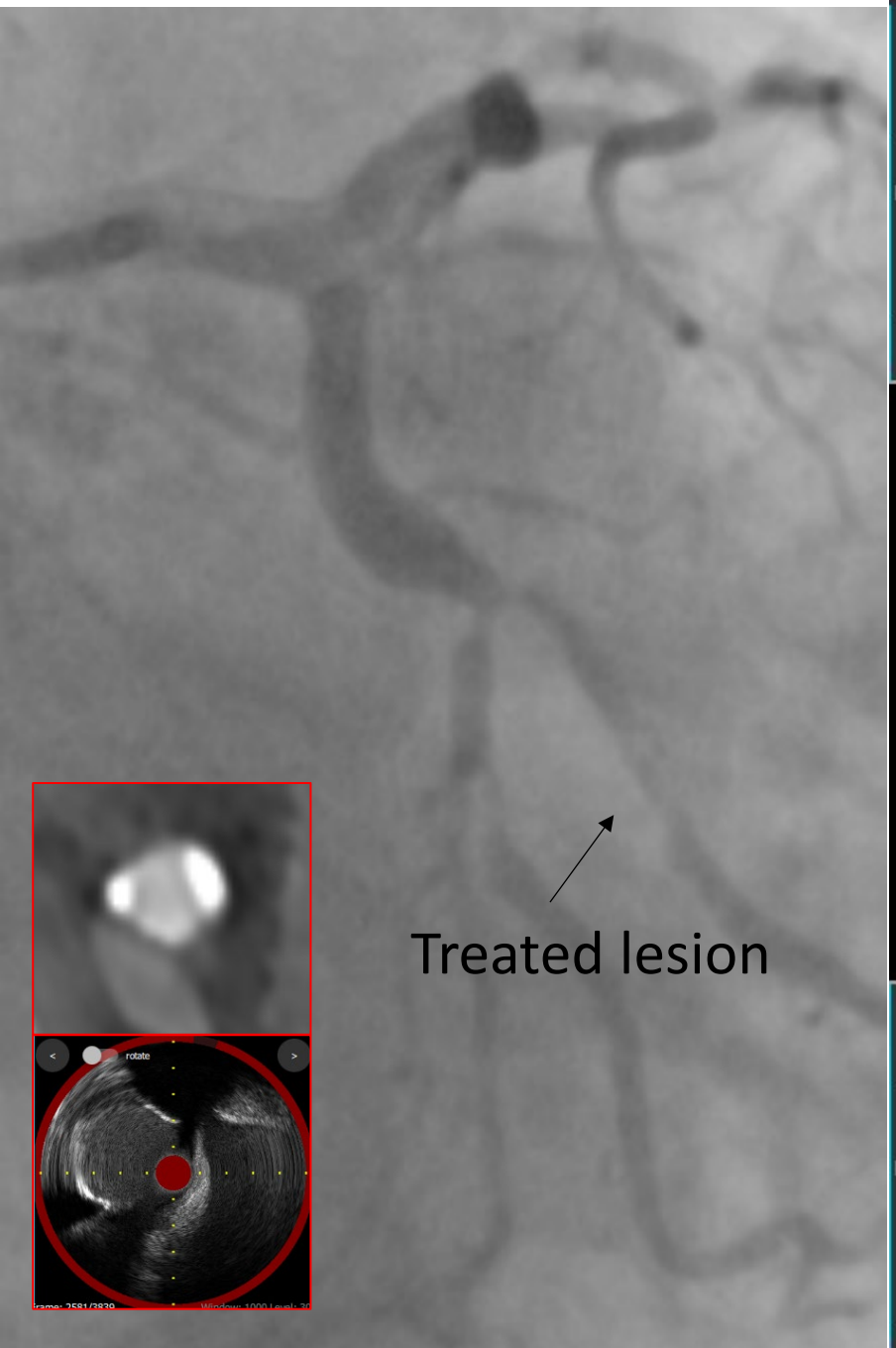
Treated lesion

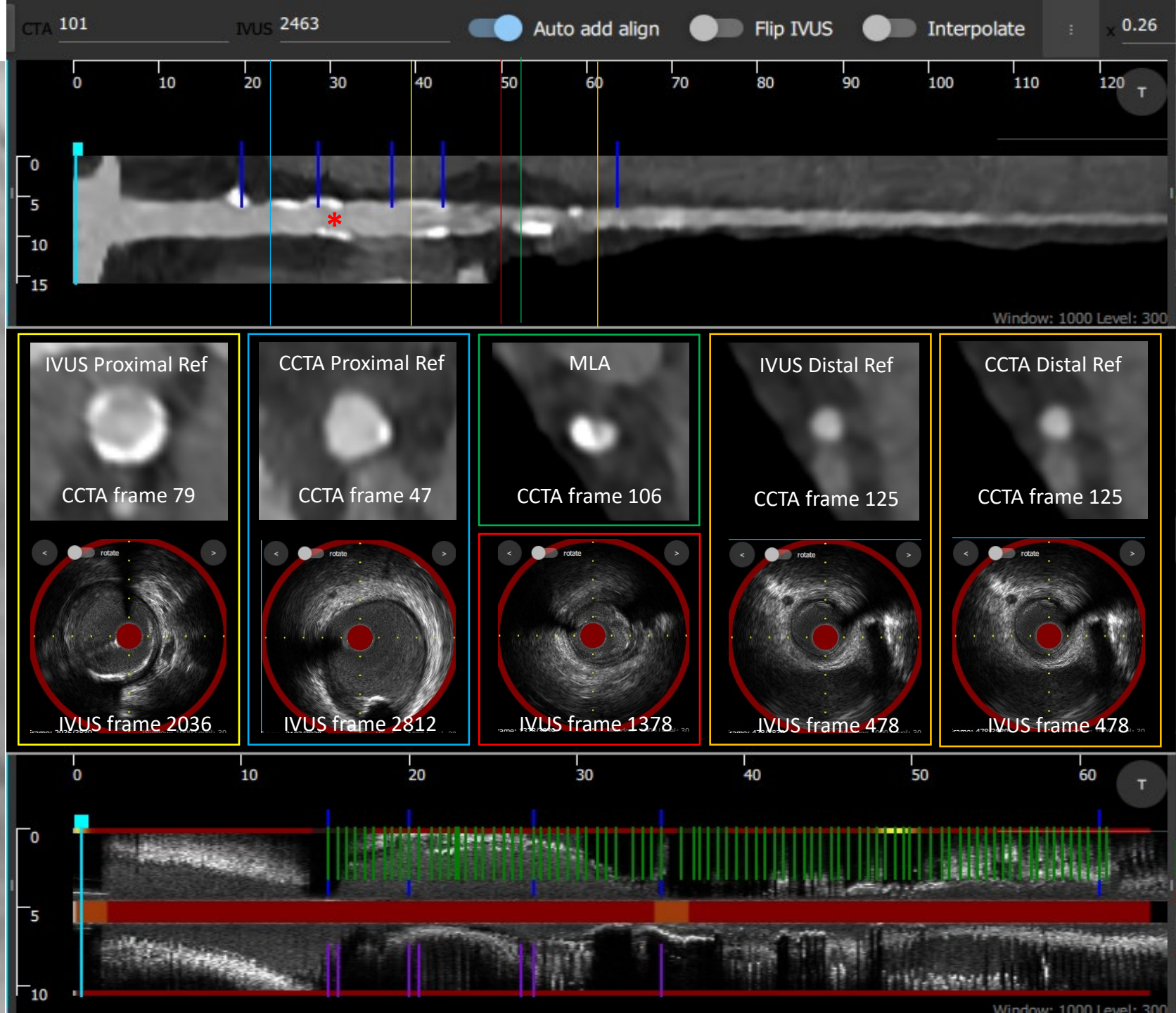
CTA 101
IVUS 2463
Auto add align
Flip IVUS
Interpolate
0.26
Window: 1000 Level: 300
IVUS Proximal Ref
CCTA frame 79
IVUS frame 2036
CCTA Proximal Ref
CCTA frame 47
IVUS frame 2812
MLA
CCTA frame 106
IVUS frame 1378
IVUS Distal Ref
CCTA frame 125
IVUS frame 478
CCTA Distal Ref
CCTA frame 125
IVUS frame 478

Case 30


Treated lesion

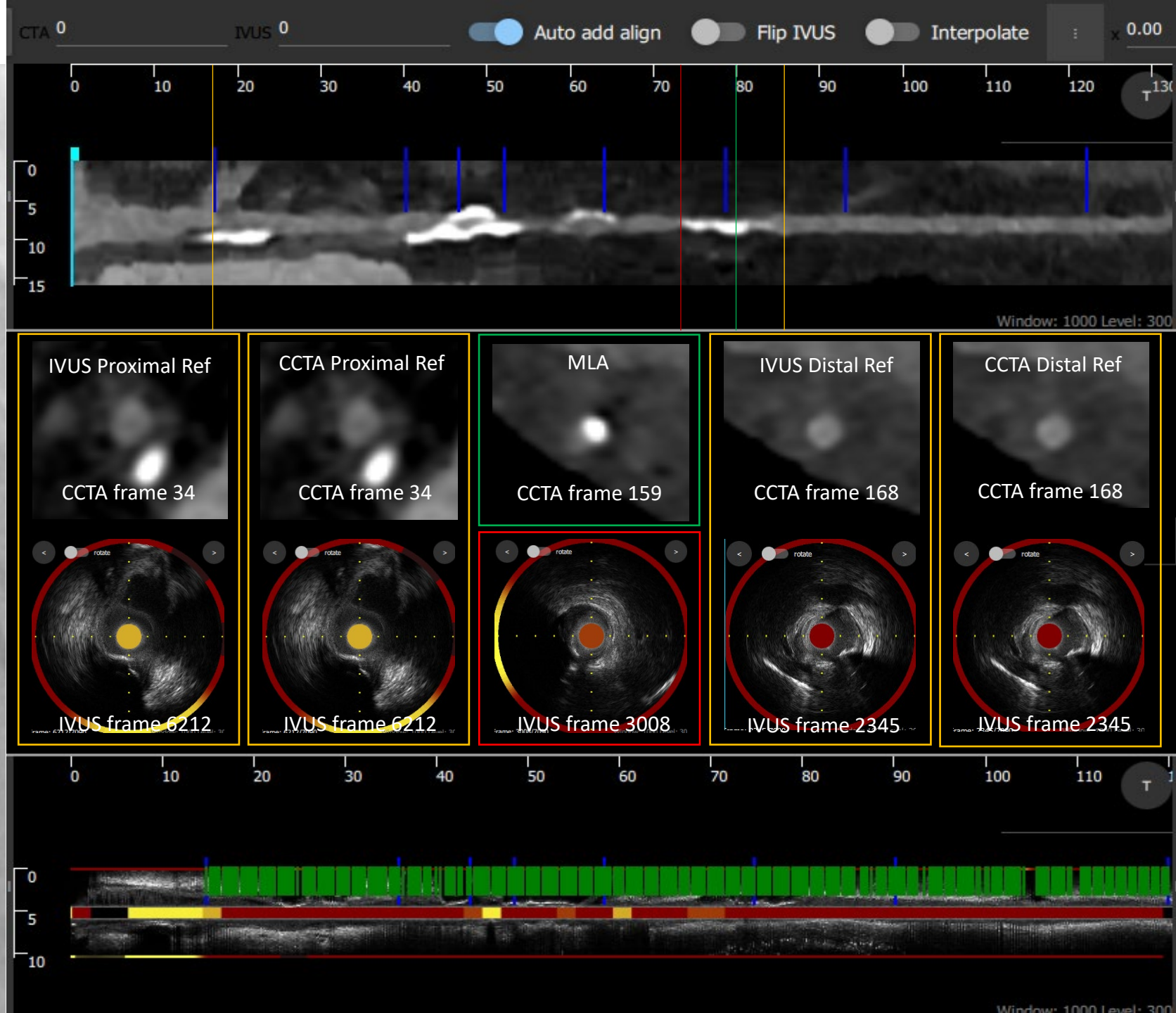
CTA 0
IVUS 0
Auto add align
Flip IVUS
Interpolate
0.00
0 10 20 30 40 50 60 70 80 90 100 110 120
0 5 10 15
Window: 1000 Level: 300
IVUS Proximal Ref
CCTA frame 34
IVUS frame 6212
CCTA Proximal Ref
CCTA frame 34
IVUS frame 6212
MLA
CCTA frame 159
IVUS frame 3008
IVUS Distal Ref
CCTA frame 168
IVUS frame 2345
CCTA Distal Ref
CCTA frame 168
IVUS frame 2345
0 10 20 30 40 50 60 70 80 90 100 110
0 5 10

Case 31

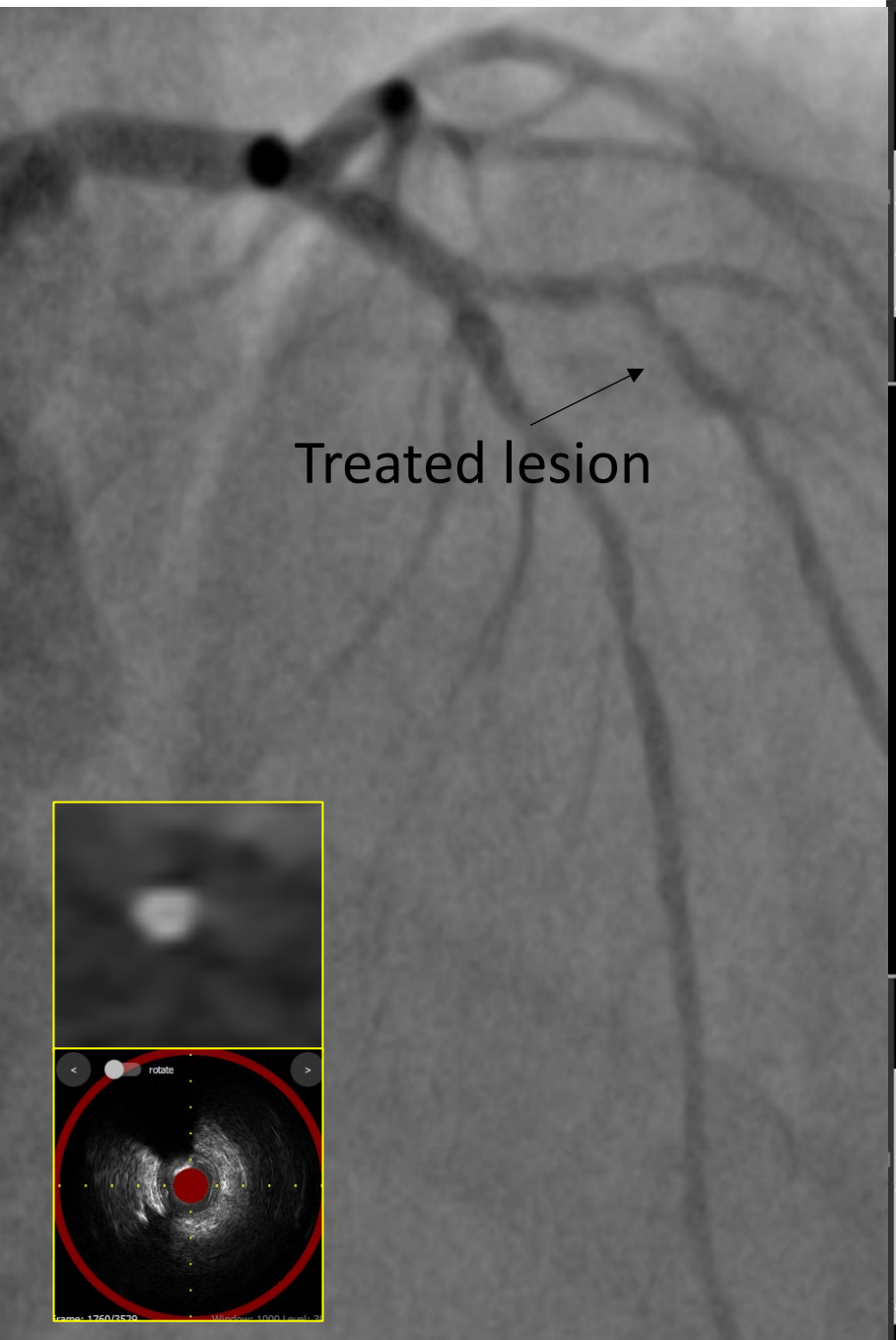
Treated lesion

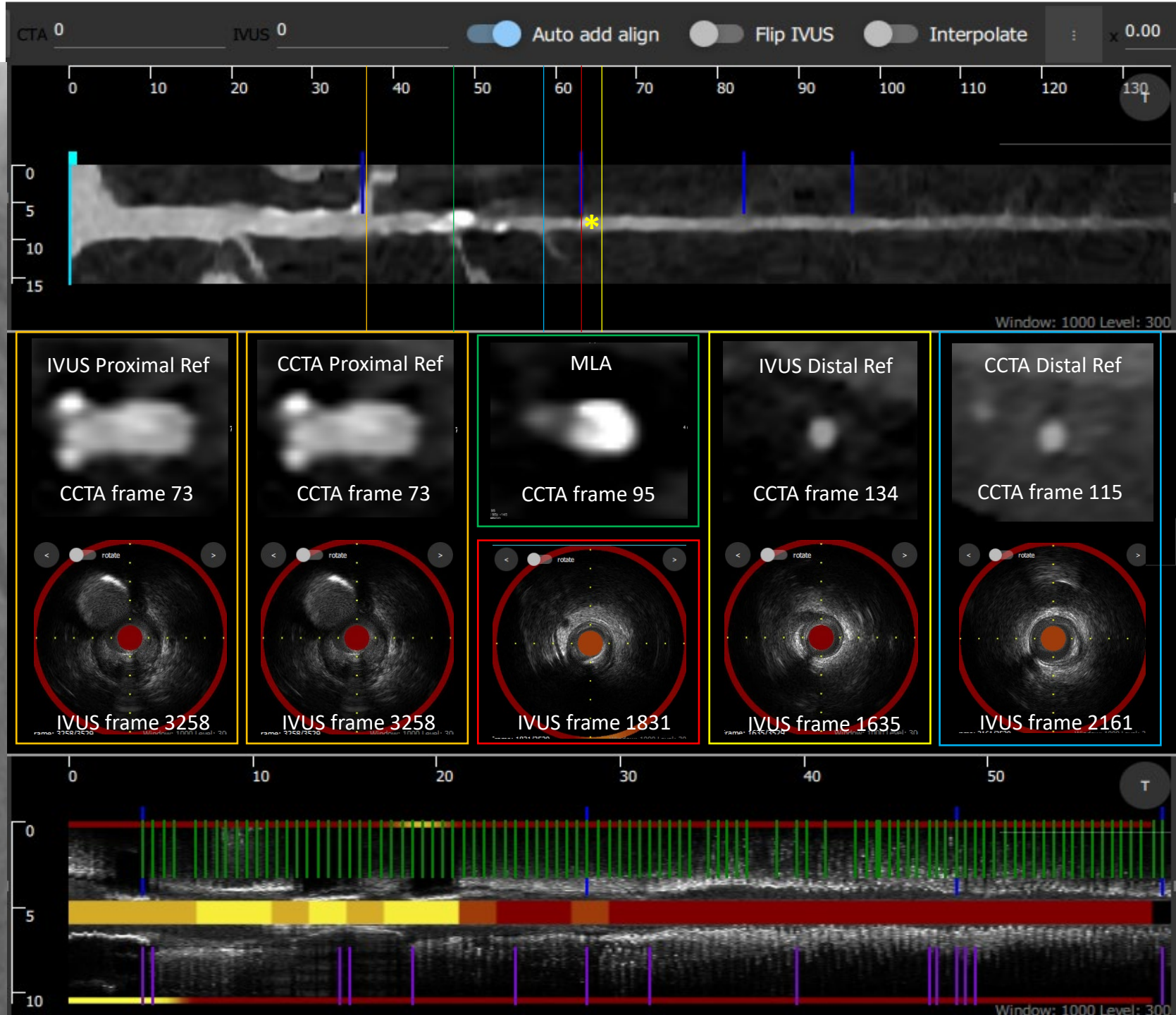
CTA 0
IVUS 0
Auto add align
Flip IVUS
Interpolate
0.00
Window: 1000 Level: 300
IVUS Proximal Ref
CCTA frame 73
IVUS frame 3258
CCTA Proximal Ref
CCTA frame 73
IVUS frame 3258
MLA
CCTA frame 95
IVUS frame 1831
IVUS Distal Ref
CCTA frame 134
IVUS frame 1635
CCTA Distal Ref
CCTA frame 115
IVUS frame 2161
Window: 1000 Level: 300

Case 32


Treated lesion

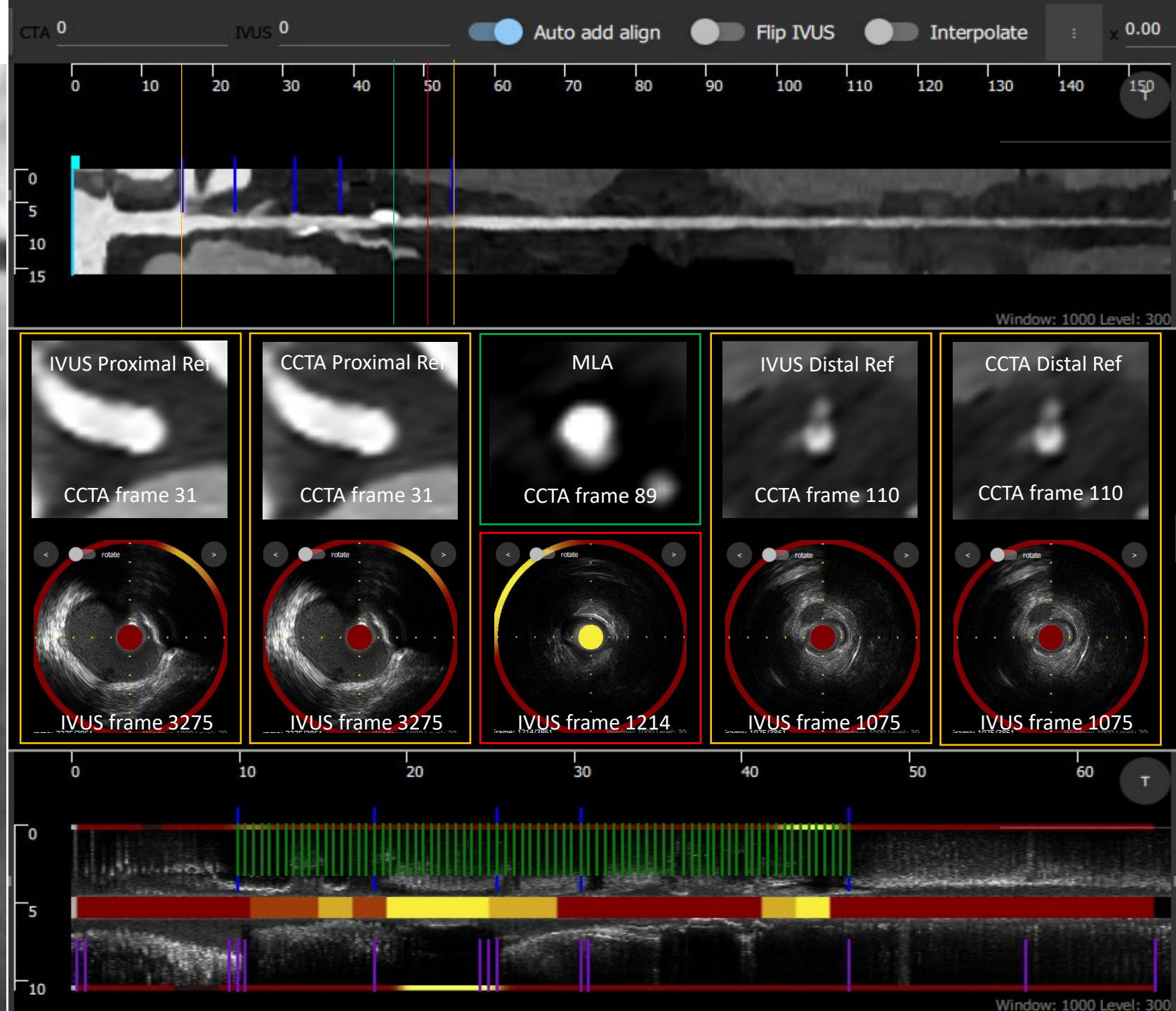
CTA 0
IVUS 0
Auto add align
Flip IVUS
Interpolate
0.00
Window: 1000 Level: 300
IVUS Proximal Ref
CCTA frame 31
IVUS frame 3275
CCTA Proximal Ref
CCTA frame 31
IVUS frame 3275
MLA
CCTA frame 89
IVUS frame 1214
IVUS Distal Ref
CCTA frame 110
IVUS frame 1075
CCTA Distal Ref
CCTA frame 110
IVUS frame 1075
Window: 1000 Level: 300

Case 35

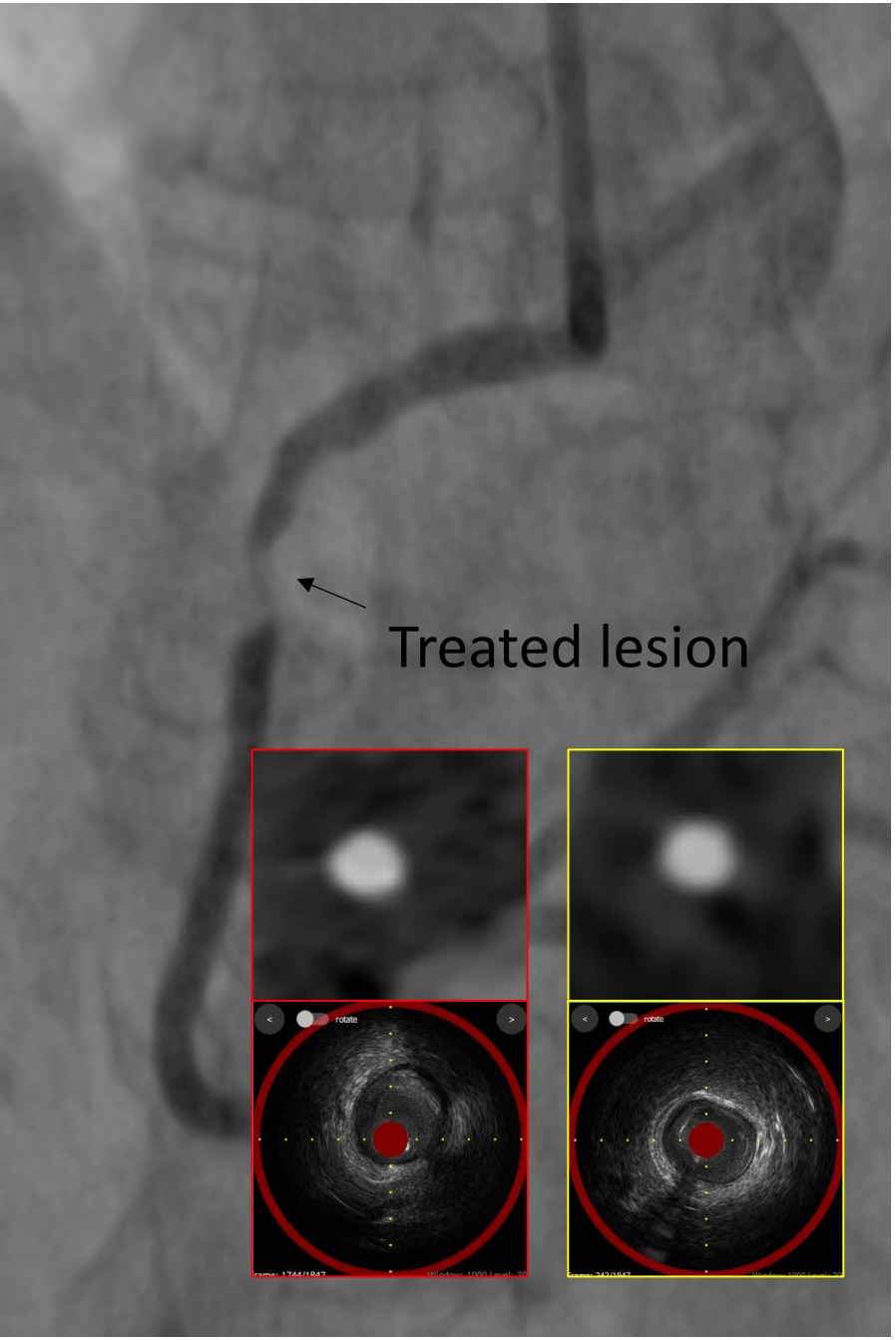
Treated lesion

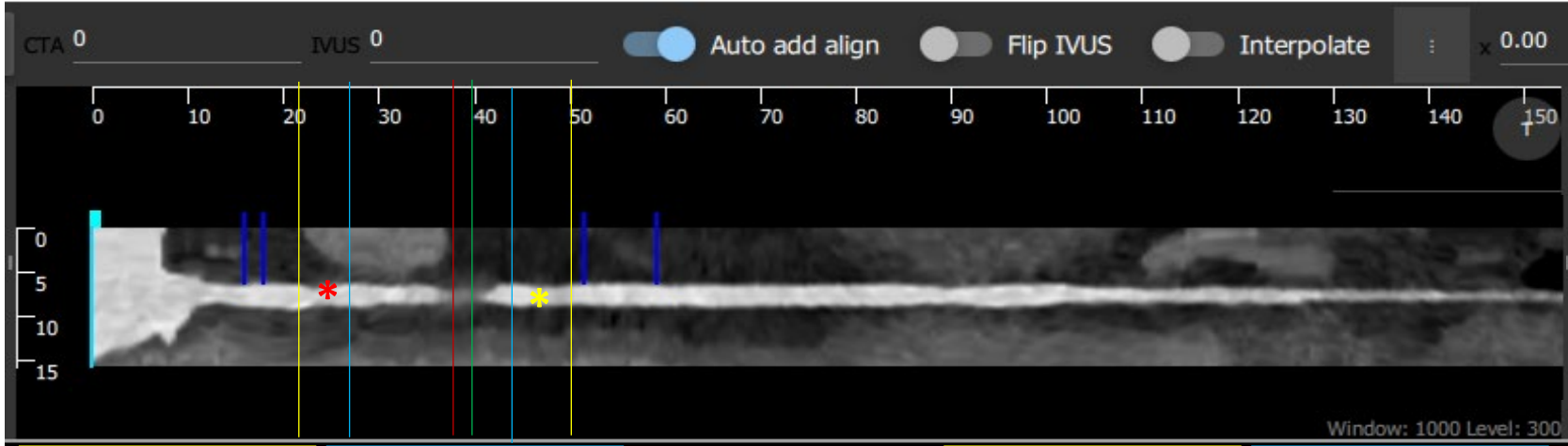
CTA 0
IVUS 0
Auto add align
Flip IVUS
Interpolate
0.00
0 10 20 30 40 50 60 70 80 90 100 110 120 130 140 150
0 5 10 15
Window: 1000 Level: 300

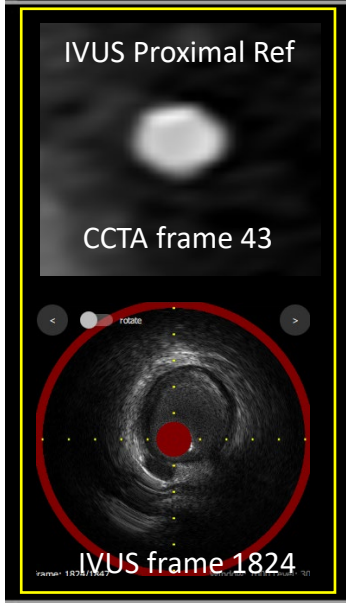
IVUS Proximal Ref
CCTA frame 43
IVUS frame 1824

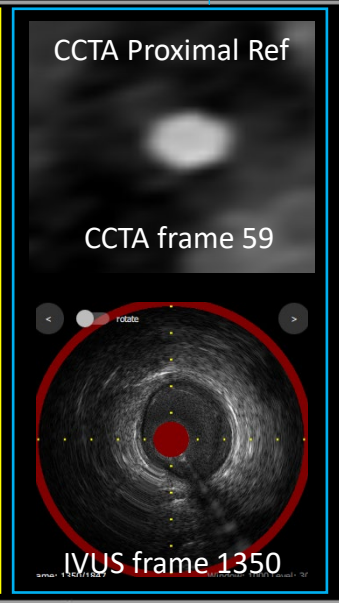
CCTA Proximal Ref
CCTA frame 59
IVUS frame 1350

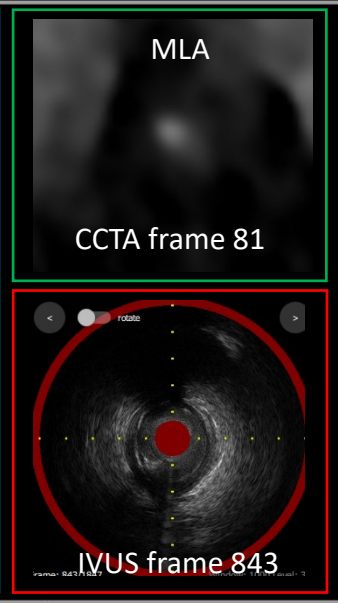
MLA
CCTA frame 81
IVUS frame 843

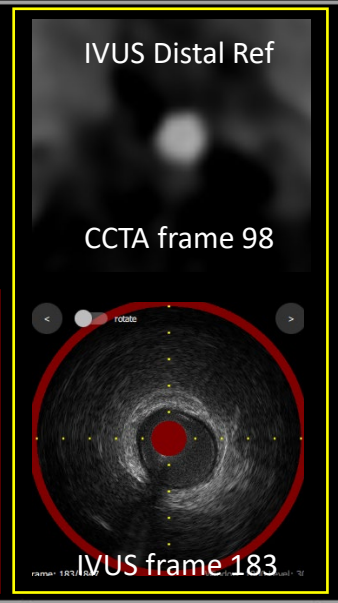
IVUS Distal Ref
CCTA frame 98
IVUS frame 183

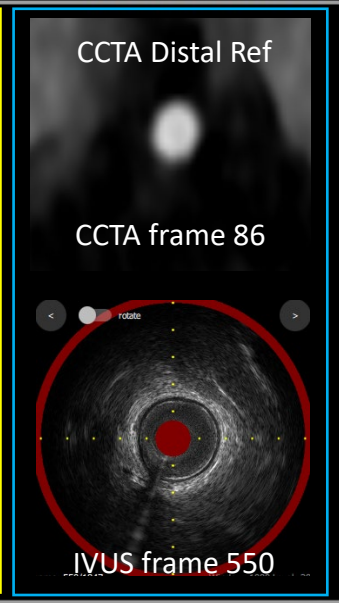
CCTA Distal Ref
CCTA frame 86
IVUS frame 550

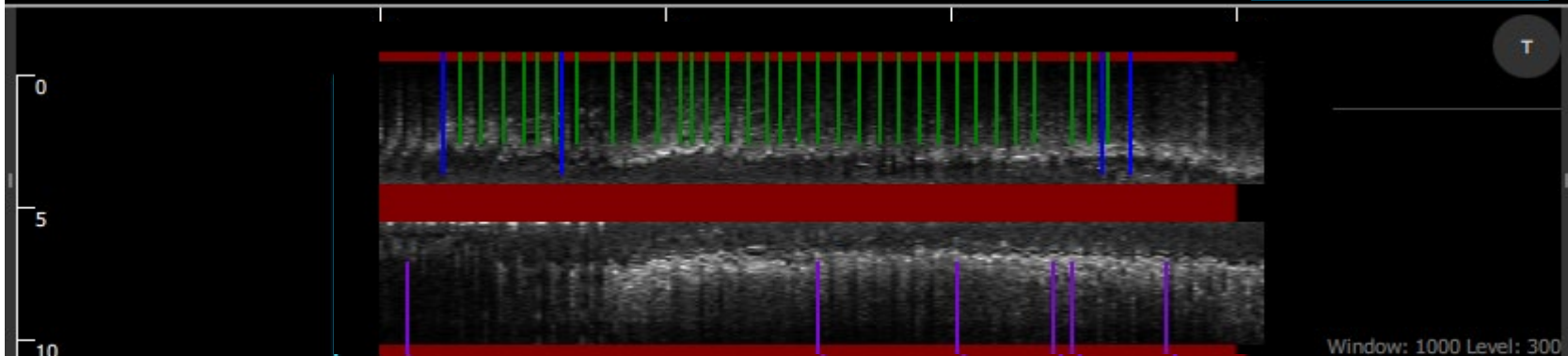
0
5
10
Window: 1000 Level: 300

Case 36


Treated lesion

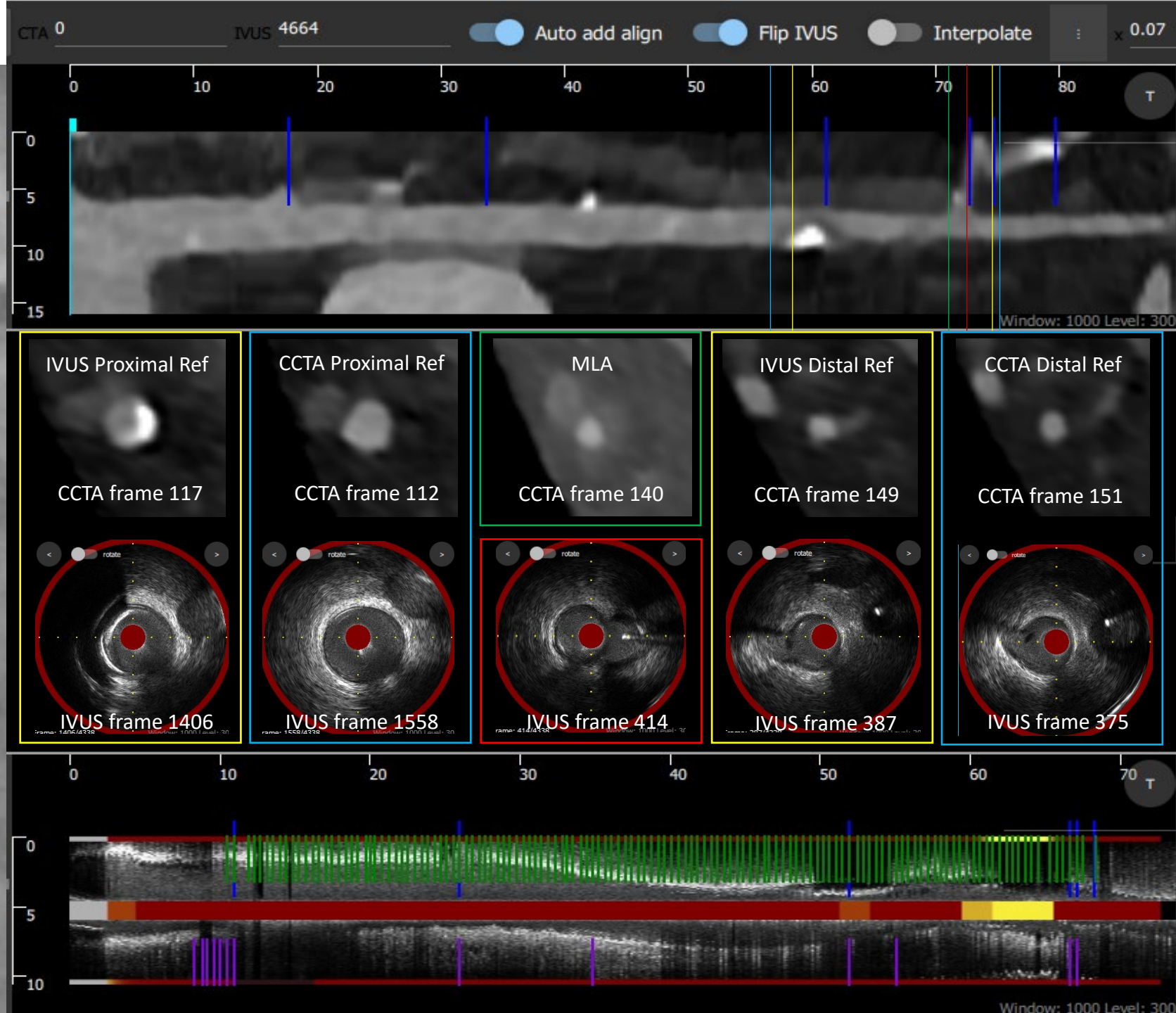
CTA 0
IVUS 4664
Auto add align
Flip IVUS
Interpolate
x 0.07
Window: 1000 Level: 300
IVUS Proximal Ref
CCTA frame 117
IVUS frame 1406
CCTA Proximal Ref
CCTA frame 112
IVUS frame 1558
MLA
CCTA frame 140
IVUS frame 414
IVUS Distal Ref
CCTA frame 149
IVUS frame 387
CCTA Distal Ref
CCTA frame 151
IVUS frame 375
Window: 1000 Level: 300

Case 35

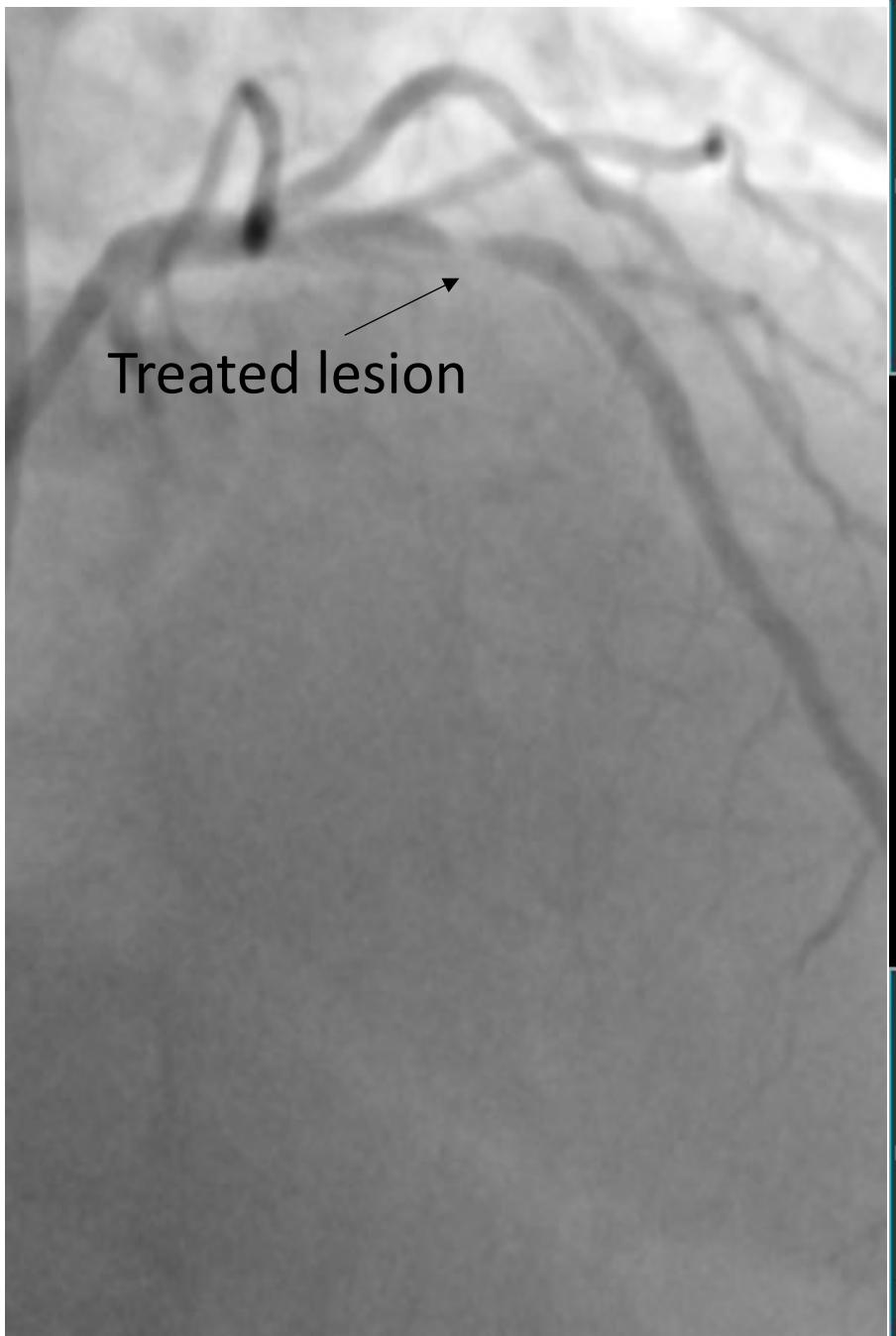
Treated lesion

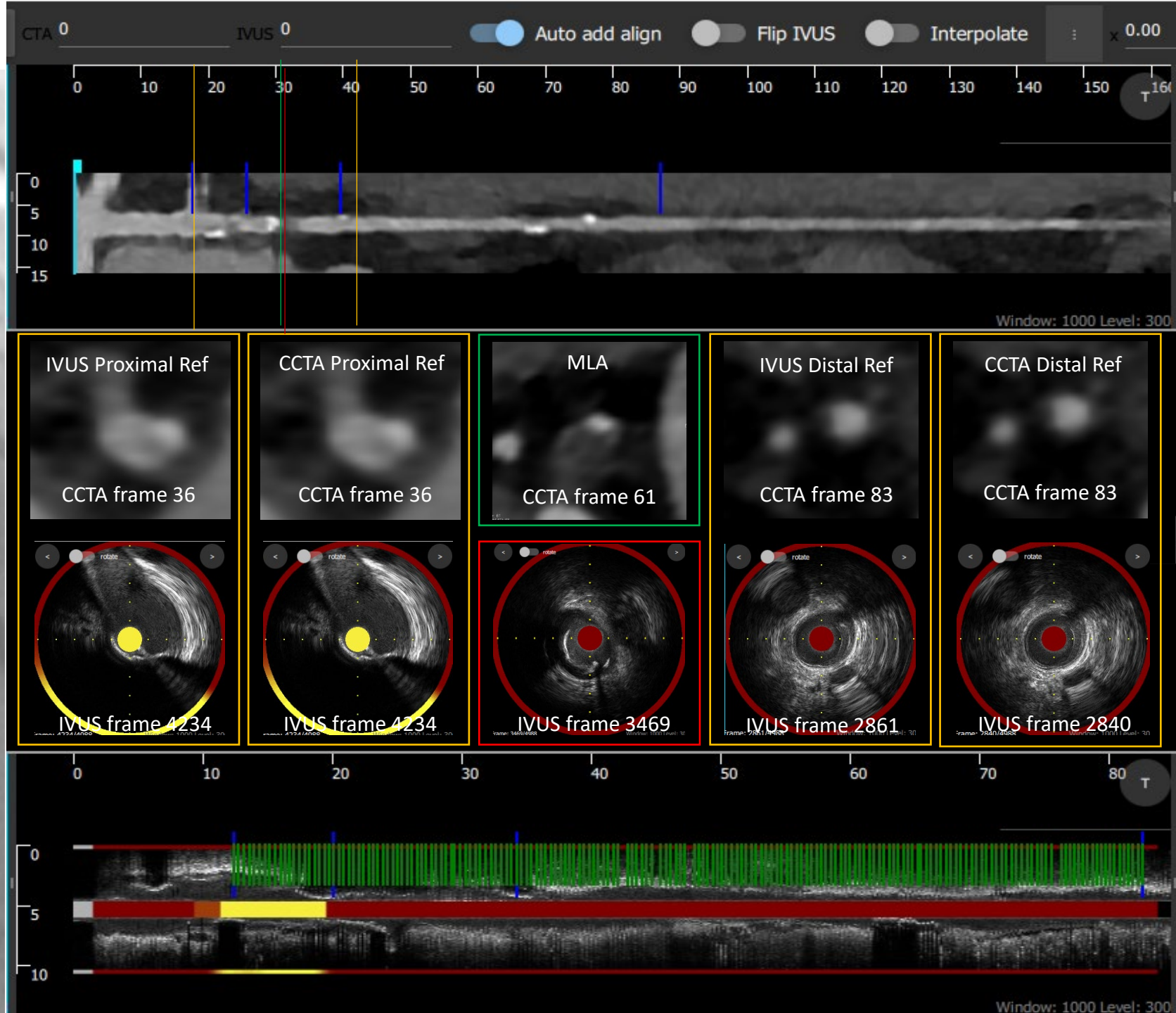
CTA 0
IVUS 0
Auto add align
Flip IVUS
Interpolate
0.00
Window: 1000 Level: 300
IVUS Proximal Ref
CCTA frame 36
IVUS frame 4234
CCTA Proximal Ref
CCTA frame 36
IVUS frame 4234
MLA
CCTA frame 61
IVUS frame 3469
IVUS Distal Ref
CCTA frame 83
IVUS frame 2861
CCTA Distal Ref
CCTA frame 83
IVUS frame 2840
Window: 1000 Level: 300

Case 36

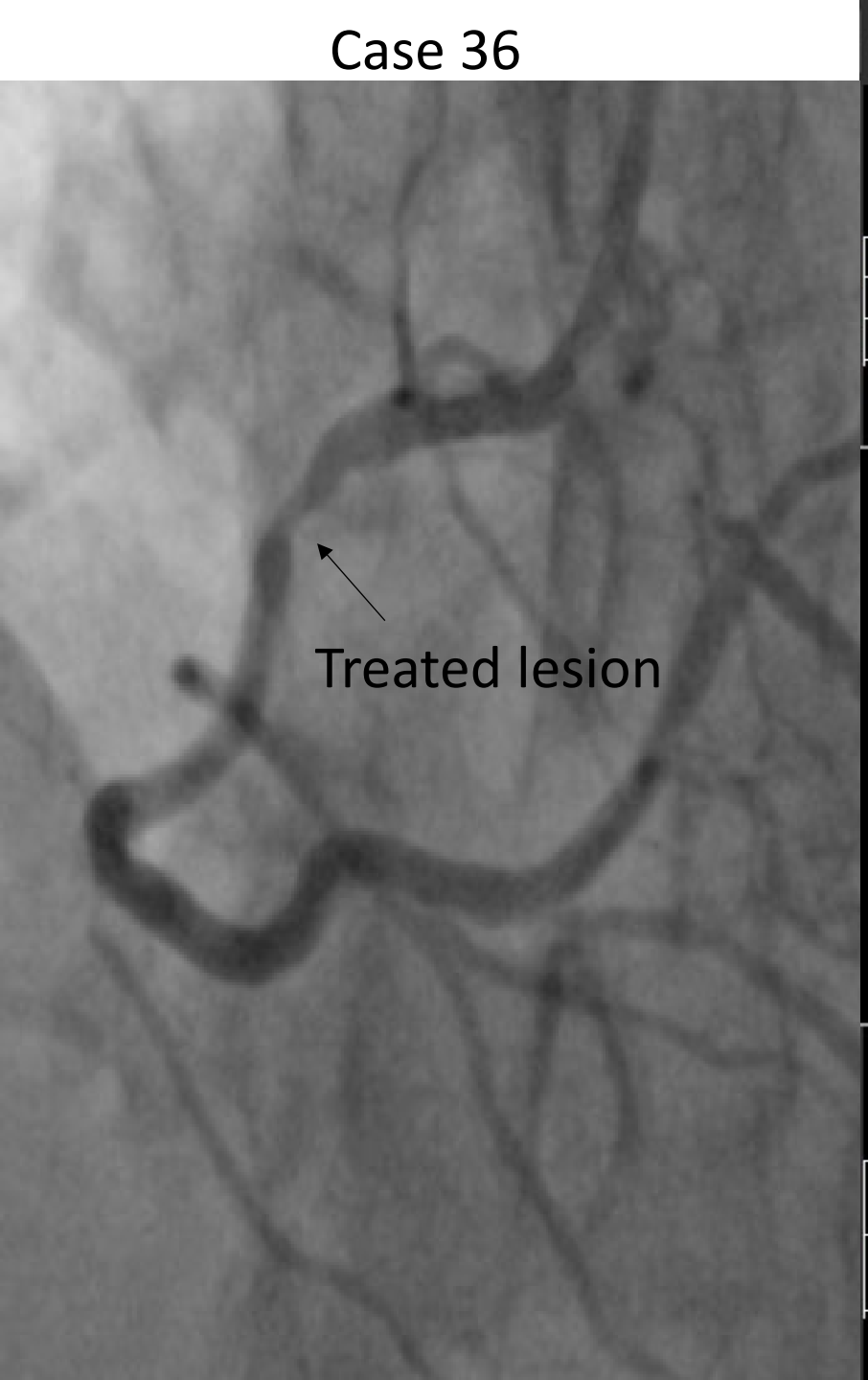
Treated lesion

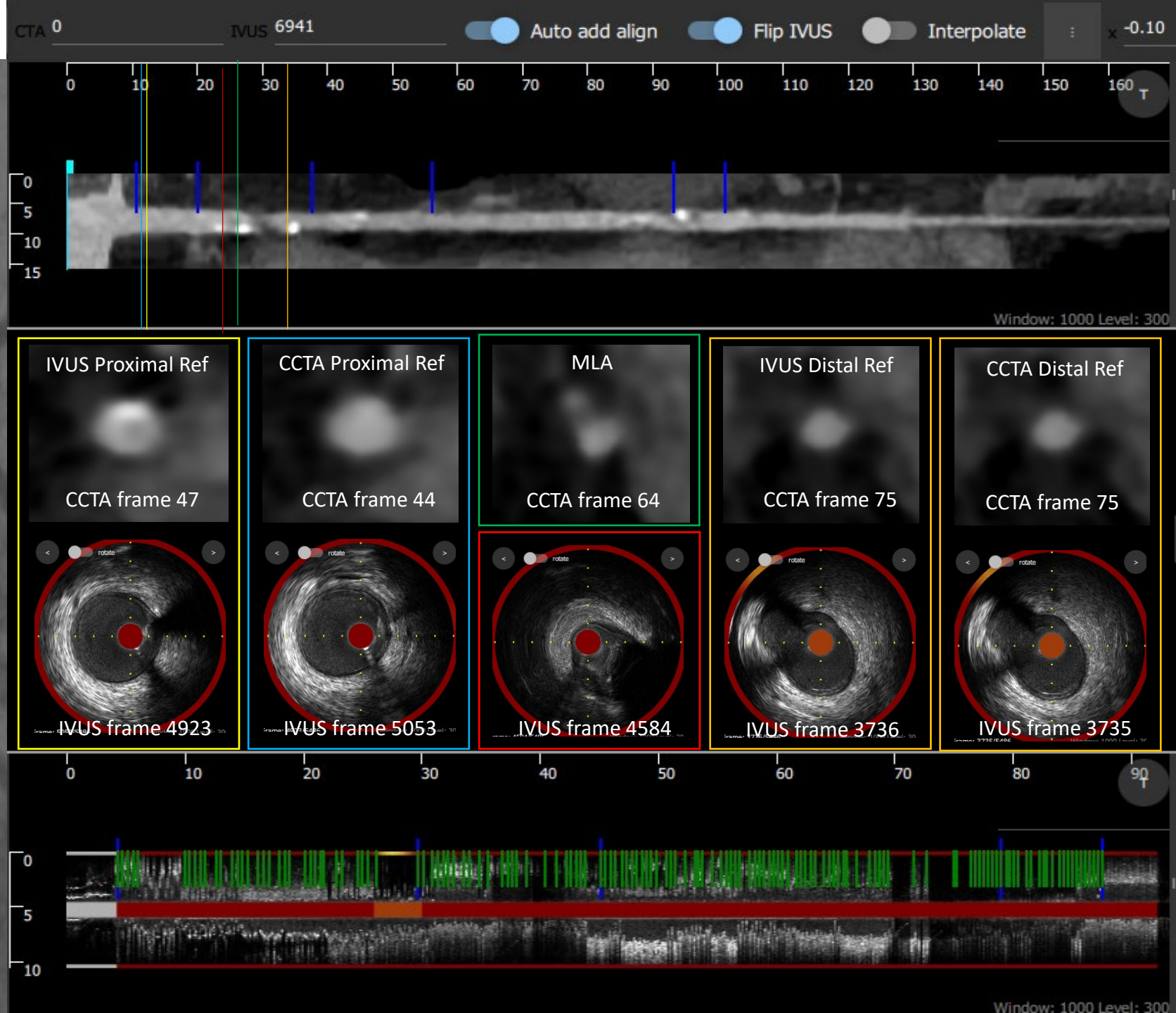
CTA 0
IVUS 6941
Auto add align
Flip IVUS
Interpolate
-0.10
Window: 1000 Level: 300
IVUS Proximal Ref
CCTA frame 47
IVUS frame 4923
CCTA Proximal Ref
CCTA frame 44
IVUS frame 5053
MLA
CCTA frame 64
IVUS frame 4584
IVUS Distal Ref
CCTA frame 75
IVUS frame 3736
CCTA Distal Ref
CCTA frame 75
IVUS frame 3735
Window: 1000 Level: 300

Case 37

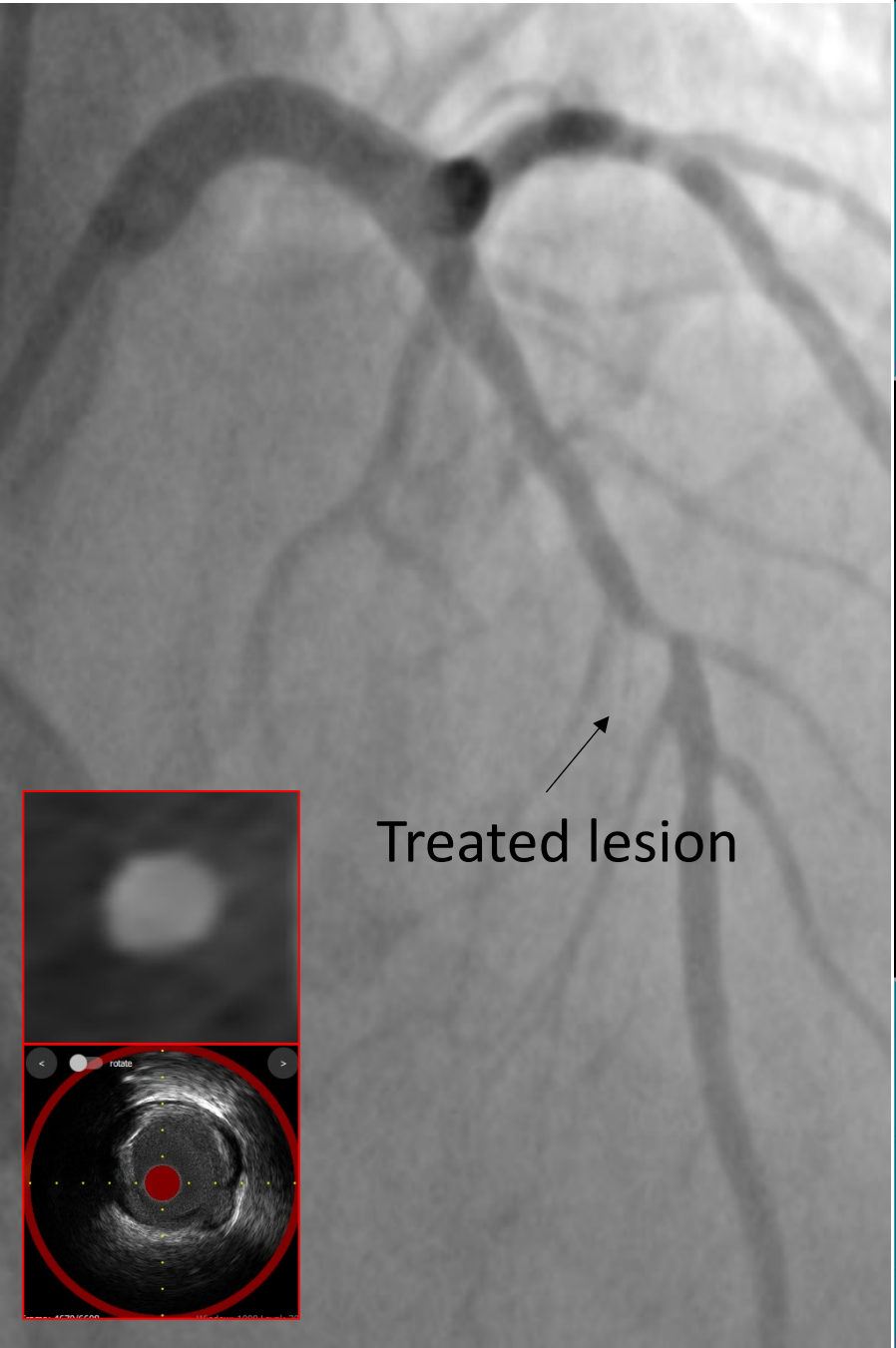
Treated lesion

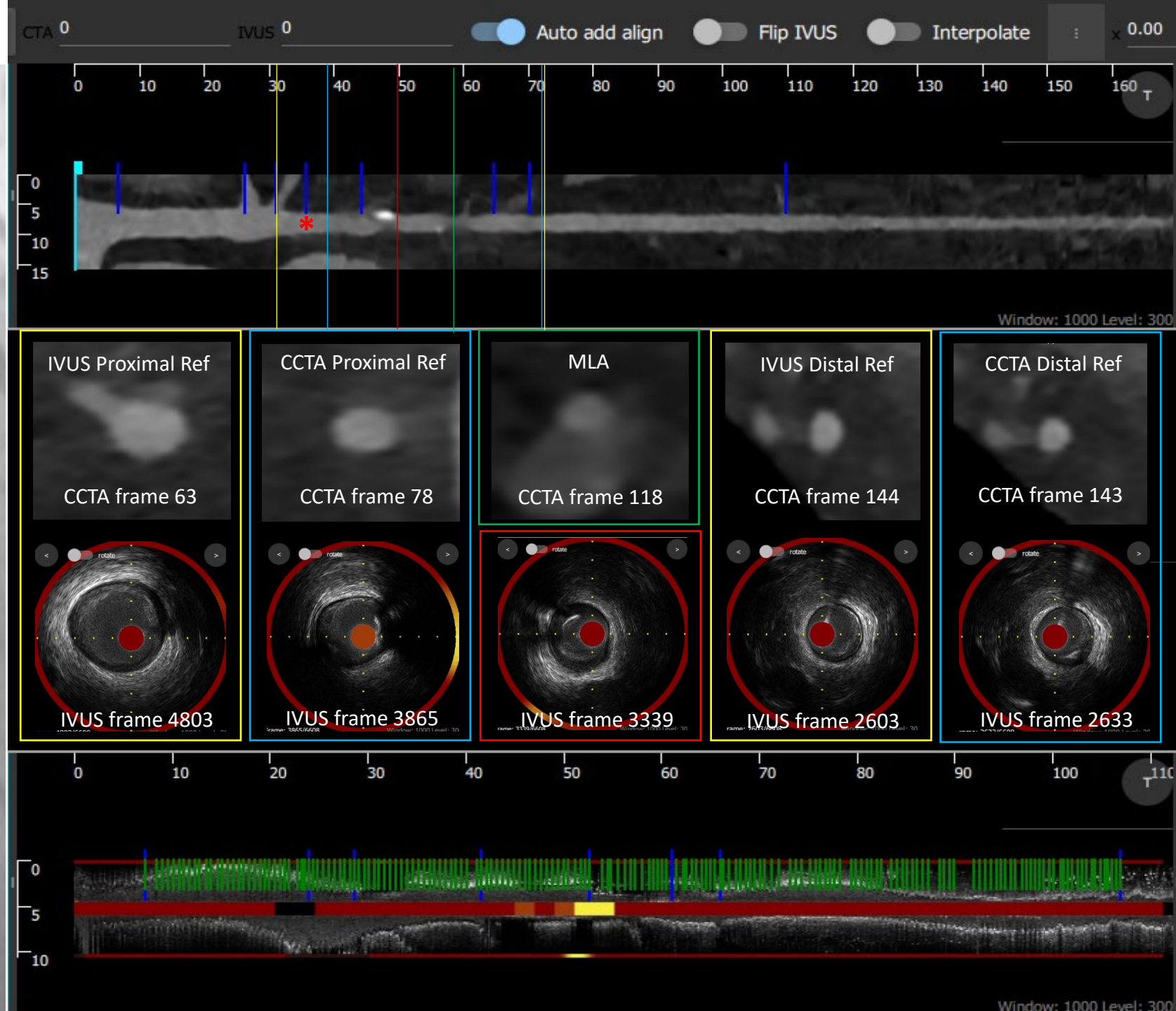
CTA 0
IVUS 0
Auto add align
Flip IVUS
Interpolate
0.00
Window: 1000 Level: 300
IVUS Proximal Ref
CCTA frame 63
IVUS frame 4803
CCTA Proximal Ref
CCTA frame 78
IVUS frame 3865
MLA
CCTA frame 118
IVUS frame 3339
IVUS Distal Ref
CCTA frame 144
IVUS frame 2603
CCTA Distal Ref
CCTA frame 143
IVUS frame 2633
Window: 1000 Level: 300

Case 38


Treated lesion

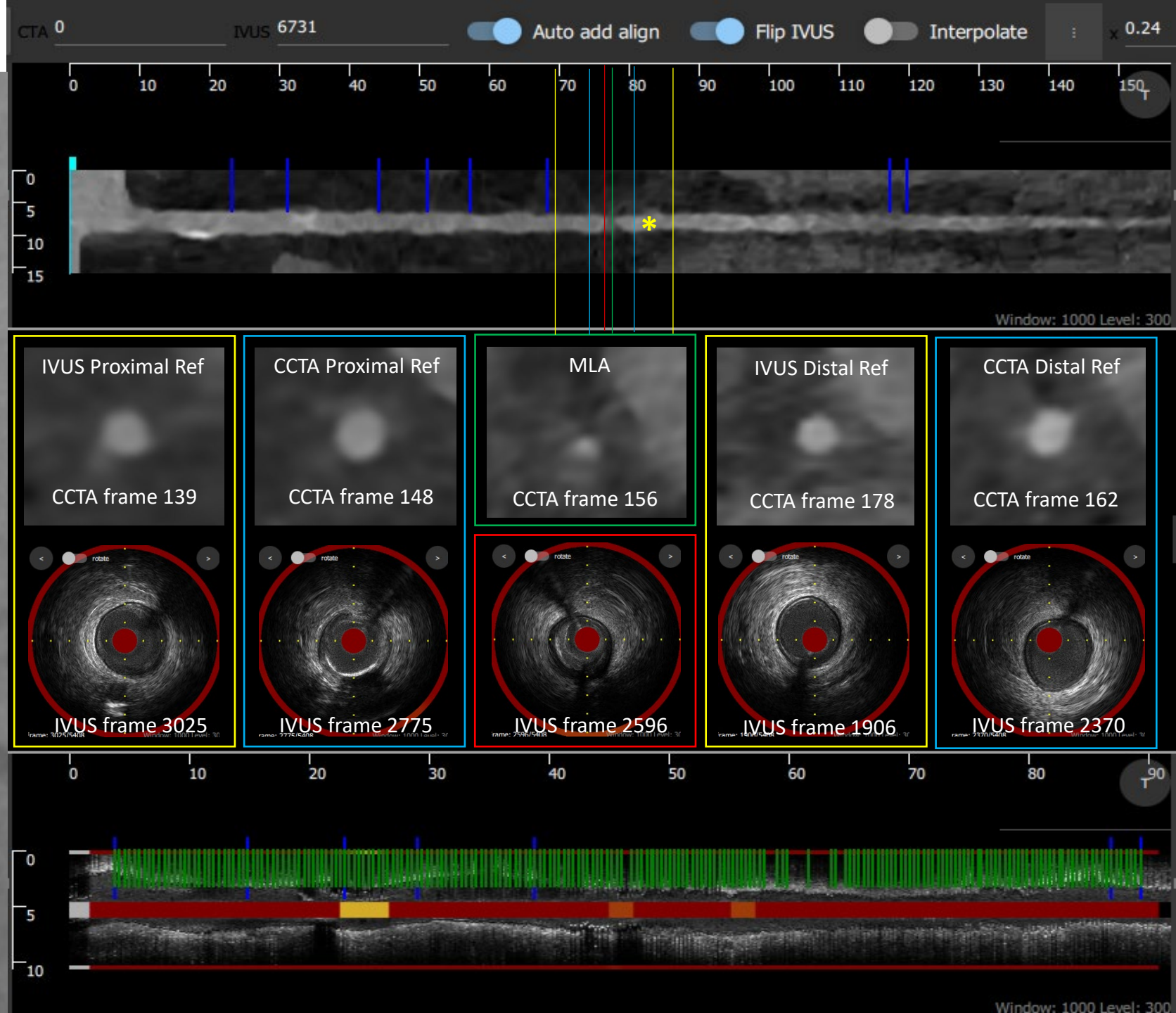
CTA 0
IVUS 6731
Auto add align
Flip IVUS
Interpolate
0.24
Window: 1000 Level: 300
IVUS Proximal Ref
CCTA frame 139
IVUS frame 3025
CCTA Proximal Ref
CCTA frame 148
IVUS frame 2775
MLA
CCTA frame 156
IVUS frame 2596
IVUS Distal Ref
CCTA frame 178
IVUS frame 1906
CCTA Distal Ref
CCTA frame 162
IVUS frame 2370
Window: 1000 Level: 300

Case 39

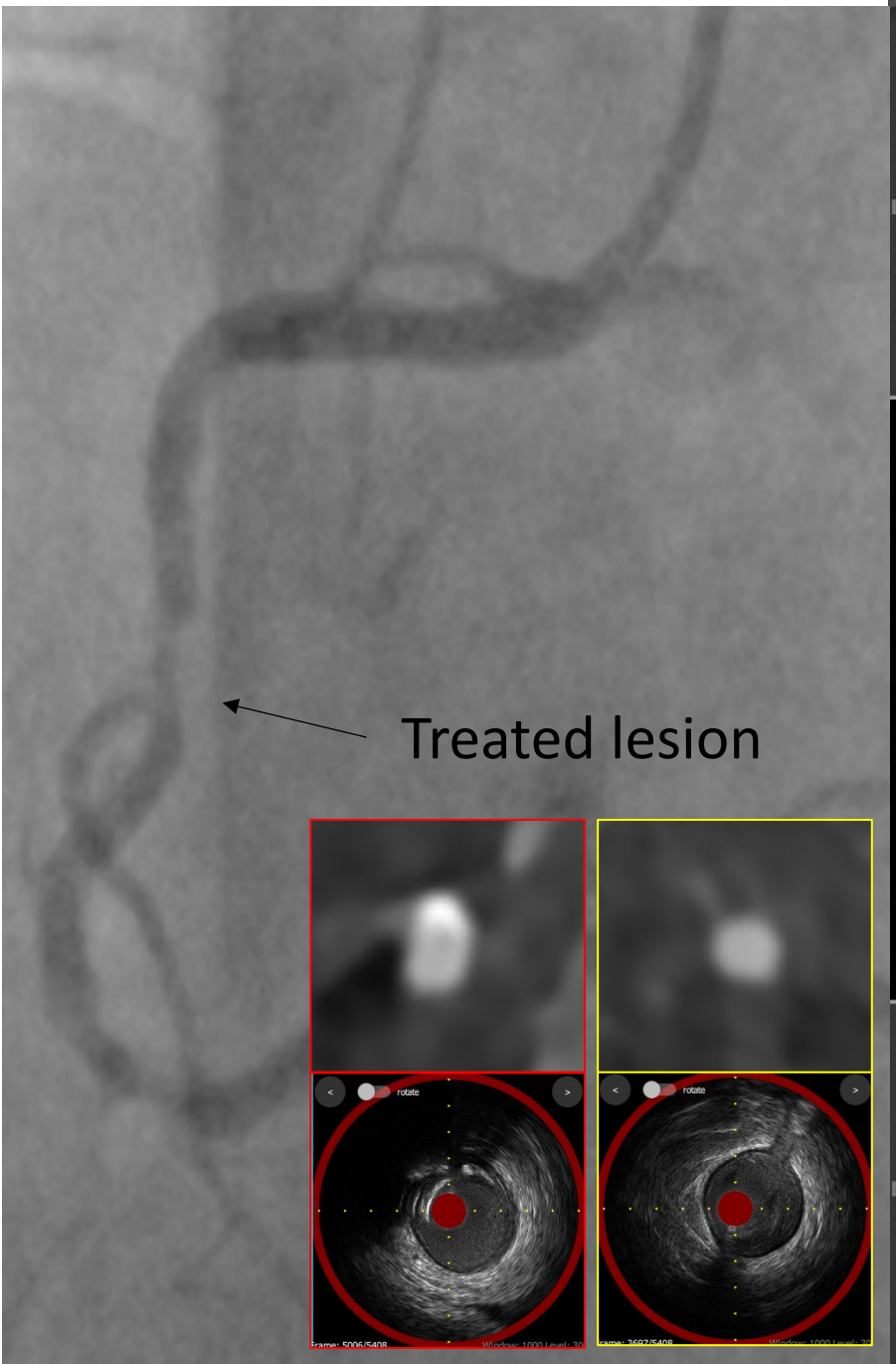
Treated lesion

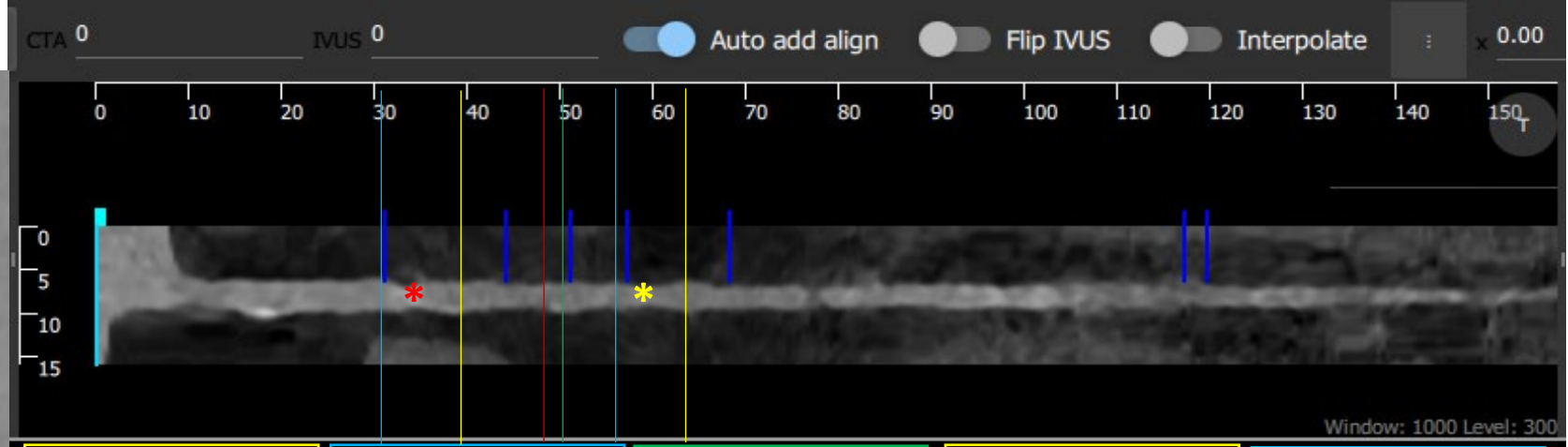
CTA 0
IVUS 0
Auto add align
Flip IVUS
Interpolate
0.00
0 10 20 30 40 50 60 70 80 90 100 110 120 130 140 150
0 5 10 15
Window: 1000 Level: 300

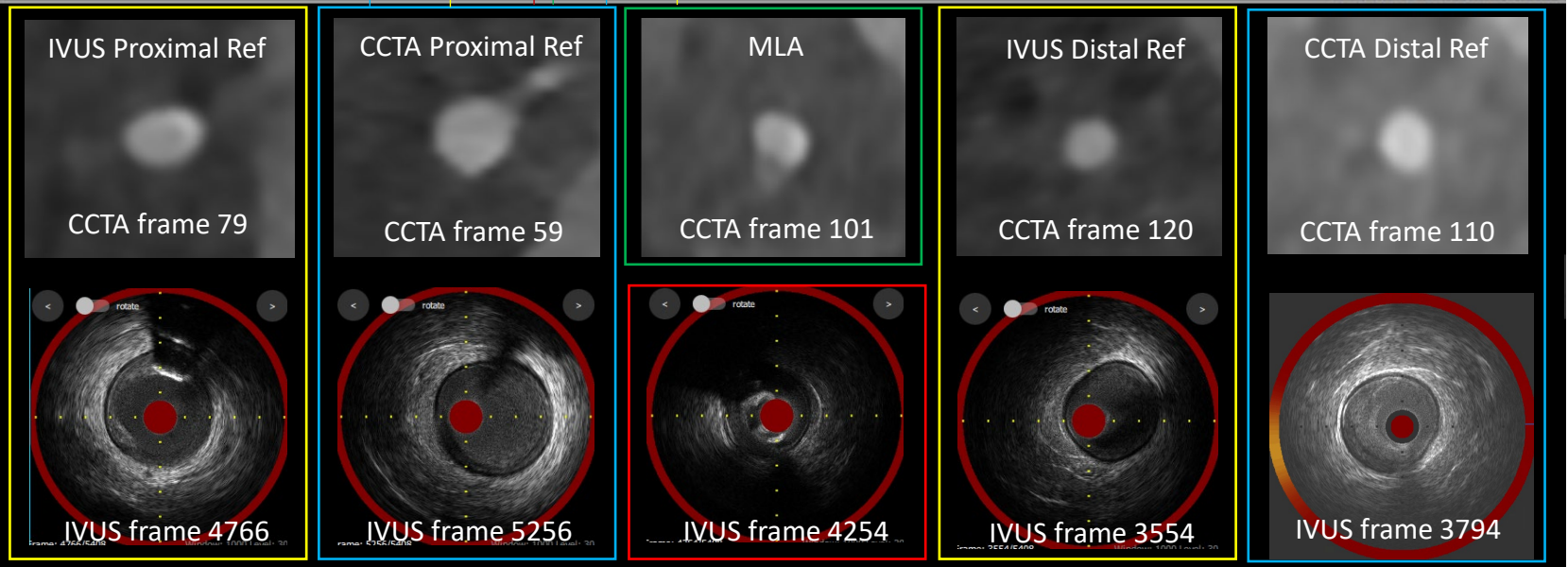
IVUS Proximal Ref
CCTA frame 79
IVUS frame 4766
CCTA Proximal Ref
CCTA frame 59
IVUS frame 5256
MLA
CCTA frame 101
IVUS frame 4254
IVUS Distal Ref
CCTA frame 120
IVUS frame 3554
CCTA Distal Ref
CCTA frame 110
IVUS frame 3794

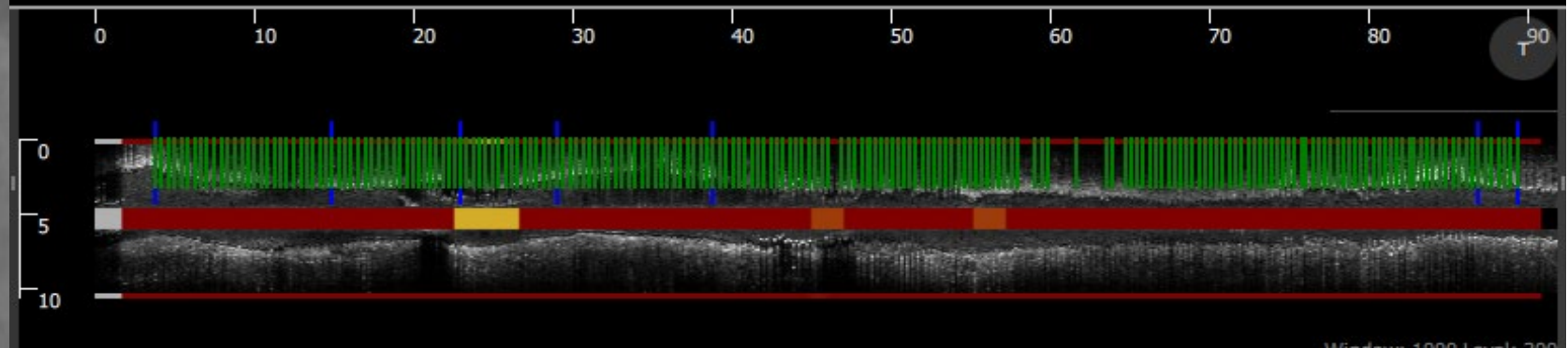
0 10 20 30 40 50 60 70 80 90
0 5 10

Case 40


Treated lesion

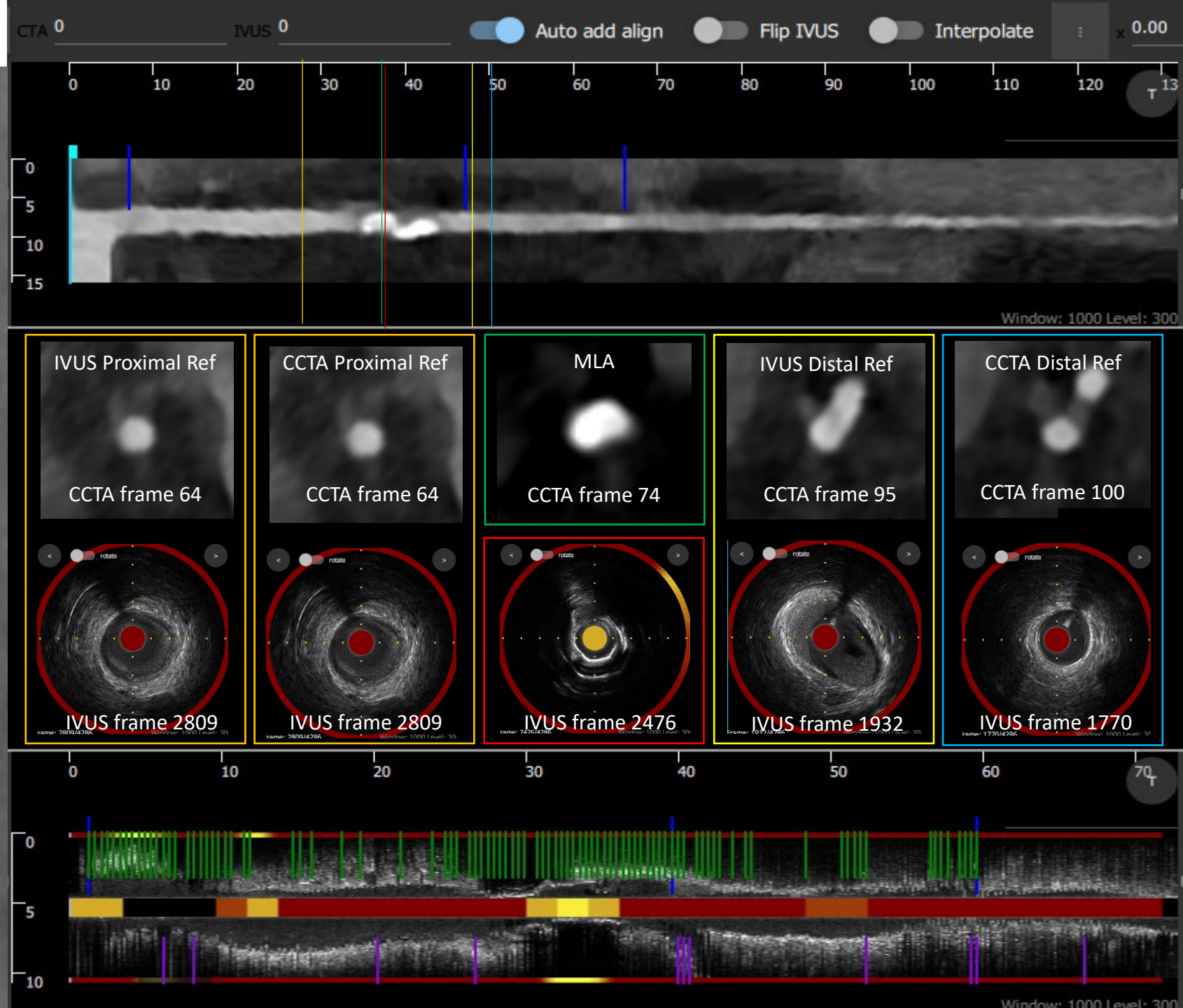
CTA 0
IVUS 0
Auto add align
Flip IVUS
Interpolate
0.00
0 10 20 30 40 50 60 70 80 90 100 110 120
0 5 10 15
Window: 1000 Level: 300
IVUS Proximal Ref
CCTA frame 64
IVUS frame 2809
CCTA Proximal Ref
CCTA frame 64
IVUS frame 2809
MLA
CCTA frame 74
IVUS frame 2476
IVUS Distal Ref
CCTA frame 95
IVUS frame 1932
CCTA Distal Ref
CCTA frame 100
IVUS frame 1770
0 10 20 30 40 50 60 70
0 5 10
Window: 1000 Level: 300

Case 41


Treated lesion
CTA 151
IVUS -719
Auto add align
Flip IVUS
Interpolate
IVUS Proximal Ref
CCTA frame 81
IVUS frame 1392
CCTA Proximal Ref
CCTA frame 77
IVUS frame 1519
MLA
CCTA frame 96
IVUS frame 1005
IVUS Distal Ref
CCTA frame 98
IVUS frame 878
CCTA Distal Ref
CCTA frame 102
IVUS frame 763

Case 42


Treated lesion

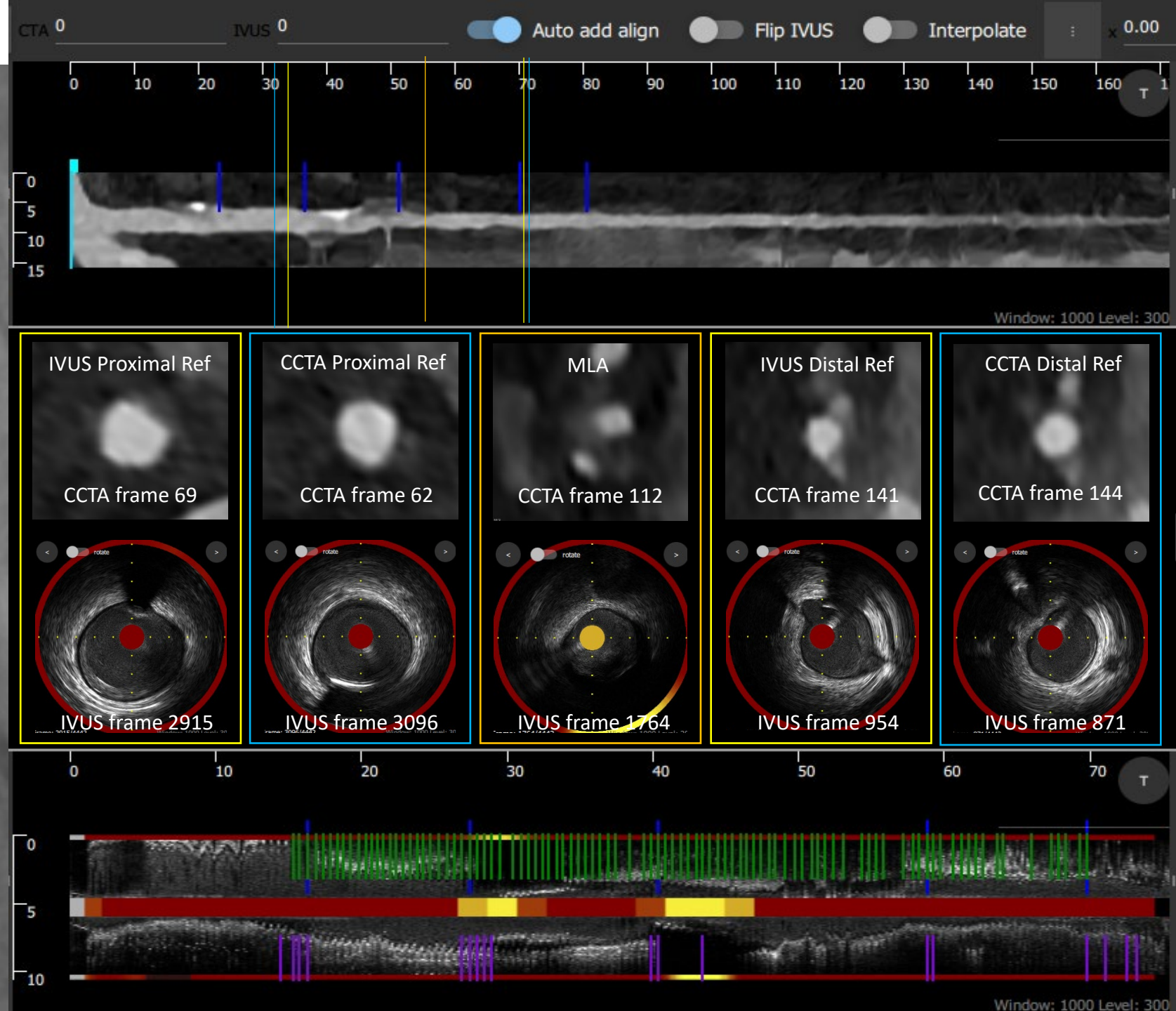
CTA 0
IVUS 0
Auto add align
Flip IVUS
Interpolate
0.00
0 10 20 30 40 50 60 70 80 90 100 110 120 130 140 150 160
0 5 10 15
Window: 1000 Level: 300
IVUS Proximal Ref
CCTA frame 69
IVUS frame 2915
CCTA Proximal Ref
CCTA frame 62
IVUS frame 3096
MLA
CCTA frame 112
IVUS frame 1764
IVUS Distal Ref
CCTA frame 141
IVUS frame 954
CCTA Distal Ref
CCTA frame 144
IVUS frame 871
0 10 20 30 40 50 60 70
0 5 10
Window: 1000 Level: 300

Case 43

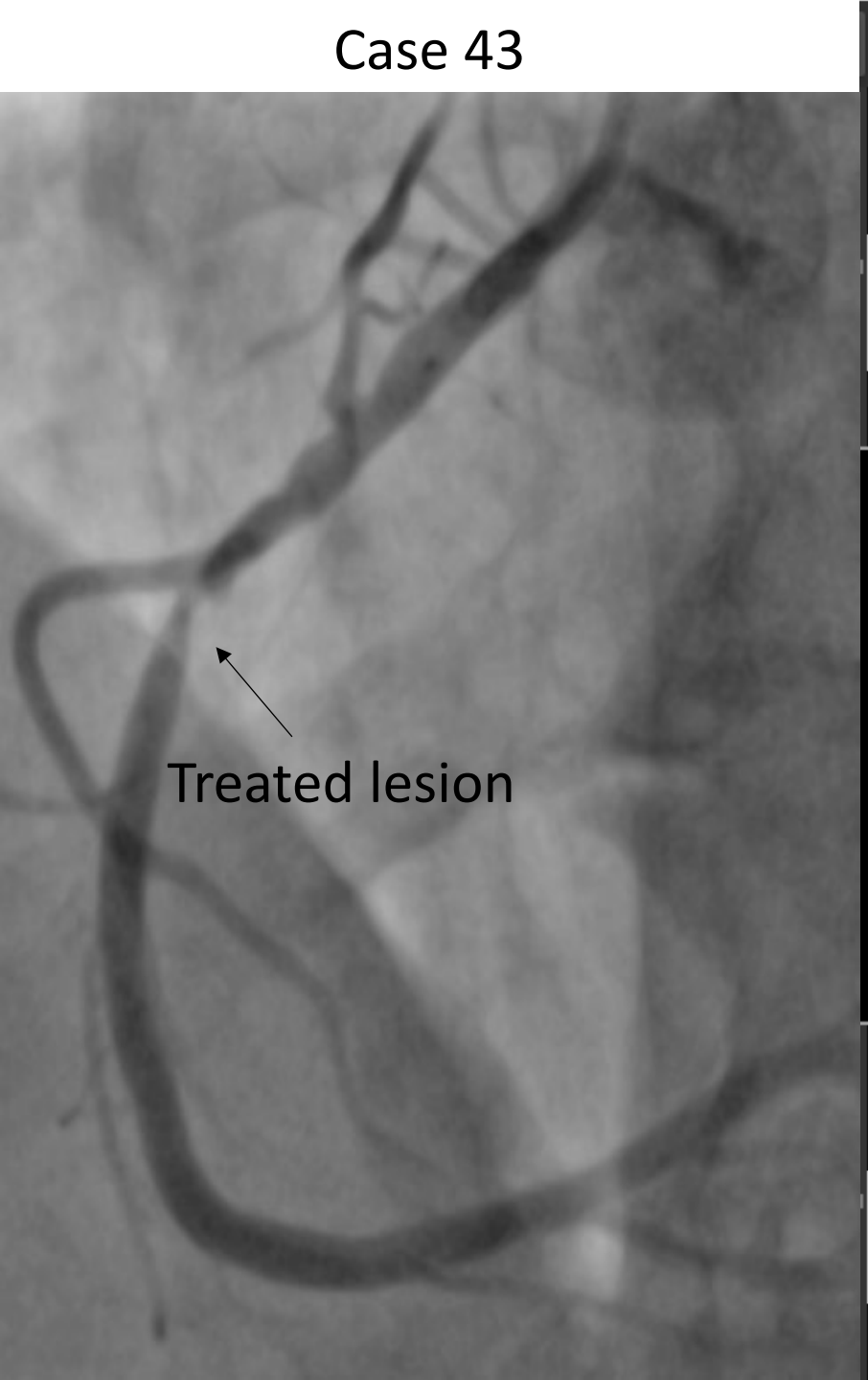
Treated lesion

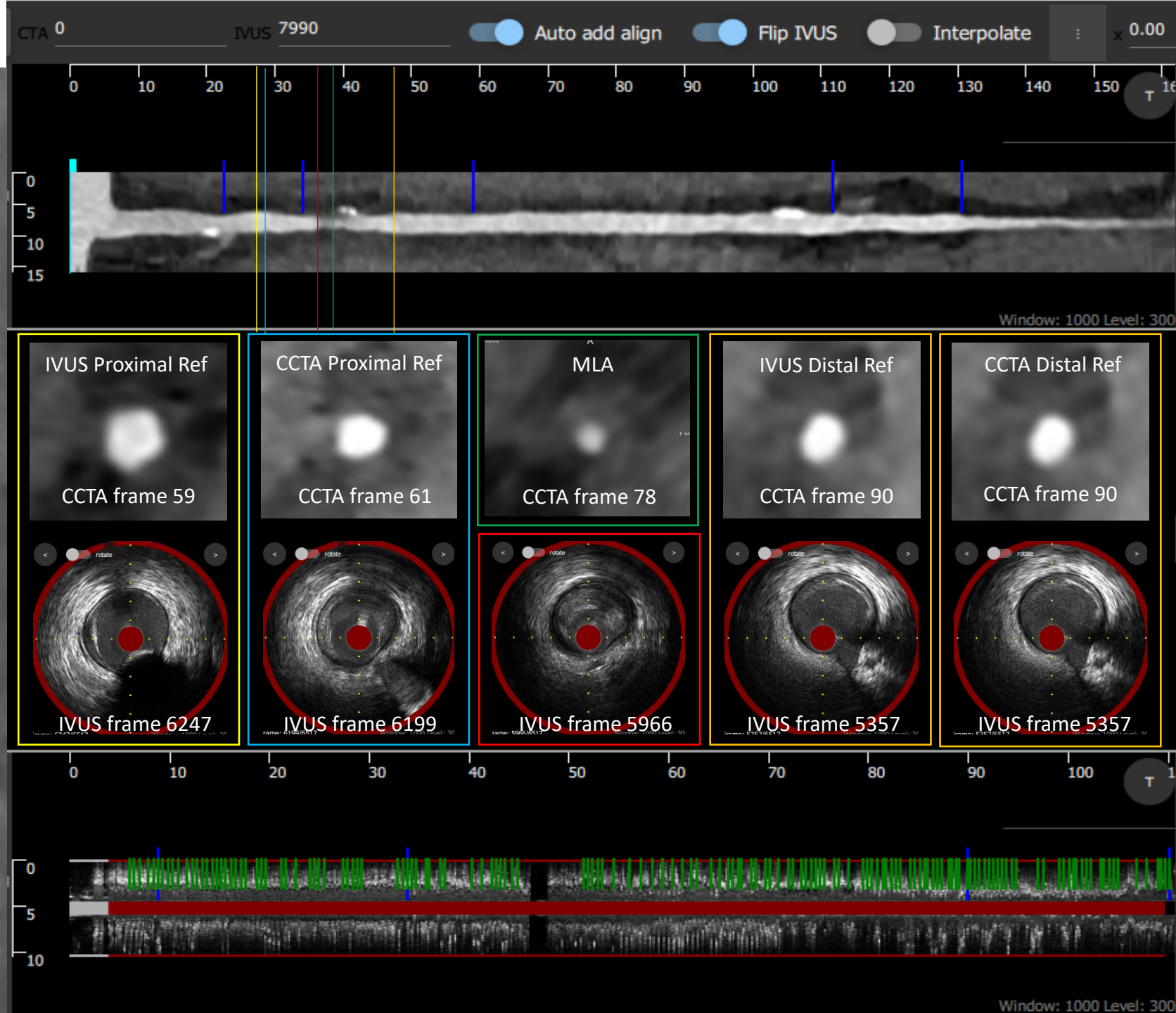
CTA 0
IVUS 7990
Auto add align
Flip IVUS
Interpolate
x 0.00
0 10 20 30 40 50 60 70 80 90 100 110 120 130 140 150
0 5 10 15
Window: 1000 Level: 300
IVUS Proximal Ref
CCTA frame 59
IVUS frame 6247
CCTA Proximal Ref
CCTA frame 61
IVUS frame 6199
MLA
CCTA frame 78
IVUS frame 5966
IVUS Distal Ref
CCTA frame 90
IVUS frame 5357
CCTA Distal Ref
CCTA frame 90
IVUS frame 5357
0 10 20 30 40 50 60 70 80 90 100
0 5 10
Window: 1000 Level: 300

Case 44

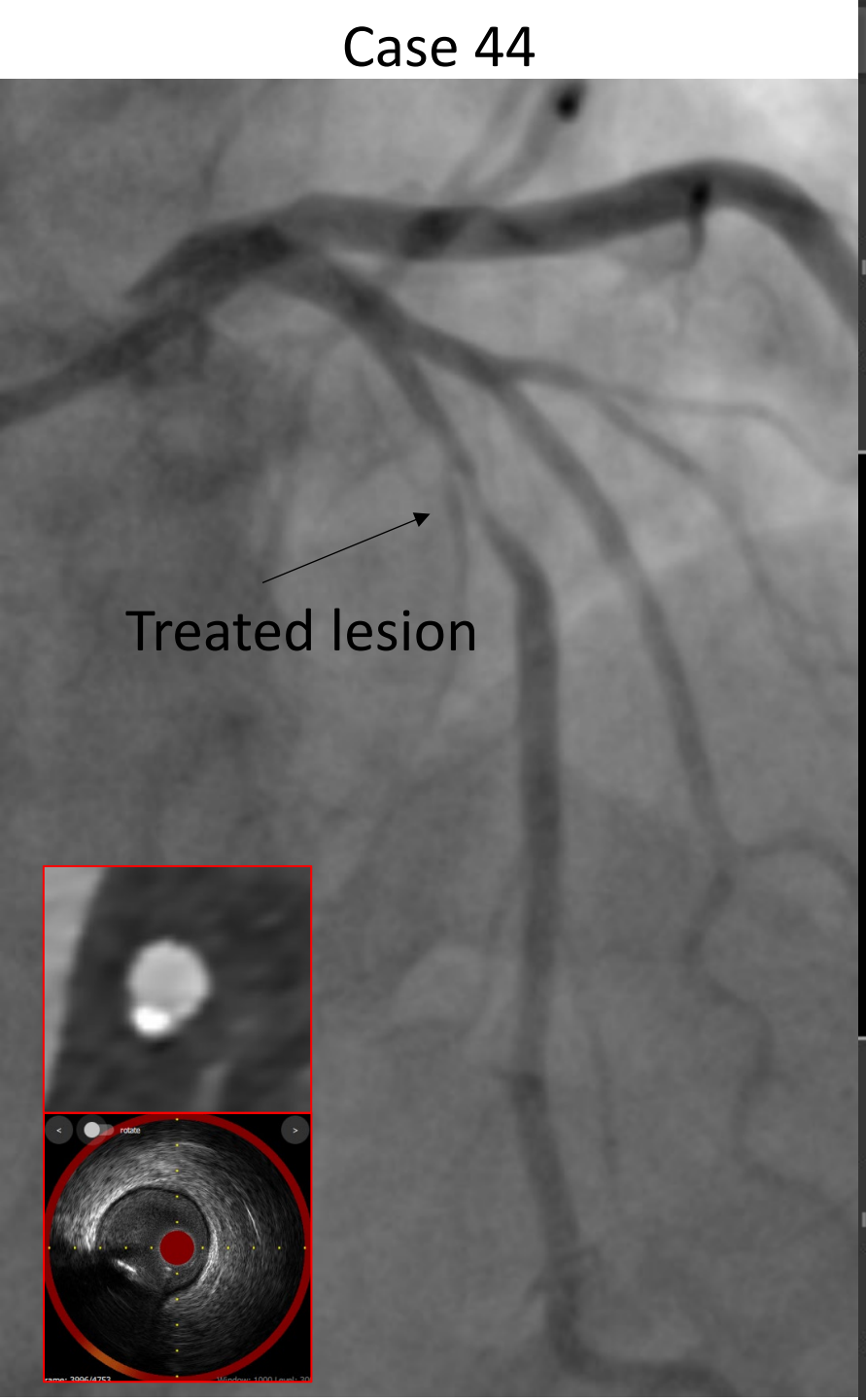
Treated lesion

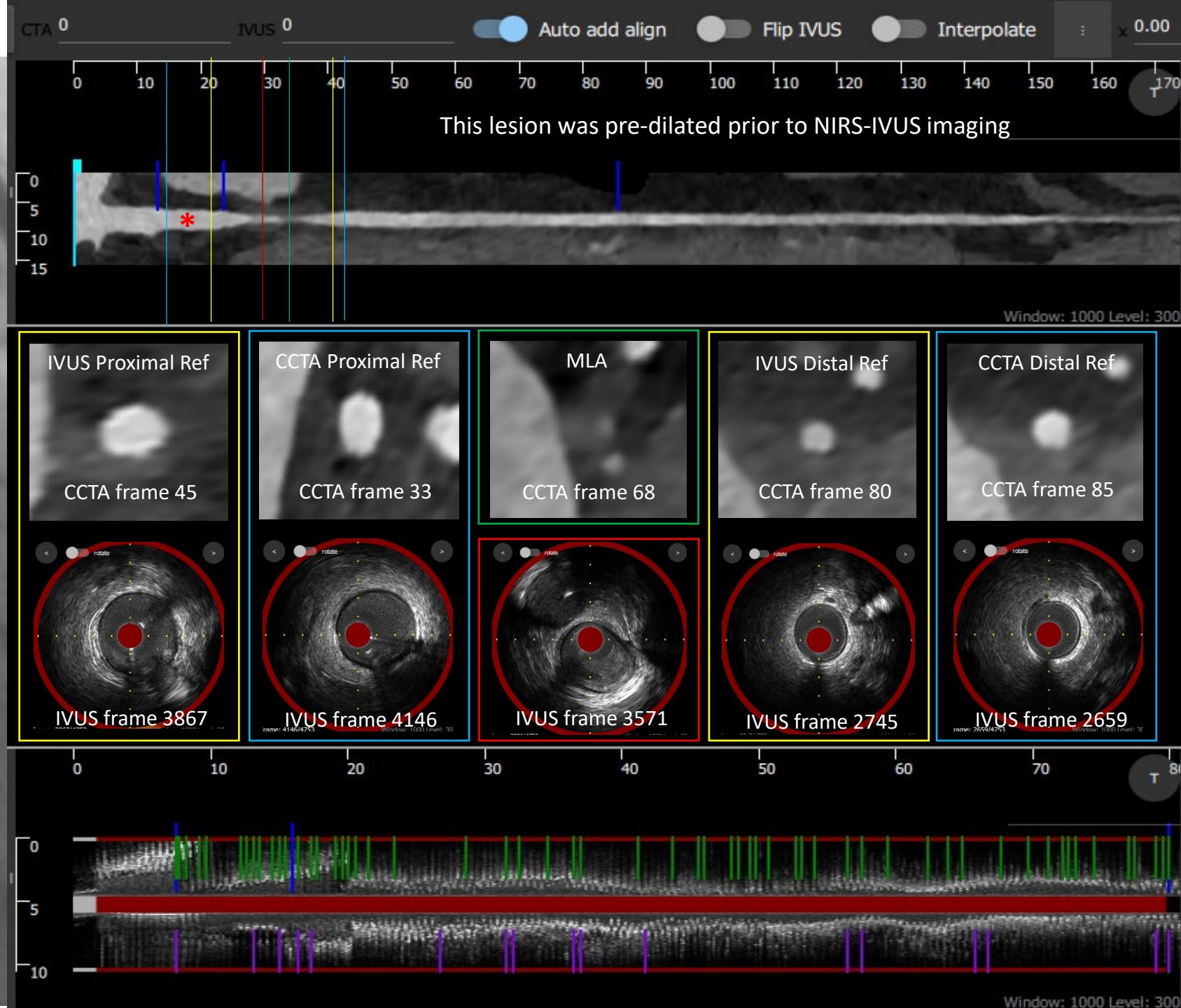
CTA 0
IVUS 0
Auto add align
Flip IVUS
Interpolate
0.00
This lesion was pre-dilated prior to NIRS-IVUS imaging
Window: 1000 Level: 300
IVUS Proximal Ref
CCTA frame 45
IVUS frame 3867
CCTA Proximal Ref
CCTA frame 33
IVUS frame 4146
MLA
CCTA frame 68
IVUS frame 3571
IVUS Distal Ref
CCTA frame 80
IVUS frame 2745
CCTA Distal Ref
CCTA frame 85
IVUS frame 2659
Window: 1000 Level: 300

Case 45

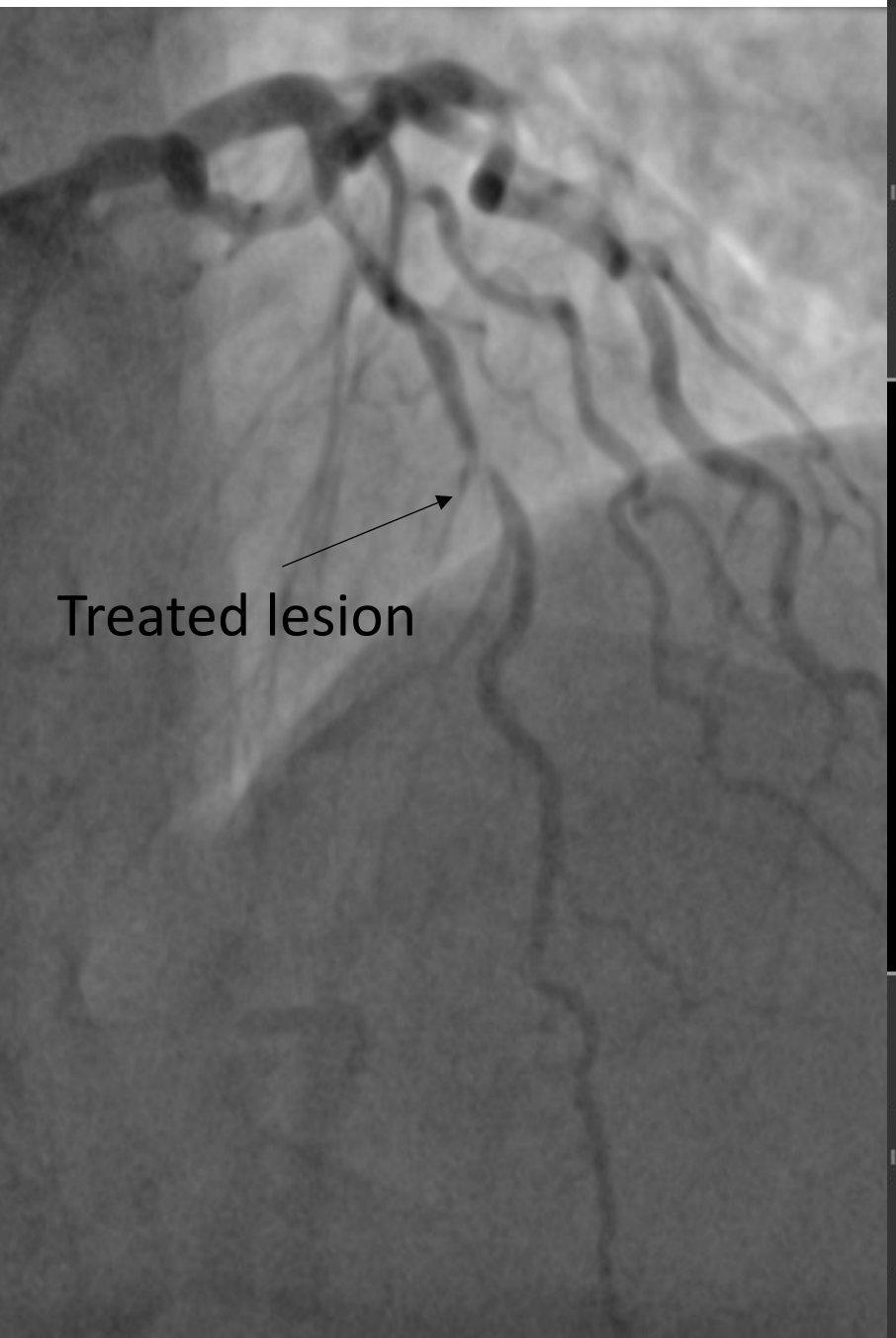
Treated lesion

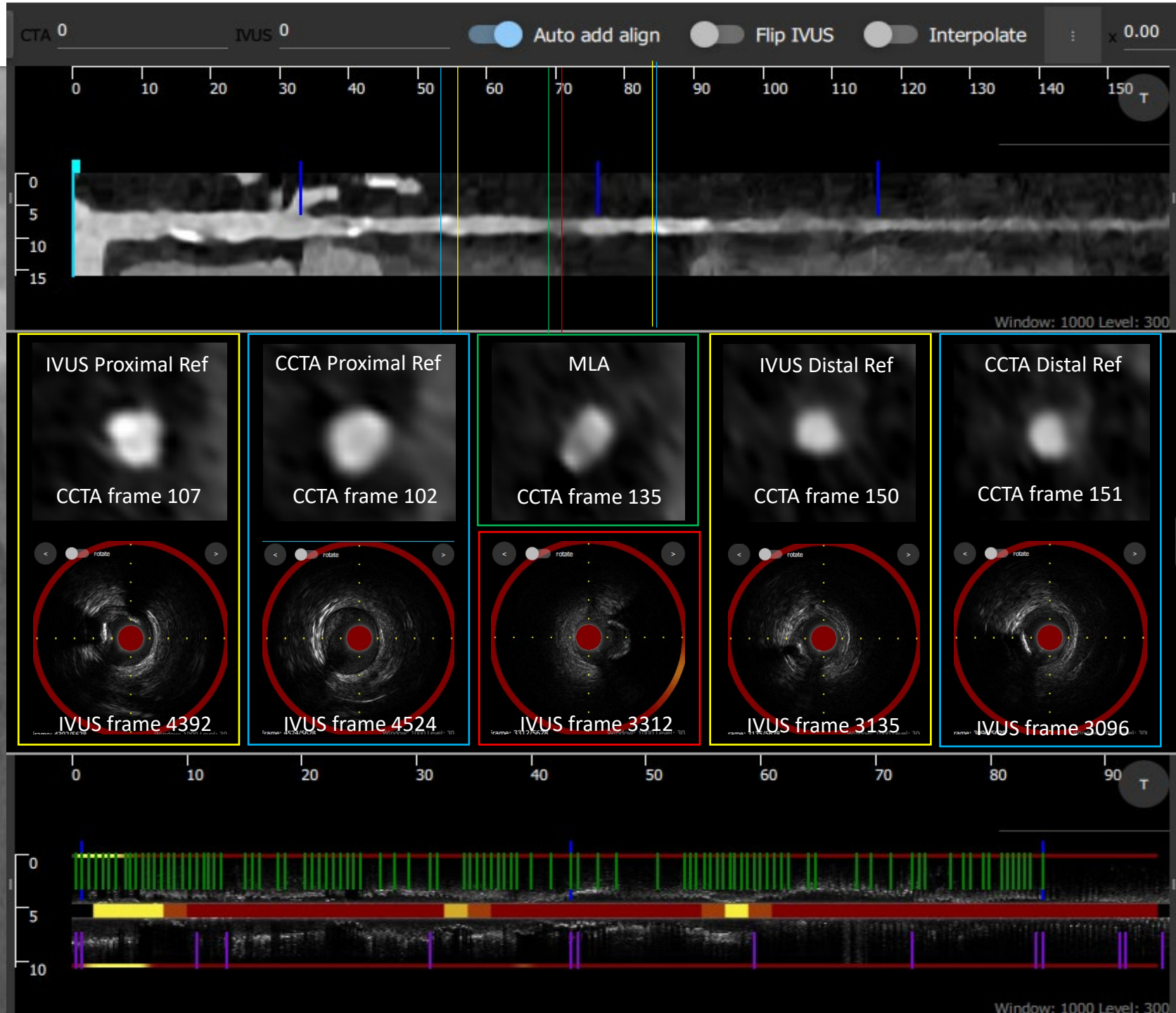
CTA 0
IVUS 0
Auto add align
Flip IVUS
Interpolate
0.00
0 10 20 30 40 50 60 70 80 90 100 110 120 130 140 150
0 5 10 15
Window: 1000 Level: 300
IVUS Proximal Ref
CCTA frame 107
IVUS frame 4392
CCTA Proximal Ref
CCTA frame 102
IVUS frame 4524
MLA
CCTA frame 135
IVUS frame 3312
IVUS Distal Ref
CCTA frame 150
IVUS frame 3135
CCTA Distal Ref
CCTA frame 151
IVUS frame 3096
0 10 20 30 40 50 60 70 80 90
0 5 10
Window: 1000 Level: 300

Case 46


Treated lesion

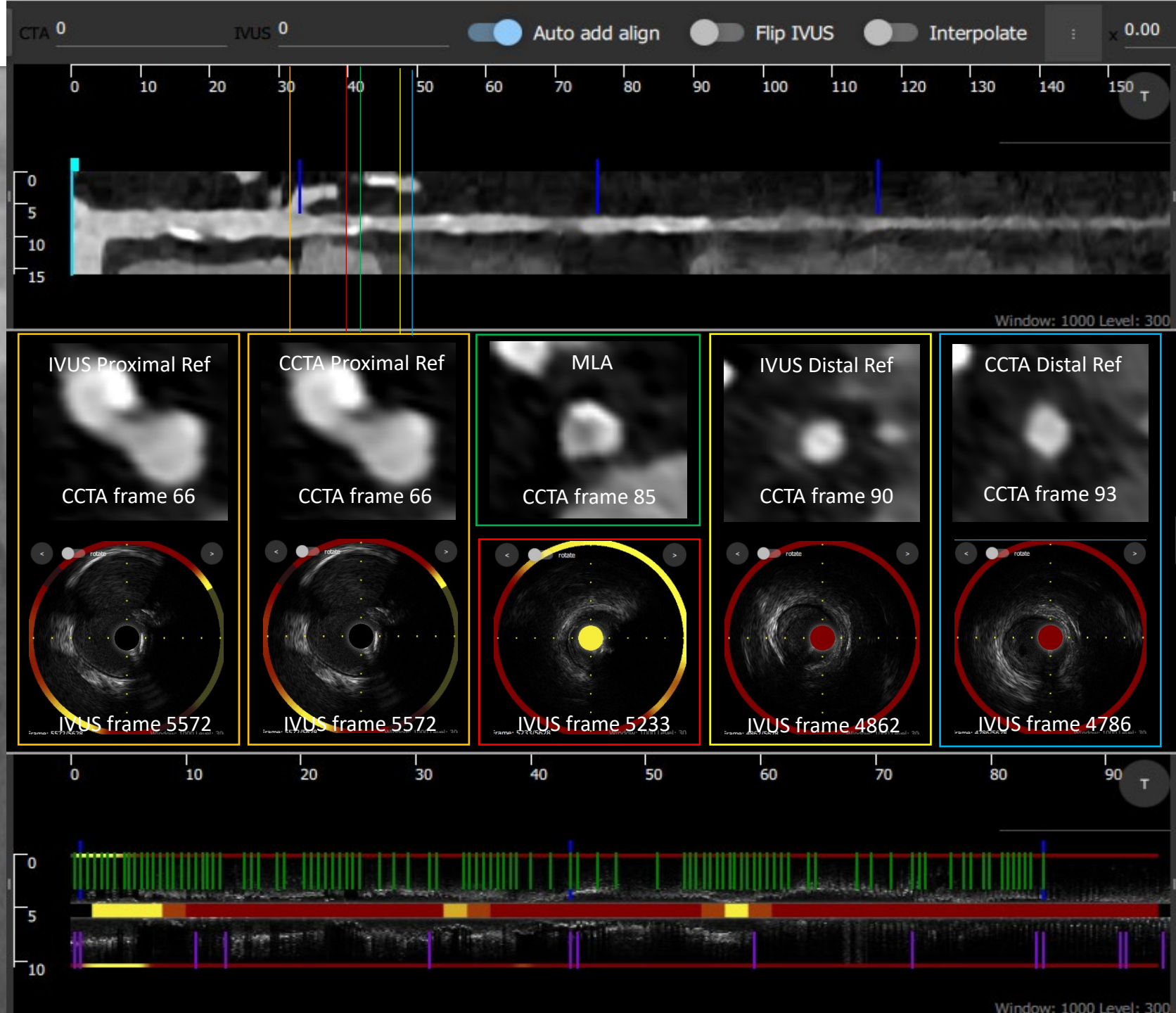
CTA 0
IVUS 0
Auto add align
Flip IVUS
Interpolate
0.00
0 10 20 30 40 50 60 70 80 90 100 110 120 130 140 150
0 5 10 15
Window: 1000 Level: 300
IVUS Proximal Ref
CCTA frame 66
IVUS frame 5572
CCTA Proximal Ref
CCTA frame 66
IVUS frame 5572
MLA
CCTA frame 85
IVUS frame 5233
IVUS Distal Ref
CCTA frame 90
IVUS frame 4862
CCTA Distal Ref
CCTA frame 93
IVUS frame 4786
0 10 20 30 40 50 60 70 80 90
0 5 10
Window: 1000 Level: 300

Case 47

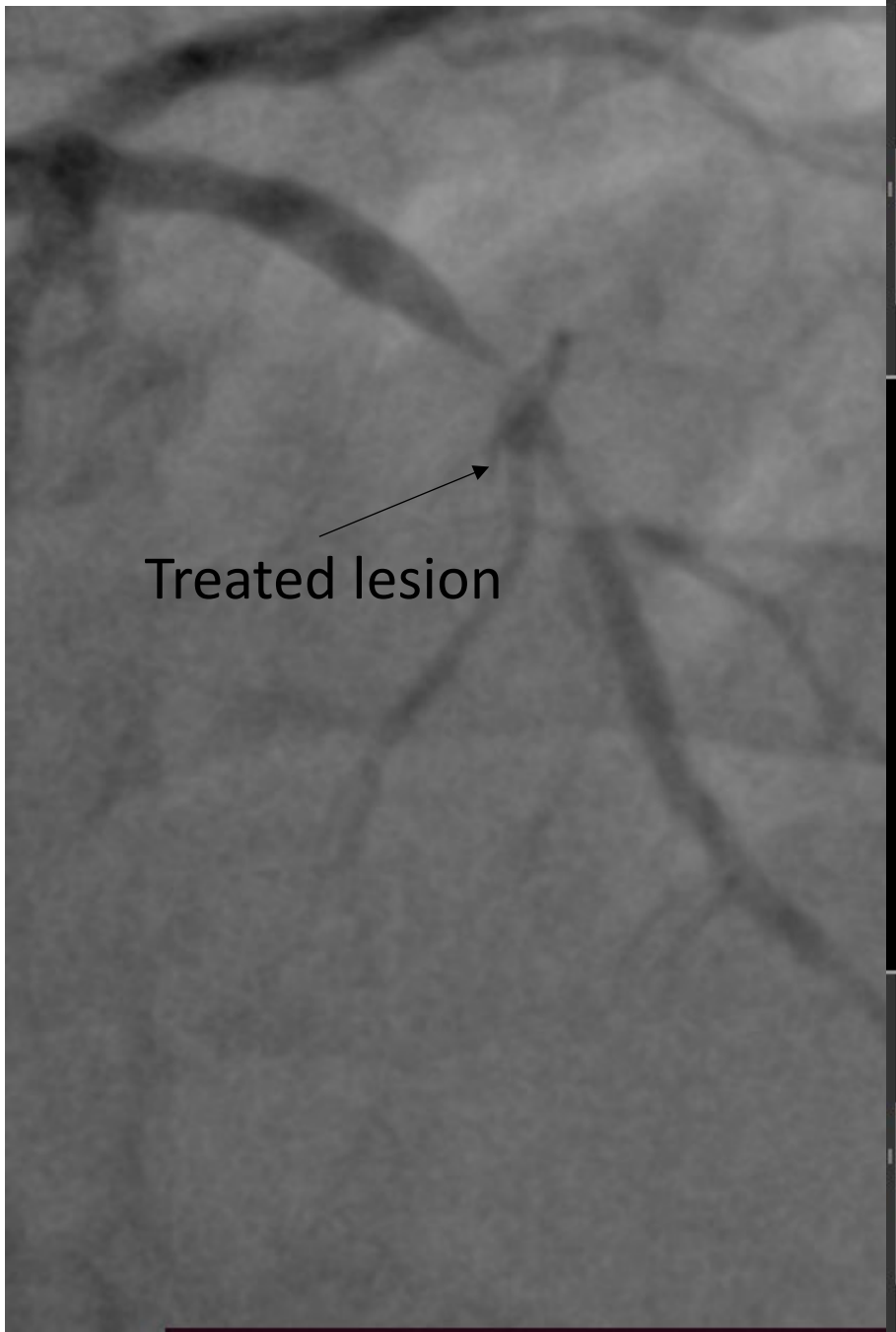
Treated lesion

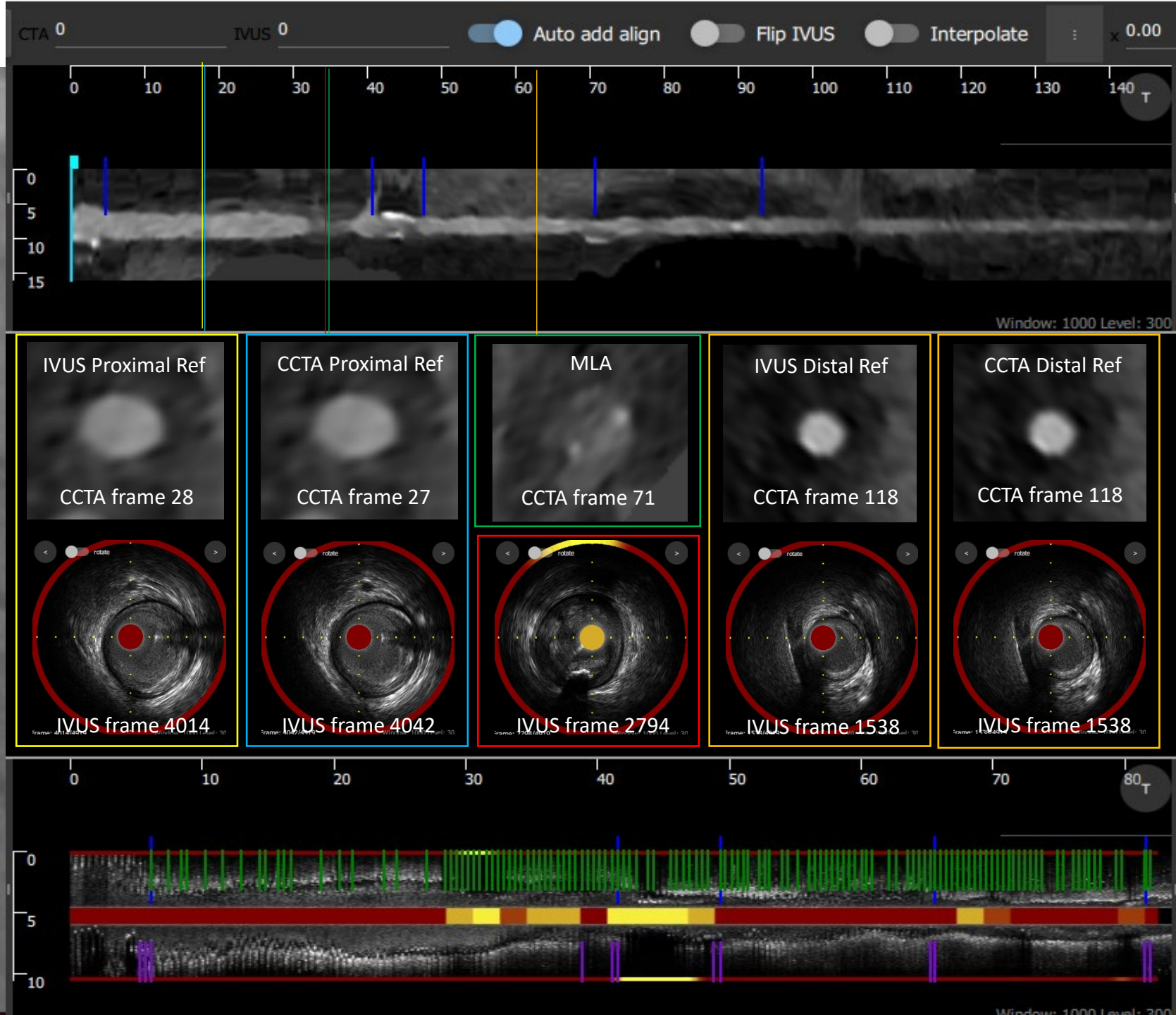
CTA 0
IVUS 0
Auto add align
Flip IVUS
Interpolate
0.00
Window: 1000 Level: 300
IVUS Proximal Ref
CCTA frame 28
IVUS frame 4014
CCTA Proximal Ref
CCTA frame 27
IVUS frame 4042
MLA
CCTA frame 71
IVUS frame 2794
IVUS Distal Ref
CCTA frame 118
IVUS frame 1538
CCTA Distal Ref
CCTA frame 118
IVUS frame 1538

Case 48

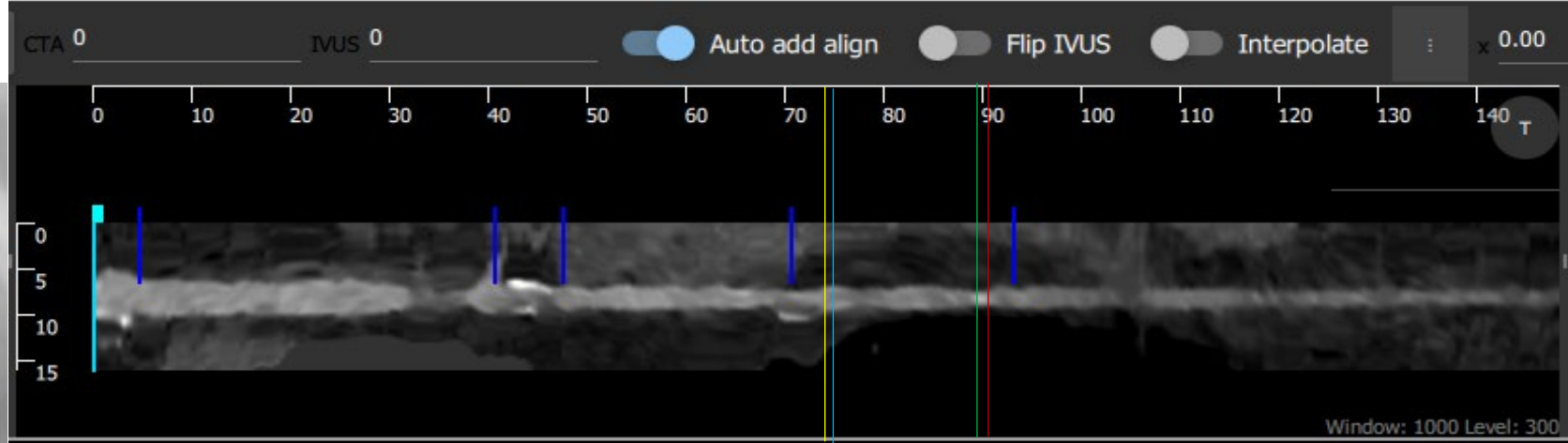

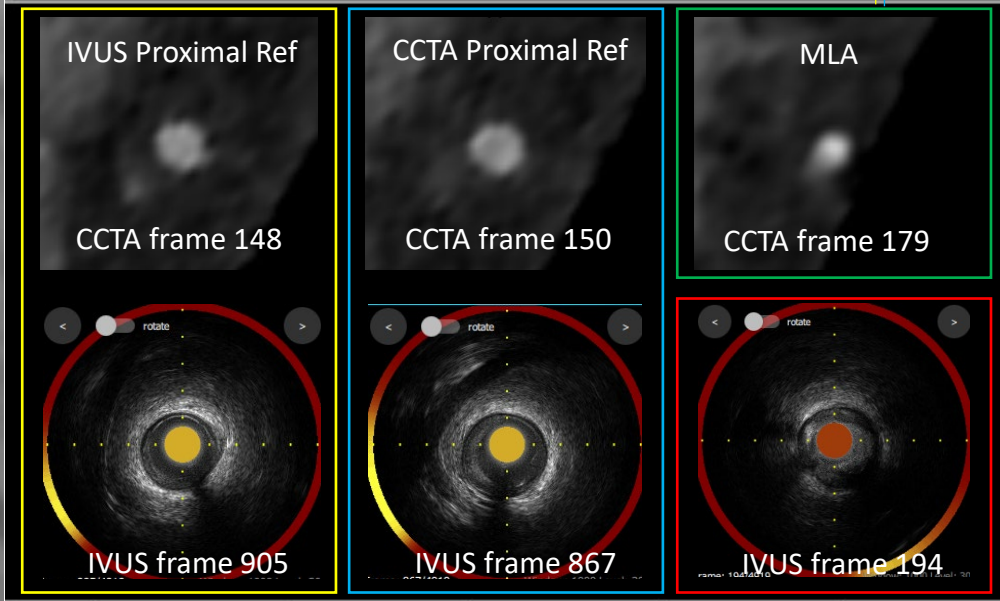

NIRS-IVUS pullback started in the plaque so distal reference areas and lesion length cannot be calculated

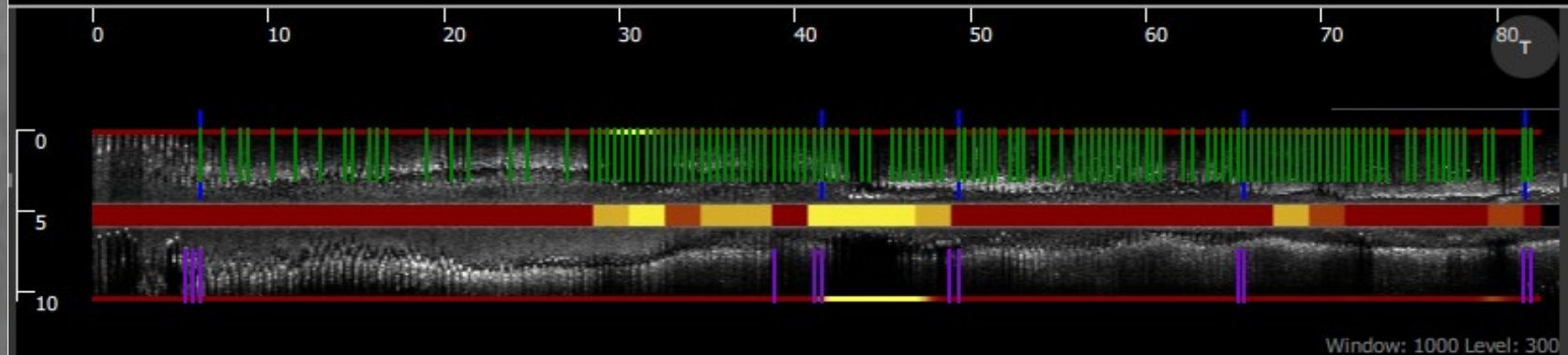

Case 49

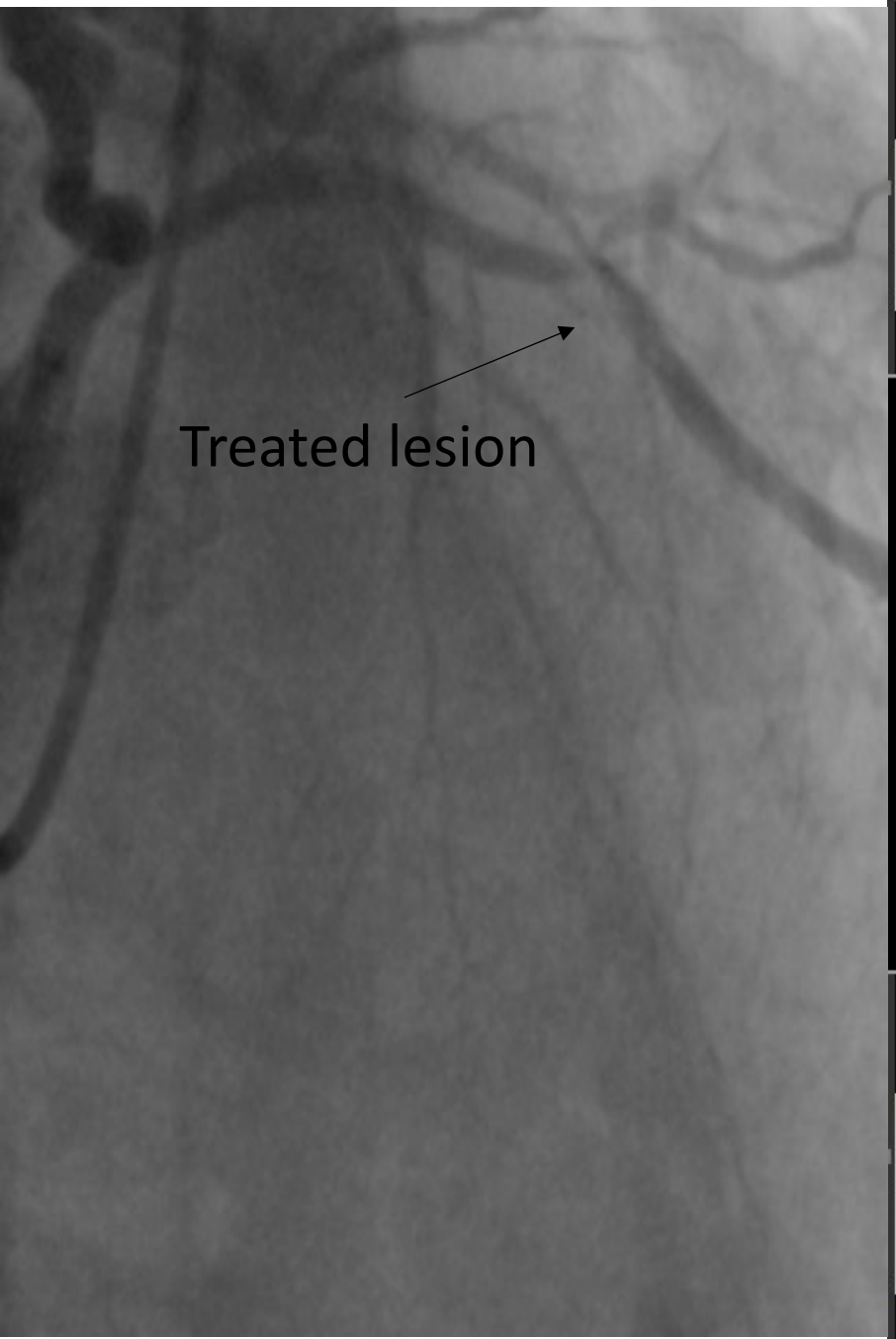
Treated lesion


CTA 2
IVUS 5428
Auto add align
Flip IVUS
Interpolate
0.01
0 10 20 30 40 50 60 70 80 90 100 110 120 130
0 5 10 15
Window: 1000 Level: 300
IVUS Proximal Ref
CCTA frame 77
IVUS frame 2990
CCTA Proximal Ref
CCTA frame 77
IVUS frame 2990
MLA
CCTA frame 98
IVUS frame 2133
IVUS Distal Ref
CCTA frame 115
IVUS frame 1783
CCTA Distal Ref
CCTA frame 115
IVUS frame 1783
0 10 20 30 40 50 60 70
0 5 10
Window: 1000 Level: 300

Case 50

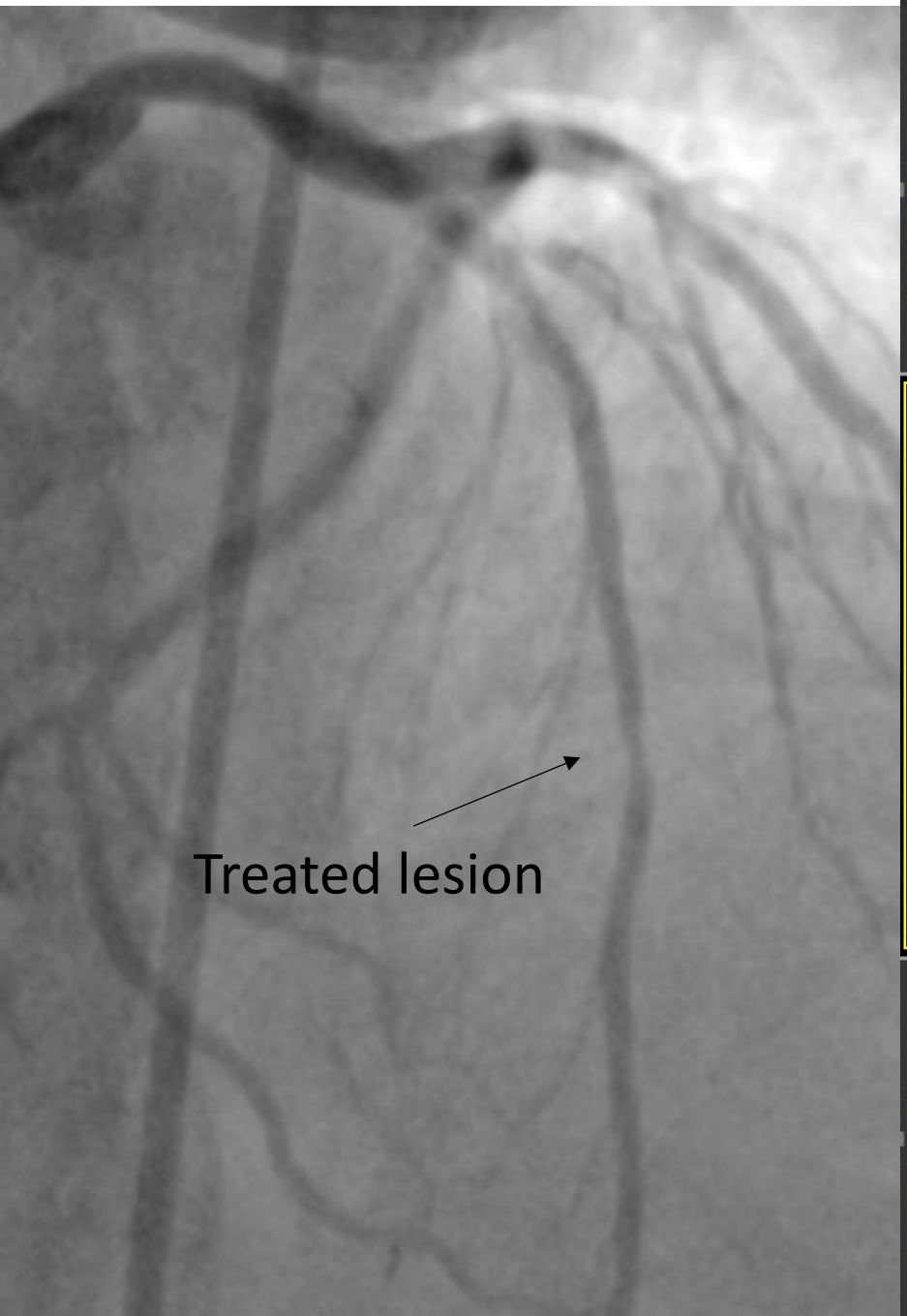
Treated lesion

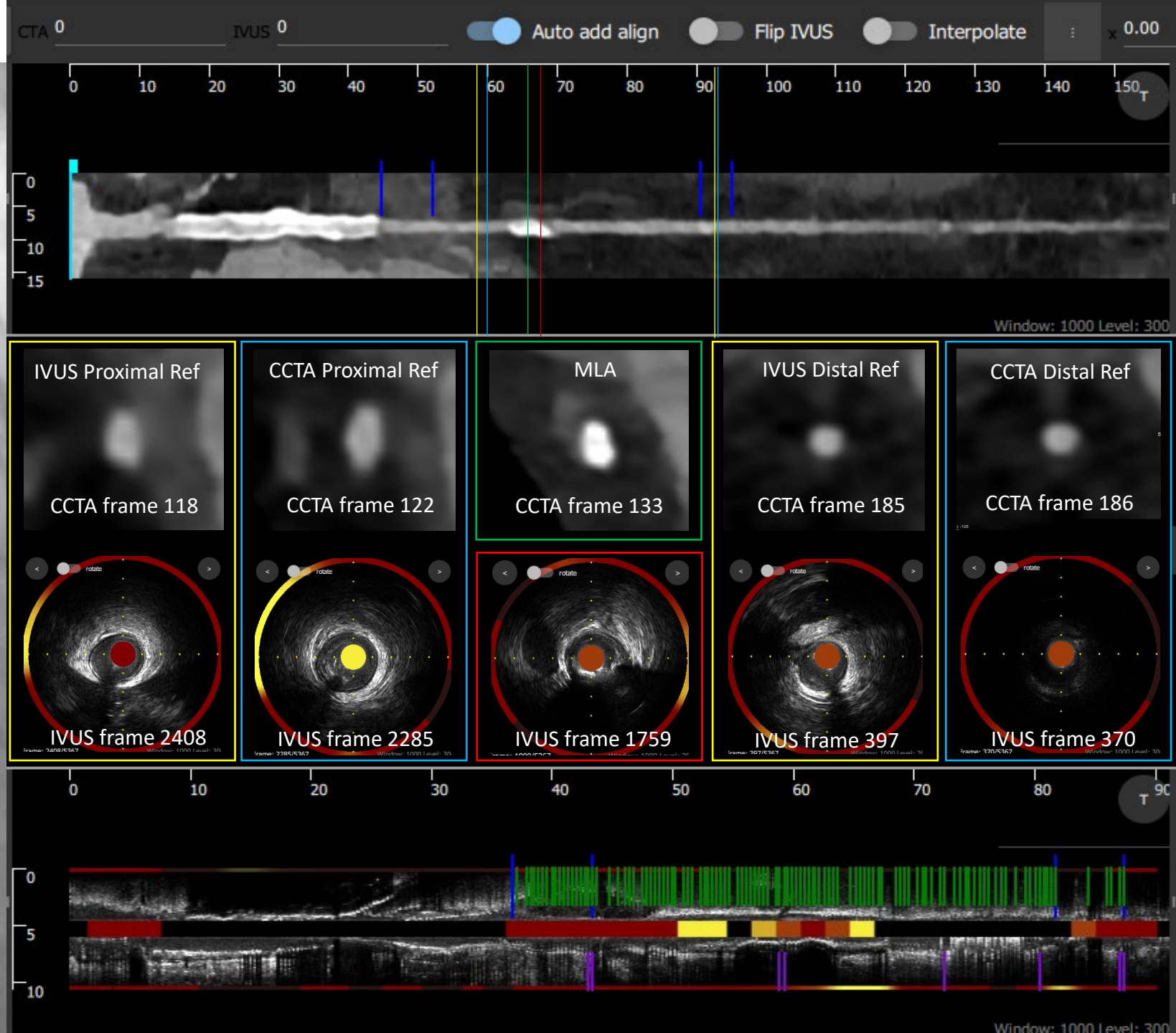
CTA 0
IVUS 0
Auto add align
Flip IVUS
Interpolate
0.00
Window: 1000 Level: 300
IVUS Proximal Ref
CCTA frame 118
IVUS frame 2408
CCTA Proximal Ref
CCTA frame 122
IVUS frame 2285
MLA
CCTA frame 133
IVUS frame 1759
IVUS Distal Ref
CCTA frame 185
IVUS frame 397
CCTA Distal Ref
CCTA frame 186
IVUS frame 370
Window: 1000 Level: 300

Case 51

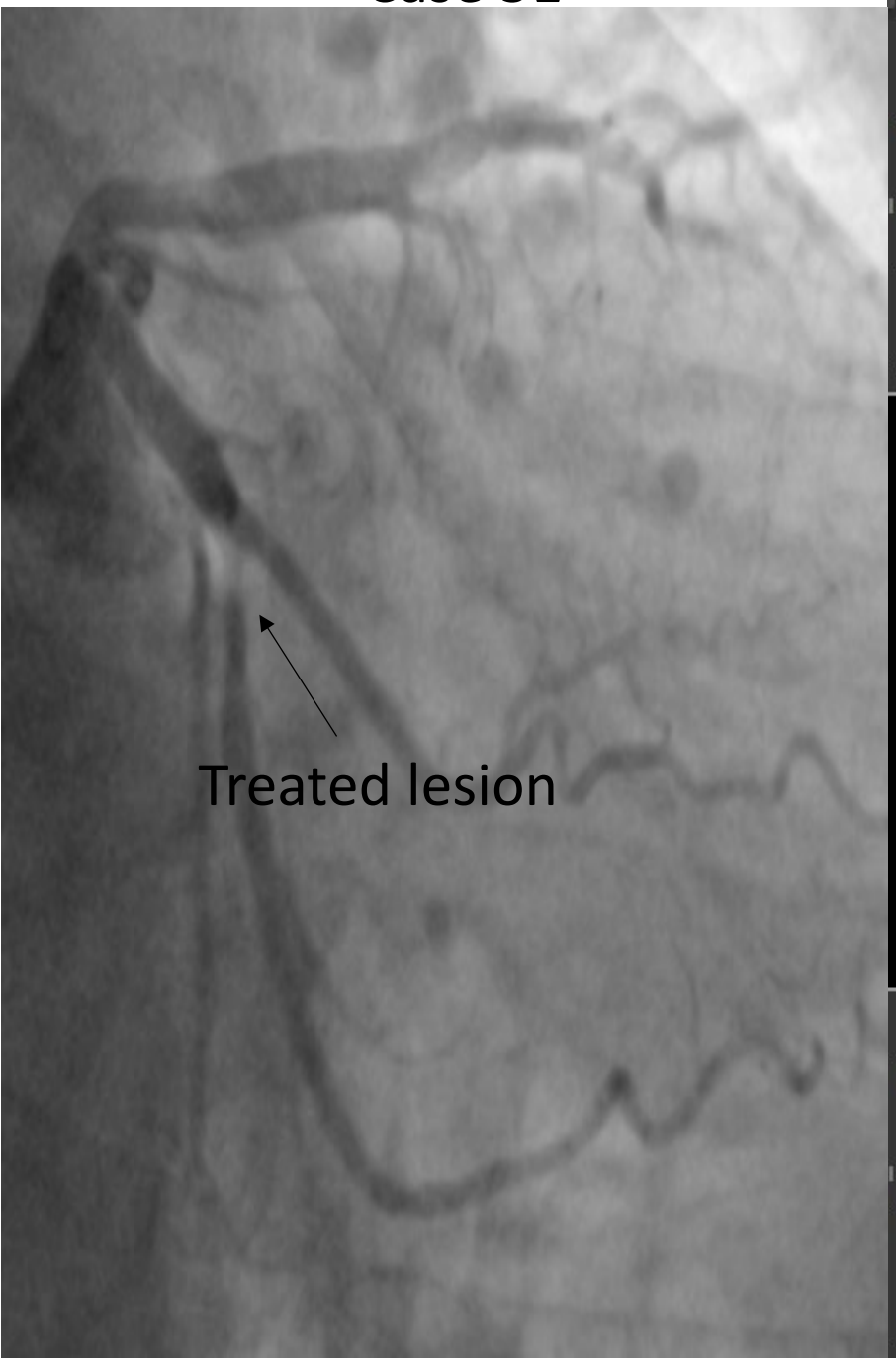
Treated lesion

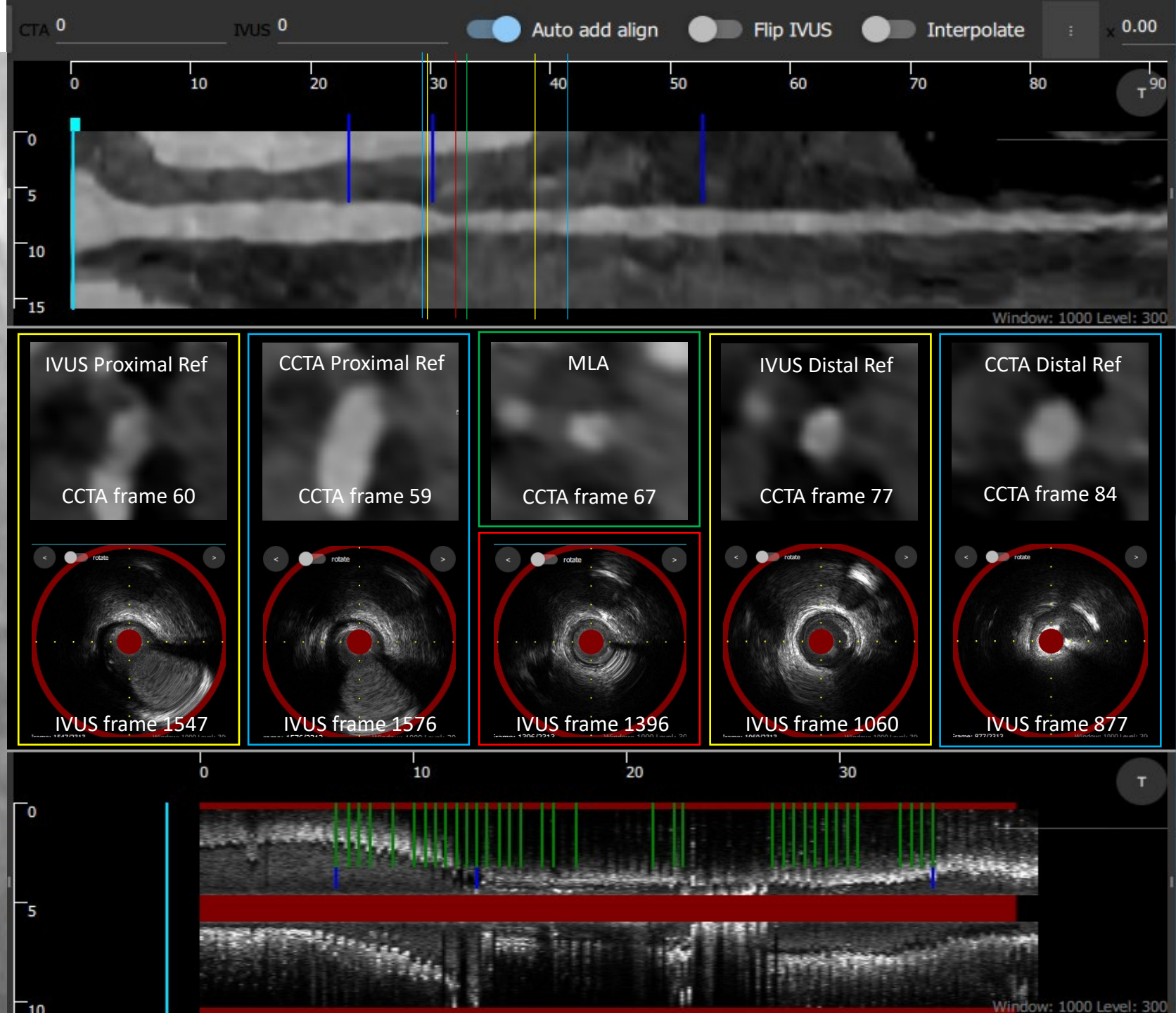
CTA 0
IVUS 0
Auto add align
Flip IVUS
Interpolate
0.00
Window: 1000 Level: 300
IVUS Proximal Ref
CCTA frame 60
IVUS frame 1547
CCTA Proximal Ref
CCTA frame 59
IVUS frame 1576
MLA
CCTA frame 67
IVUS frame 1396
IVUS Distal Ref
CCTA frame 77
IVUS frame 1060
CCTA Distal Ref
CCTA frame 84
IVUS frame 877
Window: 1000 Level: 300

Case 52


Treated lesion

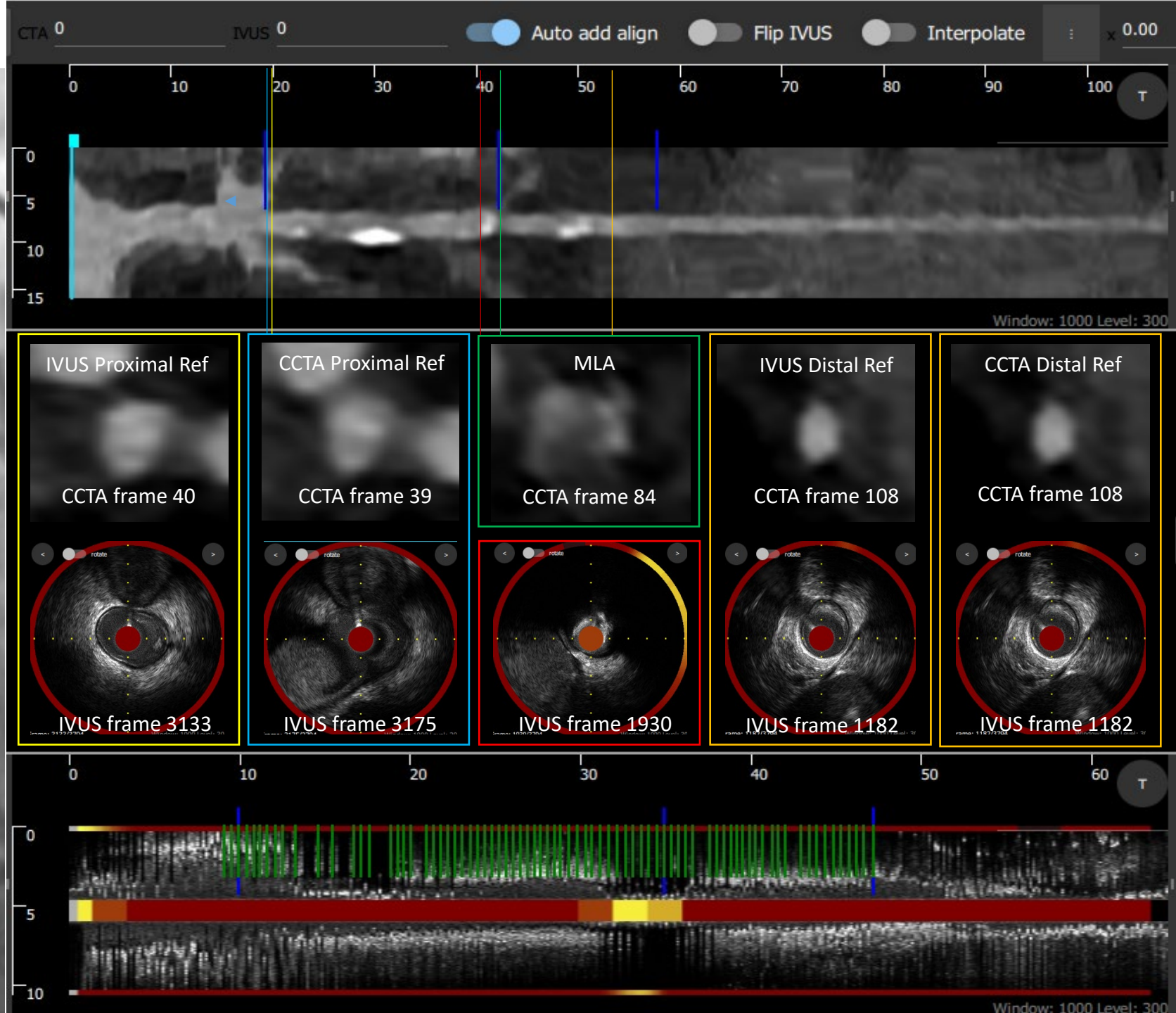
CTA 0
IVUS 0
Auto add align
Flip IVUS
Interpolate
0.00
Window: 1000 Level: 300
IVUS Proximal Ref
CCTA frame 40
IVUS frame 3133
CCTA Proximal Ref
CCTA frame 39
IVUS frame 3175
MLA
CCTA frame 84
IVUS frame 1930
IVUS Distal Ref
CCTA frame 108
IVUS frame 1182
CCTA Distal Ref
CCTA frame 108
IVUS frame 1182
Window: 1000 Level: 300

Case 53


Treated lesion

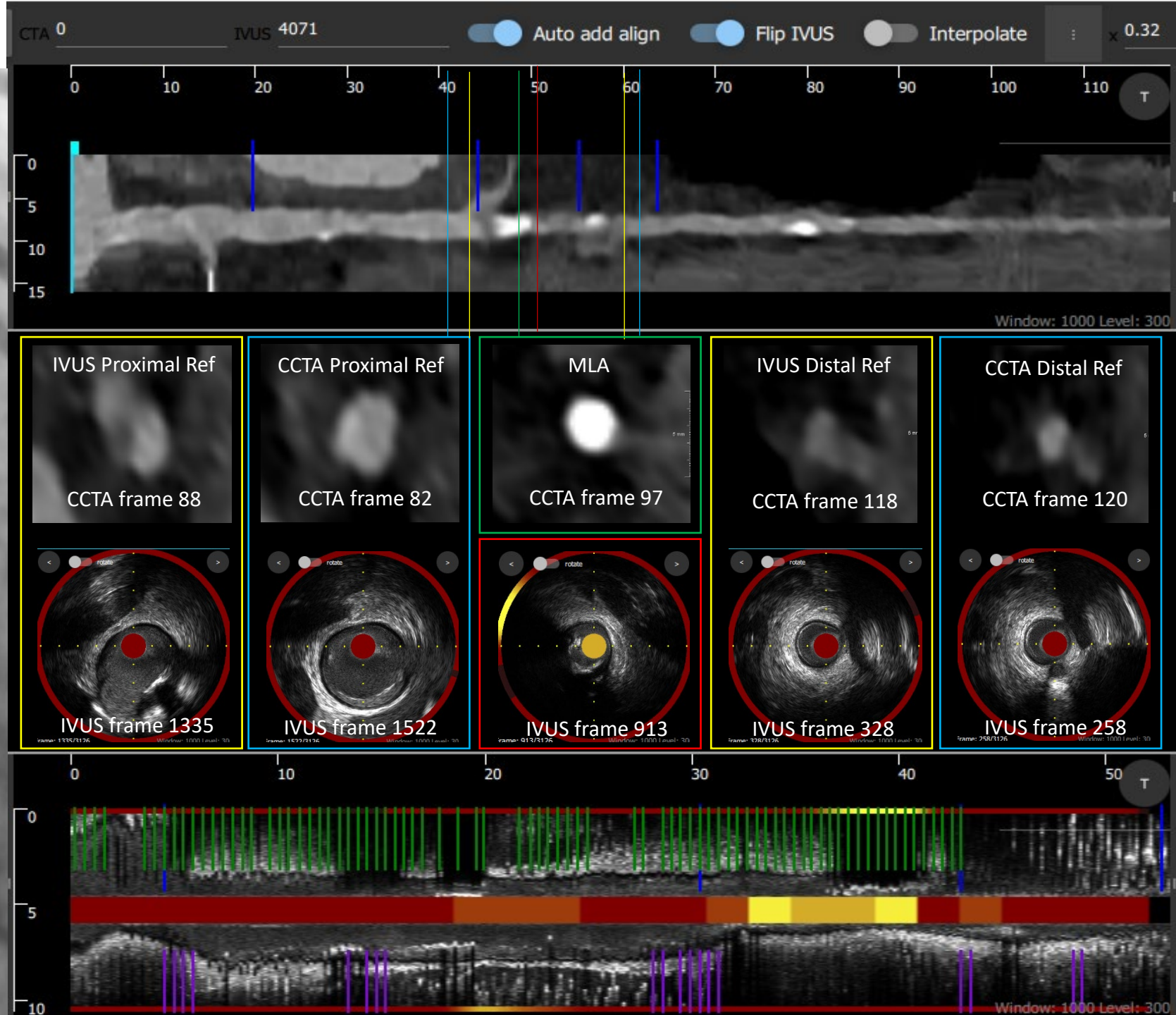
CTA 0
IVUS 4071
Auto add align
Flip IVUS
Interpolate
0.32
Window: 1000 Level: 300
IVUS Proximal Ref
CCTA frame 88
IVUS frame 1335
CCTA Proximal Ref
CCTA frame 82
IVUS frame 1522
MLA
CCTA frame 97
IVUS frame 913
IVUS Distal Ref
CCTA frame 118
IVUS frame 328
CCTA Distal Ref
CCTA frame 120
IVUS frame 258
Window: 1000 Level: 300

Case 54

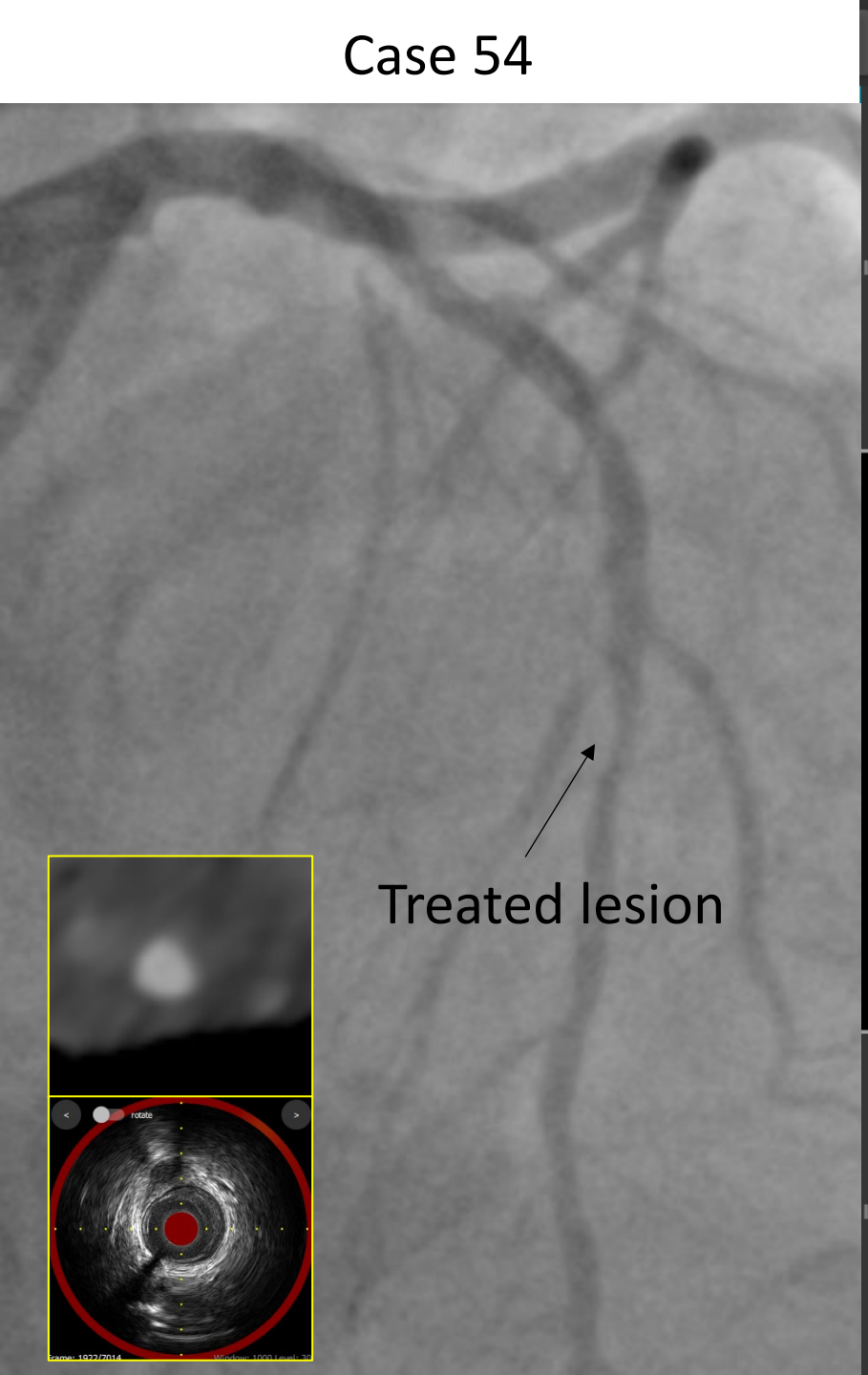
Treated lesion

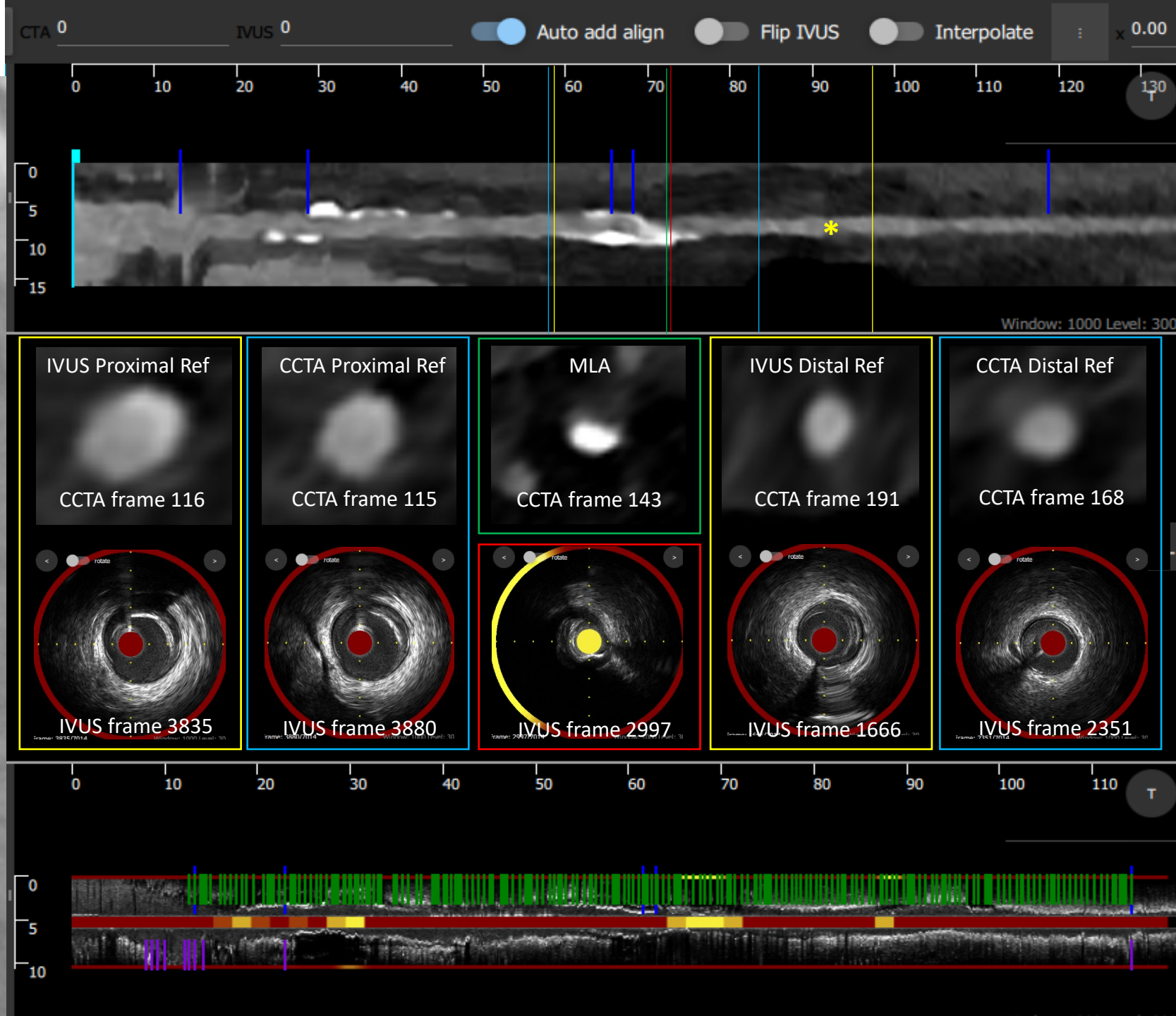
CTA 0
IVUS 0
Auto add align
Flip IVUS
Interpolate
x 0.00
Window: 1000 Level: 300
IVUS Proximal Ref
CCTA frame 116
IVUS frame 3835
CCTA Proximal Ref
CCTA frame 115
IVUS frame 3880
MLA
CCTA frame 143
IVUS frame 2997
IVUS Distal Ref
CCTA frame 191
IVUS frame 1666
CCTA Distal Ref
CCTA frame 168
IVUS frame 2351

Case 55


Treated lesion

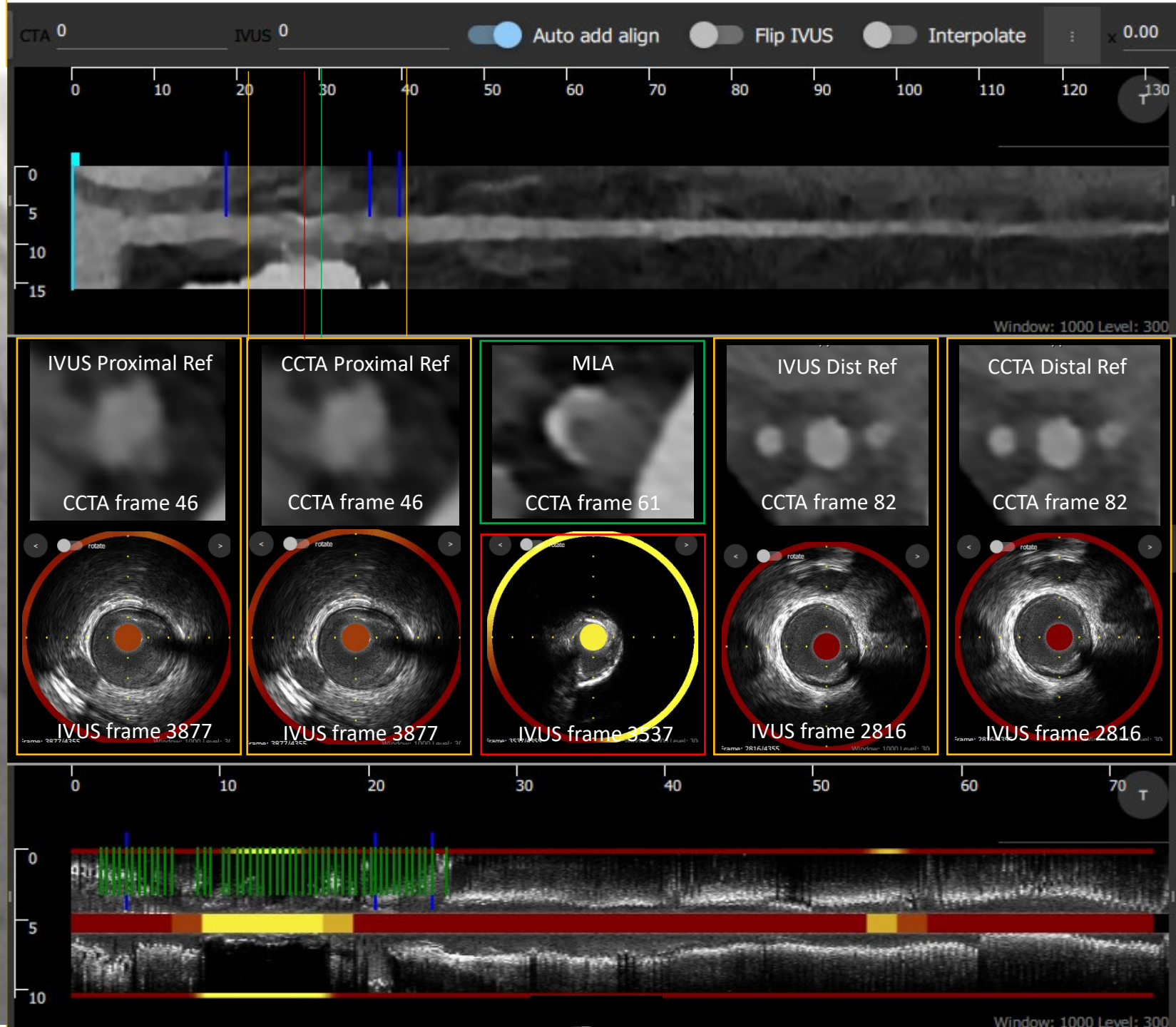
CTA 0
IVUS 0
Auto add align
Flip IVUS
Interpolate
0.00
Window: 1000 Level: 300
IVUS Proximal Ref
CCTA frame 46
IVUS frame 3877
CCTA Proximal Ref
CCTA frame 46
IVUS frame 3877
MLA
CCTA frame 61
IVUS frame 3537
IVUS Dist Ref
CCTA frame 82
IVUS frame 2816
CCTA Distal Ref
CCTA frame 82
IVUS frame 2816
Window: 1000 Level: 300

Case 56


Treated lesion

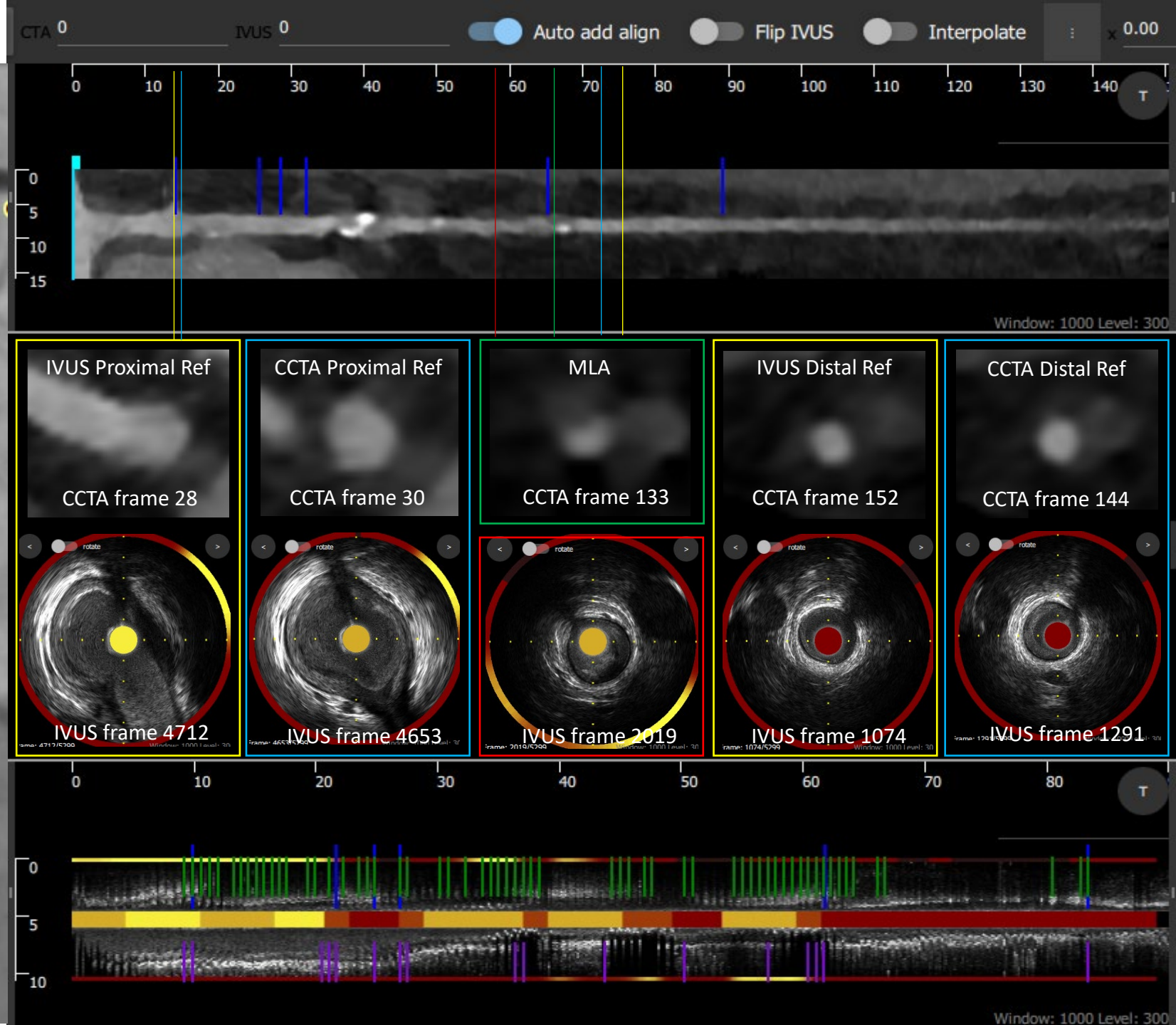
CTA 0
IVUS 0
Auto add align
Flip IVUS
Interpolate
0.00
Window: 1000 Level: 300
IVUS Proximal Ref
CCTA frame 28
IVUS frame 4712
CCTA Proximal Ref
CCTA frame 30
IVUS frame 4653
MLA
CCTA frame 133
IVUS frame 2019
IVUS Distal Ref
CCTA frame 152
IVUS frame 1074
CCTA Distal Ref
CCTA frame 144
IVUS frame 1291
Window: 1000 Level: 300

Case 57

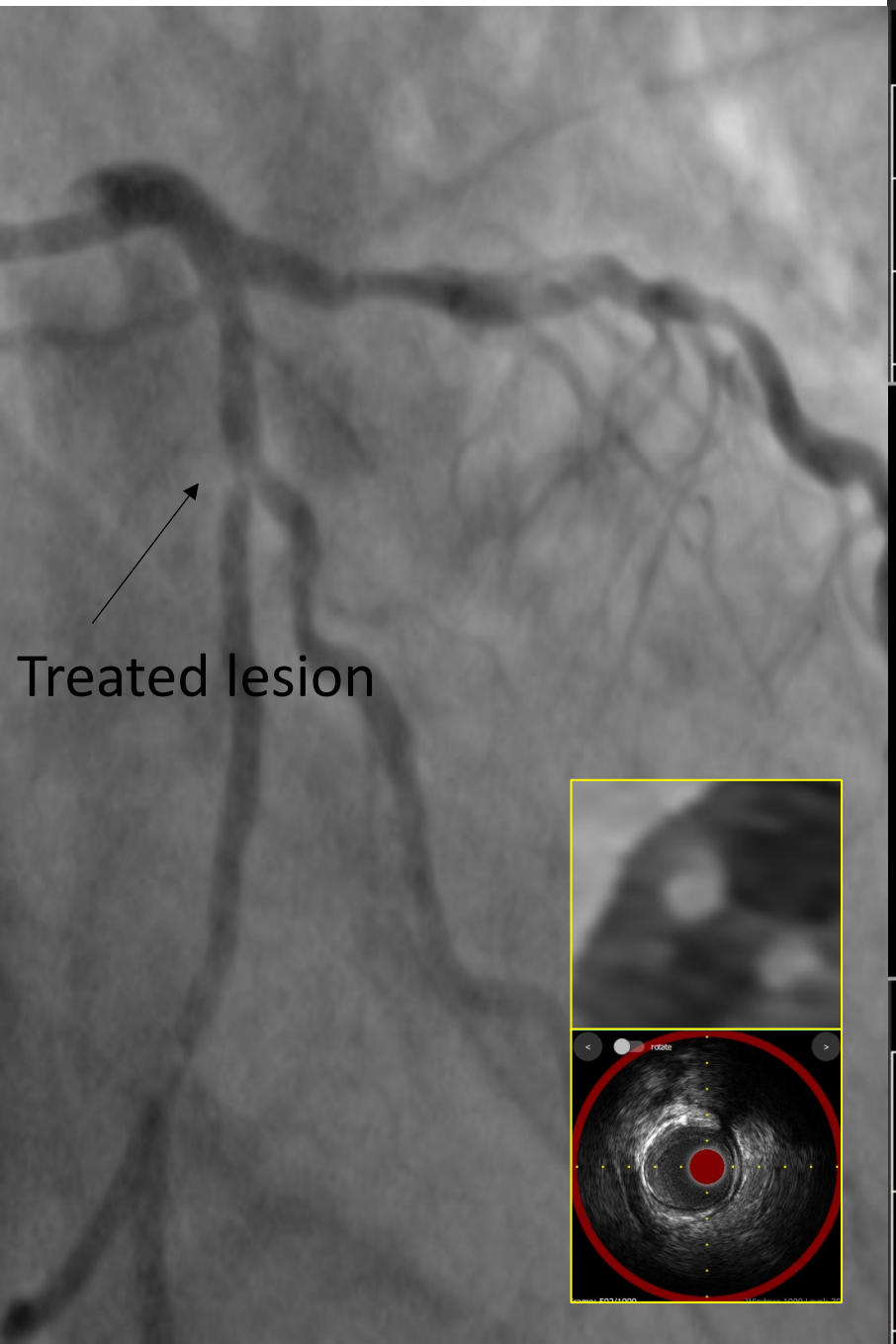
Treated lesion

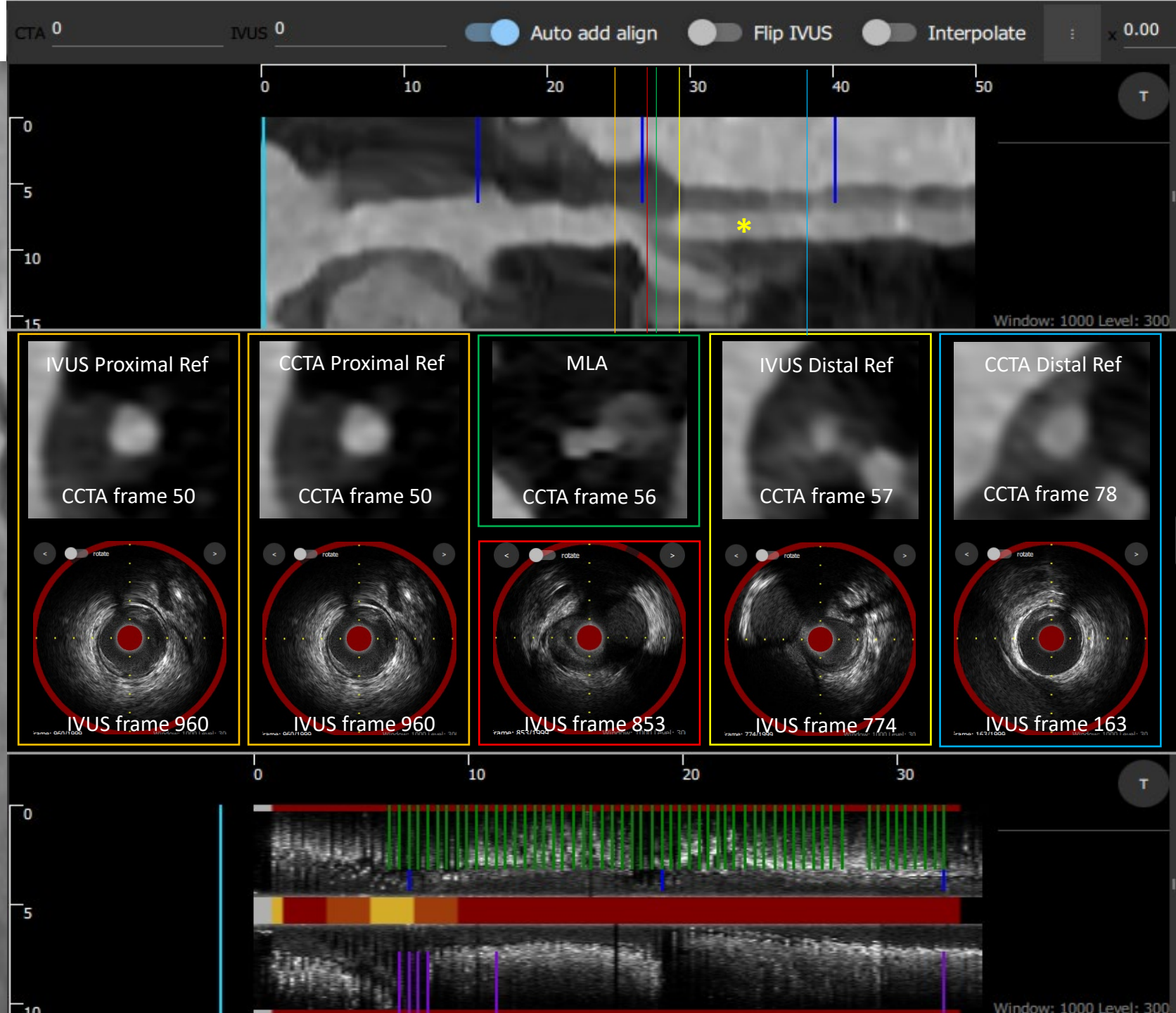
CTA 0
IVUS 0
Auto add align
Flip IVUS
Interpolate
0.00
0
10
20
30
40
50
0
5
10
15
Window: 1000 Level: 300
IVUS Proximal Ref
CCTA frame 50
IVUS frame 960
CCTA Proximal Ref
CCTA frame 50
IVUS frame 960
MLA
CCTA frame 56
IVUS frame 853
IVUS Distal Ref
CCTA frame 57
IVUS frame 774
CCTA Distal Ref
CCTA frame 78
IVUS frame 163
0
10
20
30
0
5
10
Window: 1000 Level: 300

Case 58

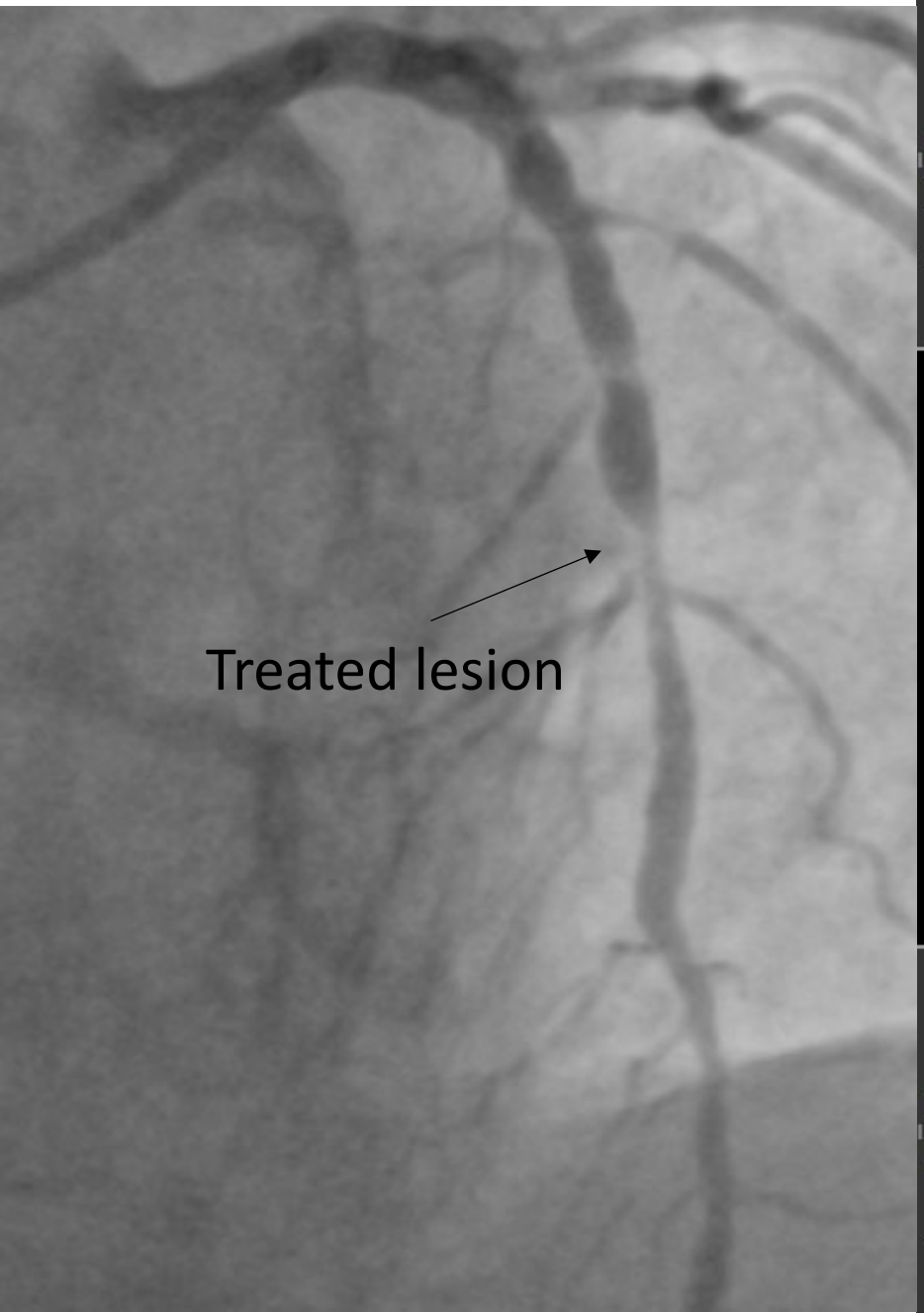
Treated lesion

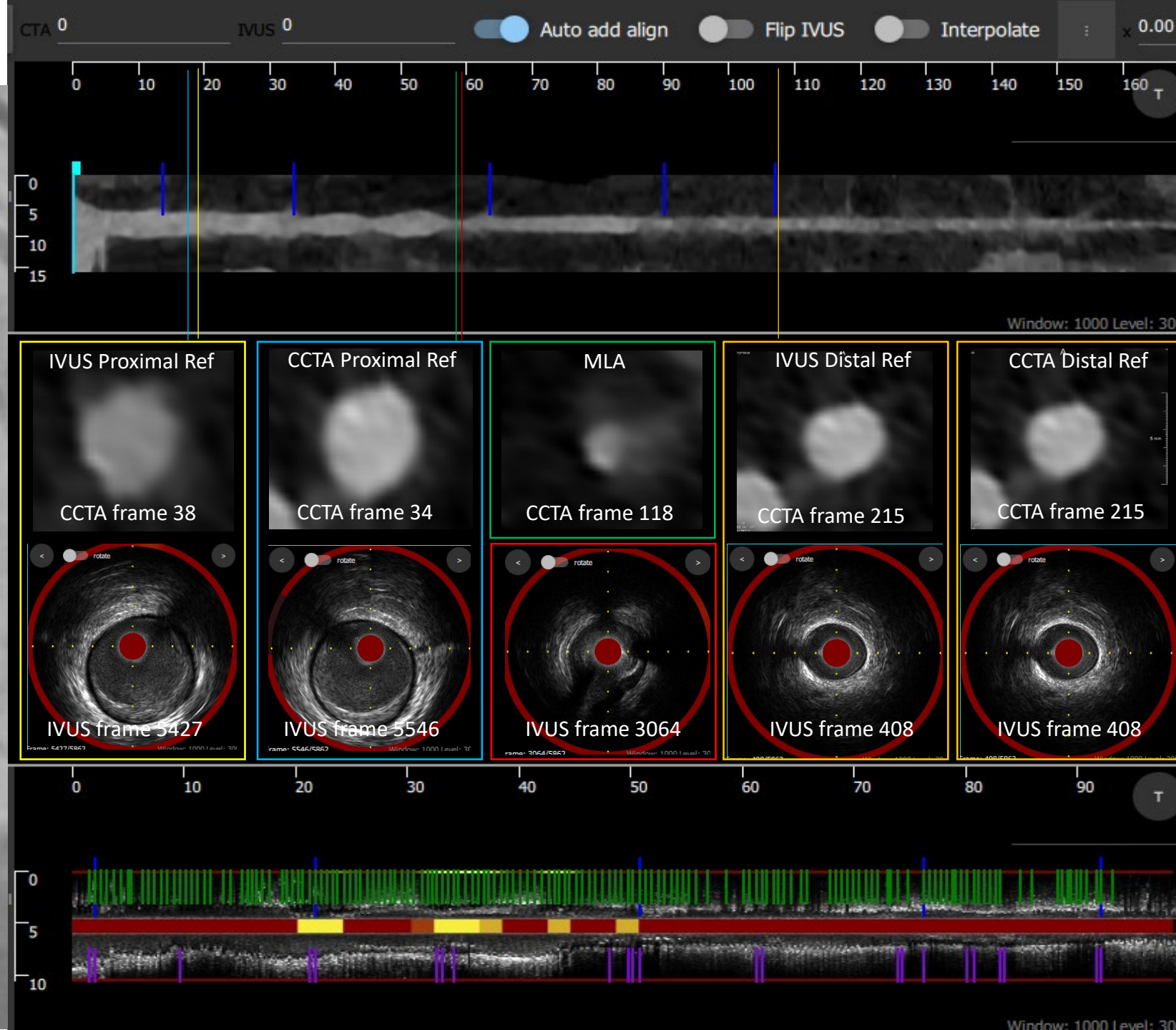
CTA 0
IVUS 0
Auto add align
Flip IVUS
Interpolate
0.00
Window: 1000 Level: 30
IVUS Proximal Ref
CCTA frame 38
IVUS frame 5427
CCTA Proximal Ref
CCTA frame 34
IVUS frame 5546
MLA
CCTA frame 118
IVUS frame 3064
IVUS Distal Ref
CCTA frame 215
IVUS frame 408
CCTA Distal Ref
CCTA frame 215
IVUS frame 408

Supplementary Figure 3. NIRS-IVUS and CCTA coregistration software.

On the top panel, a longitudinal view of the CCTA segment of interest is shown with the matched corresponding longitudinal NIRS-IVUS view shown on the bottom panel. Anatomical landmarks were used to match end-diastolic NIRS-IVUS and CCTA cross-sections, with linear interpolation applied for the in between cross-sections. The NIRS-IVUS vessel and EEM borders are then superimposed on the corresponding CCTA cross-section to enable comparison of the estimations of the two modalities as shown on the top left-hand panel, where the yellow, orange, green and red borders refer to the CCTA lumen, CCTA vessel wall, NIRS-IVUS lumen and NIRS-IVUS EEM, respectively. The corresponding NIRS-IVUS frame is shown on the bottom left panel. The side branch direction indicating correspondence is marked with a purple line.

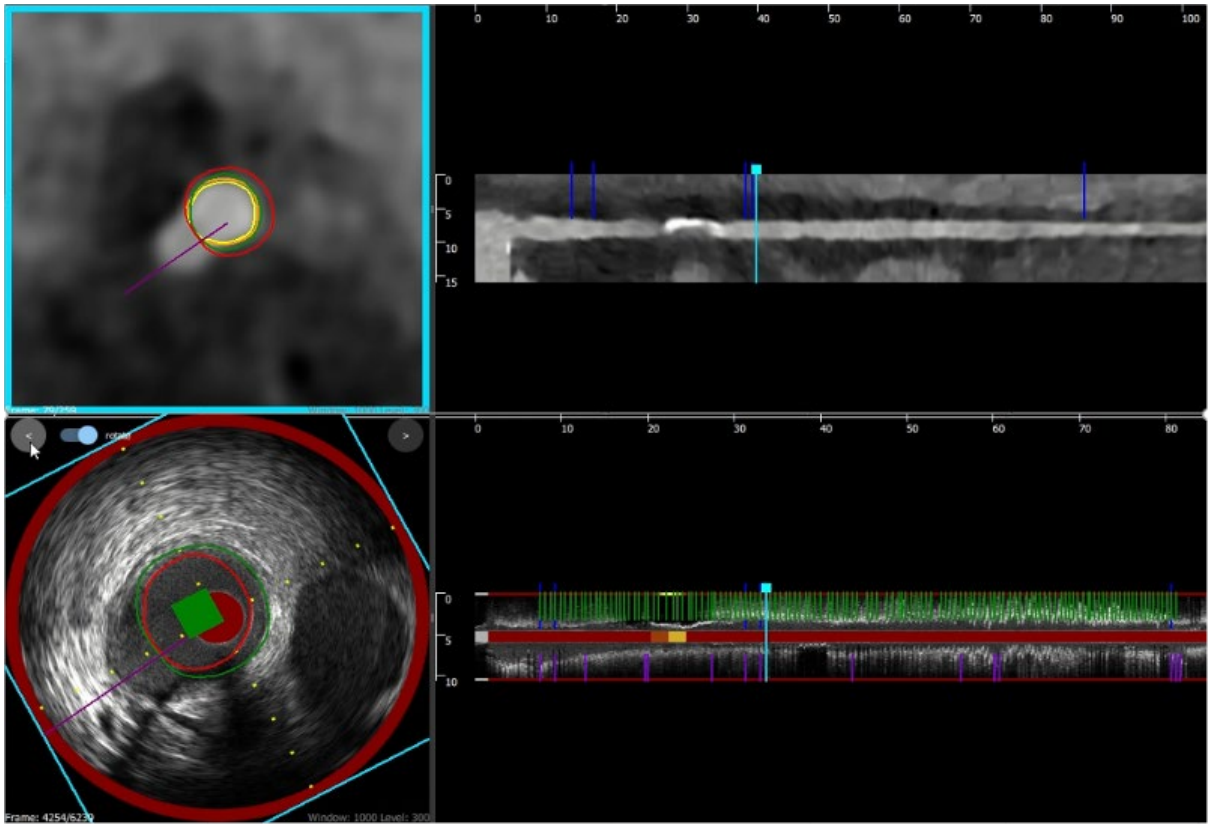

Supplementary Figure 4. A case example highlighting the limitations of Hounsfield unit-based plaque composition assessment.

The top panel shows a NIRS-IVUS spread-out plot of a segment analysed in a right coronary artery, with the yellow colour indicating presence of lipid core and the semi-transparent white showing the presence of calcific tissue. The middle panel is the output of the analysis software for this segment of interest; it is apparent that the high HU values in the lumen resulted in false classification of the vessel wall as calcific tissue. In the bottom panel, the classified tissues in the disease-free segments were replaced by the media, an option that is available in the analysis software; this resulted in improved plaque composition analysis in the disease-free segments but not in the detected plaques where the superficial plaque was erroneously classified as calcific tissue.

NIRS-IVUS spread-out plot

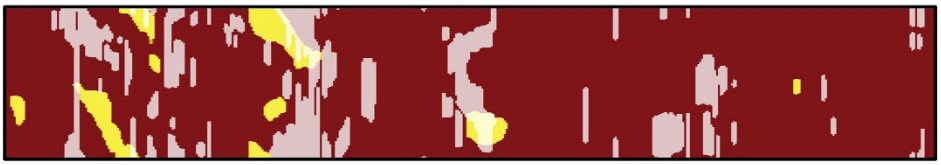

Conventional CCTA spread-out plot

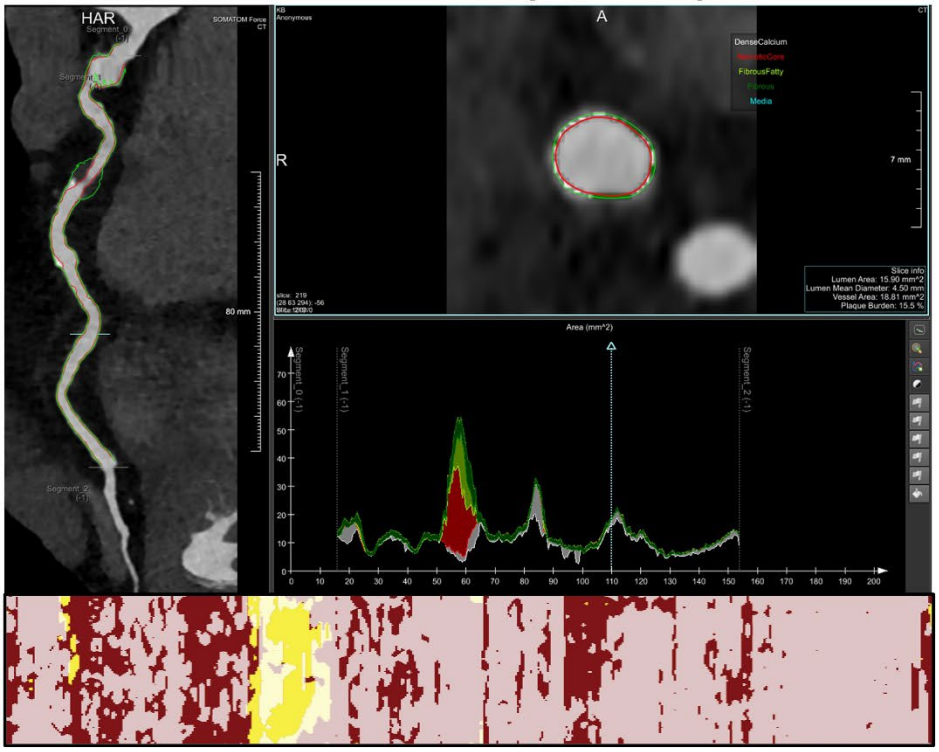

CCTA spread-out plot with ‘media’ replacement